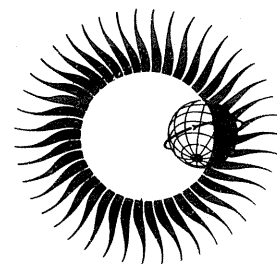


WORLD DATA CENTER A

Upper Atmosphere Geophysics



DATA ON SOLAR-GEOPHYSICAL ACTIVITY
ASSOCIATED WITH THE MAJOR
GEOMAGNETIC STORM OF MARCH 8, 1970



April 1971

WORLD DATA CENTER A

National Academy of Sciences

2101 Constitution Avenue, N. W. Washington, D. C. U.S.A., 20418

World Data Center A consists of the Coordination Office

and nine subcenters:

World Data Center A
Coordination Office
National Academy of Sciences
2101 Constitution Avenue, N.W.
Washington, D. C., U.S.A. 20418
Telephone (202) 961-1478

Solar and Interplanetary Phenomena,
Ionospheric Phenomena, Flare-Associated
Events, Aurora, Cosmic Rays, Airglow:
World Data Center A:
Upper Atmosphere Geophysics
National Oceanic and Atmospheric
Administration
Boulder, Colorado, U.S.A. 80302
Telephone (303) 447-1000 Ext. 3381

Geomagnetism, Seismology and Gravity:
World Data Center A:
Geomagnetism, Seismology and Gravity
Environmental Data Service, NOAA
Rockville, Maryland, U.S.A. 20852
Telephone (301) 496-8160

Glaciology:
World Data Center A:
Glaciology
American Geographical Society
Broadway at 156th Street
New York, New York, U.S.A. 10032
Telephone (212) 234-8100

Longitude and Latitude:
World Data Center A:
Longitude and Latitude
U. S. Naval Observatory
Washington, D. C., U.S.A. 20390
Telephone (202) 698-8422

Meteorology (and Nuclear Radiation):
World Data Center A:
Meteorology
National Climatic Center
Federal Building
Asheville, North Carolina, U.S.A. 28801
Telephone (704) 254-0961

Oceanography:
World Data Center A:
Oceanography
Building 160
Second and N Streets, S.E.
Washington, D. C., U.S.A. 20390
Telephone (202) 698-3753

Rockets and Satellites:
World Data Center A:
Rockets and Satellites
Goddard Space Flight Center
Code 601
Greenbelt, Maryland, U.S.A. 20771
Telephone (301) 982-6695

Tsunami:
World Data Center A:
Tsunami
National Oceanic and Atmospheric
Administration
P. O. Box 3887
Honolulu, Hawaii, U.S.A. 96812
Telephone (808) 546-5698

Upper Mantle Project:
World Data Center A:
Upper Mantle Project
Lamont-Doherty Geological Observatory
Palisades, New York, U.S.A. 10964
Telephone (914) 359-2900 Ext. 209

Notes:

- (1) World Data Centers conduct international exchange of geophysical observations in accordance with the principles set forth by the International Council of Scientific Unions. WDC-A is established in the United States under the auspices of the National Academy of Sciences.
- (2) Communications regarding data interchange matters in general and World Data Center A as a whole should be addressed to: World Data Center A, Coordination Office (see address above).
- (3) Inquiries and communications concerning data in specific disciplines should be addressed to the appropriate subcenter listed above.

WORLD DATA CENTER A

Upper Atmosphere Geophysics



REPORT UAG-12 PART I

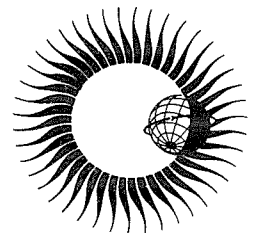
DATA ON SOLAR - GEOPHYSICAL ACTIVITY ASSOCIATED WITH THE MAJOR GEOMAGNETIC STORM OF MARCH 8, 1970

compiled by
J. Virginia Lincoln and Dale B. Bucknam
WDC-A, Upper Atmosphere Geophysics
Boulder, Colorado

Prepared by Research Laboratories, NOAA, Boulder, Colorado
and published by

U.S. DEPARTMENT OF COMMERCE
NATIONAL OCEANIC AND ATMOSPHERIC ADMINISTRATION

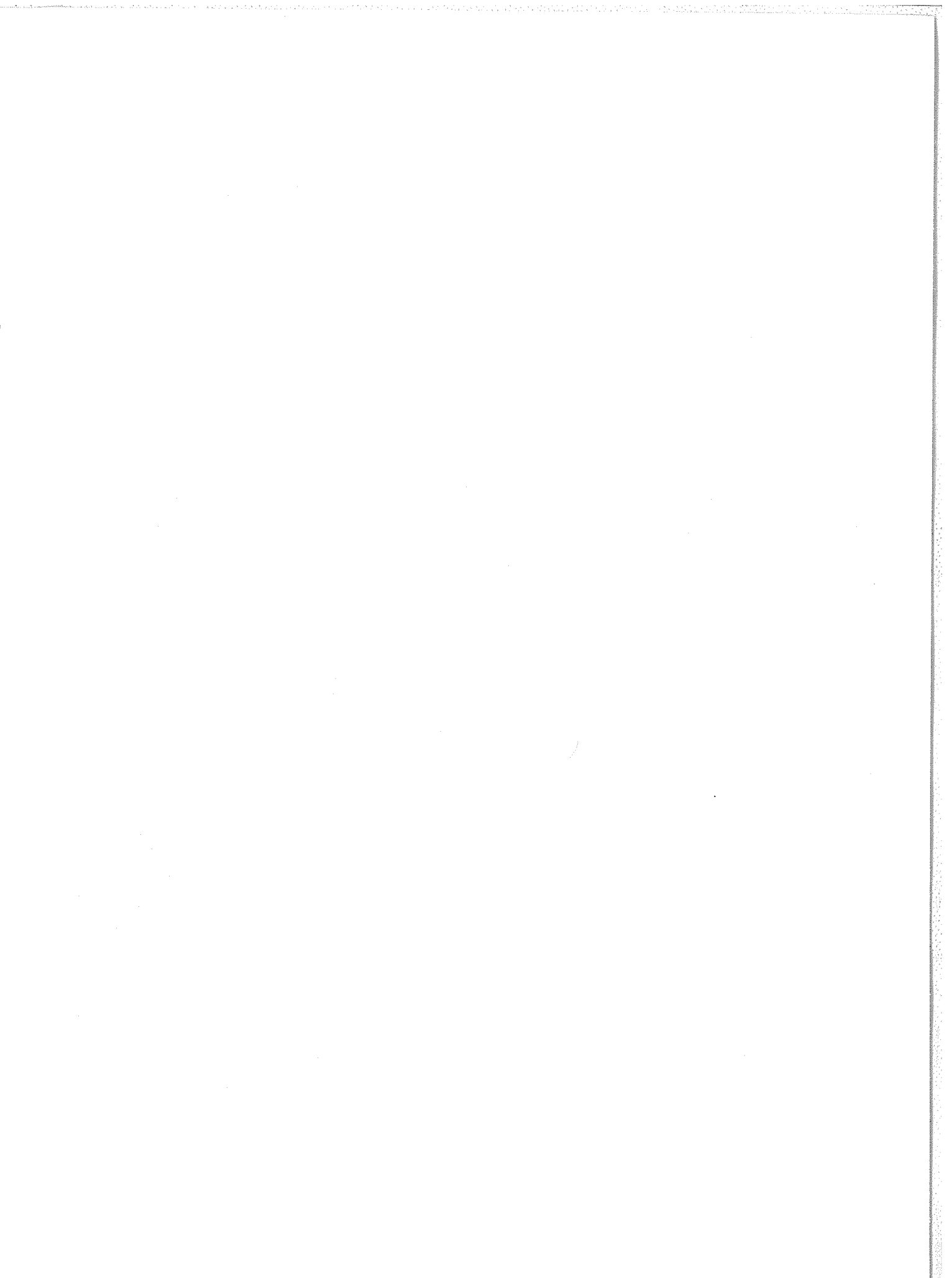
ENVIRONMENTAL DATA SERVICE
Asheville, North Carolina, USA 28801



April 1971

SUBSCRIPTION PRICE: \$9.00 a year; \$2.50 additional for foreign mailing; single issue price varies.* Order from the Superintendent of Documents, Government Printing Office, specifying the Catalog order number, C52.16/2:12. Checks and money orders should be made payable to the Superintendent of Documents. Remittance and correspondence regarding subscriptions should be sent to the Superintendent of Documents, Government Printing Office, Washington, D. C. 20402.

*Price of this issue \$3.00



FOREWORD

This compilation is the fourth in these series of reports continuing this type of international cooperation recommended by the Inter-Union Commission on Solar-Terrestrial Physics. The Chairmen or Co-Chairmen of IUCSTP Working Groups 2, 7 and 12 suggested at the IUCSTP Symposium in Leningrad, May 1970, that this period around March 6-10, 1970 was worthy of study.

Dr. Akasofu stated this period included the greatest magnetic storm to date in this solar cycle. In addition, a total solar eclipse took place on March 7.

Therefore, in July 1970 contributions were solicited from the international community. Originally it had been anticipated the report would be completed by the end of 1970. Contributions continued to be received into January 1971. Thus, the processing has only now been completed. Because of the large number of papers the report is in three parts to facilitate handling. The ones dealing primarily with the eclipse are grouped as an Appendix to Part III. There has been no attempt to cover comprehensively the March 7, 1970 total solar eclipse. The reader should refer to the collection of eclipse papers published in Nature, June 1970. A "Symposium on 1970 Solar Eclipse" will be held at the XIVth Meeting of COSPAR, June 21 - July 2, 1971 in Seattle, Washington. IUCSTP is coordinating the organization of this Symposium in consultation with all interested Unions and COSPAR. Proceedings of this Symposium are expected to be published.

This present report also includes selections from the data normally sent to World Data Centers which the compilers felt help complete the account of the solar-terrestrial phenomena for this study. The many participants are thanked for their submissions of their special data or contributions.

The compilers wish to acknowledge with special thanks the huge task of typing and correcting the manuscript that was done by Mrs. Lorraine Bower and Miss May Starr.

J. Virginia Lincoln
Dale B. Bucknam

TABLE OF CONTENTS

	<u>Page</u>
PART I	
FOREWORD	i
1. INTRODUCTION AND SUMMARY OF GENERAL ACTIVITY	1
2. SOLAR DISK AND LIMB PHENOMENA	8
3. SOLAR RADIO PHENOMENA	43
4. SOLAR X-RAYS	98
5. SUDDEN IONOSPHERIC DISTURBANCES	109
6. SOLAR WIND	122
7. SOLAR ENERGETIC PARTICLES	130
PART II	
8. IONOSPHERIC PHENOMENA	179
9. AIRGLOW	272
10. AURORA	298
PART III	
11. COSMIC RAYS	312
12. INTERDISCIPLINARY STUDIES	325
13. GEOMAGNETIC DATA	359
14. INTERPLANETARY MAGNETIC FIELD	408
APPENDIX: ECLIPSE	413
ACKNOWLEDGEMENTS	461
ALPHABETICAL INDEX	461
AUTHOR INDEX	464

TABLE OF CONTENTS

PART I

	<u>Page</u>
FOREWORD	i
J. Virginia Lincoln Dale B. Bucknam	
1. INTRODUCTION AND SUMMARY OF GENERAL ACTIVITY	
J. Virginia Lincoln	1
2. SOLAR DISK AND LIMB PHENOMENA	
Synoptic Chart of Solar Magnetic Fields (Robert Howard)	8
The Solar Active Region Associated with Geophysical Events 6-8 March 1970 (Patrick S. McIntosh)	10
Geoactive Phenomena Beyond the Western Limb on March 6, 1970 (L. Krivsky and S. Pinter)	16
Green Corona in Connection with the Possible Proton Event March 6, 1970 (M. Rybanský and J. Sýkora)	20
A Two-ribbon Flare on March 7, 1970 (Eijiro Hiei and Fumio Moriyama)	23
Optical Flares and VLF Anomalies Related to the Great Magnetic Storm of March 8, 1970 (Richard A. Miller, S.J. and Allan R. Trinidad)	29
High Velocity Mass-ejection Evidence Related to a Solar Flare of March 8, 1970 (Marta Rovira, Marcos Machado and Hugo Grassi Gallegos)	37
Importance 2 Active Prominences at Limb Observed at Catania Astrophysical Observatory on March 8, 1970 (G. Godoli, O. Morgante and M. L. Sturiale)	40
3. SOLAR RADIO PHENOMENA	
Summary of Worldwide Outstanding Solar Radio Emission Events - Fixed Frequency and Spectral (Hope I. Leighton and J. Virginia Lincoln)	43
Type I Noise Active Regions and Energetic Electrons from 1 to 10 March 1970 (Kunitomo Sakurai)	52
Solar Radio Emission for March 6-10, 1970 (H. Tanaka)	61
The Microwave Spectroheliograms of March 6-10, 1970 (J. S. Deuter and R. N. Bracewell)	64
Solar Emission at 8.3 mm on March 6-12, 1970 (G. Feix)	68
Characteristics of Noise Storms and the S-component of Solar Radio Emission in March, 1970 (A. Böhme and A. Krüger)	71
Radioheliograph Observations of Harmonic Type III Bursts (D. J. McLean)	76
Solar Radio Emission, Hiraïso, Japan (F. Yamashita)	81
The Type IV Event on 6 March, 1970 (L. Fritzkova-Svestkova and J. Olmr)	82
Microwave Burst of 6 March 1970 Proton Flare (V. L. Badillo)	85
High-resolution Observations of a Microwave Burst on March 7, 1970 (Ahinzo Enomé)	88
Data Submitted by Ahmedabad, India for the Period March 2-10, 1970 (K. R. Ramanathan)	92
4. SOLAR X-RAYS	
Solar Activity and Earth Atmospheric Densities in March, 1970 (D. E. Knight, R. J. Uribe and B. E. Woodgate)	98
Physical Models of Two Plage-associated X-ray Emitting Regions During the Period March 1 to 14, 1970 (P. R. Sengupta)	101
Solar X-ray Emission March 5-10, 1970 (D. M. Horan and R. W. Kreplin)	105

PART I (continued)

	<u>Page</u>
5. SUDDEN IONOSPHERIC DISTURBANCES	
Sudden Ionospheric Disturbance Summary from WDC-A Archive (J. Virginia Lincoln)	109
Multi-frequency Radiowave Observations of SID Events During 1-6 March, 1970 (T. B. Jones and R. E. Evans)	110
On the SID Activity of Early March 1970 (P. Triska and J. Lastovicka)	115
Atmospherics and SEA During the Period 1970 March 4-10 (V. Barocas)	120
6. SOLAR WIND	
Vela 5 Solar Wind Observations During the Geomagnetic Storm of March 8, 1970 (Michael D. Montgomery and S. J. Bame)	122
Energetic Electrons and Protons Observed on OGO-5, March 6-10, 1970 (H. I. West, Jr., J. R. Walton, R. M. Buck and R. G. D'Arcy, Jr.)	124
7. SOLAR ENERGETIC PROTONS	
HEOS-A1 Solar Proton ($1 \leq E \leq 13$ Mev, $E > 360$ Mev) and Interplanetary Magnetic Field Data for March 6-10, 1970 (A. Balogh, C. Dyer, A. Engel, P. Hedgecock, R. Hynds and J. Sear)	130
Observation of Energetic Solar Particles During March 6-10, 1970 (R. P. Lin and K. A. Anderson)	132
Solar Protons and Alpha Particles in the March 6-9, 1970 Events (J. C. Armstrong and C. O. Bostrom)	134
Proton, Alpha and Bremsstrahlung Fluxes Measured Aboard OY5-6 (G. K. Yates, L. Katz, J. G. Kelley, B. Sellers, F. A. Hanser and P. R. Morel)	139
Temporal Variations in the 100 kev to 8 Mev Protons over the Northern Polar Cap During the March 7, 1970 Event (H. R. Lindalen, K. Aarsnes, R. Amundsen and F. Søråas)	147
Trapped Particles over the Northern Polar Cap between 6 and 10 March 1970 (V. Domingo, D. E. Page and M. L. Shaw)	150
Redistribution of Trapped Protons following the 8 March 1970 Magnetic Storm (S. M. Krimigis, P. Verzariu, D. Venkatesan and B. A. Randall)	156
Proton and Alpha Particle Measurements over the Northern Polar Cap with the Satellite GRS-A/Azur during the March 1970 Solar Proton Event (E. Lammers and J. Moritz)	160
Observation of Solar Particles in March 1970 and Correlated Effects in the Outer Radiation Belt (E. Achtermann, B. Häusler, D. Hovestadt, and M. Scholer)	168

1. INTRODUCTION AND SUMMARY OF GENERAL ACTIVITY

by

J. Virginia Lincoln
 Aeronomy and Space Data Center
 National Oceanic and Atmospheric Administration, Boulder, Colorado

As with previous reports of this series, the scientists submitting contributions have not had the benefit of seeing each other's contributions. This leads to some repetition, but from different viewpoints. In a few cases the compilers have supplied introductory text to the data submitted. Some minor editing has been done to make the contributions consistent or to clarify the English. Some data as published in "Solar-Geophysical Data" are repeated here for the user's convenience.

General Activity

The Abbreviated Calendar Record from "Solar-Geophysical Data", Number 314, Part II, pages 86-87, shows a rise in the level of activity on March 6 continuing through the storm on March 8.

The two McMath regions mentioned as candidates for the source of the solar disturbance are Regions 10595 and 10614. Their region histories are reprinted in Table 1 below. See "Solar-Geophysical Data" Descriptive Text for units used. The calcium plage data are from McMath-Hulbert Observatory; the sunspot magnetic field data from Mt. Wilson Observatory; the area, count and Zürich classification from NOAA, Boulder, Colorado; and the 9.1 cm data from Stanford University.

Table 1

Histories of McMath regions 10595 and 10614

MCMATH REGION 10595				CMP DATE		27.0 Feb		RETURN OF REGION 10549 & 10561				ROTATION		2					
				CALCIUM		PLAGE		DATA		SUNSPOT DATA				9.1 CM					
YR	MO	DA	MC NO.	LAT	CMD	L	AREA	INT	MW NO.	LAT	CMD	L	MAG.	H	AREA	CNT	C	INT	FLUX
70	2	20	10595	N15	E88	273	600	2.0											
70	2	21	10595	N16	E76	230	3000	3.5	17759	N16	E70	232		0	100	15	D	19	8
70	2	22	10595	N16	E62	232	4000	3.5	17759	N15	E59	234	(O)	4	430	9	D	25	11
70	2	23	10595	N16	E47	274	4000	3.5	17759	N16	E44	234	(O)	4	0	20	D	41	17
70	2	24	10595	N17	E34	234	4100	3.5	17759	N16	E31	234	(O)	5	430	44	E	33	13
70	2	25	10595	N17	E20	235	4500	3.5	17759	N16	E16	236	(BY)	4	260	48	E	35	14
70	2	26	10595	N17	E05	236	4000	3.0	17759	N15	E04	235	(BY)	4	260	38	E	41	17
70	2	27	10595	N17	W18	246	4100	3.5	17759	N11	W26	249		0	10	3	B	38	16
70	2													0	180	44	D		
70	2	28	10595	N17	W22	237	4000	3.0							220	43	D	33	13
70	3	1	10595	N17	W36	237	3800	3.5							250	35	D	21	8
70	3	2	10595												200	7	C	19	8
70	3	3	10595												160	6	G	63	25
70	3	4	10595												0	3	D	19	8
70	3	5	10595	N17	W39	238	700	1.0										12	5
70	3	6	10595															4	2

MCMATH REGION 10614				CMP DATE		7.6 Mar		RETURN OF REGION 10567*				ROTATION		4					
				CALCIUM		PLAGE		DATA		SUNSPOT DATA				9.1 CM					
YR	MO	DA	MC NO.	LAT	CMD	L	AREA	INT	MW NO.	LAT	CMD	L	MAG.	H	AREA	CNT	C	INT	FLUX
70	3	1	10614	S10	E80	121	800	1.5							70	4	D	13	5
70	3	2													60	4	D		
70	3	3													100	4	D		
70	3														0	1	A		
70	3														10	1	A		
70	3														50	1	G		
70	3	4	10614												80	13	D	18	7
70	3														0	2	B		
70	3														10	4	C		
70	3														20	1	G		
70	3	5	10614	S10	E28	121	3700	3.5	17770	S12	E26	120	(BP)	4				13	5
70	3	6	10614	S10	E16	119	3200	3.5	17770	S12	E15	120	(BP)	4				8	3
70	3	7	10614	S10	W01	122	2800	3.0	17770	S12	W02	123	(BP)	3	40	20	C	6	2
70	3	8	10614	S10	W14	123	2400	3.0	17770	S12	W14	122	(BY)	3	50	18	D	9	4
70	3														0	1	A		
70	3	9	10614	S10	W28	124	2400	3.0	17770	S11	W26	121	(O)	4	40	18	D	6	2
70	3														30	7	D		
70	3	10	10614	S10	W40	123	2200	3.0										8	3
70	3	11	10614	S10	W53	123	1800	3.0	17770	S12	W54	122	(AF)	2				14	5
70	3	12	10614	S11	W66	122	1600	3.0										14	5
70	3	13	10614	S11	W80	123	800	2.0										9	3

The University College London-Leicester University 9.1-10.5Å x-ray maps from OSO-5 indicate activity in Region 10595 as it passes the west limb on March 6, 1970.

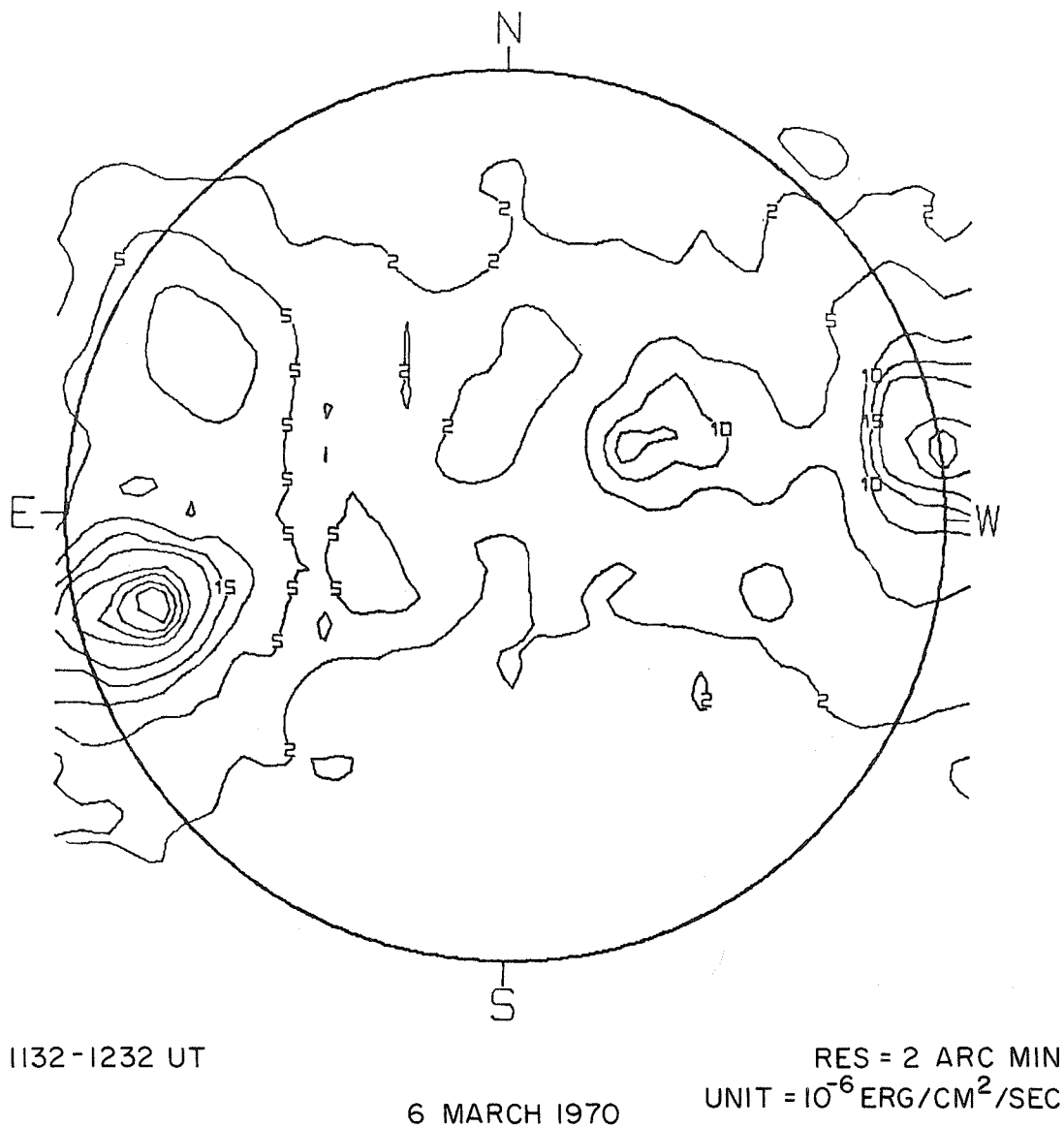


Fig. 1.

Table 2 and the histogram (Figure 2) present the final Rz sunspot numbers and 2800 MHz solar flux associated with the passage of these two regions February 20 - March 13, 1970.

Table 2

2800 MHz solar flux (S) and final Zurich sunspot numbers (Rz) for February 20 - March 13, 1970

	<u>Rz</u>	<u>S</u>		<u>Rz</u>	<u>S</u>		<u>Rz</u>	<u>S</u>		<u>Rz</u>	<u>S</u>
Feb. 20	125	201									
21	128	195	Feb. 26	143	182	Mar. 4	107	168	Mar. 10	125	160
22	132	187	27	150	180	5	107	173	11	103	158
23	164	188	28	146	178	6	103	170	12	88	166
24	166	190	Mar. 1	137	179	7	111	171	13	104	154
25	173	183	2	129	176	8	118	175			
			3	113	170	9	120	167			

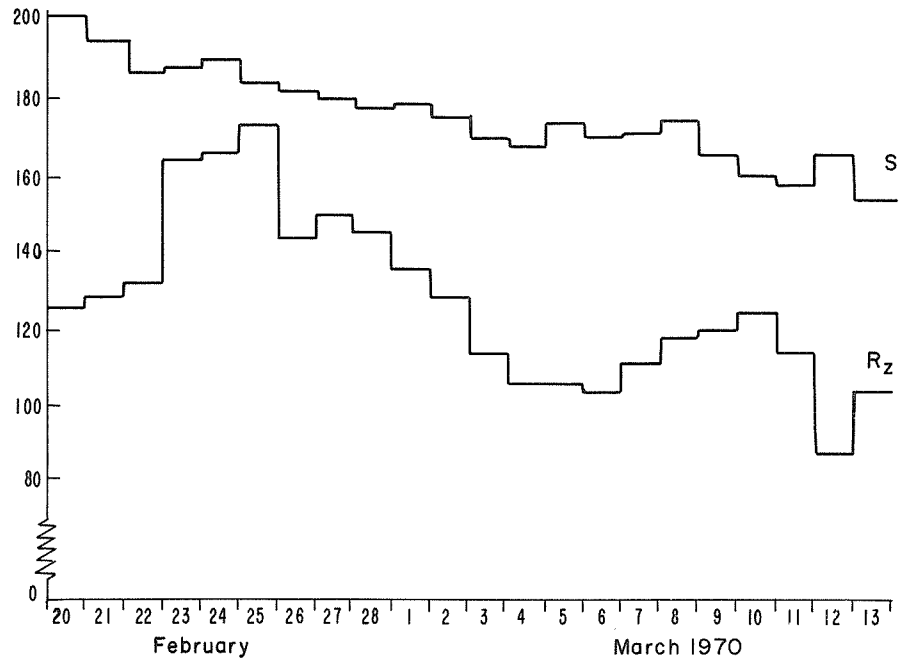


Fig. 2. Daily solar flux at 2800 MHz, S, and final relative sunspot numbers, Rz.
 The confirmed solar flares for March 6-8, 1970 are reprinted on the following pages.

SOLAR FLARES

Confirmed

MARCH 1970

OBSERVATORY	OBSERVED UT			MAX. PHASE	APPROX. LAT.	MER. DIST.	LOCATION			DURATION MIN.	IM-POR-TANCE	OBS. COND. TYPE	MEASUREMENTS				REMARKS
	DATE	START	END				CENTRAL DISTANCE	MCMATH PLAGE REGION	CMP DAY				MEAS AREA Sq. Deg.	CORR AREA Sq. Deg.	MAX WIDTH Ha	MAX INT %	
1970 MAR																	
GRP28512	05	0426	0522	0436	N15	W88	1.000	10595	26.6	56	1N		.70				4 2 2 5
CRON	05	0412	0428	0416	N14	W90	1.000	10595	26.4	16	-N	C	0416	.30	1.20		
MANI	05	0421E	0521D	0436	N15	W86	.999	10595	26.7	60D	1N 2		0436	.77	2.30		
CULG	05	0430	0522	0436	N16	W87	1.000	10595	26.7	52	1N	C	0436	.62			A
SIBE	05	0447	0458		N15	W90	1.001	10595	26.4	11	-F	V					H
4 STATIONS REPORTING GROUP 28516. 1 STATIONS OBSERVING AND NOT REPORTING.																	
GRP28516	05	1226	1304	1234	N05	W05	.229	10607	5.1	38	-E		1.73				4 4 4 5
CATA	05	1225	1310	1240	N05	W05	.229	10607	5.1	45	-N		1240	1.39	1.43		141
RAMY	05	1227	1306	1234	N05	W06	.236	10607	5.1	39	-B	C		1.29			FH
HERS	05	1228E	1250	1228E	N06	W03	.235	10607	5.3	22D	1N	P	1230	3.40	3.50		BE
MCMA	05	1242E	1308		N05	W06	.236	10607	5.1	26D	-E	C	1242	.83	.90		E
516 CATA	05	1235	1240	1235	N06	E02	.232	10607	5.7	5	*-N		1235	.23	.24		153
4 STATIONS REPORTING GROUP 28518. 1 STATIONS OBSERVING AND NOT REPORTING.																	
GRP28518	05	1455	1529	1505	S12	E29	.484	10614	7.8	34	-N		1.03				2 2 2 5
CATA	05	1455E	1510D	1505	S12	E29	.484	10614	7.8	15D	-B		1505	1.33	1.53		204
MCMA	05	1504E	1529		S11	E29	.483	10614	7.8	25D	-F	C	1504	.72	.80		E
28518	05	1436	1513	1450	S10	E29	.482	10614	7.8	37	*-F		.80				2 2 2 4
RAMY	05	1435	1510	1453	S10	E29	.482	10614	7.8	35	-N	C		.88			F
HTPR	05	1437	1515	1447	S10	E29	.482	10614	7.8	38	-F	C	1447	.72	.80		EU
GRP28521	05	1616	1645	1623	S16	E70	.933	10618	10.9	29	1B		1.21				3 3 2 3
MCMA	05	1615E	1640	1623	S16	E70	.933	10618	10.9	25D	1B	C	1623	1.29	3.70		EHV
RAMY	05	1616	1649	1623	S16	E71	.939	10618	11.0	33	1B	C					UH
HTPR	05	1618	1629D	1623	S15	E70	.933	10618	10.9	11D	1B	C	1623	1.13			H
522 MCMA	05	1822	1910	1826	N11	W90	1.000	10595	27.0	48	--F	C	1826				AK
523 MCMA	05	1825	1850		S15	E45	.704	10618	9.1	25	--F	C	1830	.72	1.00		E
GRP28524	05	1909	1937	1915	S15	E72	.944	10618	11.2	28	-N		.93				2 2 2 2
MCMA	05	1909	1936	1912	S16	E70	.933	10618	11.0	27	-N	C	1912	.62	1.80		E
RAMY	05	1911E	1938	1917	S14	E74	.955	10618	11.3	27D	1N	C		1.24			F
GRP28525	05	1919	1958	1931	S13	E26	.442	10614	7.8	39	--N		.78				2 2 2 2
RAMY	05	1917	1955	1929	S15	E23	.404	10614	7.5	38	-N	C		.93			F
MCMA	05	1921	2000	1932	S11	E28	.468	10614	7.9	39	-N	C	1932	.62	.70		E
GRP28526	05	1921	1932	1922	N12	W90	1.000	10595	27.1	11	--F						2 2 0 2
RAMY	05	1920	1929	1922	N13	W90	1.000	10595	27.1	9	-N	V					DE
MCMA	05	1922	1935		N11	W90	1.000	10595	27.1	13	-F	C	1925				
GRP28527	05	1940	1953	1942	N05	W09	.262	10607	5.1	13	--F		.49				2 2 2 2
RAMY	05	1939	1951	1942	N05	W10	.272	10607	5.1	12	-F	C		.46			DEH
MCMA	05	1940	1955	1942	N05	W07	.244	10607	5.3	15	-F	C	1942	.52	.50		E
528 RAMY	05	2042	2103	2044	S15	E73	.950	10618	11.3	21	--N	C		.21			DE
529 RAMY	05	2103	2108	2104	S07	E14	.240	10614	6.9	5	--F	C		.46			DE
	05	2158	2235	NO FLARE PATROL													
GRP28530	06	0015	0033	0018	N03	W17	.339	10607	4.7	18	-N		.99				3 3 3 5
MANI	06	0013	0048	0018	N04	W17	.348	10607	4.7	35	-N	2	0018	1.03	1.10		
MITK	06	0015	0028	0018	N04	W17	.348	10607	4.7	13	-N	C	0018	.93	1.00		E
VORO	06	0016	0022	0018	N02	W18	.345	10607	4.7	6	-B	C	0018	1.02	1.07		74
GRP28532	06	0545	0614	0553	S09	E65	.901	10618	11.1	29	1N		1.38				2 2 2 6
CULG	06	0543	0612	0553	S10	E64	.893	10618	11.0	29	1N	P	0553	1.65	3.20		
CRON	06	0546	0615	0552U	S08	E65	.902	10618	11.1	29	1N	C	0552	1.10	2.30		
6 STATIONS REPORTING GROUP 28534. 0 STATIONS OBSERVING AND NOT REPORTING.																	
GRP28534	06	0747	0821	0751	S14	E18	.324	10614	7.7	34	-N		2.33				4 4 4 5
CRON	06	0745	0825	0755	S14	E18	.324	10614	7.7	40	1N	C	0755	2.40	2.50		
BUCA	06	0745	0824	0748	S14	E16	.294	10614	7.5	39	-N	C	0748	1.99	2.10		
TACH	06	0748E	0810		S11	E19	.328	10614	7.8	22D	1F	V	0749	3.19	3.39		2.26
CATA	06	0750	0825	0750	S15	E17	.315	10614	7.6	35	-E		0750	1.73	1.84		48
28534	06	0755	0816	0808	S14	E19	.339	10614	7.8	21	*-N		1.78				263
HTPR	06	0747	0817	0806	S15	E18	.330	10614	7.7	30	1N	C	0806	2.37	2.40		3 3 3 8
MANI	06	0758E	0813D		S14	E19	.339	10614	7.8	15D	-F	1	0800	1.86	1.96		E
CATA	06	0800	0825	0810	S11	E20	.344	10614	7.8	25	-N		0810	.58	.62		199
CATA	06	0805	0815	0810	S17	E22	.400	10614	8.0	10	-B		0810	.52	.57		204
536 RAMY	06	1241	1300	1251	N04	W27	.488	10607	4.5	19	--F	C		.46			DEH

SOLAR FLARES

Confirmed

MARCH 1970

OBSERVATORY	OBSERVED UT			LOCATION				DURATION	IM-POR-TANCE	OBS. COND. TYPE	MEASUREMENTS				REMARKS		
	DATE	START	END	MAX. PHASE	APPROX. LAT.	APPROX. MER. DIST.	CENTRAL DISTANCE				MCMATH PLAGE REGION	CMP DAY	MIN	TIME UT		MEAS AREA Sq. Deg.	CORR AREA Sq. Deg.
1970 MAR																	
GRP28537	06	1321	1341	1326	S14	E60	.859	10618	11.1	20	1N					4 4 3 5	
RAMY	06	1318	1349	1326	S12	E59	.850	10618	11.0	31	1N	C				F	
NERA	06	1319E	1335D	1323	S15	E60	.859	10618	11.1	16D	2N	2					
HTPR	06	1321	1350	1327	S14	E62	.876	10618	11.2	29	1N	C	1327	1.55	3.00	E	
ZURI	06	1326	1329	1326	S14	E60	.859	10618	11.1	3	1N	C	1326	2.10	4.00		
GRP28538	06	1447	1510	1458	N03	W26	.468	10607	4.7	23	--F			.70		4 4 4 4	
RAMY	06	1445	1517	1452	N02	W27	.477	10607	4.6	32	-F	C		.72		DEH	
HTPR	06	1449	1508	1458	N03	W26	.468	10607	4.7	19	-F	C	1458	1.03	1.10		
CATA	06	1500E	1510D	1505	N03	W25	.454	10607	4.8	10D	-B		1505	.75	.85	282	
MCMA	06	1501E	1506		N03	W27	.482	10607	4.6	5D	-F	C	1503	.31	.40	EH	
GRP28539	06	1534	1544	1536	N08	W23	.462	10607	4.9	10	--F			.31		2 2 1 4	
RAMY	06	1533	1543	1536	N07	W23	.454	10607	4.9	10	-F	C		.31		DE	
BOUL	06	1534	1544	1536	N08	W22	.450	10607	5.0	10	-F	S					
GRP28540	06	1700	1717	1703	N03	W27	.482	10607	4.7	17	--F			.26		3 3 2 3	
RAMY	06	1658	1724	1703	N03	W27	.482	10607	4.7	26	-F	C		.31		DEH	
BOUL	06	1700	1709	1703	N03	W26	.468	10607	4.8	9	-N	V	1703		.50		
HTPR	06	1702	1703D		N04	W28	.502	10607	4.6	1D	-F	C	1703	.21	.20		
GRP28541	06	1723	1743	1726	S07	E12	.206	10614	7.6	20	-N			1.27		2 2 2 2	
RAMY	06	1723	1746	1726	S06	E12	.208	10614	7.6	23	-N	C		1.03		DE	
BOUL	06	1723	1737	1725	S08	E13	.223	10614	7.7	14	-N	C		1.50	1.50	E	
BOUL	06	1724	1740	1725	S07	E12	.206	10614	7.6	16	-N	V	1725		2.00		
542 BOUL	06	1749	1805	1752	S21	W67	.913	10621	1.7	16	-N	V	1752		.50		2
GRP28544	06	2057	2115	2100	S12	E37	.598	10618	9.6	18	--F			.52		2 2 1 2	
RAMY	06	2057	2114	2100	S12	E39	.625	10618	9.8	17	-F	C		.52		DE	
BOUL	06	2059E	2115	2059	S12	E35	.571	10618	9.5	16D	-N	V					
545 BOUL	06	2141	2200	2143	N07	W29	.534	10607	4.7	19	--F	V	2143		.80		1
546 BOUL	06	2217	2221	2219	N03	W29	.511	10607	4.8	4	--F	V	2219		.80		2
GRP28548	06	2348	0001	2349	S14	E25	.489	10618	9.2	13	--N			.78		3 3 2 5	
BOUL	06	2348	2352	2348	S15	E30	.506	10618	9.2	4	-N	S	2348		1.00		
MANI	06	2349E	0010	2350	S13	E29	.486	10618	9.2	21D	-B	1	2350	.72	.81		
MITK	06	2352E	0000		S15	E28	.477	10618	9.1	8D	-F	C	2352	.83	1.00	E	
GRP28549	07	0117	0132	0121	N07	W33	.586	10607	4.6	15	-N			1.02		2 2 2 4	
MANI	07	0115	0138	0121	N11	W33	.610	10607	4.6	23	-N	3	0121	1.13	1.44		
CRON	07	0118	0125	0121	N03	W33	.566	10607	4.6	7	-N	C	0121	.90	1.10	H	
GRP28550	07	0138	0331	0152	S12	E10	.190	10614	7.8	113	2B			8.37		6 4 4 6	
CULG	07	0131	0329	0153	S11	E09	.168	10614	7.7	118	3B	P	0153	13.41	13.00	HLSRU	
MANI	07	0140	0410	0148	S11	E09	.168	10614	7.7	150	2B	3	0148	5.98	6.03		
CRON	07	0141	0240	0150	S12	E11	.205	10614	7.9	59	1N	C	0150	5.00	5.00		
MITK	07	0141	0333D	0146	S13	E10	.198	10614	7.8	112D	2N	C	0146	9.08	9.20	FH	
KODA	07	0143E	0254	0202	S11	E08	.152	10614	7.7	71D	2B	C	0203	10.44	10.40	CIKU	
VORO	07	0244E	0330D		S11	E10	.183	10614	7.9	46D	1B	P	0246	3.88	3.90	2.00 81 EJ	
GRP28558	07	0630	0703	0641	S14	E55	.813	10618	11.4	33	--F			.87		4 4 3 7	
TEHR	07	0625	0650D		S12	E53	.792	10618	11.2	25D	1F						
HTPR	07	0632	0700	0636	S13	E55	.813	10618	11.4	28	-F	C	0636	.41	.70	E	
ABST	07	0634	0658	0646	S16	E55	.813	10618	11.4	24	-F	C	0646	1.07	1.80	D	
MANI	07	0636E	0712		S13	E57	.832	10618	11.6	36D	-N	1	0640	1.13	1.89		
GRP28563	07	0718	0752	0719	S20	W78	.972	10602	1.5	34	1N			.90		3 3 1 10	
TEHR	07	0655E	0810D		S15	W79	.977	10602	1.4	75D	1F						
ABST	07	0716	0730	0719	S21	W77	.967	10602	1.5	14	1N	C	0719	.90		D	
ISTA	07	0720	0755		S24	W78	.971	10602	1.5	35	-B						
GRP28564	07	0722	0735	0725	N04	W35	.598	10607	4.7	13	1N			1.83		7 7 5 9	
TEHR	07	0720E	0735D	0723	N04	W30	.530	10607	5.1	15D	1N						
CAPE	07	0721	0735	0724	N04	W37	.624	10607	4.5	14	-N	C	0724	1.41	1.80	H	
HTPR	07	0721	0733	0724	N04	W35	.598	10607	4.7	12	1B	C	0724	2.06	2.40		
ABST	07	0722	0736	0724	N04	W36	.611	10607	4.6	14	1N	C	0724	2.25	2.80	D	
MANI	07	0723E	0726D		N04	W35	.598	10607	4.7	3D	1F	1	0725	2.27	2.71		
CATA	07	0725	0735	0725	N03	W36	.607	10607	4.6	10	-B		0725	1.16	1.45	234 H	
ISTA	07	0725	0737	0727	N03	W35	.593	10607	4.7	12	1N						

SOLAR FLARES

Confirmed

MARCH 1970

OBSERVATORY	OBSERVED UT			LOCATION				DURATION	IMPOR-TANCE	OBS. COND. TYPE	MEASUREMENTS				REMARKS	
	DATE	START	END	MAX PHASE	APPROX. LAT.	CENTRAL DISTANCE	MCMATH PLAGE REGION				CMP DAY	TIME UT	MEAS. AREA Sq. Deg.	CORR. AREA Sq. Deg.		MAX WIDTH H ₀
1970 MAR																
GRP28565	07	0803	0815	0809	N07	W33	.586	10607	4.9	12	--F		.64			4 4 2 7
TEHR	07	0737E	0815D		N06	W32	.567	10607	4.9	38D	-F					
TEHR	07	0750E	0810D		N04	W30	.530	10607	5.1	20D	-F					
TEHR	07	0755E	0812D		N08	W31	.566	10607	5.0	17D	-F					
ISTA	07	0800	0804		N05	W30	.535	10607	5.1	4	-N					
HTPR	07	0805	0812	0808	N08	W35	.617	10607	4.7	7	-F	C	0808	.41	.50	E
CATA	07	0810	0830	0810	N07	W35	.612	10607	4.7	20	-N		0810	.87	1.09	199 Z
GRP28567	07	0840	0907	0843	S06	E04	.073	10614	7.7	27	-N		2.03			9 9 8 10
MONT	07	0837	0913	0842	S04	E04	.090	10614	7.7	36	1B	C	0842	2.58		
CAPE	07	0839	0900	0843	S06	E03	.056	10614	7.6	21	-F	C	0843	1.20	1.20	
ZURI	07	0839	0850D	0840	S06	E02	.041	10614	7.5	11D	1N	P	0840	3.16	3.20	
HTPR	07	0840	0904	0842	S06	E04	.073	10614	7.7	24	-E	C	0842	2.06	2.00	
CATA	07	0840	0920	0845	S06	E03	.056	10614	7.6	40	-B		0845	1.91	1.92	339
MANI	07	0840E	0906D		S06	E04	.073	10614	7.7	26D	-N	1	0845	1.44	1.44	
UCCL	07	0841	0904D	0841	S05	E02	.052	10614	7.5	23D	1N	P	0841	2.06	2.10	E
ISTA	07	0844	0903	0848	S09	E07	.124	10614	7.9	19	-N					
ABST	07	0845E	0905	0845	S06	E04	.073	10614	7.7	20D	-N	P	0845	1.79	1.80	E
GRP28572	07	1013	1030	1015	S19	W80	.979	10621	1.4	17	-N		.59			5 2 2 9
TEHR	07	0900E	1150D	0943	S15	W79	.977	10621	1.4	170D	1B					V
MONT	07	1012	1038	1017	S21	W77	.967	10621	1.6	26	-N	C	1017	.52		
UCCL	07	1012	1039	1014	S18	W80	.979	10621	1.4	27	1N	C	1014	.77		D
ZURI	07	1013	1016	1015	S22	W77	.967	10621	1.7	3	-N	C	1015	.57		
HTPR	07	1014	1021	1016	S20	W80	.979	10621	1.4	7	-N	C	1016	.41		
5 STATIONS REPORTING GROUP 28573.					3 STATIONS OBSERVING AND NOT REPORTING.											
GRP28573	07	1046	1150	1056	N09	W45	.740	10606	4.1	64	-F		1.20			3 3 3 7
MONT	07	1045	1102D	1055	N08	W44	.725	10606	4.1	17D	-N	C	1055	1.55		
CAPE	07	1045	1150	1100	N08	W43	.713	10606	4.2	65	-F	C	1100	1.02	1.50	
UCCL	07	1047	1110D	1054	N11	W47	.768	10606	3.9	23D	1F	P	1054	1.03	2.40	F
28573	07	1045	1210	1109	N07	W44	.721	10606	4.1	85	*-B		2.08			2 2 2 6
CATA	07	1045	1210	1110	N09	W44	.728	10606	4.1	85	1B		1110	2.61	3.83	234
RAMY	07	1107E	1130D	1107U	N05	W43	.702	10606	4.2	23D	-N	C		1.55		F
574 TEHR	07	1050E	1205D		N08	W35	.617	10607	4.8	75D	2N					V 6
7 STATIONS REPORTING GROUP 28576.					0 STATIONS OBSERVING AND NOT REPORTING.											
GRP28576	07	1122	1205	1128	S14	E48	.738	10618	11.1	43	1B		2.35			5 5 4 7
NERA	07	1118E	1135D	1125	S15	E47	.727	10618	11.0	17D	1B	2				
RAMY	07	1121	1217	1127	S11	E49	.749	10618	11.1	56	1B	C		2.48		F
HTPR	07	1122	1136		S13	E49	.749	10618	11.1	14	1B	C	1124	1.65	2.60	EH
CAPE	07	1123	1212	1130	S14	E48	.738	10618	11.1	49	1B	C	1130	2.03	3.00	
CATA	07	1125	1215	1130	S15	E49	.750	10618	11.2	50	1B		1130	3.25	4.85	372
28576	07	0000	1205	(1139)	S14	E49	.749	10618	10.7	725	*1N		.62			3 2 1 6
TEHR	07	1122E	1122D		S13	E50	.760	10618	11.2		1B					VE
ONDR	07	1133E	1159		S14	E48	.738	10618	11.1	26D	2N	V	1134		2.70	K
HTPR	07	1142E	1210		S13	E49	.749	10618	11.2	28D	-N	C	1143	.62	1.00	2.70 B
GRP28580	07	1601	1637	1609	S14	E45	.703	10618	11.0	36	1N		2.63			4 4 2 4
MCMA	07	1600	1650		S15	E45	.704	10618	11.0	50	1N	C	1608	1.55	2.20	E
RAMY	07	1601	1651	1608	S13	E46	.714	10618	11.1	50	1B	C		3.71		UF
BOUL	07	1601	1635	1610	S13	E42	.665	10618	10.8	34	2N	V	1610		6.50	
ONDR	07	1607E	1613		S15	E45	.704	10618	11.0	6D	2N	V	1611		2.40	
584 BOUL	07	1919	1930	1920	S17	W21	.386	10626	6.2	11	--F	V	1920	1.00		2
GRP28585	07	2017	2043	2020	N06	W54	.824	10606	3.8	26	--F		.52			2 1 1 2
RAMY	07	2017	2043	2020	N06	W54	.824	10606	3.8	26	-F	C		.52		DE
BOUL	07	2021	2050	2031	N10	W55	.843	10606	3.7	29	-F	V				
	07	2044	2057		NO FLARE PATROL											
GRP28586	07	2115	2139	2122	S21	W83	.987	10621	1.7	24	1N					2 1 0 3
BOUL	07	2115	2139	2122	S21	W83	.987	10621	1.7	24	1N	V	2122		4.00	
RAMY	07	2119	2143	2123	S23	W88	.997	10621	1.3	24	-N	C				DE
587 RAMY	07	2139	2156	2144	N06	W45	.729	10607	4.5	17	--F	C		.83		DE 2
GRP28589	08	0009	0124	0111	S21	W89	.998	10602	1.3	75	--F		.51			2 2 2 4
MANI	08	0009	0127	0111	S21	W88	.997	10602	1.4	78	-F	2	0111	.52	1.60	
CRON	08	0108	0121	0111	S21	W90	.999	10602	1.3	13	-N	C	0111	.50	2.00	IE

SOLAR FLARES

Confirmed

MARCH 1970

OBSERVATORY	OBSERVED UT			LOCATION				DURATION	IMPOR-TANCE	OBS COND. TYPE	MEASUREMENTS				REMARKS		
	DATE	START	END	MAX. PHASE	APPROX. LAT.	APPROX. MER. DIST.	CENTRAL DISTANCE				MCMATH PLAGE REGION	CMP DAY	MIN	TIME UT		MEAS. AREA Sq. Deg.	CORR. AREA Sq. Deg.
1970 MAR																	
GRP28594	08	0657	0708	0701	S12	W08	.160	10614	7.7	11	--N		.65				4 4 3 6
KODA	08	0656	0702	0700	S12	W09	.175	10614	7.6	6	-N	V	0658	.65	6.60	1.64	CD
MANI	08	0657	0712	0702	S11	W08	.152	10614	7.7	15	-N	3	0702	.41	.42		
ONDR	08	0659E	0707		S12	W08	.160	10614	7.7	8D	-N	V	0701			2.20	CD
ABST	08	0700E	0710	0701	S14	W08	.180	10614	7.7	10D	-N	P	0701	.90	.90		D
GRP28595	08	0714	0730	0718	N08	W46	.747	10607	4.9	16	1N			1.32			5 5 4 7
CULG	08	0712	0735	0717	N08	W44	.725	10607	5.0	23	1N	C	0717	1.75	2.55		
CRON	08	0715	0722	0717	N09	W46	.750	10607	4.9	7	-N	C	0717	.70	1.10		E
MANI	08	0716	0738	0719	N08	W45	.736	10607	4.9	22	-F	3	0719	1.03	1.50		
ABST	08	0717E	0725	0717	N09	W46	.750	10607	4.9	8D	1F	P	0717	1.79	2.70		D
ONDR	08	0718E	0732		N07	W47	.755	10607	4.8	14D	1N	V	0719			2.20	CE
GRP28598	08	1218	1243	1224	N08	W04	.272	10616	8.2	25	--F			.96			2 2 2 5
CATA	08	1215	1250	1223	N07	W03	.251	10616	8.3	35	-N		1223	1.39	1.43	195	
RAMY	08	1221	1236	1225	N08	W05	.276	10616	8.1	15	-F	V		.52			F
GRP28600	08	1330	1356	1341	S10	E16	.277	10618	9.8	26	-N			.97			4 3 3 4
ONDR	08	1327E	1356		S16	E30	.509	10618	10.8	29D	1N	V	1330			2.40	CK
RAMY	08	1329	1351	1341	S10	E16	.277	10618	9.8	22	-N	V		1.03			F
CATA	08	1330	1405	1340	S11	E16	.280	10618	9.8	35	-E		1340	1.27	1.33	278	
MCMA	08	1343E	1353D		S10	E16	.277	10618	9.8	10D	-N	P	1343	.62	.60		E
GRP28601	08	1335	1403	1348	N08	W51	.800	10607	4.7	28	--N			.46			4 4 3 4
RAMY	08	1334	1406	1350	N08	W53	.819	10607	4.6	32	-N	V		.52			DE
CATA	08	1335	1400	1350	N11	W51	.808	10607	4.7	25	-B		1350	.34	.59	246	
MCMA	08	1343E	1353D	1345	N07	W52	.807	10607	4.7	10D	-N	P	1345	.52	.90		E
ONDR	08	1349E	1402		N07	W47	.755	10607	5.1	13D	-F	V	1350			2.00	DH
GRP28604	08	1513	1524	1515	S12	W12	.221	10614	7.7	11	--B			.79			2 2 2 4
RAMY	08	1511	1523	1515	S12	W12	.221	10614	7.7	12	-N	V		.83			DE
CATA	08	1515	1525	1515	S12	W12	.221	10614	7.7	10	-B		1515	.75	.77	251	
GRP28605	08	1607	1649	1618	S16	E29	.495	10618	10.8	42	-N			1.13			2 1 1 3
RAMY	08	1607	1649	1618	S16	E29	.495	10618	10.8	42	-N	V		1.13			DE
MCMA	08	1630E	1639D		S16	E31	.523	10618	11.0	9D	-N	P	1630	.31	.40		E
	08	1817	1836		NO FLARE PATROL												
	08	1840	1853		NO FLARE PATROL												
	08	1854	1952		NO FLARE PATROL												
GRP28606	08	1933	2007 (1955)		S12	W15	.268	10614	7.7	34	-F			.62			2 2 1 2
BOUL	08	1933E	1952D		S11	W15	.263	10614	7.7	19D	1N	S					
MCMA	08	1952E	2007D		S13	W15	.273	10614	7.7	15D	-F	C	1955	.62	.60		E
607 MCMA	08	2002	2007D	2004	N08	W52	.809	10607	4.9	5D	--F	C	2004	.31	.50		D 1
	08	2007	2016		NO FLARE PATROL												
GRP28608	08	2244	2314	2259	S11	W17	.296	10614	7.7	30	-N			1.53			4 4 3 4
CULG	08	2234	0011	2302	S12	W17	.299	10614	7.7	97	1N	C	2302	2.58	2.62		
BOUL	08	2248E	2254D		S09	W17	.291	10614	7.7	6D	-N	S					
VORO	08	2249	2306	2256	S12	W16	.283	10614	7.8	17	-B	C	2256	1.29	1.33	98	EJ
MANI	08	2250E	2321D		S11	W17	.296	10614	7.7	31D	-N	1	2255	.72	.75		
GRP28613	09	0416	0508	0423	S13	E25	.427	10618	11.1	52	1F			2.24			3 3 3 5
MANI	09	0415	0513	0421	S12	E25	.424	10618	11.1	58	1F	2	0421	2.48	2.70		
CULG	09	0416	0510	0427	S13	E24	.412	10618	11.0	54	1F	C	0427	2.68	2.86		
MITK	09	0416	0500	0422	S14	E25	.430	10618	11.1	44	-N	C	0422	1.55	1.70		E
GRP28614	09	0535	0633	0541	S15	E25	.434	10618	11.1	58	-F			2.58			3 3 3 5
MITK	09	0534	0539		S15	E27	.463	10618	11.3	5	-F	C	0539	1.75	2.00		E
CULG	09	0535	0638	0539	S16	E24	.424	10618	11.0	63	1N	P	0539	4.64	4.95		RS
MANI	09	0537	0627	0543	S15	E25	.434	10618	11.1	50	-F	2	0543	1.34	1.40		
GRP28615	09	0802	0815	0805	S11	E15	.263	10618	10.5	13	--N			.46			3 3 3 5
MANI	09	0800	0818	0805	S11	E15	.263	10618	10.5	18	-F	2	0805	.62	.65		
HTPR	09	0802	0811	0805	S11	E15	.263	10618	10.5	9	-F	C	0805	.31	.30		
CATA	09	0805	0815	0805	S12	E15	.268	10618	10.5	10	-B		0805	.46	.48	234	
GRP28616	09	1104	1116	1110	S12	W22	.378	10614	7.8	12	--N			.67			3 3 3 6
HTPR	09	1103	1116	1113	S12	W22	.378	10614	7.8	13	-F	C	1113	.62	.60		
RAMY	09	1104	1118	1106	S12	W22	.378	10614	7.8	14	-F	C		.52			DE
CATA	09	1105	1115	1110	S13	W22	.381	10614	7.8	10	-B		1110	.87	.95	209	
618 MCMA	09	1700	1726	1708	S10	W29	.482	10614	7.5	26	--N	C	1708	.36	.40		E 3

2. SOLAR DISK AND LIMB PHENOMENA

"Synoptic Chart of Solar Magnetic Fields"

by

Robert Howard
Mount Wilson Observatory
Hale Observatories
Pasadena, California

This Synoptic Chart is constructed from the digital data of the daily magnetograms obtained at the 150-foot Tower Telescope at Mount Wilson. The spectrum line employed is λ 5250.2, Fe I. The magnetograph at the Tower Telescope measures only the longitudinal component of the Zeeman effect. The aperture is 17 arc seconds on a side, and the whole area of the sun is generally covered in one magnetogram with no overlapping.

The Synoptic Chart is made up of computerdrawn segments from individual day's observations. In order to get a standardized chart covering one half of a solar rotation, the chart has been redrawn. There is no averaging done at any point from more than one day's observation.

The solid horizontal lines represent the equator, $\pm 20^\circ$, $\pm 40^\circ$, and $\pm 60^\circ$ latitude. This is an equal-area projection, so that the line at the top of the chart represents the north pole, and the line at the bottom of the chart represents the south pole.

The Carrington longitudes are given at the bottom of the chart. The solid vertical lines represent each even 10 degrees in longitude.

Straight horizontal dashed lines represent the dividing line between regions where there is data and regions where there is no data due to incomplete observations.

Vertical dashed lines represent the dividing lines between observations from different days.

The longitude of central meridian at the time of observation is indicated by a short vertical line and date at the bottom, and by the caret at the top of the chart.

Solid magnetic contour lines represent positive fields (magnetic vector pointed toward the observer), and dashed contour lines represent negative fields. Exceptions to this rule are made when a contour line represents a lower rather than a higher value. Thus if there is a positive 10 gauss contour line that is solid surrounding a dashed contour line, the latter represents positive 10 gauss, and within it is less than positive 10 gauss. This rule applies only to contours which are not open at a boundary.

The gauss levels are ± 5 , ± 10 , ± 20 , ± 40 , ± 80 gauss. Corrections are made to compensate for limb darkening or any other decrease in the brightness of the signal, but no corrections are made for possible geometrical effects such as the inclination of the line of sight to the lines of force at high latitudes.

Positions are generally accurate to about 15 arc seconds. There is some smearing of the data at high latitudes because of the geometry of the situation. Data greater than 40° from central meridian should be treated with some caution. Serious inaccuracies of fit at the boundary between two day's observations are normally due to rapid growth of a region.

"The Solar Active Region Associated with Geophysical Events 6-8 March 1970"

by

Patrick S. McIntosh
NOAA Environmental Research Laboratories
Boulder, Colorado

The geophysical activity during the period 5-8 March 1970 can be associated with two separate active regions on the sun. The minor geomagnetic disturbance which commenced about 0805 UT on the 5th may be associated with the central meridian passage of McMath region 10607 at N06 and Carrington longitude 158 degrees. This region produced numerous X-ray flares during its eastern disk passage [Solar-Geophysical Data]. The polar cap absorption and satellite-detected protons beginning late on 6 March must surely be associated with an energetic flare event on west limb at 0926 UT that day. The event was described as an importance two limb surge, but its rapid motion may classify it better as a spray. It was located at N09 and it was associated with an X-ray burst of 2.8×10^{-2} ergs cm^{-2} sec^{-1} in the 1-8 Angstrom band, placing it in the M category on the scale devised by the NOAA Space Environment Services Center (formerly Space Disturbance Forecast Center of ESSA). The event was followed by importance one loop prominences, which continued until the occurrence of an importance three spray at 1838 UT (see Figure 1). The severe geomagnetic storm beginning on 8 March followed by 43 hours the west limb event at 06/0926 UT.

The source of the 6 March flare was McMath region 10595, located at N15 and nine degrees beyond the west limb at the time of the event. Figures 2 and 3 illustrate the abnormal evolution of this region prior to the west limb event.

The region formed on the disk on 1 February in the trailing portion of an old and distended region, McMath plage 10547. The new region was designated region 10561. It reached maximum sunspot area on 2 February as a small type-D group of 150 millionths hemispheric area. Its location was N18 and Carrington longitude 236.

The return of region 10561 on 21 February as region 10595 brought a bright calcium plage (3.0 to 3.5) with area of about 4000 millionths of the hemisphere. The calcium plage area and brightness remained nearly constant throughout the disk passage, although the H-alpha plage appeared to fade in overall brightness as the region approached west limb (Figure 3).

The sunspot group on 21 February was small and growing, as if new magnetic fields had emerged through the old region only a day or two prior to east limb appearance. The spots developed into a type-E group of about 400 millionths area by 24 February. The total spot area declined during the remainder of the disk passage, but on every day some new spots appeared so that the area decline was irregular and the group configuration changed radically during the western disk passage.

Two principal growth phases were evident. The first was the overall region growth to maximum area from 21 through 24 February. The second phase began on 27 February with the appearance of bright H-alpha plage and small spots south of the strong spot near the center of the region (last frame of Figure 2). Simultaneously, north polarity spots came into contact with the large leader spot of south polarity, and the joining of the spots apparently led to their rapid decay over the next four days. During the same four days the central spot became darker and new spots and plage encircled it. On 2 March spots of south polarity were detected on the edge of penumbra which also enveloped two, strong north-polarity spots, thus creating a delta-configuration with the line of polarity change oriented nearly east-west. This magnetic configuration is highly correlated with proton flares [Warwick, 1966].

Foreshortening interfered with observations of sunspot evolution after 2 March. The increase in H-alpha plage brightness south of the strong spots on 3 and 4 March indicates that the south-polarity magnetic fields may have continued growth until the last observations on 4 March. This growth would have enhanced the magnetic field gradients across the longitudinal neutral line in the delta configuration, and we might infer that the conditions for a proton flare were improving during west limb passage of region 10595.

The occurrence of the significant flare activity in region 10595 is plotted on time-lines in Figure 4. Preference was given to events associated with X-ray bursts exceeding 10^{-2} ergs cm^{-2} sec^{-1} in the 1-8 Angstrom band. Other events were included if they were at least importance one on the disk or at least importance two on the limb. Two periods of high activity are evident, corresponding well with the two phases of sunspot growth described above. Large surges at east limb and several small X-ray events were associated with the general growth of the region until 24 February. A sudden increase in strong X-ray events, including a large X-event, accompanied the growth of new magnetic fields in the center of the region. Enhanced activity continued until well after west limb passage, presumably due to the gradual complication of magnetic fields near the central spot. The lack of X-ray events near central meridian may be due in part to center-limb variations in X-ray emission, with a tendency toward limb brightening.

LOOPS FOLLOWED BY GREAT SPRAY N15 W90+
6 MARCH 1970

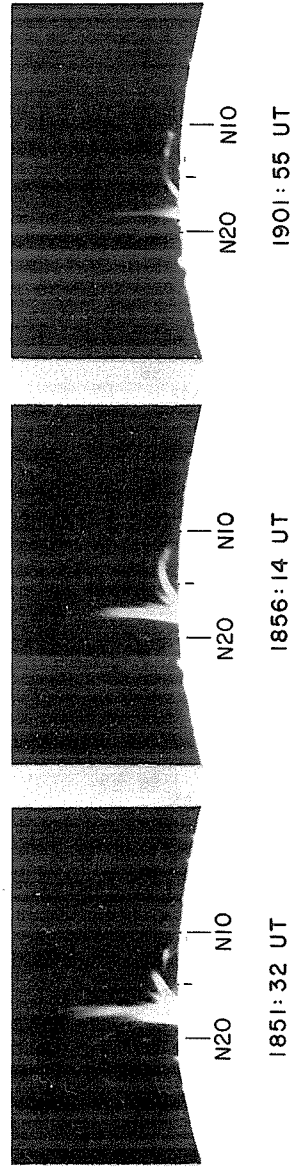
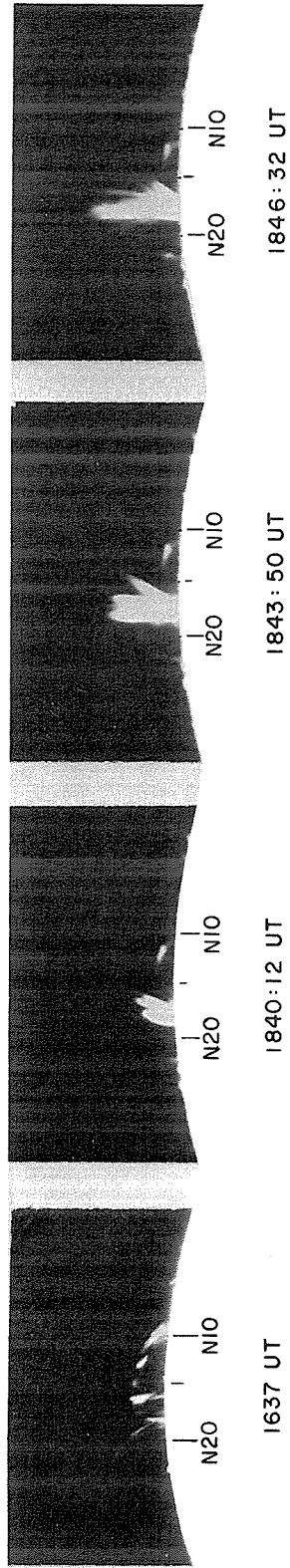


Fig. 1. Loops and a large spray from McMath region 10595 followed the energetic event at 0926 UT on 6 March 1970. Overexposures with a 35 mm eyepiece camera enabled Joe Sutorik to obtain this sequence without interrupting the SPAN flare patrol in Boulder.

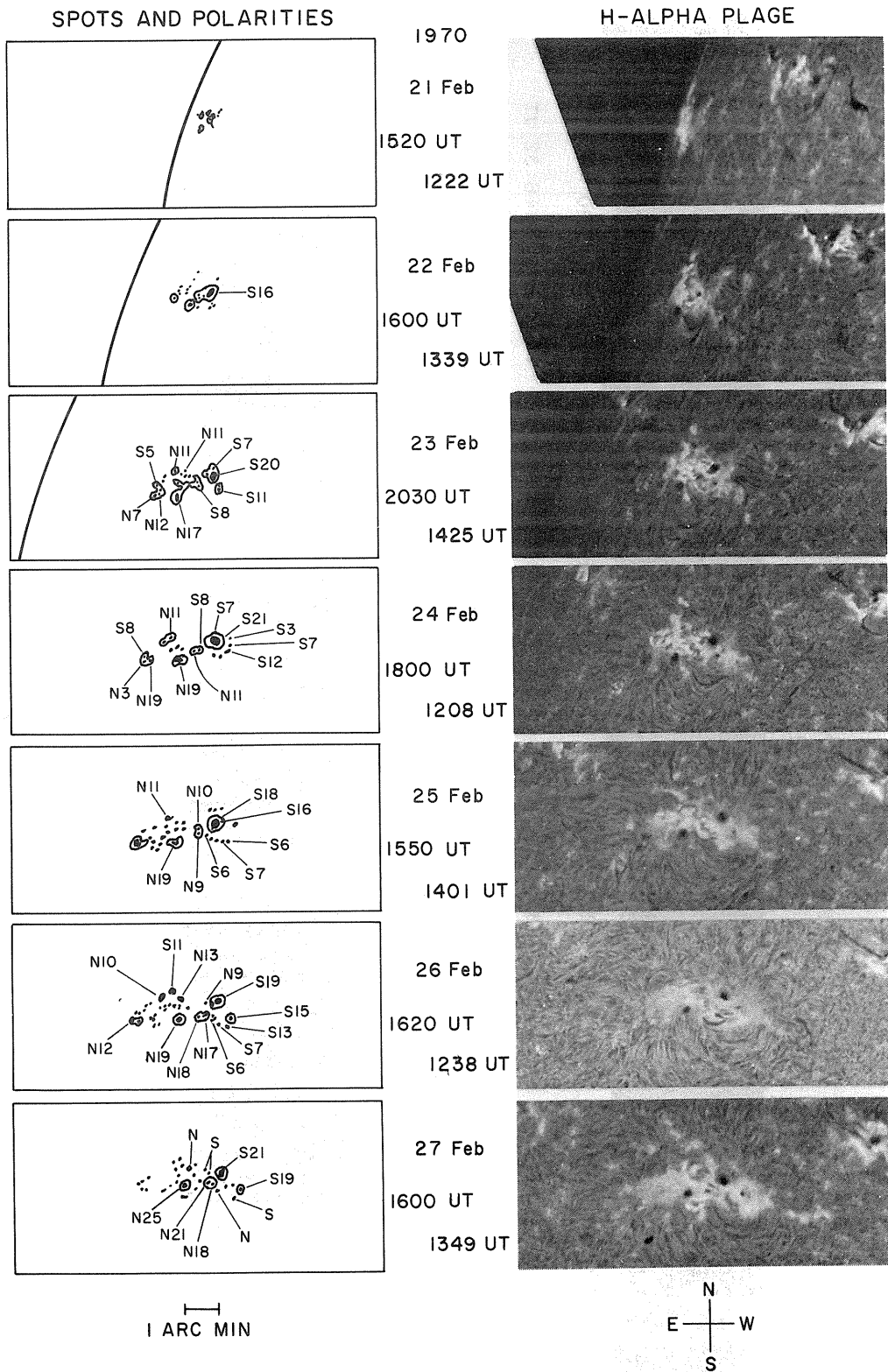


Fig. 2. Eastern disk passage of McMath region 10595. Sunspot drawings from the NOAA/NASA SPAN Observatory in Boulder. Spot polarities from Crimean Astrophysical and Mt. Wilson Observatories. H-alpha patrol photographs from Ramey Air Force Base, Puerto Rico.

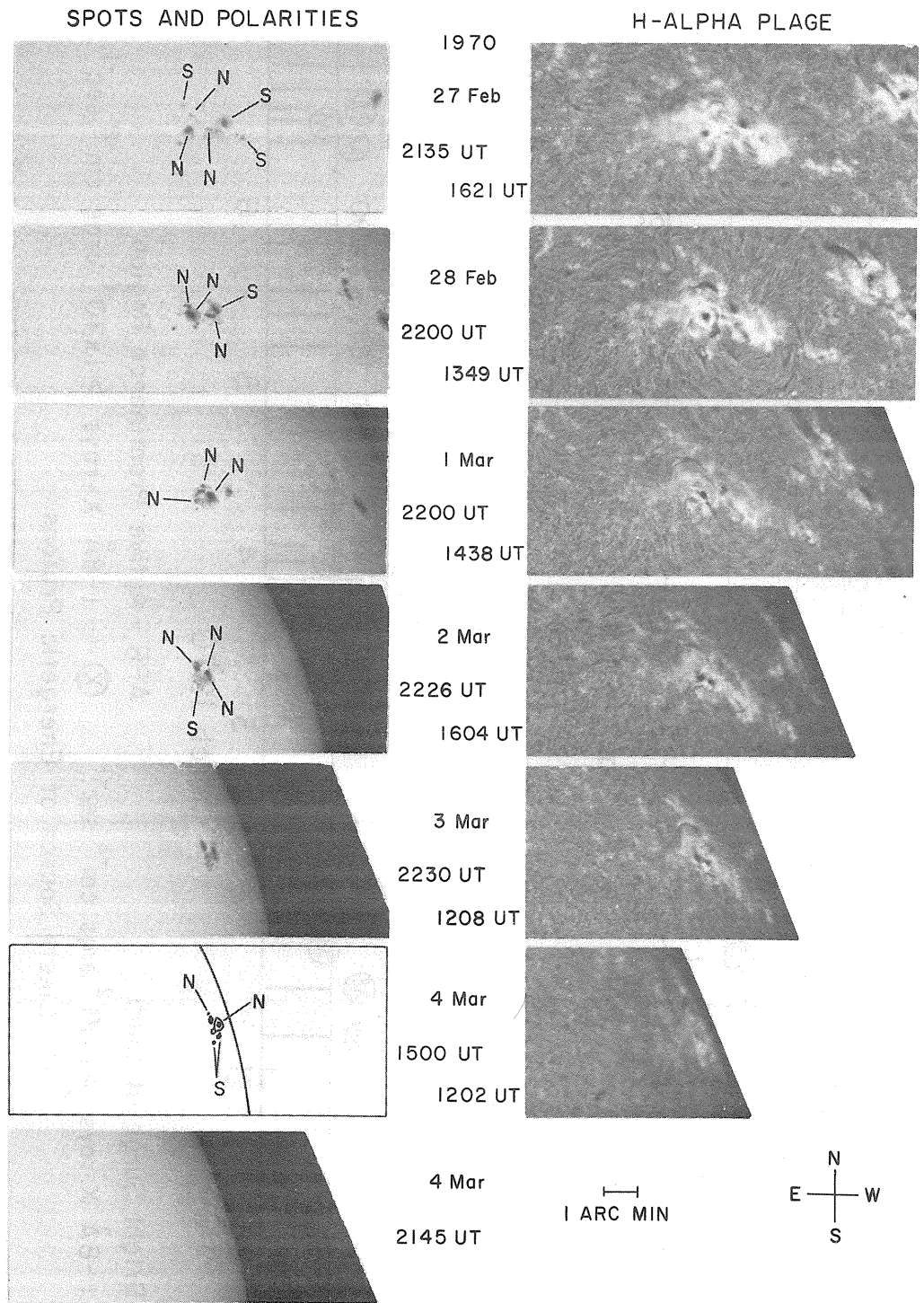
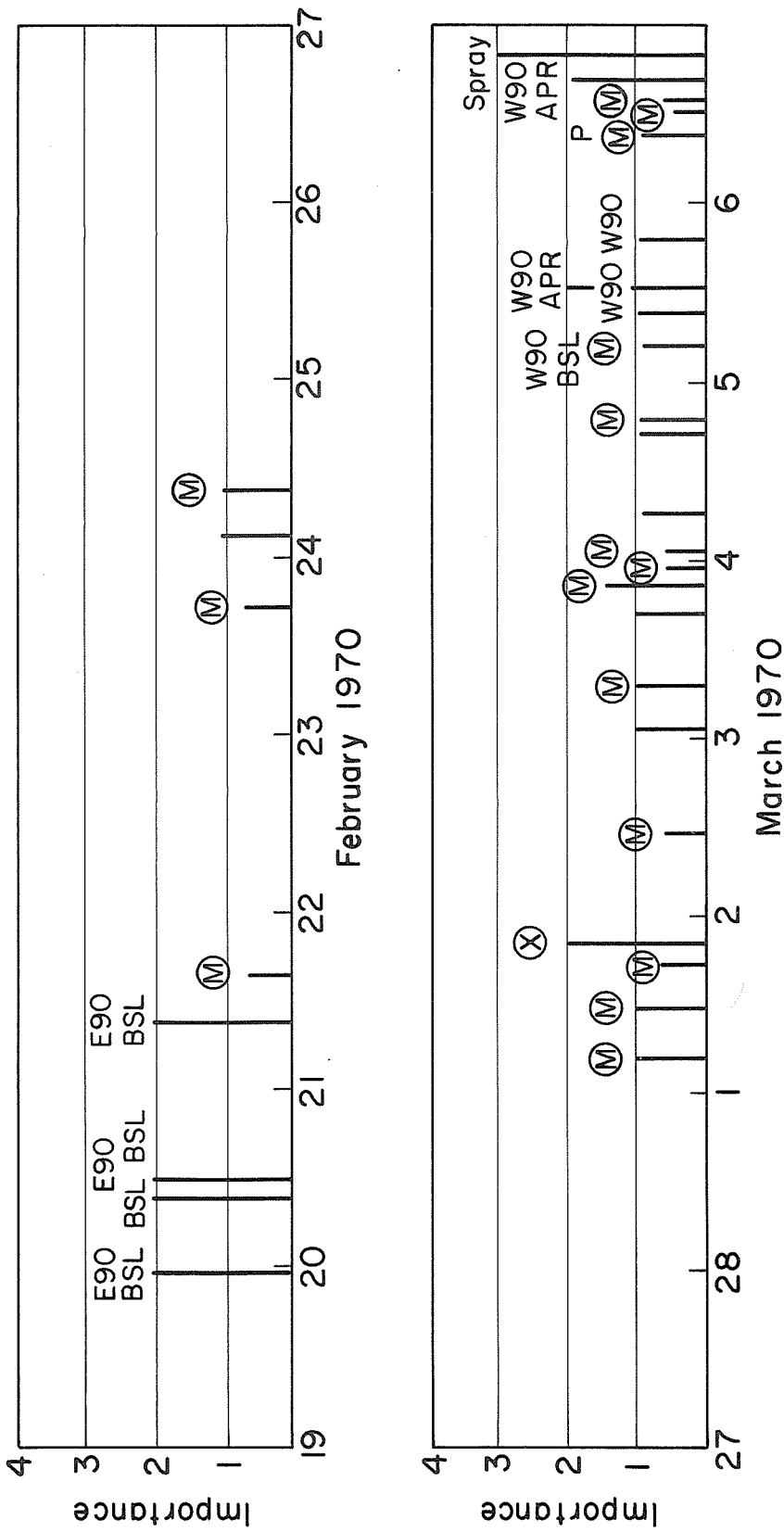


Fig. 3. Western disk passage of McMath region 10595. White-light photographs from Culgoora Solar Observatory, C.S.I.R.O., Australia. Polarities from Crimean Astrophysical Observatory. H-alpha patrol photographs from NOAA/NASA SPAN Observatory in Boulder (27 Feb.) and Ramey Air Force Base, Puerto Rico.

FLARE EVENTS IN McMATH REGION 10595



The choice of region 10595 as the source of the energetic particle effects on 6-8 March is strengthened by the occurrence of a proton flare from this region on its subsequent disk passage. A portion of McMath region 10641 represented the third rotation for the region. The early part of the disk passage brought another phase of redevelopment, with a maximum sunspot area of over 500 millionths of the hemisphere in a type-D group. Class X flares occurred at 1203 UT on 25 March and 0011 UT on 29 March. The latter was followed by satellite-detected protons and a small polar cap absorption event [Solar-Geophysical Data]. Weak plage with no sunspots returned in April.

The outstanding feature of the solar active region with McMath numbers 10561-10595-10641 was the repeated emergence of strong new magnetic fields at nearly identical heliographic coordinates during a period of two months. The interaction of each new field with older fields was accompanied by increases in energetic flares. The birth of new spots near older spots was seen to be related to proton flares in other regions [McIntosh, 1969a, 1969b, 1970].

REFERENCES

- | | | |
|-----------------|-------|---|
| MCINTOSH, P. S. | 1969a | Birth and development of the sunspot group associated with the proton flare of July 1966, <u>Annals of the IQSY</u> , <u>3</u> , 40-43 |
| MCINTOSH, P. S. | 1969b | Sunspots associated with the proton flare of 23 May 1967, <u>World Data Center A, Upper Atmosphere Geophysics Report UAG-5</u> , 14-19, February 1969 |
| MCINTOSH, P. S. | 1970 | Sunspots associated with the proton flares of late October 1968, <u>World Data Center A, Upper Atmosphere Geophysics Report UAG-8</u> , 22-29, March 1970 |
| | 1970 | <u>Solar-Geophysical Data</u> , U. S. Department of Commerce, (Boulder, Colorado, U.S.A., 80302). |
| WARWICK, C. S. | 1966 | Sunspot configurations and proton flares, <u>Astrophys. J.</u> , <u>145</u> , 215-223. |

"Geoactive Phenomena Beyond the Western Limb on March 6, 1970"

by

L. Krivsky
Astronomical Institute of the Czechosl. Acad. Sci.
Ondrejov near Prague

and

S. Pinter
Geophysical Institute of the Slovak Acad. Sci.
Hurbanovo

An H-J type active region (position \sim N15), which had displayed increased activity with flare occurrences (McMath No. 10595) on the disk in the preceding days, set on March 3, 1970. Great flares, the upper parts of which were at a minimum height of 20,000 - 25,000 km above the photosphere and represented sources of exceptionally intense x-ray emissions, occurred in this region when it was about 13° beyond the W-limb on March 6, 1970. The first great phenomenon occurred after 0926 UT. A second great phenomenon, originating beyond the limb of the disk after 1200 UT, the central and upper parts of which emerged at about 1300 UT, represents a typical case of a perfectly developed proton flare of the ascending magnetic channel type in the shape of a loop channel as can be seen from the photographs of this phenomenon [Krivsky 1968, 1969a,b, 1970]. This flare was also the source of sub-cosmic particles which caused a minor PCA effect beginning at 1410 UT on the same day, and one and a half hours later 20 - 70 MeV particles were detected by the geostationary ATS-1 satellite.

The purpose of this report is to compare direct x-ray emission measurements made by the SOLRAD 9 satellite with the SEA effects on 27 and 35 kHz. As regards the former phenomenon from beyond the limb it was possible to determine the variation of the electron temperature of the source and the approximate vertical dimension of the flare nodes which ascended rapidly above the disk limb and radiated in the x-ray emission.

Characteristics of x-ray emissions and SEA effects

If the variation of the x-ray emission on the three channels observed is compared with the variation of the SEA effects on 35 kHz (Figure 1) very good agreement can be seen in particular as regards channels 0 - 3 Å and 1 - 8 Å, including secondary increases; as regards SEA there is, of course, a time delay of several minutes as a result of the reaction time of the ionosphere. Unfortunately, there are gaps in the satellite x-ray emission records corresponding to the time of passage through the Earth's shadow; then the better record is that of the variation provided by SEA effects where there are no interruptions.

Firstly, the characteristic variations of the x-ray emission and of the SEA effects are quite analogous: the first effect after 0930 UT is a typical flare effect with a sudden increase and a gradual decrease. This effect and its emission are probably affected by the emission from a very weak flare of important SF after 1049 UT, but only towards the end. The second, less typical SEA effect due to the increase of the x-ray emission after 1200 UT was caused by a series of active phenomena located beyond the W-limb of the disk, as well as by phenomena on the disk. All the data pertinent to the commencements of the observed phenomena are in Figure 1, denoted by arrows on the SEA record. As a result of the complicated multiple events after 1200 UT the electron temperatures were not calculated.

Secondly, provided x-ray emission satellite measurements are available outside the shadow it is also possible to observe the response of the secondary increases, e.g. around 1330 or 1500 UT, on the SEA 35 kHz records. This again substantiates the previous results concerning the importance of SEA effect recordings on some frequencies for obtaining an idea of the variation of the original x-ray emission. A suitable choice of atmospheric frequencies may provide a rough idea of the anomalous x-ray emission in some different intervals [Krivsky and Nestorov 1968]. An SEA record on 27 kHz (Ondrejov, Czechoslovakia) was also available for analysis; with the exception of certain detailed features it displayed a variation similar to that of the 35 kHz record from the observatory of Vsetin (Czechoslovakia). The comparison of both frequencies affected by the slightly different x-ray emission ranges will be the subject of a future paper.

Table 1 gives a comparison of some of the characteristic of the observed x-ray emission with the characteristics of SEA effects on 35 and 27 kHz. The time data and the comparison of the maxima of the emissions and of the SEA effects are sufficiently representative and also important for certain calculations concerning the reaction time of the lower ionosphere.

The first observed x-ray emission burst in the 1-8 Å range reached an intensity of $0.05 \text{ erg cm}^{-2} \text{ s}^{-1}$, and in the 8 - 20 Å range an intensity of $0.12 \text{ erg cm}^{-2} \text{ s}^{-1}$.

Table 1

First burst of the x-ray emission and SEA					
\AA	Start UT	Max. UT	End UT	Duration of event min	Duration of the phase of increase min
0 - 3	(0931)	(>0938)	?	?	(>7)
1 - 8	0930	0940	1136	126	10
8 - 20	0931	0943	1148	137	12
SEA 35 kHz	0937	0944	(1143)	126	7
	t (1-8,SEA) 7 min	t (1-8,SEA) 4 min	t (1-8,SEA) 7 min	t (1-8,SEA) 0	t (1-8,SEA) -3 min
	t (8-20,SEA) 6 min	t (8-20,SEA) 1 min	t (8-20,SEA) -5 min	t (8-20,SEA) -11 min	t (8-20,SEA) -5 min
SEA 27 kHz	0935	0942	(1113-1143)	(128)	7
	t (1-8,SEA) 5 min	t (1-8,SEA) 2 min	t (1-8,SEA) (7) min	t (1-8,SEA) (2) min	t (1-8,SEA) -3 min
	t (8-20,SEA) 4 min	t (8-20,SEA) -1 min	t (8-20,SEA) -5 min	t (8-20,SEA) -11 min	t (8-20,SEA) -5 min

The Height and the Vertical Dimension of the Source Emitting the X-ray Emission (first phenomenon 0926 UT)

It is known that this x-ray emission burst was not caused by a phenomenon on the disk but by a phenomenon based beyond the limb at a distance of about 13° . The nature of the phenomenon cannot be critically assessed because photographs in H α were not available. This phenomenon was classified at the time by the now NOAA Space Environment Services Center as BSL, imp. 2, N09 at its beginning. It later was transformed into loops, imp. 1, N15 lasting for about five hours. The x-ray emission was radiated towards the Earth only when the radiating "sources" reached a minimum height of about 20,000 km above the photosphere. The existence of an x-ray emission due to these phenomena from beyond the limb at these heights has already been described before [Kleczek and Krivsky 1960, Krivsky and Nestorov 1969].

Let it be assumed that the ascending nodes of the phenomenon, which were the source of the x-ray emission, emitted the emission prior to appearing over the disk limb; also assume that the rate of ascent could have amounted to about 30 km/s in the first instance, and to about 100 km/s in the second instance, and also that the emission did not vary too much in the course of the emergence of the "nucleus". It is known that in the harder interval of 1 - 8 \AA the increasing phase lasted for 10 min, and in the softer of 8 - 20 \AA for 12 min. One can also consider the fact that exposure of the source of the x-ray emission when the emitting sources are ascending lasts over an interval from the onset of the x-ray emission to its maximum (to the full exposure of the "nucleus"). As regards the 1 - 8 \AA channel the following vertical dimensions of the "nucleus" are obtained for the two alternatives of the rate of ascent considered: 1) 18,000 km and 2) 60,000 km; for the 8 - 20 \AA channel: 1) 22,000 km and 2) 72,000 km. Should the actual rates of ascent of the bright nodes of the phenomenon above the disk limb be available these data could be made more accurate. It is also necessary to point out that the dimensions of the "nucleus" with the first alternative of the rate of ascent roughly correspond to the height of the brightly radiating nodes in H α at the peaks of loops of proton flares [Krivsky 1969 b].

Electron Temperatures and Source Energy (First Event)

Since measurements of the intensity of the x-ray emission burst are available for two frequency ranges, 0.5 - 3 and 1 - 8 \AA , the electron temperature, T_e , can be computed according to Bogen [1968]. The computed temperature is shown in the bottom half of Figure 1. One can see that the temperature increased sharply at the time of the increase in the 1 - 8 \AA intensity, and that the temperature decreased quite rapidly at the time of the decline of the x-ray emission intensity. The maximum electron temperature T_e amounted to 5.8×10^7 $^\circ\text{K}$. It appears that the temperature determined in this manner should characterize the temperature of the small "nucleus" itself.

As regards the comprehensive study of the phenomenon it is very important to have data on the overall radiated energy for various x-ray emission ranges. The energy was computed by means of the time integral of the radiation intensity curve. The computed energies are given in the following table; it can be seen that the total energy radiated decreases with decreasing wavelength.

SOLRAD 9 X-RAY

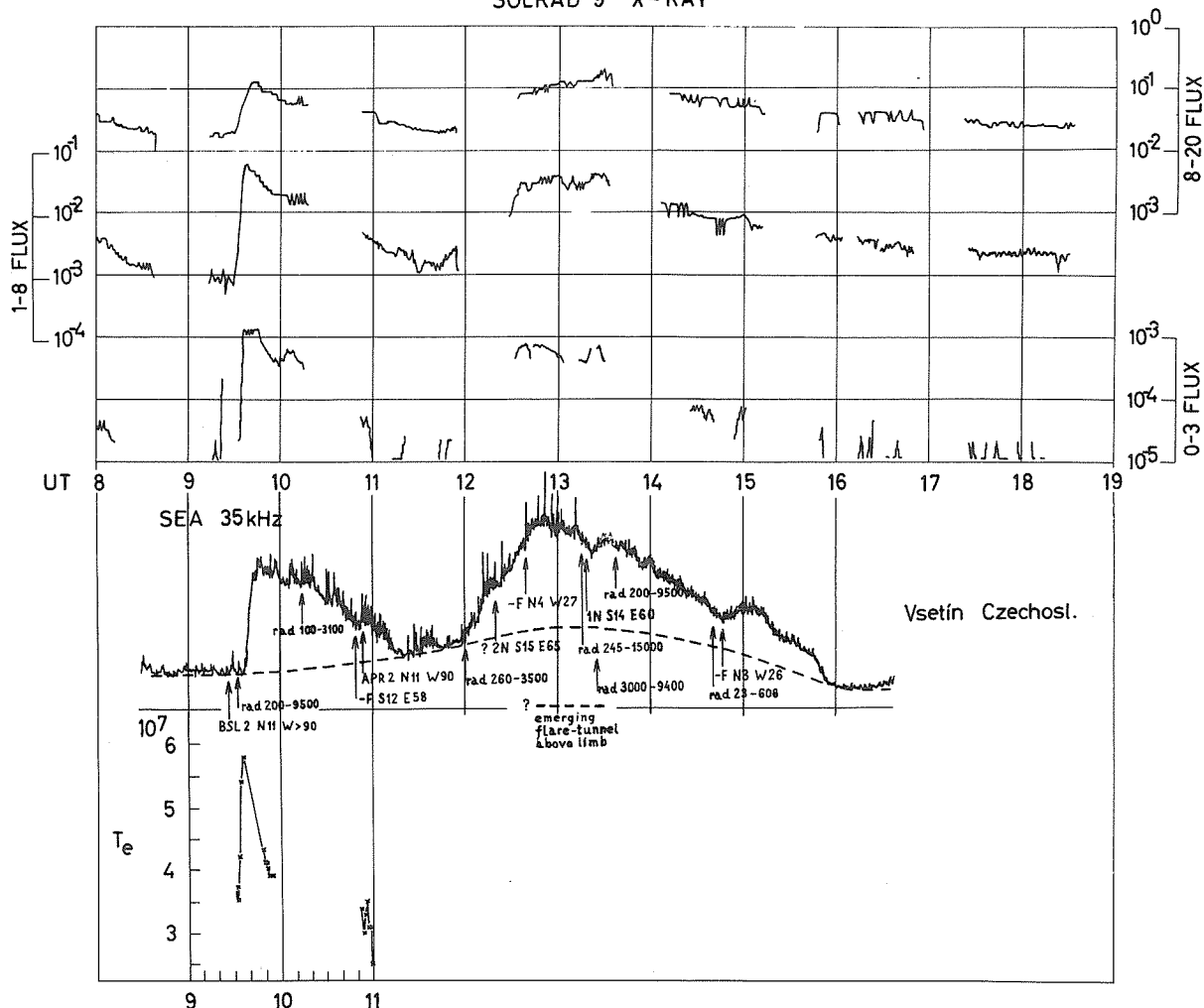


Fig. 1. The upper three records represent the x-ray emission on three channels of the SOLRAD 9 satellite. The middle record is a copy of SEA effect recording (sudden enhancement of atmospheric) on 35 kHz, the bottom boundary line is the zero level, the dashed line is the fitted normal level corresponding to days with no effect. The arrows on this record indicate the beginnings of all confirmed and unconfirmed flares together with their positions, the adopted data are also given concerning the character of the active events beyond the W-limb, and the interval in which the flare-loops channel probably emerged on the disk is also marked at the lower boundary. Arrows indicate the beginnings of radio bursts giving the observed frequency range. The bottom curve represents the computed electron temperature, T_e , of the "nucleus" emitting the x-ray emission according to Bogen's formula [1968].

	Passbands	Energy erg	Satellite
soft	8 - 20 Å	5×10^{29}	} Explorer 37
soft	1 - 8 Å	5×10^{28}	
hard	0-5 - 3 Å	6×10^{26}	

Using a large amount of statistical data the total energy radiated in the said energy ranges was determined in dependence on the importance of the flare [Pinter 1970]. By comparing the energy from the flare from beyond the limb on March 3, 1970 with the values of the energy computed for the various flares, it is possible to conclude that the flare was of importance 2B or 2F.

Proton Flare Beyond the Limb (Second Event)

Using the photographs of the flare beyond the limb, furnished by the NOAA Space Environment Services Center, Boulder, Colorado, it was possible to determine the trend in the rate of ascent of the upper nodes in the interval 1406 - 1539 UT as about 4.5 km/s, which is the usual trend of the rate for the second slower phase of ascent of the peaks of the nodes on the loops in proton flares [Krivsky 1969 a,b]. By extrapolating the second trend into the past (since the authors did not have photographs made prior to 1406 UT) and considering the approximate onset of the first trend to be about 20 km/s, one arrives at the conclusion that the peaks of the loop-tunnel flare with their base beyond the limb by 14° emerged approximately at 1300 UT \pm 20 min. This could agree with the radio emission in the 245 - 15,000 MHz range which began at 1317 UT and with another emission at 1325 and 1339 UT [Solar-Geophysical Data, U.S. Department of Commerce (Boulder, Colorado U.S.A. 80302)]. See Figure 1.

With a view to the character of this event one may judge that this flare was the main source of the ejection of particles of sub-cosmic radiation which caused the PCA effect on the same day. Moreover, it may be said that the particles which were responsible for this effect and the increase in the particle flux at the satellites were generated in the first instance in the regions of the peak nodes on the loop tunnel [Krivsky 1968, 1970], whereas the particles with much higher energies were generated in the bottom parts of this formation unobservable from the Earth, and this was probably the reason why they did not arrive at the region near the Earth.

The authors would like to thank Mr. D. Horan of the NRL Research Laboratory, Washington, for providing them with the measurements of the x-ray emission from the Explorer 37 satellite prior to their publication. The authors would also like to extend their thanks for cooperation to Mr. T. Skandera and Mr. Z. Kamarad of the observatory in Vsetin.

REFERENCES

- | | | |
|--------------------------------|--------|--|
| BOGEN, P. | 1968 | <u>Plasma Diagnostics</u> , ed. W. Locte-Holtgreven, North-Holland Amsterdam, 424. |
| KLECZEK, J. and
L. KRIVSKY | 1960 | <u>Nature</u> , <u>186</u> , 1035. |
| KRIVSKY, L. | 1968 | <u>IAU Symp. No. 35 (Budapest 1967)</u> , ed. K. O. Kiepenheuer, Dordrecht-Holland, 465. |
| KRIVSKY, L. | 1969 a | Development and spatial structure of proton flares near the limb and coronal phenomena I. Flare on 5 IV 1960, <u>Bull. Astr. Inst. Czech.</u> , <u>20</u> , 139. |
| KRIVSKY, L. | 1969 b | Development and spatial structure of proton flares near the limb and coronal phenomena II. Flare of 26 IX 1963 and its emission, <u>Bull. Astr. Inst. Czech.</u> , <u>20</u> , 163. |
| KRIVSKY, L. | 1970 | Development and spatial structure of proton flares near the limb and coronal phenomena III. Cosmic rays flare on Nov. 18, 1968, <u>Bull. Astr. Inst. Czech.</u> , <u>21</u> , 67. |
| KRIVSKY, L. and
G. NESTOROV | 1968 | Development of proton region with flares and ionospheric effects (26.7 to 5.9. 1966), <u>Bull. Astr. Inst. Czech.</u> , <u>19</u> , 197. |
| KRIVSKY, L. and
G. NESTOROV | 1969 | Ionospheric effects of x-ray emission from an active region with a proton flare (30 June - 11 July 1966), <u>Annals of the IQSY</u> , Vol. 3, The Proton Flare Project, M.I.T., 137. |
| PINTER, S. | 1970 | Unpublished. |

"Green Corona in Connection with the Possible Proton Event March 6, 1970"

by

M. Rybanský and J. Sýkora
Astronomical Institute of the Slovak Academy of Sciences
Skalnate Pleso, Czechoslovakia

Our short note is written with the assumption that McMath region 10595 was the source of the possible proton event of March 6, 1970 which caused remarkable manifestations in the whole spectrum and which was accompanied by extraordinary geophysical effects. This is chiefly suggested by low energy solar cosmic ray measurements carried out by spacecrafts Pioneers 6 and 8. At the time the possible proton flare occurred, the region 10595 was already behind the solar limb. From the fact that disturbances occurred in the Earth's atmosphere and from the known positions of Pioneers 6 and 8 it is clear that a sector of the interplanetary medium more than 180 degrees in extent was affected.

The position of region 10595 (N15, L = 238°) in the period March 4 - 7, 1970 was very suitable for coronal observations. The region was crossing the sun's west limb. Unfortunately, during this period there were no observations at any corona station, except for a March 4 observation of Kislovodsk, evidently owing to bad weather. In consequence of the generally small number of observations in the winter period it was not even possible to construct synoptic coronal charts separately for the east and west limb passages of the given region. Therefore, we approached a certain compromise. Coronal activity, brightness of the green corona emission line - 5303 Å, was calculated for the central meridian as an average of values when the proper meridian passed the east and west limbs. When the observation from only one limb existed, as in most cases, this observation was considered as belonging to the central meridian.

Measurements of the different stations (Pic du Midi, Kislovodsk, Lomnický Stit, Norikura) were transformed to a common Pic du Midi photometric scale by the method designed by Gnevyshev [1963]. Systematic errors between different corona station data were eliminated using results of Sýkora [1971].

In Figure 1 five synoptic charts of the five successive passages of the studied region through the central meridian are demonstrated (Carrington rotations No. 1556-60). It can be clearly seen that in rotation No. 1558, which is associated with the critical period of March 6th, there is a remarkably enhanced green corona intensity just at the location of the 10595 region, N15, L = 238°. The intensity reaches 175 so-called absolute coronal units. This is an intensity about 3-4 times higher than one could expect in this part of the solar cycle and in heliographic latitude N15. There is a justifiable assumption that at the time when the possible proton event occurred the corona intensity was even significantly higher. High corona intensity occurred during all five rotations in the neighborhood of this heliographic position. This implies that the 10595 region was a part of an active complex in which the active regions were successively occurring and fading out.

In Figure 2 the daily maps of the green corona for March 16 and 17 are shown. The studied region was just about to appear at the east limb. The isophotes were obtained by measuring a radial slit spectrogram. On such spectrograms it is possible to measure the corona intensity from the limb outwards. The intensities are expressed in the scale of Lomnický Stit and measured by the method as described by Lexa [1965] and Rybanský [1967]. Except for generally enhanced intensity, 150 absolute units, in comparison with, for example, the southern hemisphere, no clean-cut details can be seen in the NE quadrant.

REFERENCES

- | | | |
|------------------|------|--|
| GNEVYSHEV, M. N. | 1963 | <u>Astron. Zhu.</u> , <u>40</u> , 401 |
| LEXA, J. | 1965 | <u>Publ. Astron. Inst. Czech. Acad. Sci.</u> , <u>51</u> , 125 |
| RYBANSKÝ, M. | 1967 | <u>Bull. Astron. Inst. Czech.</u> <u>18</u> , 51 |
| SÝKORA, J. | 1971 | <u>Bull. Astron. Inst. Czech.</u> , <u>22</u> , No. 1 |

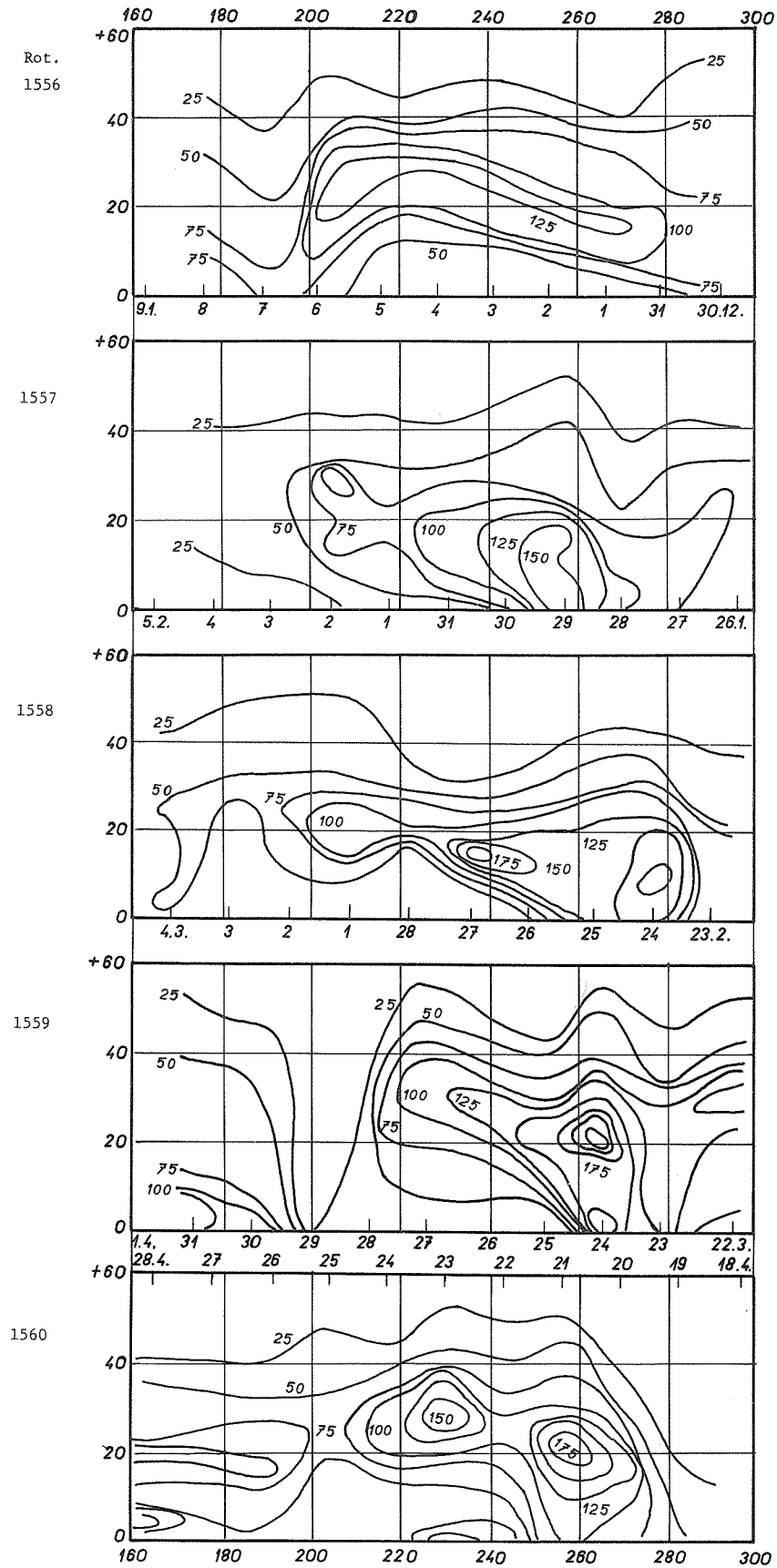


Fig. 1. Parts of the green emission corona synoptic charts for the Carrington rotations No. 1556-1560. Inscribed numbers indicate intensities expressed in Pic du Midi photometric scale.

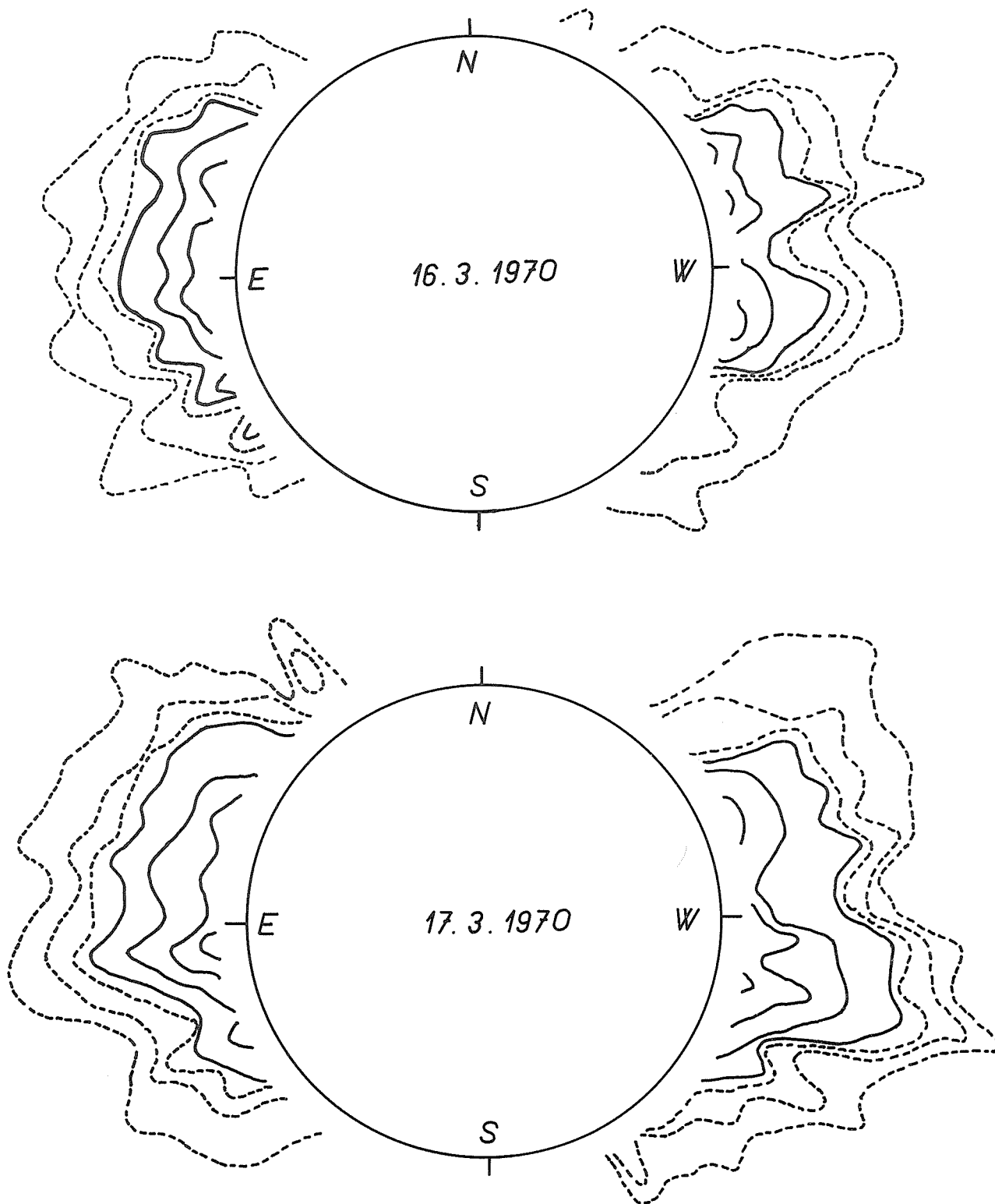


Fig. 2. Daily maps of green corona. The outermost isophote is 20 absolute units, and the dotted contours are shown in increasing steps of 10 units. The intensities equal or larger than fifty absolute units are shown by the solid lines and they are graduated in fifty unit steps. The linear scale is four times enlarged in comparison with the dimensions of the sun's disk.

"A Two-Ribbon Flare on March 7, 1970"

by

Eijiro Hiei and Fumio Moriyama
Tokyo Astronomical Observatory
Mitaka, Tokyo, Japan

Introduction

An importance 2n flare took place in McMath region No. 10614 on March 7, 1970. This flare was observed simultaneously with a 14 cm monochromatic heliograph at Mitaka and an echelle spectrograph of the solar telescope at the Okayama Astrophysical Observatory. The active region, which produced the flare, appeared at the east limb on March 1. On March 2, a small sunspot of type C appeared. The development of the sunspot as observed at Mitaka is shown in Fig. 1.

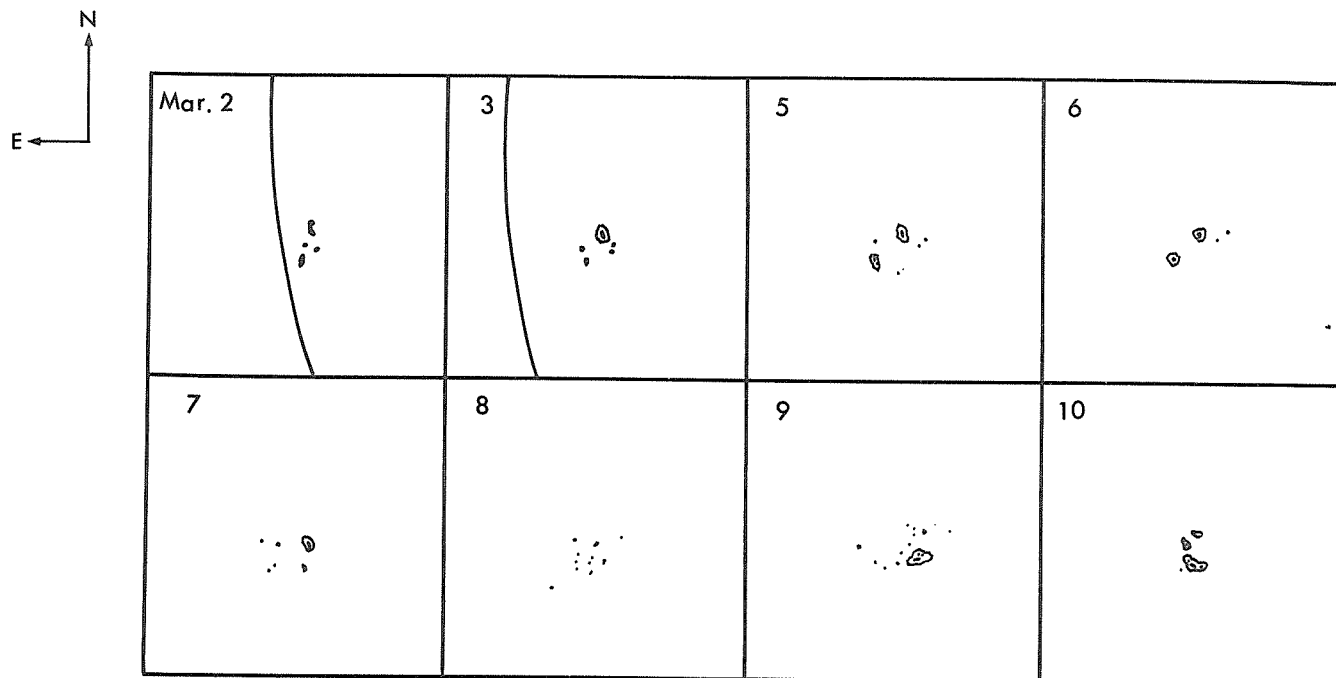


Fig. 1. Disk passage of the sunspot.

The flare activity of the region was very low and only the flare of March 7 was observed in this active region during its disk passage at Mitaka.

Instrument

The solar telescope is of Coude type with a 65 cm objective mirror and makes a solar image of 36 cm in diameter on the spectrograph slit. Sunlight passing through the slit is collimated by a mirror with 500 cm in focal length and 15 cm in aperture. The collimated beam is directed to a transmission grating of Bausch & Lomb with 83 grooves/mm blazed into λ 7700 A 1st order. In order to save an area of "inter-spectra" of an echelle spectrogram, the 1st order spectrum of the transmission grating is used from λ 4900 A to λ 6700 A and the 2nd order from λ 3400 A to λ 5000 A. Then the beam falls on an echelle grating of Bausch & Lomb with 73.25 grooves/mm of a size 128 mm x 254 mm and is diffracted into a series of 36th- to 71st- order spectra. The spectra of 40 cm x 18 cm is formed by a camera mirror with 400 cm in focal length and 100 cm in aperture. A camera is set at the center of the mirror and the echelle grating, and the image forming system is of a correctorless Schmidt. A field flattening lens is put just before the image of the spectra. A date, time, 12 marks from a tube sensitometer for the blue, and the other 12 marks for the red are impressed at one corner of the film. A roll film of 24 cm x 60 m is loaded in the camera, and the spectrum can be taken at a maximum speed of 1 frame per 15 sec. A slit jaw picture is simultaneously taken with spectra by a reflecting light through a Lyot filter of 0.5 A passband at H α .

Development of Flare

At about 0010 UT on March 7, a dark filament was formed on the east side of the spot as is shown in Fig. 2. The filament gradually extended towards north and south with increasing darkness, and

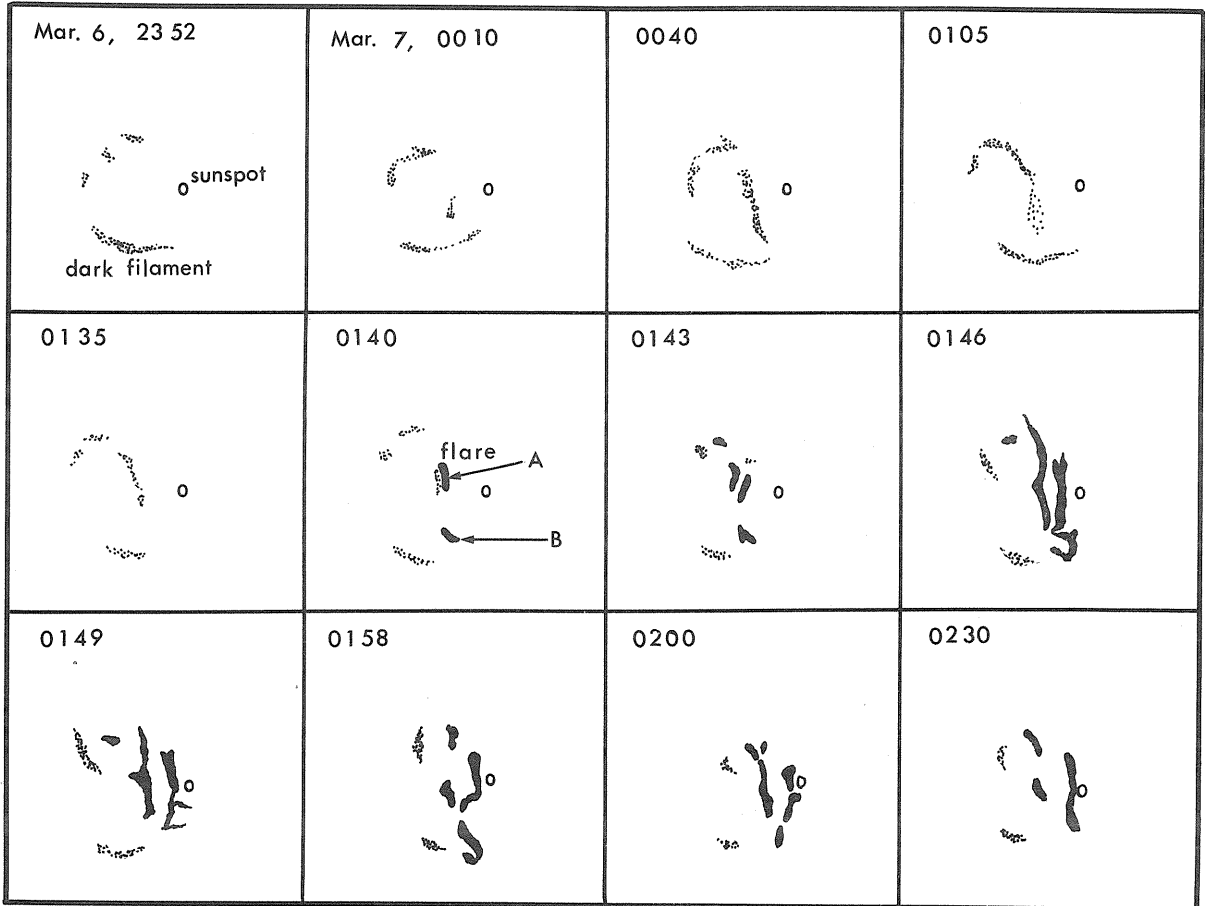


Fig. 2. Development of the flare.

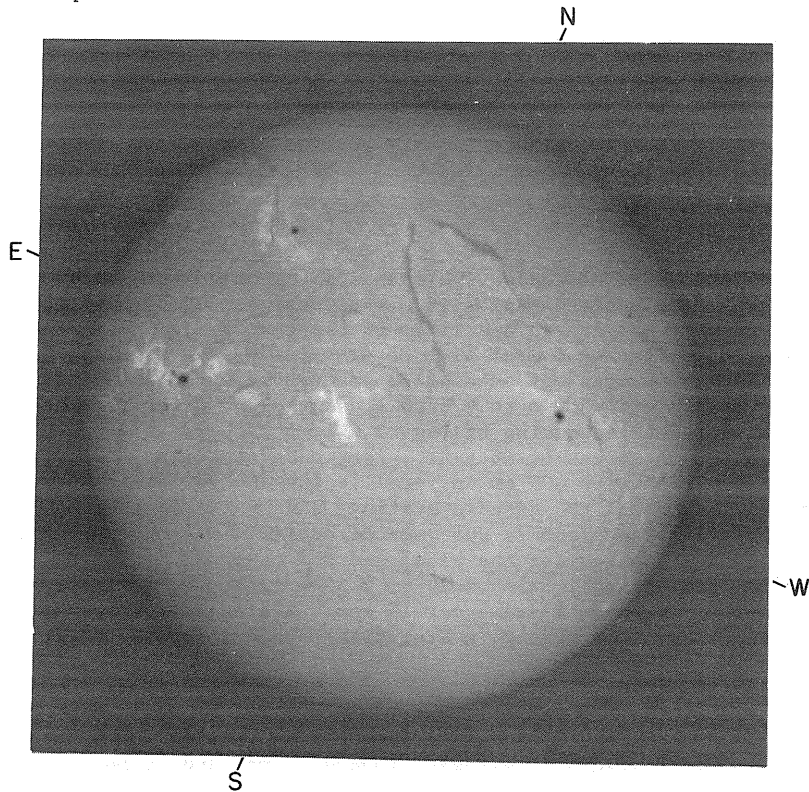


Fig. 3. Filtergram taken at 0146 UT March 7, 1970.

attained maximum visibility at 0040 UT. At 0045 UT it joined with pre-existing dark markings, each encircling the north and south sides of the active region, respectively. After that the filament began to fade from the southern part, followed by diminution of the northern part. At 0135 UT the southern part was completely gone, but the northern part left faint traces of darkness. At 0140 UT the flare started as brightening of two regions, one (A in Fig. 2) along the fading northern part, and the other (B in Fig. 2) previously occupied by the southern part of the filament. At 0143 UT another brightening appeared parallel to the pre-existing flare at A, and they advanced rapidly towards north and south to take the shape of two-ribbon structure. The flare developed into two prolonged bright filaments which were receding one from the other, and attained maximum brightness at 0145 UT. After that the brightness fell gradually. See Figure 3.

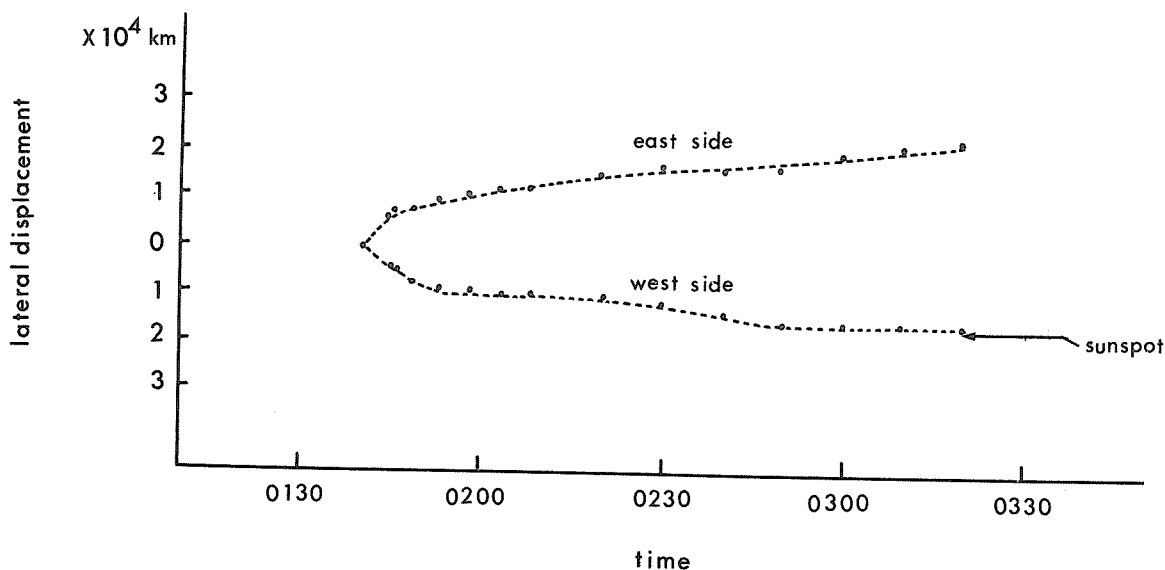


Fig. 4. Lateral motion of flare.

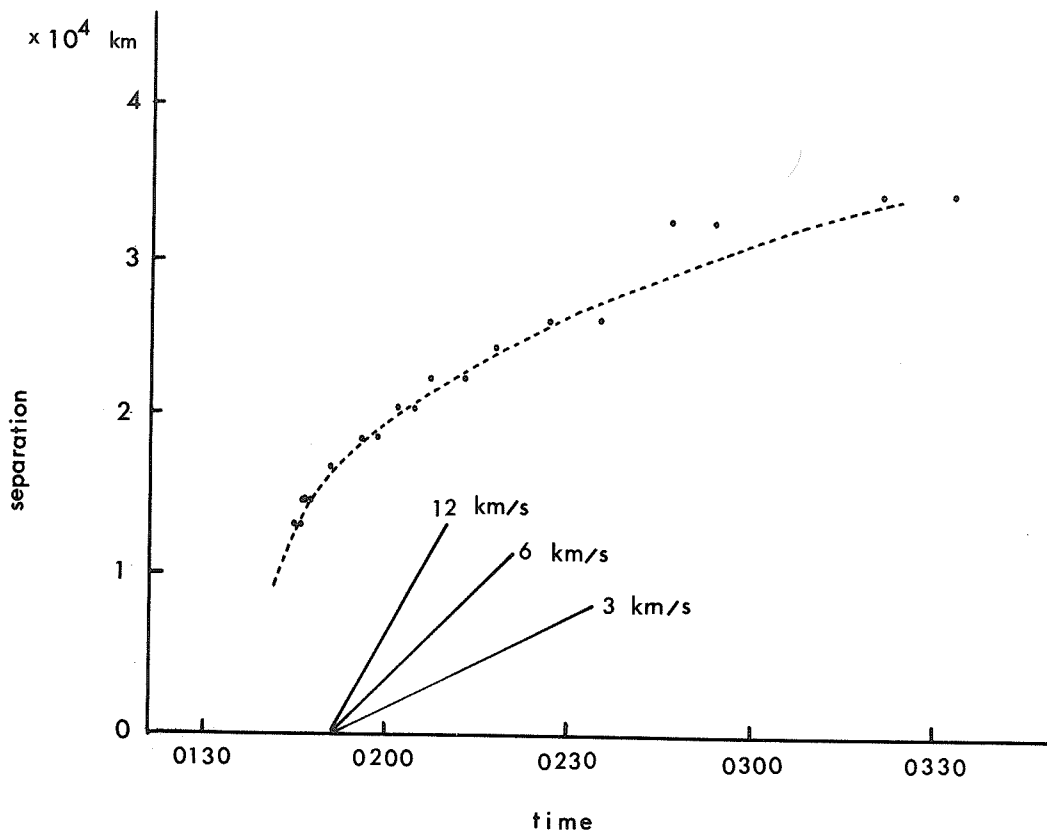


Fig. 5. Separation of flare ribbons.

Figures 4 and 5 show the lateral displacement of flare ribbons. In the earlier phase the separation proceeded with a velocity of about 12 km/s, but in the later phase the motion was decelerated and the velocity decreased to about 3 km/s. In particular the one ribbon at west side appeared to be stopped near the sunspot.

The H α patrol observation at Mitaka ceased at 0330 UT because of unfavorable weather, and the last phase of the flare was not observed.

Spectrographic Observation

The observation with the echelle spectrograph was made from 1 min. before the time of maximum brightness of the flare. Total 18 spectrograms were obtained during 90 min. of the whole development of the flare with an exposure time of 1 sec. A slit of 50 μ in width and 3 mm in length was used. The slit jaw picture was taken at the same time as the exposure of the spectrograph by a Nikon Motor Drive with an exposure time of 1/4 sec. Figure 6 shows a spectrogram of the flare taken at 1 min. before the maximum time. Linear dispersions on the spectrogram are ranging from 0.25 A/mm at 3500 A to 0.50 A/mm at 7000 A.

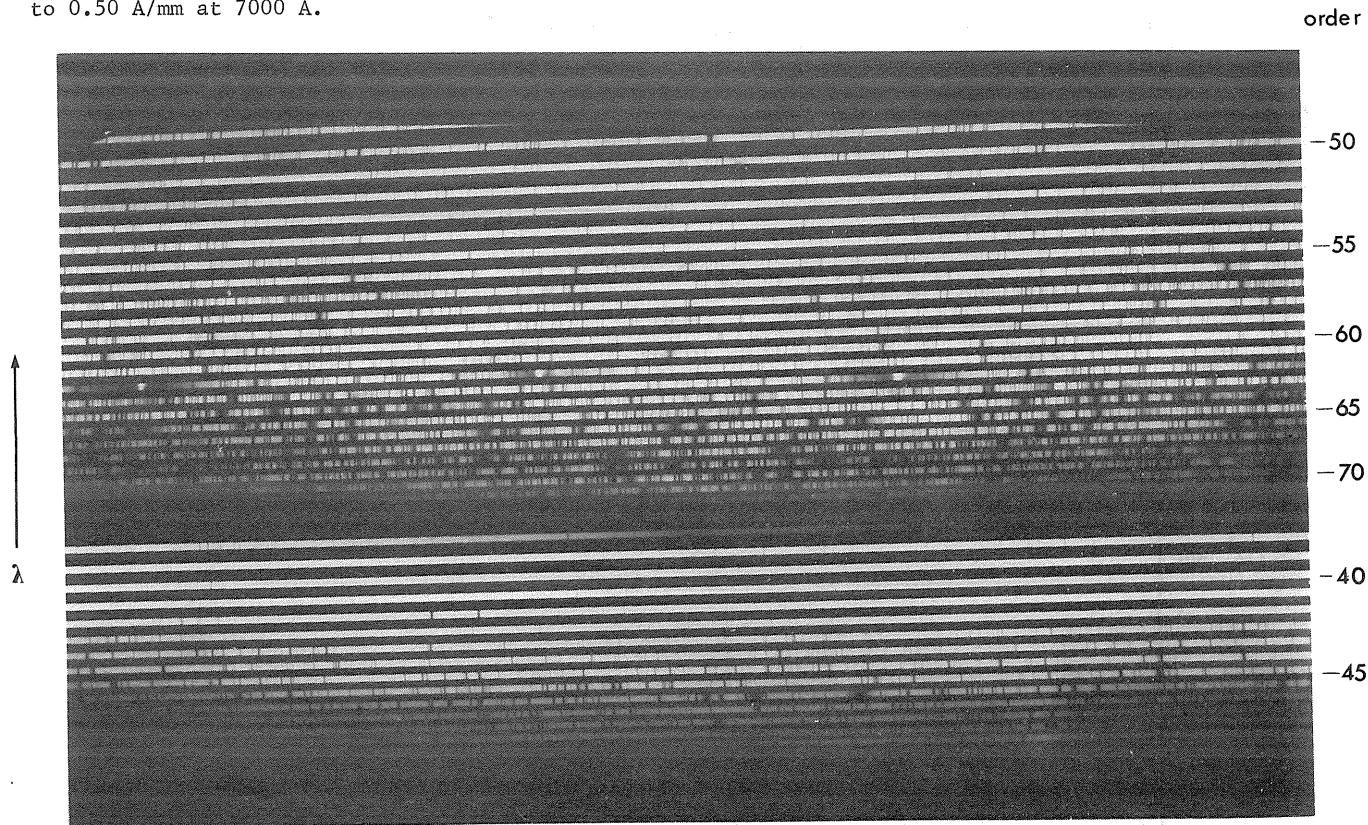
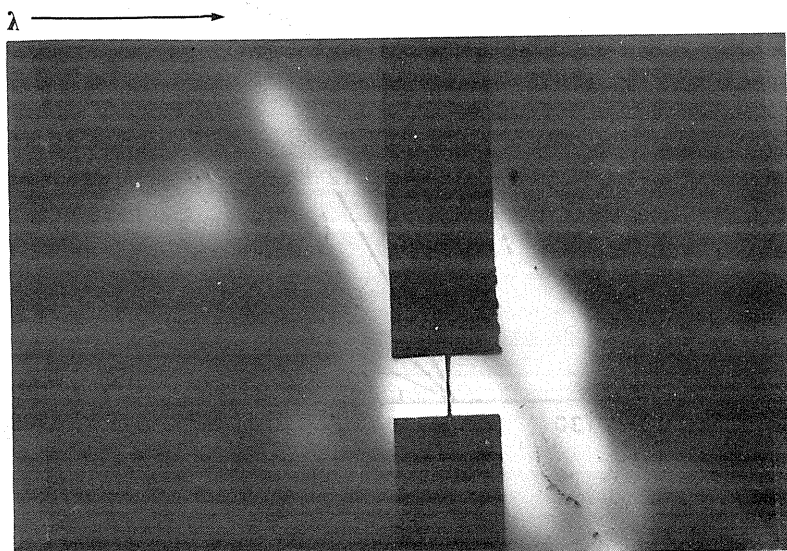


Fig. 6. Echelle spectrogram.

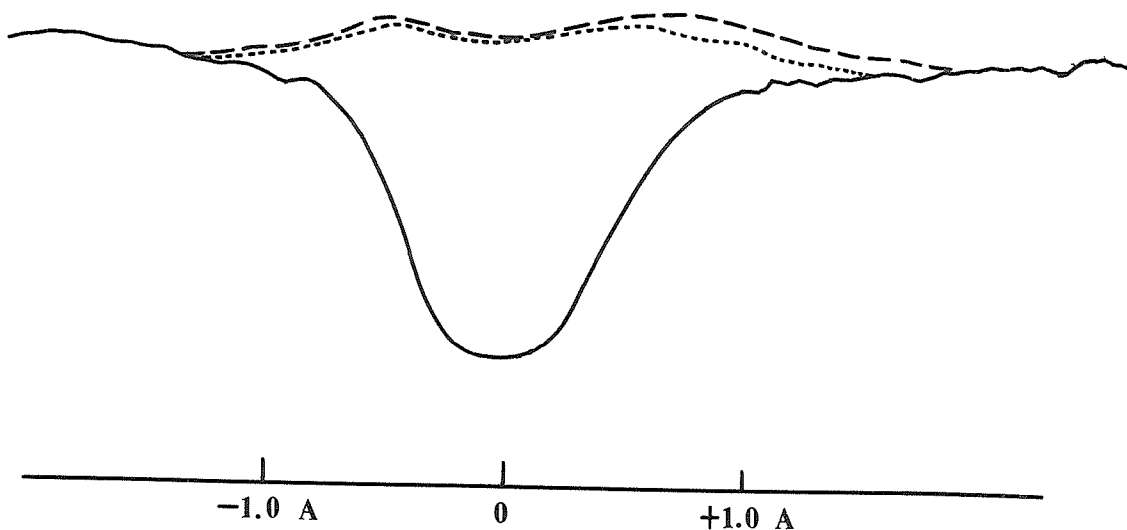
slit jaw picture



Microphotometer tracings were made for the lines of $H\alpha$, He, Ca II H and K, Si I λ 3905.53 A, and Fe I λ 3719.95 A at the brightest region of the flare. Figure 7 shows the tracings for these lines. A red asymmetry of profiles for some lines is seen in the figure.

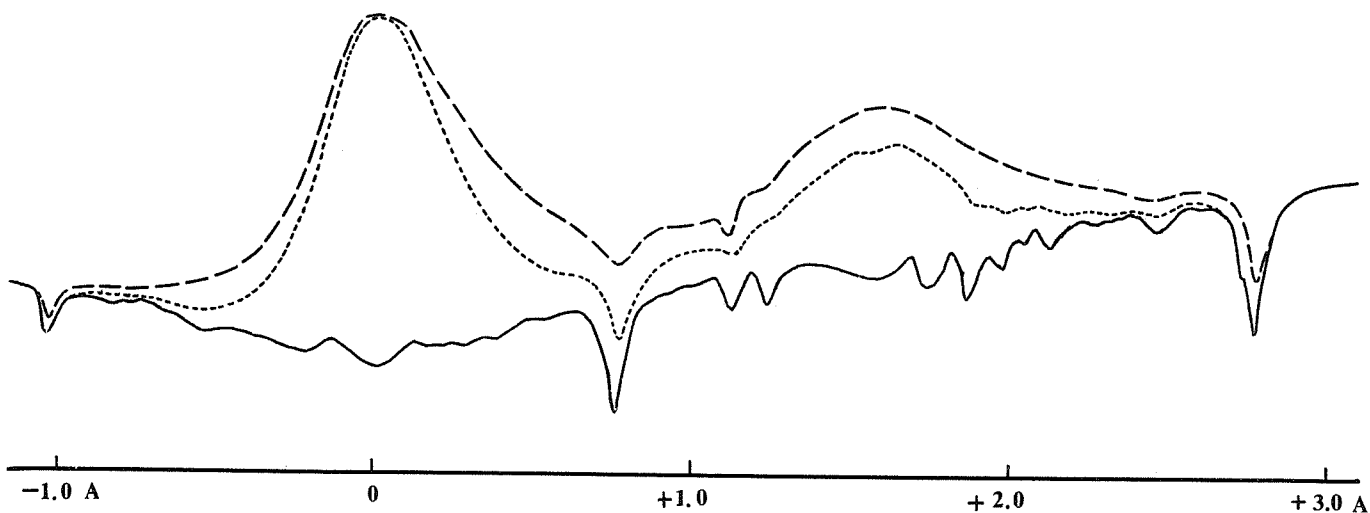
----- 1 min. before
 5 min. after the max.

(A)



$H\alpha$

(B)



Ca II H

$H\epsilon$

Fig. 7. Line profile of emission lines

"Optical Flares and VLF Anomalies Related to the Great Magnetic Storm of March 8, 1970"

by

Richard A. Miller, S.J. and Allan R. Trinidad
Solar Division, Manila Observatory, Philippines

Introduction

This paper will confine itself first to a description of the photographic aspects of two of the three largest solar events, as rated by x-ray emission, in the three and a half days preceding the most severe part of the March 8, 1970 great magnetic storm, and second, to a description of some of the VLF effects, especially at the height of the storm.

Observations of Flares

A glance at Solar-Geophysical Data [ESSA, 1970] shows that of the three largest x-ray events, in the range 1 - 8 Å, measured by satellite Solrad 9 - Explorer 37, for the period March 5 to March 10, 1970, two were occasioned by the double flare of March 5 at 0420 UT and by the flare of March 7 at 0130 UT. The double flare at opposite sides of the sun, on March 5, possibly predisposed the

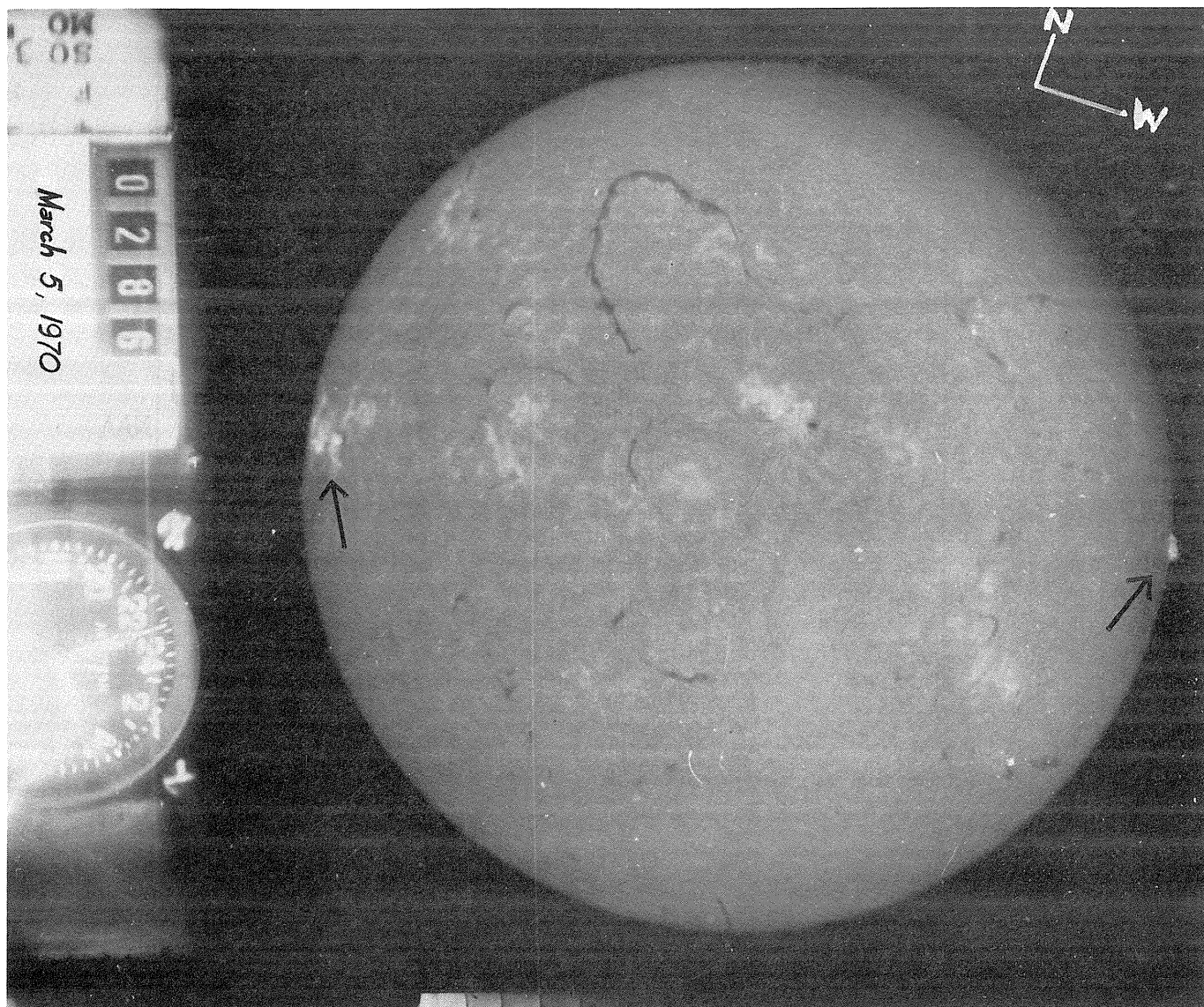


Fig. 1. Double flare at opposite limbs, March 5, 0457 UT, 1970, taken near maxima of SPA's, but after optical maximum. Arrows point to flares.

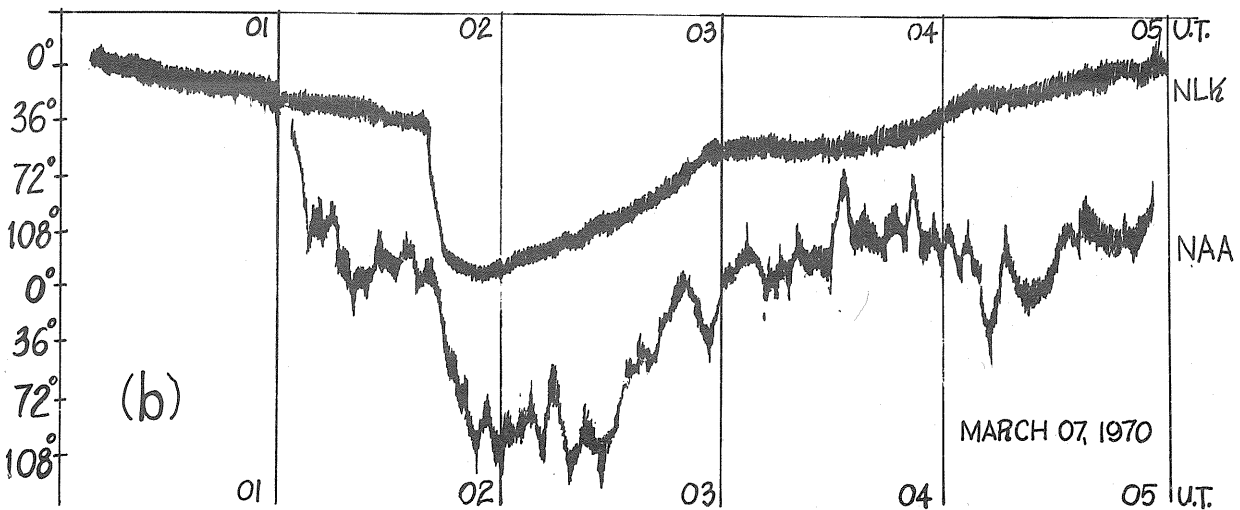
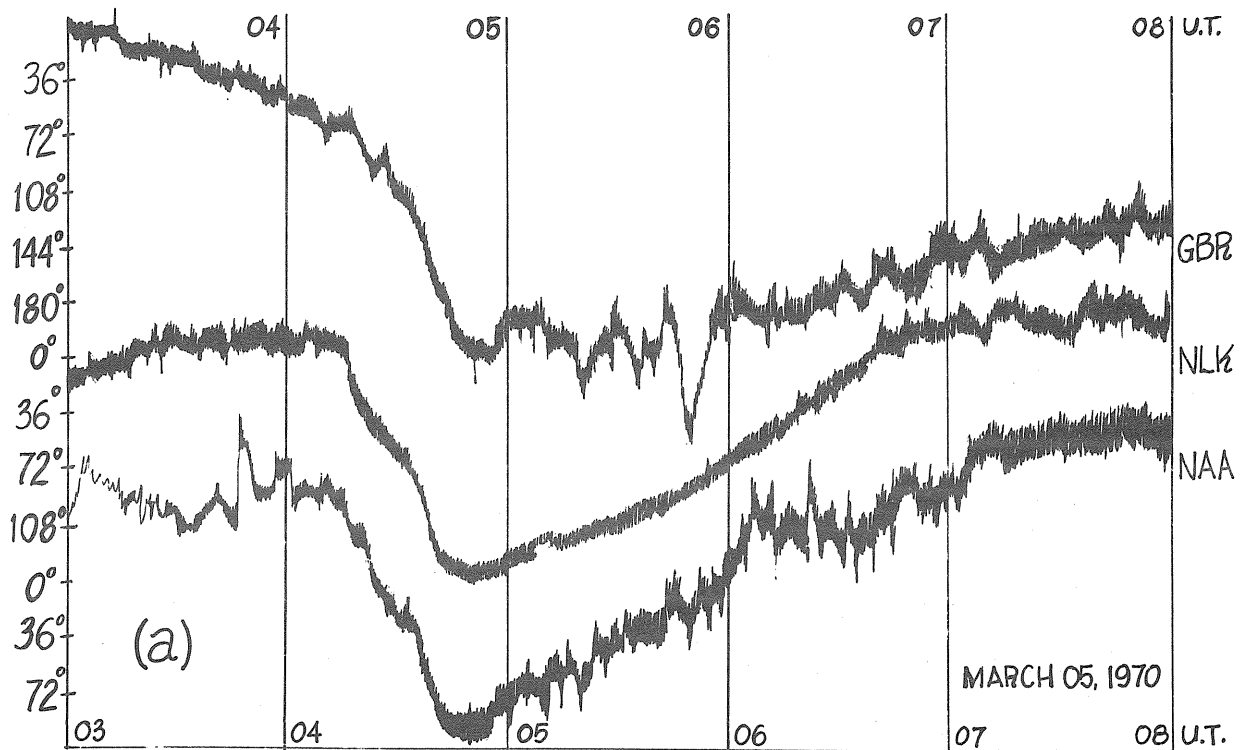


Fig. 2. Sudden Phase Anomalies corresponding
 a) to the double flare of March 5, 0457 UT and
 b) to the flare of March 7, 0130 UT

magnetic field about the sun for the penetration of the particles from subsequent flares. Ionospheric effects were strong and lasted on the local VLF circuits from 0418 UT to 0656 UT. Practically simultaneously two flares began, one at S15 E71 and the other at N15 W86 to the limb. Figure 1 is a photograph of this event taken near SPA maximum, twenty minutes after the maximum of the western flare. The 1N rating for the western flare may have been an underestimate, due chiefly to spotty coverage of the flare here through clouds. Figure 2a shows major SPA's on all three of our locally monitored transmissions. The advances were 134°, 148° and 142° on circuits tuned to GBR, Rugby, England, NLK, Jim Creek, Wn. and NAA, Cutler, Me., respectively. Duration for the longest SPA, on the GBR circuit, was two hours and thirty seven minutes.

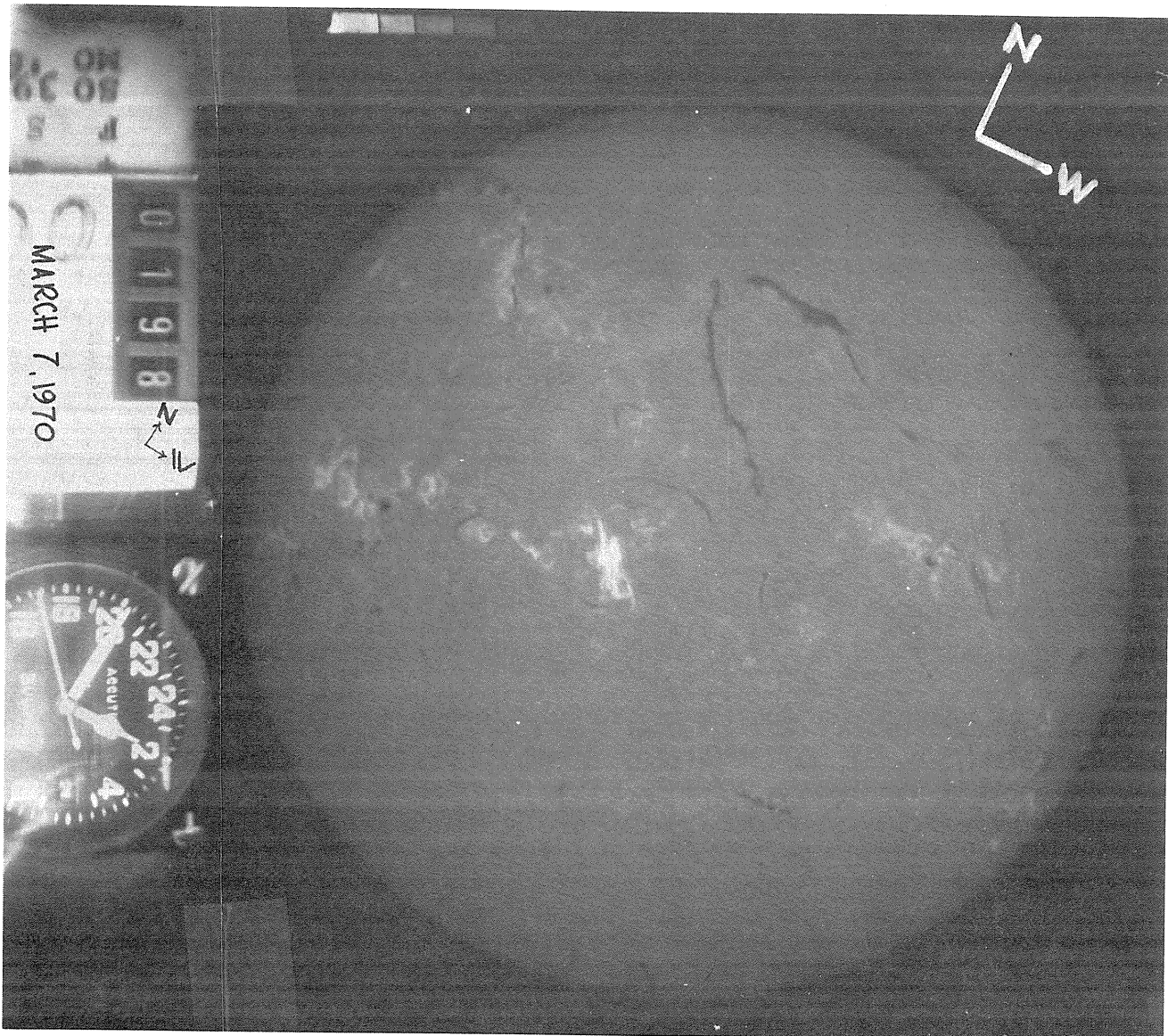


Fig. 3. Major flare of March 7, 0150 UT, S11 E09, at end of flash phase with parallel ribbon emission.

Figure 3 shows the hydrogen alpha filtergram of the event of March 7, 1970. The photograph taken at 0150 UT is of flare maximum. Figure 2b shows the corresponding VLF disturbances. Maximum phase advances on the NLK and NAA circuits were 97° and 144° , respectively. The original filtergram of Figure 3 was photometered at one of the brightest regions and found to be 0.47 in log intensity above the local background. This is considerably below the 0.63 log increase of the October 31, 1968 3b flare, photographed through the same telescope [Miller and Trinidad, 1970]. The March 7 flare, while not especially bright, was of considerable tenacity.

It would not have been easy to predict a large flare in this region. There was a wishbone-shaped formation or a gamma configuration in hydrogen alpha emission. This configuration has been observed at Manila as a necessary, but not sufficient condition for a vigorous flare. The calcium spectroheliogram taken shortly before the flare (Figure 4a) shows one particularly sharp corner and three angular bends in that part of the plage region which flared, in contrast to the spectroheliogram taken the next day (Figure 4b) after the flare. This latter photo shows that the tubes of flux were by then well rounded. Arrows point to the location of the sharpest feature.

There was nothing impressive about the spot group of the region, which was classified as D 14 by the Manila Observatory just prior to the flare. An accurate superposition of a simultaneously photographed white-light heliogram and an H-alpha filtergram, taken before the flare on March 5 at 2321 UT, shows a cross formed by the intersection of a dark fibril coming out from a small spot at the NE side of the group and another dark fibril just appearing off the south end of a line of three

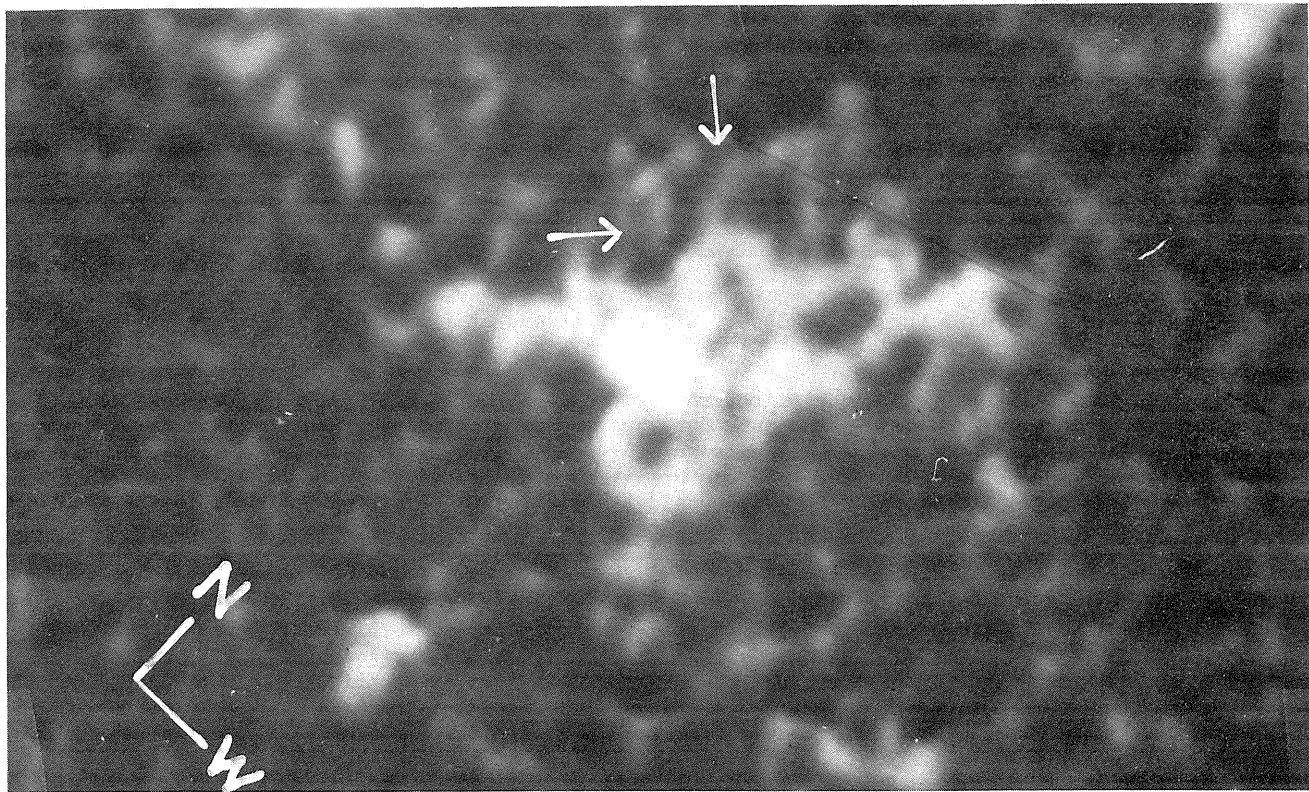
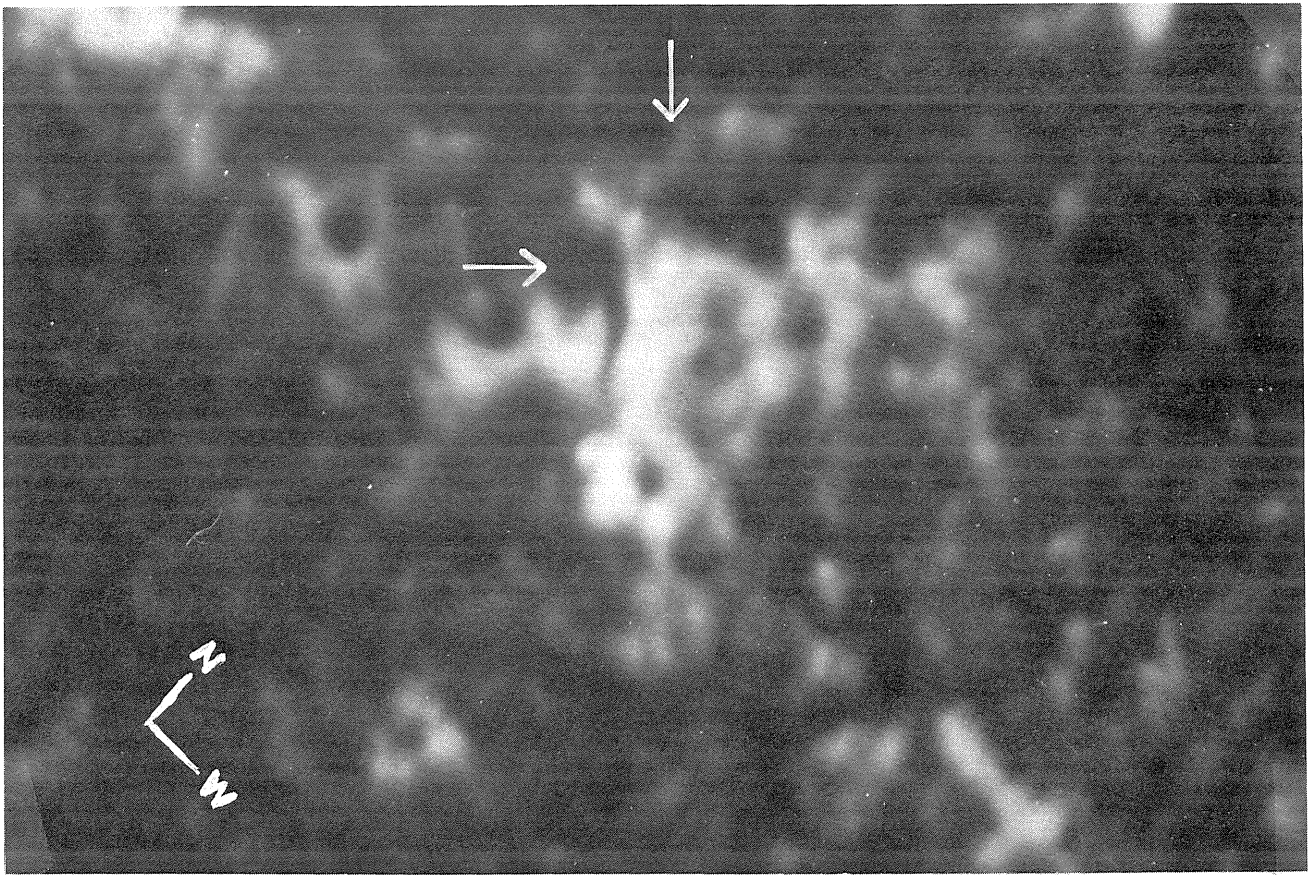


Fig. 4. K₃ spectroheliograms of flare region (McMath plage No. 10614) taken (a) before the flare, March 7, 0040 UT and (b) after the flare March 8, 0024 UT. The flux tubes have considerably rounded and smoothed in the interim. Arrows point to the location of the sharpest feature.

faint north-south oriented spots. This is a somewhat common phenomenon in white light. The "X" was at the location of the most vigorous part of the flare at the beginning of the flash phase. Curiously, the area of the spot group of the flare region notably declined near flare time. It measured 2.4 square degrees a day before the flare, March 5, 2321 UT, 1.3 square degrees at 2354 UT March 6, shortly before the flare, and then 2.5 square degrees by the next day, March 7, 2320 UT. The region showed only very minor flare activity for the rest of its disk passage.

At 0015 UT, March 7, shortly before the flare, a dark filament in hydrogen alpha intensified along the stronger or western edge of the gamma configuration on the inside (eastern) edge. The film patrol showed fluctuations in the filament at 0023 UT and more intensification at 0030 UT. The filament cut across the weaker (eastern) arm of the gamma configuration.

At 0115 UT, March 7, there began an SN flare at N11 W33, with a dark surge pushing out from this flare at 0124 UT. Possibly the disturbance gave rise to a brightening on the edge of the filament mentioned in the preceding paragraph, at 0130 UT, which may be taken as the beginning of the importance 2 flare. Propagation would be ≤ 1400 km/sec. The brightening gradually increased till 0141 UT and then in nine minutes, from 0141 UT to 0150 UT it flashed to a maximum. The flare formed parallel streamers at about 0145 UT. These streamers then separated. At 0150 UT they were one degree apart, two degrees apart by 0216 UT, and three degrees apart by 0252 UT. This was at a slightly increasing rate. The average rate was seven km/sec. Divergent motion of two parallel streamers is common especially to many proton flares [Bruzek, 1964]. At 0252 UT two faint parallel emission ribbons filled the gap between the main parallel flare ribbons. The flare lasted for as long as three hours, if ending is to be taken as 0430 UT, though any ending time between 0410 UT and 0430 UT would be satisfactory.

At the beginning of the flash phase the curved filament to the NE of the region disappeared, and reappeared after the flare. The filament to the SE almost disappeared completely at 0145 UT midway in a five minute interval of fade and restoration. At 0159 UT, five degrees to the SE of the flare center, a glob of matter approached a ribbon. The ribbon, as though hinged at its inner end, swung towards the glob. At the junction, when the glob and the ribbon met, a dark surge moved out to the SE. There was no visible shock wave, on band, at least.

VLF Circuits

The Manila Observatory monitors three VLF stations, GBR, NLK, and NAA. The first two paths are geographically similar, going from Manila NW and NE to Rugby, England and Jim Creek, near Seattle, Wn. The third, to Cutler, Me., is a transpolar route, running two degrees from the pole at its closest. The GBR trace reaches its apex at N. Lat. 62.5° and E. Long. 47° which is 76° magnetic north, whereas the NLK route reaches its apex at the tip of the Aleutian Peninsula, N. Lat. 54° , W. Long. 160° , which is 66° magnetic north. The GBR path runs above the 74° magnetic line for a third of its length, namely from Tomsk, (N. Lat. 56° , E. Long. 85°) to Petrozavodsk, (N. Lat. 62° , E. Long. 34°). The highest magnetic latitude of the NLK path, 70° , is at Seattle, its terminus.

Worthy of note is the sensitive performance of the GBR circuit to the magnetic storm and especially to the very severe phase of the storm. Signal attenuation for the most part cut out our signal from NAA, except at the height of the storm, and the NLK path did show the disturbance but not spectacularly. The GBR circuit shows an SPA-like advance of 30 degrees, beginning March 7 at 2008 UT, ending at 2100 UT and with maximum at 2019 UT. The amplitude correlates negatively. The maximum was two minutes later than the 2.4 dB maximum in riometer absorption reported by Shepherd Bay.

The severely disturbed geomagnetic field began March 8 at 1418 UT. Vela low energy proton counts reached a maximum March 8 at 1617 UT. Figure 5 shows that by 1440 UT the phase trace of the GBR circuit was definitely advancing, peaking at 1615 UT and at 1840 UT. There is negative correlation with the amplitude trace. The sharp advance to a pre-maximum at 1458 UT may be related to Thule's maximum riometer absorption, 5.9 dB, at 1455 UT. NLK's advance shows much the same as a typical SPA, with start at 1550 UT, end at 1640 UT and maximum of 50° at 1620 UT. This maximum nearly coincided with the maximum of Vela low energy proton counts at 1617 UT after which the counting rate began declining. The dotted lines on Figure 5 indicate the normal direction of the phase traces for the three circuits. The added advance on the GBR trace, upbending sharply at 1820 UT and maxing at 1837 UT is reflected in the more gradual advance of the NLK trace, shown to begin about 1845 UT at the latest. The advance of GBR at 1837 UT reached 144° or minus 25 micro-seconds. NAA showed some disturbance, an advance of 72° , beginning March 8 at 1628 UT, ending at 1900 UT and maximizing at 1715 UT. The local circuits seem to respond to the particles which cause both polar cap absorptions as well as the lowering of the ionospheric side of the VLF wave guide.

Figure 6 has been constructed with nine days of data from the phase trace of the GBR circuit. The first three days, March 3, 4 and 5, have been used to establish a norm, much in the manner of Potemra *et al.* [1959]. The points have been chosen from the base line in the case of an obvious SPA. The mean of the hourly values for these days has been established and then a five hour running mean used to give the sinusoidal curves used as reference. Hourly values for the days from the 6th to the 11th were then graphed with a horizontal time scale, and smoothed out with a solid line.

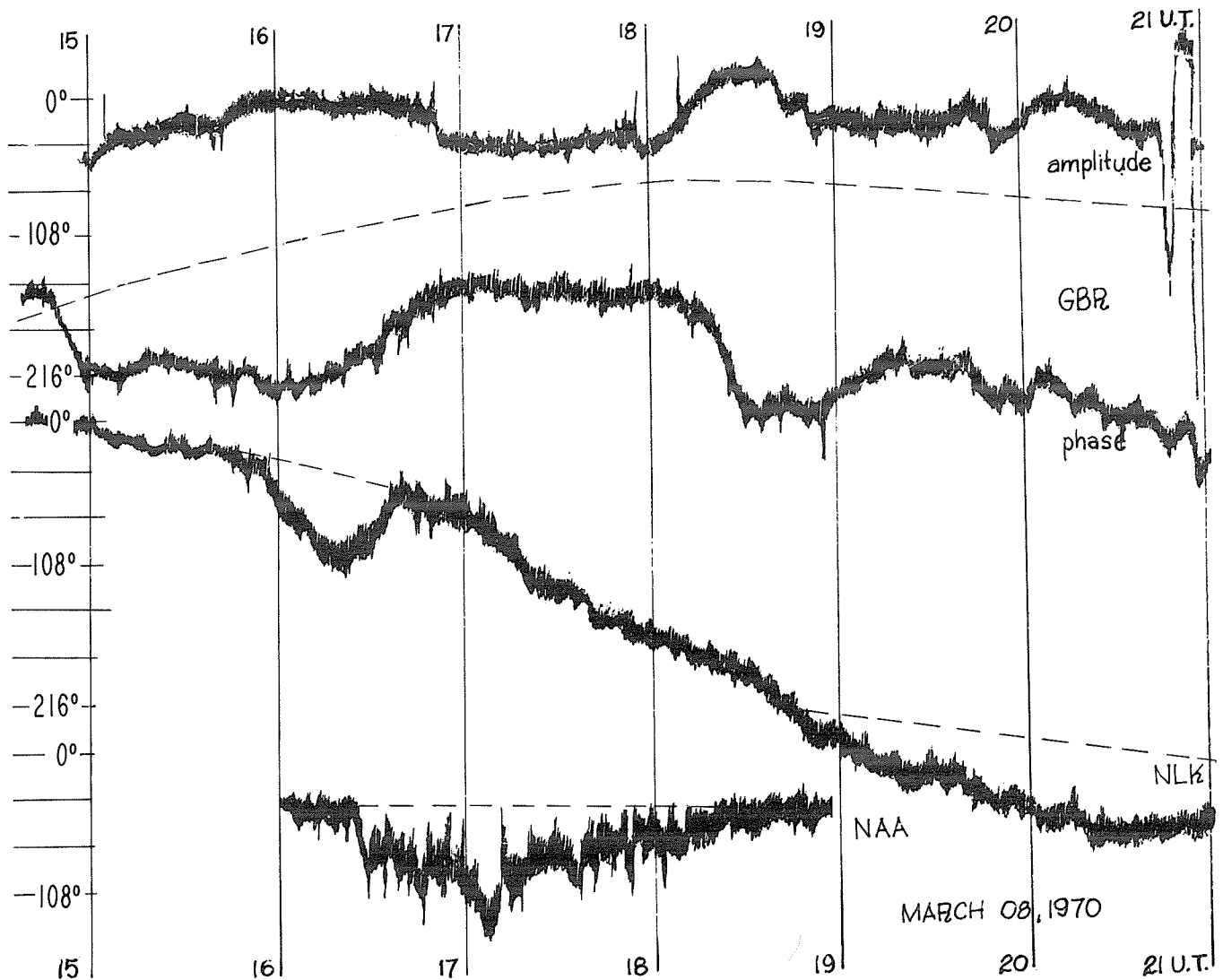


Fig. 5. The VLF circuits, at time of the most severe part of the magnetic storm, March 8, 1430 UT to 2100 UT; top to bottom: GBR amplitude, phase of GBR, of NLK and of NAA. All paths are to Manila.

The norm appears as a series of X's. The Kp daily sums of the three-hour Kp indices for the 3rd through the 11th are 23+, 24+, 20, 29-, 37, 53-, 36+, 13-, and 5+. The days which have a higher index than the norm tend to advance in phase, while the days with lower index than that here taken as an average, on the Kp scale, tend to fall below the average in phase. The same conclusion would hold for the Ap indices. As the magnetic index changes so inversely does the height of the upper side of the wave guide, especially for the GBR path. The end of the severe part of the magnetic storm, about March 9, 0700 UT is reflected in the curve of Figure 6.

Conclusion

This study shows that not only the transpolar VLF paths, but those which pass under the polar cap for a substantial part of their length, should be monitored for confirmation of Polar Cap Absorption. Though central meridian passages of regions with flares of importance three correlate well with geomagnetic storms, [Smith and Smith, 1963] the flare of March 7, 0130 UT treated in the study, does not seem sufficient of itself to produce the observed intensity of the magnetic storm. Undoubtedly a congeries of events determined that the path of the particles to the earth

should be so unobstructed. The whole picture will be clarified by the many contributions in this UAG report and by studies certain to follow.

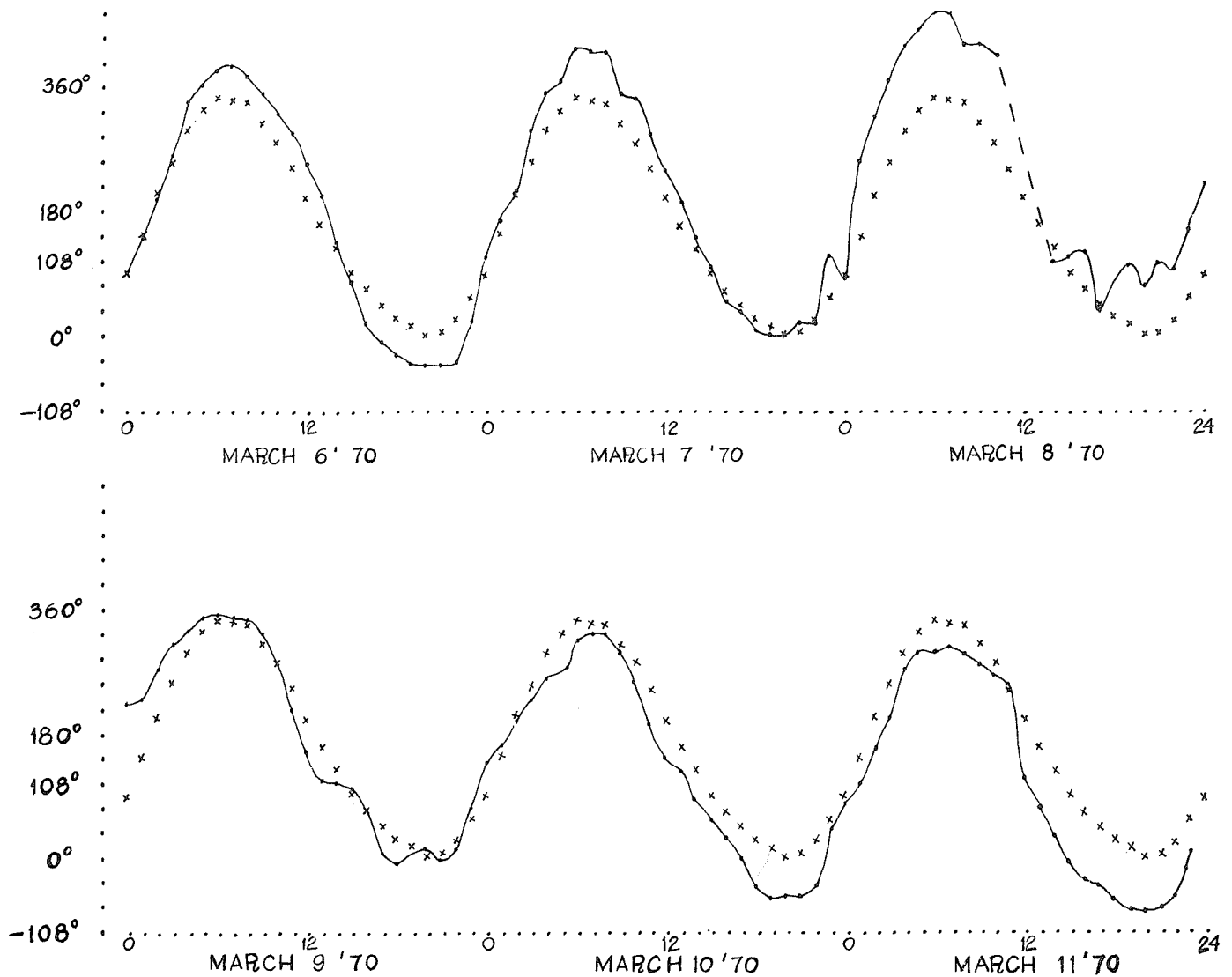


Fig. 6. Phase traces (solid line) of GBR - Manila VLF circuit March 6 to March 11, 1970 compared to the smoothed averaged (x x x x) of March 3 to March 5, 1970. Days with higher Kp values than the average are advanced and these with lower values are retarded in phase.

Acknowledgements

Thanks are due to A. Ambion for some of the figures and to the Air Weather Service of the U. S. Air Force for the film used in the patrol.

REFERENCES

- BRUZEK, A. 1964 Case Histories of Flares: The Large Flares of July 11, 12, 18 and 20, 1961, AAS - NASA Symposium on the Physics of Solar Flares, Ed. W. N. Hess NASA SP-50, Washington, D. C.
- 1970 Solar-Geophysical Data, 309 Part 1, pp. 78-81, May 1970, U. S. Department of Commerce, (Boulder, Colorado, U.S.A. 80302).
- MILLER, R. A., and 1970 A study of the Film Record of H- α Flare of October 30-31, 1968, World Data Center A, Upper Atmosphere Geophysics Report UAG-8, Part I, 48 - 53.
- POTEMRA, T. A., 1969 VLF Phase Disturbances, HF Absorption and Solar Protons in the Events of August 28 and September 2, 1966, J. Geophys. Res., 74, 6444-6458.
- SMITH, H. J., and 1963 Solar Flares, Macmillan, New York, 232.
- E. V. R. SMITH

"High Velocity Mass-Ejection Evidence Related to a Solar Flare of March 8, 1970"

by

Marta Rovira, Marcos Machado and Hugo Grossi Gallegos
Observatorio Nacional de Fisica Cosmica
San Miguel, Argentina

Mass motion in the solar atmosphere can be analyzed by means of off-band filtergrams taken systematically. On our flare-patrol material at San Miguel's Observatory, we can get filtergrams at the center and both sides of H α by using a line-shifter mechanism. This mechanism has been installed on a 140 mm aperture telescope (SECASI) which takes one photograph every 15 seconds.

One of the main investigating subjects on our work is to analyze motions in dark features recorded on our films. The phenomena that we are considering here may be observed on the film of March 8, 1970, and can be described as follows. Figure 1 shows a dark filament at it's maximum visibility in the center of H α at 1408 UT. Figure 2 shows the development of this filament in the center of H α and in the violet and red wings.

- a) in the first series of photographs, taken at 1335 UT, the presence of a dark condensation near the active zone can be seen.
- b) 1357 UT: We can see now enhanced evidence of a mass condensation constituting a dark filament which traverses the flare, and reaches near the West limb. One may not determine a general movement of the dark feature as it can be seen on both sides of H α ; but it is evident that the violet wing is preponderant.
- c) 1400 UT: Note the definite enhancement of the violet image, as an evidence of the ascending movement of the material.
- d) 1430 UT: The fourth series of photographs shows that the dark filament has disappeared as it has been ejected to the upper zones of the solar corona. This has been suggested by the ascending movement noticeable on the previous series of photos.

A further evidence of the mass ejection is given by the 73 cm registered band obtained with the solar radiotelescope of San Miguel's Observatory, showing a growth of the integrated flux coincident with the optical evidence of this phenomenon. This can be taken as another evidence, considering the results obtained by Westin and Liszka [1970], that shows a high percentage of coincidences between this kind of mass-ejection and radiation in metric and centimetric waves.

REFERENCE

WESTIN, H. and 1970 Motion of Ascending Prominences, Solar Phys., 11, 409.
L. LISZKA

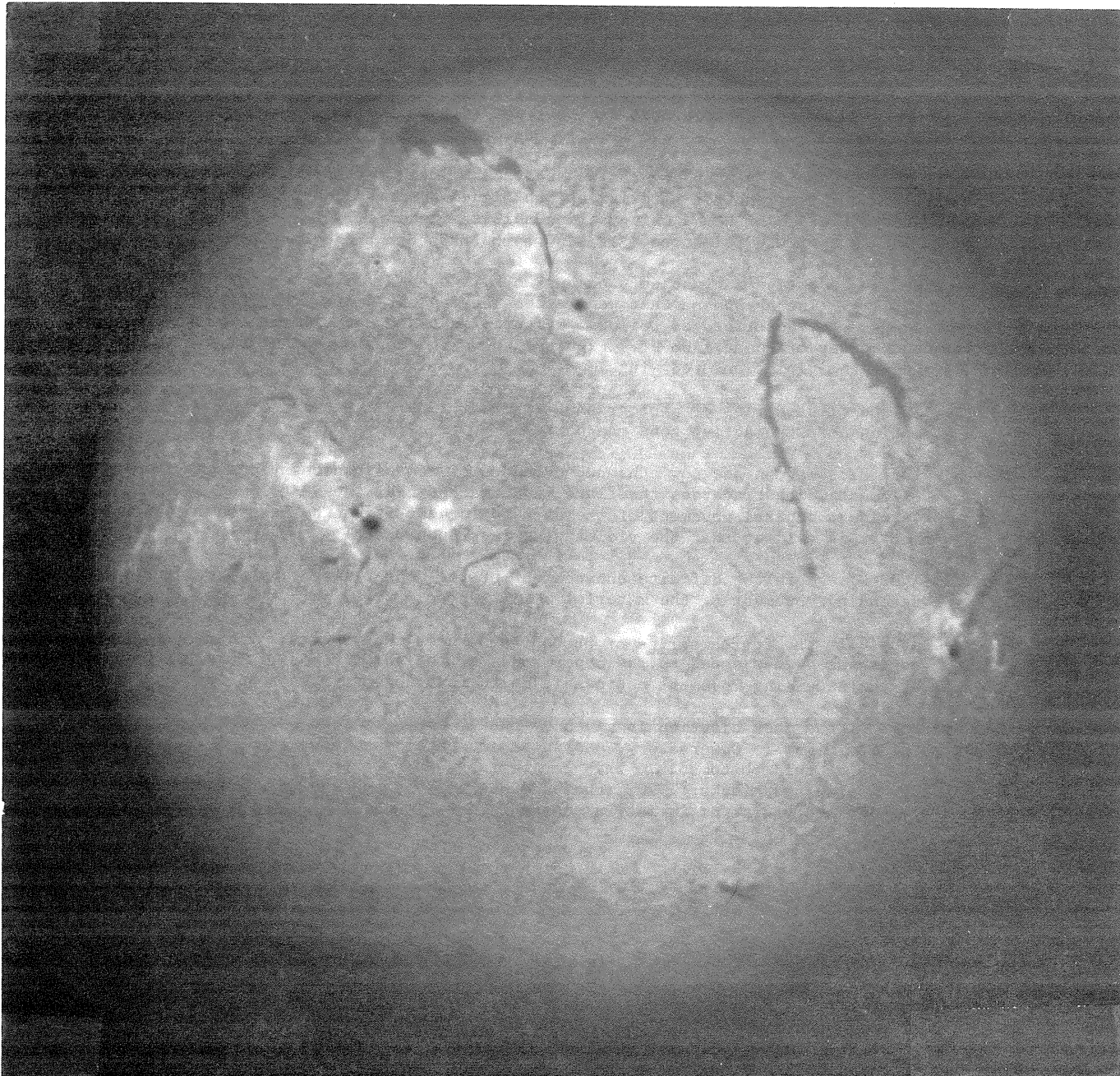


Fig. 1. Filament at center of H α March 8, 1970 at 1408 UT.

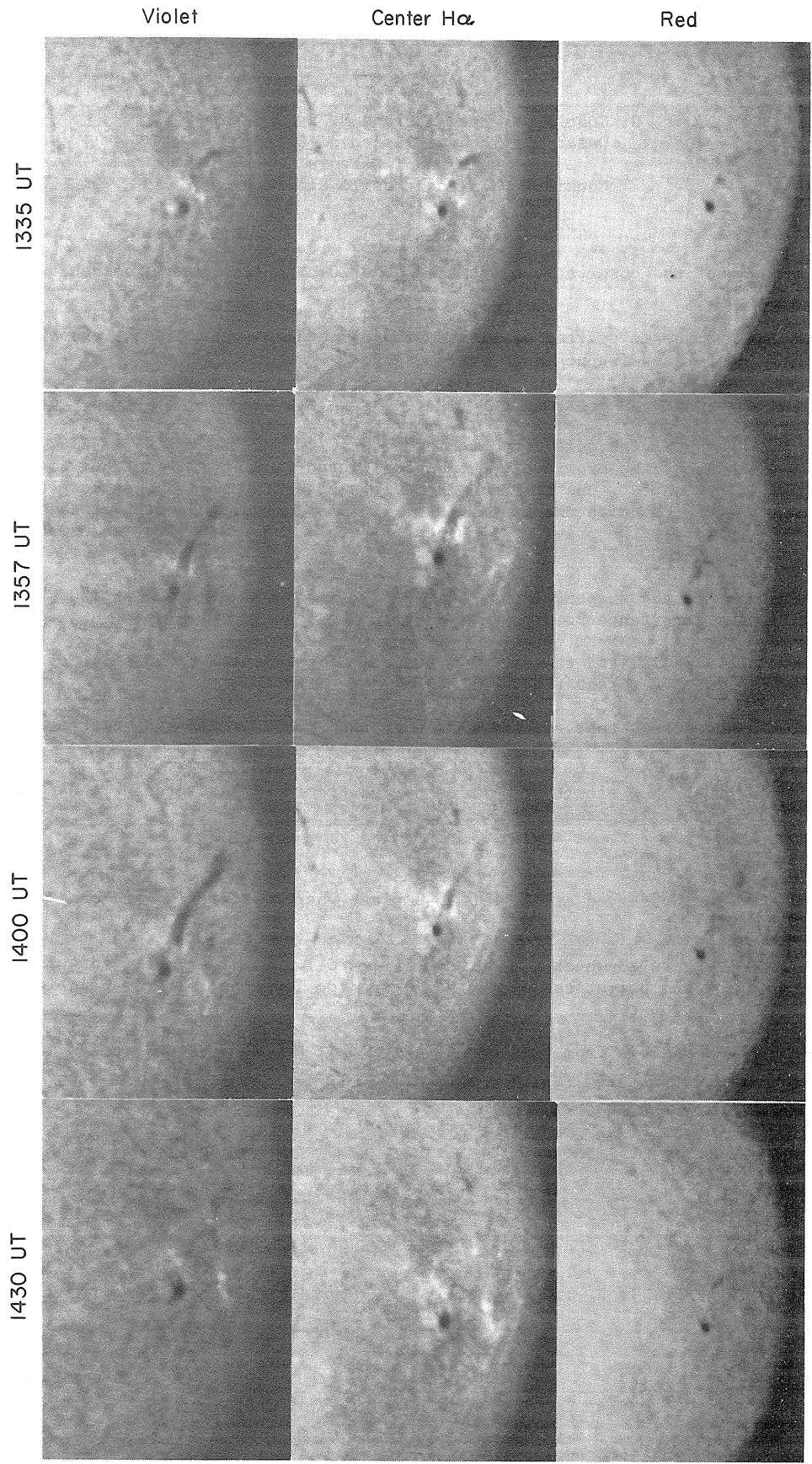


Fig. 2 Development of filament March 8, 1970 in center of H α and violet and red wings.

"Importance 2 active prominences at limb observed at
Catania Astrophysical Observatory on March 8, 1970"

by

G. Godoli, O. Morgante and M. L. Sturiale
Osservatorio Astrofisico di Catania
Universita di Catania
Consiglio Nazionale delle Ricerche

EPL at S40 E90

At the beginning of the observations on March 8, 0720 UT a quiescent prominence was observed at S40 E90.

At 1125 UT the prominence started developing rapidly and subsequently the phenomenon was followed continuously up to its disappearance.

Pictures showing some phases of the active prominence are given in Figure 1.

The first picture shows the quiescent prominence at 0720 UT. From 1125 to 1142 UT morphological changes are visible but the prominence can be considered as a whole. Between 1142 and 1145 UT the object breaks in two parts: one of these is moving southwards as a suspended prominence, the other part keeps steady with quite unchanged shape. It must be pointed out that the shape of this quiescent part is similar to the previous prominence, before its activation, as is shown from the two pictures of 0720 and 1200 UT.

The disappearance of the suspended part of the prominence was observed at 1200 UT. The event has been classified as importance 2.

In Figures 2 and 3 radial and tangential distances of the lowest south point of the detached prominence have been plotted versus time.

Both Figures 2 and 3 show that, at the time when the active prominence detaches, the curves became steeper.

This fact shows that the velocity of the suspended prominence was greater than the velocity of the whole prominence before its breaking up.

BSL at N43 W90

On March 8 a BSL was observed at N43 W90 in a place where no activity had been visible in the preceding days.

Phases of the surge are shown at the bottom of Figure 1. For this event, drawings are given instead of pictures for the brightness of the surge was too low to permit the printing of filtergrams.

The phenomenon was visible from 1440 to 1453 UT and it has been classified as importance 2.

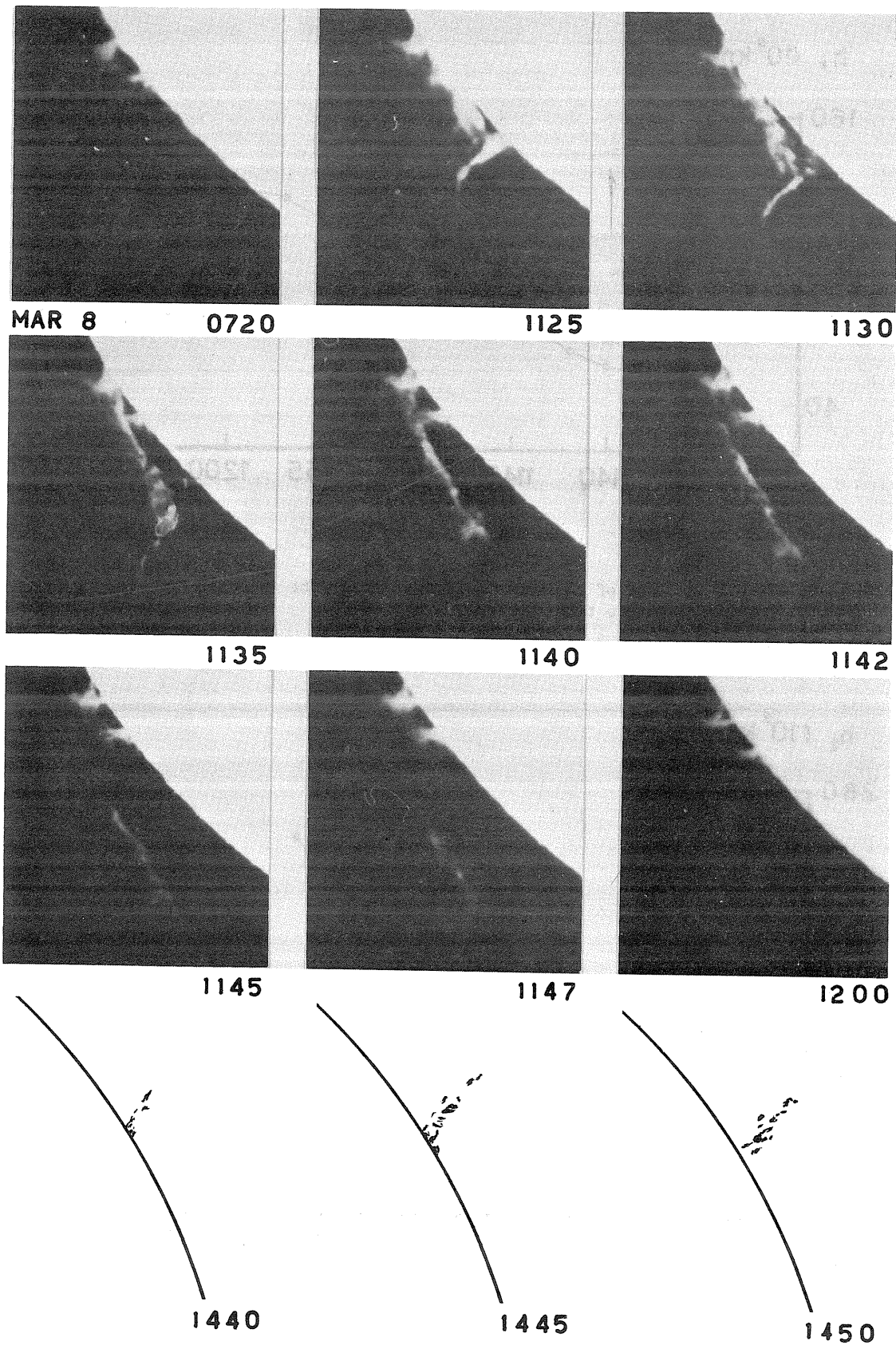


Fig. 1. Active prominences at limb on March 8, 1970, observed at Catania.

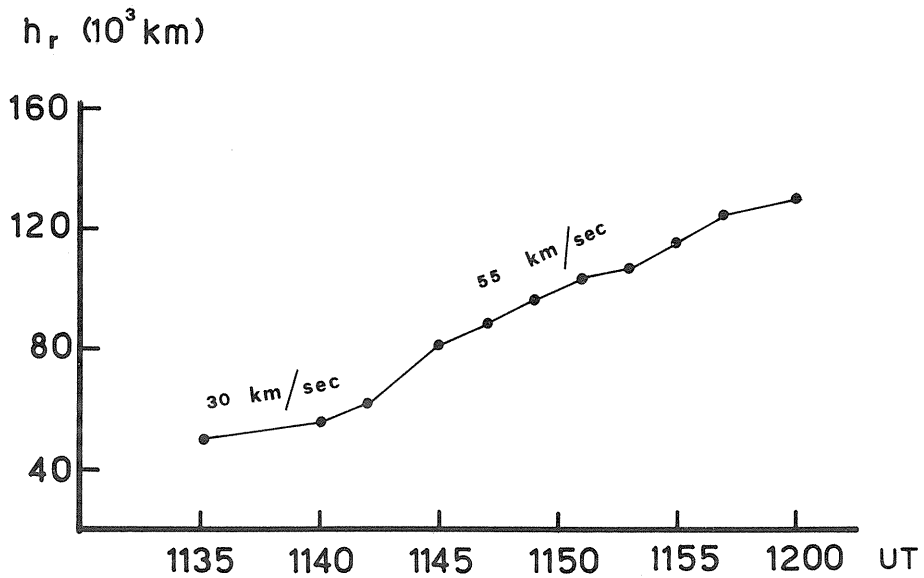


Fig. 2. Radial distance of the lowest south point of the detached prominence versus time.

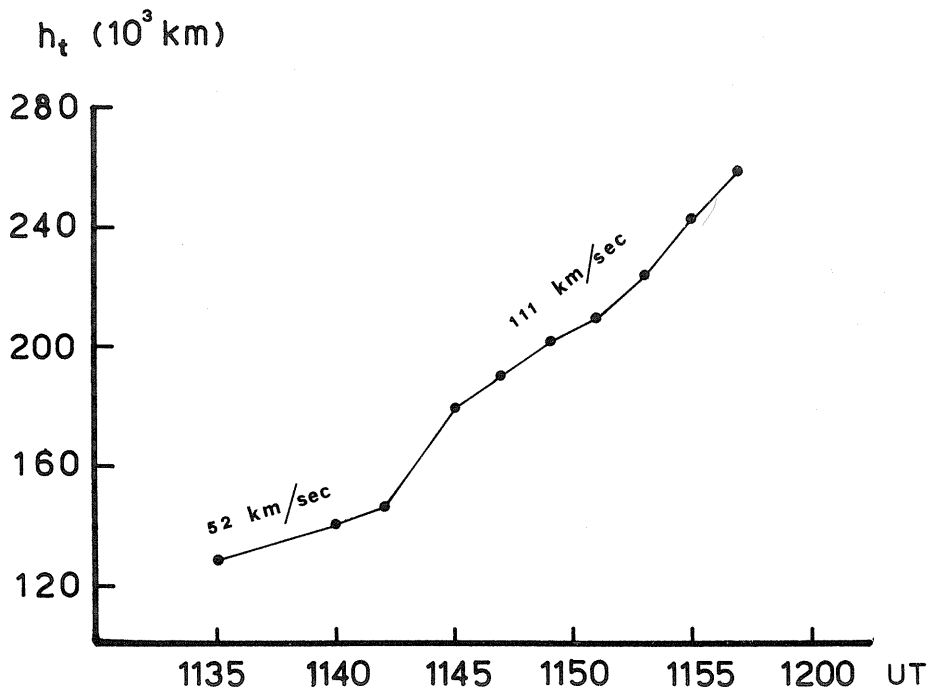


Fig. 3. Tangential distance of the lowest south point of the detached prominence versus time.

3. SOLAR RADIO PHENOMENA

"Summary of Worldwide Outstanding Solar Radio Emission Events - Fixed Frequency and Spectral"

by

Hope I. Leighton and J. Virginia Lincoln
Aeronomy and Space Data Center
National Oceanic and Atmospheric Administration, Boulder, Colorado

The tables are reprinted from "Solar-Geophysical Data". The outstanding events from the world-wide observatories reporting to World Data Center A are presented for March 6-8, 1970. The station abbreviations are explained in the table below.

Code Name	Station	Alternate Name	Geographic Lat	Long	Frequencies Reported (MHz)
<u>Fixed Frequencies</u>					
ABST	Abastumani		42N	43E	221
ARCE	Arcetri		44N	11E	9285, 1420
BERL	Berlin-Adlershof		52N	13E	9489, 2920, 1470
BORD	Bordeaux	Floriac	44N	01W	930
BOUL	Boulder		40N	105W	18 (Univ. of Colo.) 184 (ESSA)
CRIM	Simferopol	Crimea	44N	34E	3100
GORK	Gorky	Zimenki	56N	44E	9100, 3800, 2950, 650, 200, 100
HARS	Harestua	Blindern	60N	10E	225
HIRA	Hiraiso		36N	140E	500, 200
HUAN	Huancayo		12S	75W	9400
IRKU	Irkutsk	Siberian IZMIR	52N	104E	9570
IZMI	Moscow IZMIRAN	Krasnaja Pakhra	55N	37E	202
KIEL	Kiel		54N	10E	1420, 420, 240
KIEV	Kiev		50N	30E	204
KISV	Kislovodsk		43N	42E	15000, 6100
KODA	Kodaikanal		10N	77E	100
MANI	Manila		14N	121E	8800, 4995, 2695, 1415
MCMA	McMath-Hulbert		42N	83W	18
NERA	Nederhorst		52N	05E	9500, 3000, 610, 200
NEUS	Neustrelitz		53N	13E	9139, 1490
ONDR	Ondrejov		49N	14E	9400, 808, 536, 260
OTTA	Ottawa ARO	Algonquin	45N	78W	2800
PENN	Penn. State Univ.		41N	78W	10700, 2700, 960, 328
PENT	Penticton		49N	119W	2695
POTS	Potsdam	Tremsdorf	52N	13E	234, 111, 23
SANM	San Miguel		34S	58W	408
SAOP	Sao Paulo		22S	46W	7000
SLOU	Slough		51N	00E	71000, 19000, 2800
SGMR	Sagamore Hill	AFCRL	42N	72W	35000, 15400, 8800, 4995, 2695, 1415, 606, 245
TOKO	Tokyo	Mitaka	35N	139E	17000, 612
TRST	Trieste		46N	14E	239
TYKW	Toyokawa		34N	137E	9400, 3750, 2000, 1000
UCCL	Uccle	Humain	50N	04E	600
VORO	Voroshilov	Ussurisk	43N	132E	208
<u>Spectral</u>					
BOUL	Boulder (U. of Colo.)		40N	105W	7.6-80
CULG	Culgoora (C.S.I.R.O.)		30S	150E	8-222
HARV	Fort Davis		31N	104W	10-580
SGMR	Sagamore Hill (A.F.C.R.L.)		42N	71W	19-41
WEIS	Weissenau		48N	10E	30-1000

SOLAR RADIO EMISSION OUTSTANDING OCCURRENCES

MARCH 1970

MAR 1970	FREQUENCY STATION	TYPE	STARTING TIME	TIME OF MAXIMUM	DURATION	FLUX DENSITY $10^{22} \text{ Wm}^{-2} \text{ Hz}^{-1}$		INT	REMARKS	
			UT	UT	MINUTES	PEAK	MEAN			
5	600 UCCL	20	1158.5	1201.5	8.5	4.0	2.0			
	9500 BERL	46	1158.8	1201.5	21.7	14.0	3.6			
	4995 SGMR	4	1158.8	1201.5	6	56.0	23.5			
	3000 NERA	45	1158.1	1201.6	10	64.0	20.0			
	2950 GORK	3	1158.3	1201.7	7.3	23.0	8.6			
	1500 NEUS	4	1158.5	1201.8	19	27.0	4.4			
	1415 SGMR	4	1158.9	1201.6	4.9	25.6	13.4			
	950 GORK	1	1159.8	1201.8	4.9	5.4	2.2			
	245 SGMR	6	1159.2	1200.6	2.1	69.0	35.0			
	237 TRST	42	1159.6	1200.6	10.9	175.0				
	2800 SLOU	4	1159	1201.5	8	56.0				
	2695 SGMR	4	1159	1201.6	5.5	59.0	27.3			
	650 GORK	1	1200.9	1201.8	3.2	.9	0.4			
	9400 SLOU	4	1200	1201	4	24.0				
	111 POTS	45	1203 U	1254		160.0	OU			
	100 GORK	41	1208.3	1209.6	2.5	90.0				
	408 SANM	42	1254.6	1349	62.5	260.0	25.5			
	2800 OTTA	21	1305	1415	200	16.0	4.6			
	2800 OTTA	4	1318	1324.7	14	84.0	14.0			
	2800 OTTA	20	1320	1345	35	2.8	1.4			
	600 UCCL	3	1350.5		1	112.0	40.0			
	2800 OTTA	8	1417	1417.1	.5	7.6				
	237 TRST	41	1445.5	1445.8	.6	220.0				
	536 ONDR	45	1450	1450.5	2	115.0				
	2800 OTTA	1	1457.9	1458.1	.7	2.4	1.2			
	408 SANM	3	1555.3	1556.7	1.7	118.0	33.5			
	2700 PENN	24	1609	2037.4		31.0				
	10700 PENN	24	1616.6	1929.2		19.5				
	9400 HUAN	21	1617.6	1842.6	261.1	11.2	7.5			
	9400 HUAN	45	1618.1	1621.3	11.2	16.8	10.1			
	9400 HUAN	45	1618.1	1622.1		24.3				
	2800 OTTA	24	1618	1618	3	6.2				
	10700 PENN	3	1620.8	1621.4	8.2	19.7	5.1			
	960 PENN	8	1621.4	1621.4	.1	16.7				
	2800 OTTA	40	1621	1625.7	5	25.0				
	3000 NERA	5	1625.6	1625.8	.3	23.0	13.0			
	2700 PENN	3	1625.6	1625.8	.4	28.5	9.0			
	408 SANM	3	1645.7	1645.8	.5	820.0	260.0			
	2800 OTTA	20	1655 E	1700	30 D	2.8				
	2800 OTTA	21	1830	1925	115	5.0	2.5			
	15400 SGMR	1	1908.9	1911	2.9	6.5	3.3			
	10700 PENN	3	1908.5	1909.4	4.5	19.7	9.3			
	9400 HUAN	45	1908.2	1909.4	3.3	18.7	9.7			
	9400 HUAN	45	1908.2	1911		22.4				
	8800 SGMR	45	1908.5	1911	5.2	35.1	19.4			
	4995 SGMR	45	1908.4	1911	5.6	155.0	72.0			
	2800 OTTA	2	1908.7	1911	5	8.8	4.4			
	2700 PENN	3	1908.4	1910.9	7.8	12.2	4.9			
	2695 SGMR	3	1908.8	1911	5	9.3	4.7			
	9400 HUAN	29	1911.5	1911.5	70.2	15.0	11.2			
	8800 SGMR	29	1913.7	1913.7	51.3	13.3	6.7			
	4995 SGMR	29	1914	1914	51.1	15.0	7.5			
	2695 PENT	20	2035	2037	15	2.2	1.1			
	6	3750 TKYW	5	0234	0234.9	2	8.0	3.0		
		2000 TKYW	5	0234	0234.9	3	2.0	1.0		
		3750 TKYW	5	0237	0238.3	4	11.0	5.0		
		3750 TKYW	29	0241		45	3.0	1.0		
		3750 TKYW	5	0413.5	0414.3	1.5	2.0	1.0		
		3750 TKYW	5	0436	0438.3	9	6.0	2.0		
		100 GORK	44	0520 E		220		5.0		
100 GORK		6	0540.4	0540.7U	.8	40.0D				
3750 TKYW		5	0540	0547	30	6.0	2.0			
2000 TKYW		5	0546	0548	10	2.0	1.0			
100 GORK		41	0643.1	0644.5U	7	1000.0				
100 HIRA		45	0643.5	0644	1.5	390.0	100.0			
100 GORK		41	0715.4	0717.5	4	125.0				
3000 NERA		45	0745	0746.6	2.6	90.0	45.0			
2800 SLOU		4	0745.3	0746.5	1.7	142.0				
2695 MANI		4	0745.9	0746.3	1.6	88.0	41.8			
3100 CRIM		3	0746		32					
3100 CRIM		3	0746	0747	2	41.0	13.0			
600 UCCL		2	0748.5		.6	5.0				
3100 CRIM		29	0748	0756	30	14.0	5.0			
3000 NERA		5	0753	0757	27	11.0	6.0			
204 KIEV		44	0755	1035	255 D	100.0D	23.0			
221 ABST		3	0758.3	0856.3	61.3	29.0	2.0			
100 GORK		6	0758.4	0759.2U	1.3	120.0D	30.0			
100 GORK		6	0845	0845.4	.5	130.0				
606 MANI		4	0851	0851.3	.8	15.8	6.3			
8800 MANI		4	0851	0851.3	.8	15.1	7.5			
4995 MANI		3	0851	0851.3	.8	24.0	9.0			
2695 MANI		3	0851	0851.3	.8	14.6	6.3			
1415 MANI		3	0851	0851.3	.8	10.6	3.4			
111 POTS		40	0854.5	0857.8	3.4	800.0	16.0			
237 TRST		41	0856.3	0856.4	.4	460.0				
234 POTS		45	0856.4	0856.5	.2	100.0	15.0			
202 IZMI		6	0856.1	0856.6	1	200.0	35.0			
100 GORK			0900		180 D	140.0				
2950 GORK		21	0922	0939.7U	30	10.0				

SOLAR RADIO EMISSION OUTSTANDING OCCURRENCES

MARCH 1970

MAR 1970	FREQUENCY STATION	TYPE	STARTING TIME	TIME OF MAXIMUM	DURATION	FLUX DENSITY $10^{-22} \text{ Wm}^{-2} \text{ Hz}^{-1}$		INT	REMARKS
			UT	UT	MINUTES	PEAK	MEAN		
6	202 IZMI	6	0933.6	0936	4.5	30.0	20.0		
	4995 MANI	4	0933.2	0933.9	3.5	92.0	42.0		
	3000 NERA	45	0933.6	0934	11.5	725.0	225.0		
	2950 GORK	45	0933.5	0934.2	3.6	120.0			
	2950 GORK		0933.5	0934.9		64.0			
	2800 SLOU	47	0933.5	0934.2	8.3	750.0			
	2695 MANI	4	0933.2	0933.9	3.5	1140.0	215.0		
	1500 NEUS	46	0933.5	0934.3	9	30.0			
	1500 NEUS	46	0933.5	0941.3	9	33.0			
	1415 MANI	4	0933.2	0934.3	3.5	26.4	11.9		
	950 GORK	40	0934	0941.2	7.9	4.0			
	650 GORK	40	0934	0935.3	9	6.4			
	600 UCCL	22	0934	0942	35	7.0	2.0		
	9500 BERL	22	0934	0934.2	2.5	4.9	3.0		
	9400 SLOU	45	0934	0934.1	1	25.6			
	9100 GORK	1	0934.1	0934.3	3.2	15.0	4.0		
	3100 CRIM	3	0934		11	100.0D			
	111 POTS	40	0935.6	0935.7	1.5	2800.0	150.0		
	111 POTS	45	1013 U	1022.4U	119 U	200.0	40.0		
	111 POTS	40	1013.9	1016.4	6.1	1000.0	50.0		
	237 TRST	5	1015.1	1015.2	.2	155.0	40.0		
	600 UCCL	8	1016.8		.6	122.0	60.0		
	3100 CRIM	45	1019	1021	17	39.0	30.0		
	3100 CRIM		1019	1026		58.0			
	606 SGMR	40	1200.9	1211.2	26.1	91.0	30.0		
	600 UCCL	4	1200	1212	27.5	90.0	25.0		
	536 ONDR	45	1205	1301.5	22	120.0			
	408 SANM	27	1205	1213	25	34.5	13.0		
	260 ONDR	41	1220	1232.5	37	60.0			
	3000 NERA	5	1221.8	1224.5	20	10.0	5.0		
	1500 NEUS	20	1221.5	1229	21.5	3.6	2.4		
	23 POTS	40	1247.9	1248	1.3	4000.0	800.0		
	9400 HUAN	28	1317.2	1323.9	6.7	7.5	3.7		
	4995 SGMR	23	1318.5	1327.7	31.8	15.4	6.6		
	3000 NERA	45	1318.5	1319.6	8.5	90.0	20.0		
	2800 SLOU	3	1318.4	1324.6	11.7	76.0			
	2700 PENN	3	1318.5	1324.9	16.6	85.5	10.1		
	2695 SGMR	23	1319	1326.5	12.1	7.3	3.5		
	1415 SGMR	21	1319.5	1326.5	12.1	6.5	2.9		
	15400 SGMR	20	1320.3	1324.8	8.2	26.3	11.8		
	8800 SGMR	21	1320.8	1326.6	16.5	8.6	3.9		
	245 SGMR	6	1322.8	1323.3	1	135.0	18.0		
	10700 PENN	3	1323.9	1324.8	9.7	39.7	8.4		
	606 SGMR	46	1323.2	1324.3	2.5	40.3	18.0		
	9500 BERL	3	1323.5	1324.8	11	39.0	8.3		
	9400 HUAN	3	1323.9	1324.7	1.6	58.1	24.9		
	4995 SGMR	3	1323.6	1324.8	4.1	130.0	65.0		
	2695 SGMR	3	1323.9	1324.7	2.6	56.0	28.0		
	1500 NEUS	3	1323.3	1324.8	17.2	34.0	4.3		
	1415 SGMR	3	1323.8	1324.6	2.7	37.8	18.9		
	960 PENN	1	1324	1324.9	7.4	7.9	2.3		
	600 UCCL	2	1324.3	1324.5	1	12.0	6.0		
	9500 NERA	40	1324.2	1324.9	8	12.0			
	9400 SLOU	3	1324.8	1325.7	8	84.0			
	8800 SGMR	3	1324.1	1324.8	2.5	46.0	23.0		
	9400 HUAN	29	1325.5	1325.5	55.2	16.9	5.0		
	3000 NERA	29	1327		8	10.0	5.0		
	245 SGMR	20	1338.7	1406	54.1	110.0	55.0		
	234 POTS	45	1338	1400	53 U	50.0U			
	225 HARS	45	1340	1405	50	120.0	40.0		
200 NERA	27	1354.2	1406.5	24	130.0	80.0			
1500 NEUS	20	1404.5	1420.5	38.5U	4.3				
3000 NERA	5	1405	1415	30	11.0	5.0			
9500 BERL	20	1419.5E	1419.5		5.2				
111 POTS	40	1440.7	1449.7	9	1800.0	6.0			
23 POTS	40	1440.7	1449.8	9.5	4000.0	55.0			
606 SGMR	3	1449.1	1449.2	.8	14.7	7.3			
600 UCCL	3	1449.2		.4	18.0	6.0			
245 SGMR	7	1449.1	1449.8	1.2	290.0	7.0			
237 TRST	41	1449.2	1449.7	.9	1400.0				
2800 OTTA	20	1720	1735	50	2.2	1.1			
2800 OTTA	20	1825	1832	20	2.8	1.4			
606 SGMR	1	1836.7	1838	2.3	1.2	.6			
245 SGMR	6	1836.9	1839.8	3.4	92.0	7.2			
2700 PENN	24	1905	2030		12.9				
2800 OTTA	20	1910	1918	20	3.2	1.6			
100 HIRA	45	2109.5	2110.5	2	330.0D	60.0D			
100 HIRA	44	2243	0100						
7	606 MANI	1	0050.9	0051	.2	3.2	1.1		
	2695 MANI	3	0050.9	0051	.2	10.1	4.0		
	1415 MANI	1	0050.9	0051	.2	4.1	1.4		
	200 HIRA	45	0115.5	0120	8	380.0	30.0		
	208 VORO	40	0116	0122	7	192.0			
	100 HIRA	45	0116		7	340.0D	60.0D		
	1415 MANI	46	0138.6	0144.3	22.9	690.0	307.0		
	100 HIRA	45	0139.5		25.5	360.0D	150.0D		
	606 MANI	46	0141.5	0148.3	21	104.0	49.4		
	500 HIRA	45	0141	0148	19	110.0	25.0		
208 VORO	45	0141	0145	19	360.0	200.0			

PERCENT INC.

SOLAR RADIO EMISSION OUTSTANDING OCCURRENCES

MARCH 1970

MAR 1970	FREQUENCY STATION	TYPE	STARTING TIME	TIME OF MAXIMUM	DURATION	FLUX DENSITY $10^{-22} \text{ Wm}^{-2} \text{ Hz}^{-1}$		INT	REMARKS
			UT	UT	MINUTES	PEAK	MEAN		
7	200 HIRA	45	0141	0144	21	2100.0	50.0		
	3750 TKYW	45	0141	0145.2	135	73.0	12.0		
	3750 TKYW	5	0141	0155	135	30.0	11.0		
	2000 TKYW	45	0141	0145.2	30	410.0	40.0		
	9400 TKYW	45	0142	0158	135	45.0	14.0		
	9400 TKYW	5	0142	0155	135	40.0	13.0		
	8800 MANI	22	0142.2	0158.2	43	60.0	27.9		
	4995 MANI	4	0142.2	0144.4	12.4	87.0	40.6		
	2695 MANI	4	0142.2	0144.4	12.4	119.0	56.0		
	9400 TKYW	5	0143	0145	4	20.0	8.0		
	3750 TKYW	45	0143	0145.2	4	55.0	23.0		
	612 TOKO	45	0145.7	0148	3.5	67.0			
	1000 TKYW	45	0145	0155.2	20	116.0	40.0		
	3750 TKYW	5	0147	0148.2	3	5.0	2.0		
	3750 TKYW	45	0150	0152.8	5	6.0	4.0		
	4995 MANI	29	0154.6	0154.6	62.9	43.7	18.7		
	2695 MANI	29	0154.6	0154.6	62.9	30.2	14.1		
	9400 TKYW	5	0157.5	0158	1	5.0	2.0		
	3750 TKYW	5	0158	0158.3	2	6.0	2.0		
	1415 MANI	29	0201.5	0201.5	56	6.9	2.7		
	9400 TKYW	5	0209	0209.3	1	2.0	1.0		
	2000 TKYW	29	0211		110	9.0	5.0		
	9400 TKYW	45	0255	0258	25	5.0	2.0		
	3750 TKYW	5	0255	0300	25	2.0	1.0		
	2000 TKYW	5	0255	0305	25	2.0	1.0		
	100 GORK	44	0551		69		5.0		
	100 GORK	48	0551	0553.2	2.3	1400.0			
	650 GORK	3	0552.3	0552.4	.7	16.0	8.0		
	221 ABST		0600	0722.3	180	41.0			
	950 GORK	1	0607.3	0607.4	.3	4.9	2.4		
	650 GORK	1	0607.3	0607.9	1.7	1.6	0.7		
	100 GORK	41	0607.2	0608 U	5.6	40.0D			
	100 GORK		0607.2	0612.3		40.0			
	3100 CRIM	20	0608		112				
	3100 CRIM	20	0608	0636	112	49.0	15.0		
	9400 TKYW	5	0610	0635	70	8.0	4.0		
	3750 TKYW	5	0610	0635	70	9.0	4.0		
	2000 TKYW	5	0610	0635	70	5.0	3.0		
	100 GORK	6	0633.5	0635.1U	1.9	50.0D			
	100 GORK	6	0645.1	0645.8U	.9	40.0D			
	950 GORK	2	0646.4	0646.6	.6	3.5	1.4		
	111 POTS	45	0656.3	0658.2	2.7	200.0	10.0		
	100 GORK	48	0656.4	0658.8	3.4	1800.0			
	23 POTS	5	0707.7	0707.8	.6	4000.0	1500.0		
	100 GORK	6	0708.2	0708.3	1	50.0			
	237 TRST	41	0720.7	0723.8	4.2	420.0			
	234 POTS	45	0720.8	0723.8	3.7	200.0	10.0		
	202 IZMI	48	0720	0722.3	4.8	800.0	350.0		
	200 HIRA	45	0720	0722	5	610.0	45.0		
	200 NERA	45	0720.3	0722	4.7	575.0	250.0		
	111 POTS	45	0720.2	0722.5	4.6	1200.0	120.0		
	100 HIRA	45	0720	0723	5.5	450.0D	130.0D		
	950 GORK	46	0721.9	0722.6	2.8	70.0			
	950 GORK		0721.9	0722.8		46.0			
	650 GORK	46	0721.9	0722.5	3.1	39.0			
	650 GORK		0721.9	0724.1		46.0D			
	610 NERA	45	0721.5	0724	3	140.0	25.0		
	100 GORK	48	0721	0723.5	4.7	20000.0			
	606 MANI	4	0722	0723.9	5	172.0	55.0		
	600 UCCL	4	0722	0724	3	81.0	25.0		
	500 HIRA	45	0722.1	0724	2.5	150.0	25.0		
	23 POTS	45	0722.1	0722.8	3.8	25000.0	3000.0		
	4995 MANI	4	0722	0723.9	5	9.6	3.2		
	3750 TKYW	45	0722	0722.3	3	10.0	3.0		
	3000 NERA	45	0722	0723.9	2.1	17.0	6.0		
	2950 GORK	40	0722.2	0724.1	2.4	13.0			
	2695 MANI	4	0722	0722.3	5	16.1	8.0		
	2000 TKYW	45	0722	0723.8	3	75.0	10.0		
	1500 NEUS	46	0722	0724	9 U	154.0			
	1415 MANI	4	0722	0722.3	5	226.0	54.0		
	1000 TKYW	45	0722	0722.3	3	120.0	15.0		
	3100 CRIM	3	0723	0724	2	49.0	12.0		
	100 GORK	44	0736		220 D		10.0		
	950 GORK	1	0816.8	0817.1	.6	9.2	5.6		
	234 POTS	40	0816	0826.1	18.6	175.0	1.0E		
	202 IZMI	6	0816.8	0817.2	2	1100.0	600.0		
	111 POTS	40	0816	0826.1	24.8	1400.0	20.0		
	100 GORK	48	0816	0817	3.5	1300.0			
	100 HIRA	45	0816	0818	5	450.0D	110.0D		
	23 POTS	40	0816.2	0817.3	24.5	4000.0	100.0		
	1500 NEUS	1	0817 E	0817		3.1			
	1500 NEUS	1	0819 E	0819		2.2			
	1500 NEUS	1	0823.8E	0823.8		1.3			
	950 GORK	1	0825.9	0826.1	.7	3.2	1.4		
	650 GORK	1	0825.6	0826.1	1.8	2.0			
	202 IZMI	6	0825.4	0826.1	1.2	150.0	30.0		
	200 NERA	45	0825.8	0826.1	.6	400.0	200.0		
	600 UCCL	40	0833.3	0839.8	11	27.0	5.0		
	100 GORK	6	0833.3	0834.8	1.7	1600.0			
	950 GORK	1	0834.4	0834.7	.5	1.4	0.7		

SOLAR RADIO EMISSION OUTSTANDING OCCURRENCES

MARCH 1970

MAR 1970	FREQUENCY STATION	TYPE	STARTING TIME	TIME OF MAXIMUM	DURATION	FLUX DENSITY $10^{-22} \text{ Wm}^{-2} \text{ Hz}^{-1}$		INT	REMARKS
			UT	UT	MINUTES	PEAK	MEAN		
7	650 GORK	41	0834.1	0837.2	6.5	8.7			
	650 GORK		0834.1	0839.8		19.0			
	1500 NEUS	2	0836.6E	0836.6		3.5			
	950 GORK	1	0837.1	0837.2	.4	3.5			
	606 MANI	4	0838.5	0839.7	3	21.8	1.7		
	4995 MANI	4	0838.5	0838.9	3	9.6	10.9		
	2695 MANI	2	0838.5	0838.9	3	6.0	3.2		
	1415 MANI	4	0838.5	0839.7	3	8.0	2.0		
	950 GORK	4	0839.3	0839.8	.8	26.0	8.7		
	2950 GORK	1	0839.6	0839.9	.7	2.5			
	1500 NEUS	2	0839	0839.7	1	7.7	1.3		
	204 KIEV	44	0840 E	1100 U	380 D	80.0D	31.0		
	650 GORK	3	0953.2	0953.8	.8	4.3			
	600 UCCL	41	0953	0955	2.1	20.0	4.0		
	111 POTS	45	0953.3	0953.3	.6	300.0	40.0		
	23 POTS	45	0953.5	0953.6	.5	1500.0	375.0		
	650 GORK	3	0954.9	0955	.4	9.9			
	950 GORK	1	1045.6	1045.7	.3	7.0	3.5		
	650 GORK	1	1045.5	1046.3	1.2	1.3	0.6		
	100 GORK	24	1045		30 D	200.0			
	950 GORK	40	1055.3	1056.1	2.5	6.9			
	600 UCCL	4	1055.5	1056.5	1.3	12.0	3.0		
	100 GORK	6	1055.8	1056.4	1	800.0	200.0		
	650 GORK	4	1056.7	1058.3	3	8.6			
	111 POTS	45	1056	1056.1	.3	300.0	75.0		
	600 UCCL	4	1103.3	1103.6	3.5	12.0	2.0		
	1500 NEUS	20	1104.5	1130.5	66	2.8	1.3		
	3000 NERA	27	1110	1129.2	65	20.0	10.0		
	245 SGMR	44	1115 E		240 D				
	2800 SLOU	20	1117	1124.8	53	173.0			
	9500 BERL	21	1121.5	1126.3	41.5	30.0	7.3		PERCENT INC.
	9500 NERA	5	1121.8	1127.3	9.5	11.0	5.0		
	3000 NERA	45	1121.9	1124	6.3	23.0	13.0		
	9400 SLOU	21	1122	1129	42	8.0			
	9400 SLOU	3	1124	1126	2	34.0			
	9500 NERA	5	1126	1126.4	.7	10.0	5.0		PERCENT INC.
	1500 NEUS	20	1217.5	1230.5	20	2.6	1.3		
	240 KIEL	44	1346 E	1346		2000.0	20.0		
	23 POTS	5	1349.3	1349.5	.7	6000.0	2000.0		
	23 POTS	5	1408.2	1408.4	.5	1500.0	500.0		
	9500 NERA	5	1548.8	1549.3	1.2	13.0	6.0		PERCENT INC.
	2800 OTTA	21	1550	1615	60 D	24.0			
	3000 NERA	28	1555		10	22.0	10.0		
	4995 SGMR	4	1600.8	1606.6	8	145.0	70.0		
	2695 SGMR	4	1600.4	1606.7	9.6	110.0	55.0		
	1415 SGMR	4	1600.5	1607.4	8.5	105.0	52.0		
	15400 SGMR	3	1602.4	1606.5	6.6	33.5	16.0		
	606 SGMR	3	1602.9	1607.8	7	8.1	4.0		
	8800 SGMR	4	1604.8	1606.5	3.7	59.0	28.0		
	2800 SLOU	3	1604	1606	6	110.0			
2800 OTTA	4	1604.5	1606.5	8	125.0	33.0			
9500 NERA	45	1605	1606.7	2.4	13.0	7.0		PERCENT INC.	
9400 SLOU	3	1605	1607	5	76.0U				
3000 NERA	45	1605	1606.9	3.3	110.0	55.0			
600 UCCL	2	1606.8	1607.5	1.8	10.0	4.0			
9500 NERA	29	1607.4	1607.5	40.5	11.0	6.0		PERCENT INC.	
8800 SGMR	29	1608.5	1608.5	21.5D	27.3	13.0			
4995 SGMR	29	1608.8	1608.8	21.2D	50.0	25.0			
3000 NERA	29	1608.3		82 D	38.0				
15400 SGMR	29	1609	1609	21 D	17.0	8.0			
1415 SGMR	29	1609	1609	21 D	17.2	8.0			
2695 SGMR	29	1610	1610	20 D	22.9	11.0			
200 NERA	40	1651.4	1653.1	12	900.0				
600 UCCL	3	1652.5		.5	18.0				
606 SGMR	4	1731	1732.7	2.4	52.7	20.3			
3750 TKYW	5	2347	2349	5	3.0	1.0			
2000 TKYW	45	2348	2349	3	4.0	2.0			
8	9400 TKYW	5	0037	0037.8	3	6.0	2.0		
	3750 TKYW	5	0037	0037.8	6	3.0	2.0		
	3750 TKYW	5	0103	0120	30	4.0	2.0		
	9400 TKYW	5	0108	0109	10	12.0	3.0		
	3750 TKYW	5	0108	0109	2	4.0	1.0		
	3750 TKYW	5	0150	0151.2	6	5.0	2.0		
	2000 TKYW	5	0150	0151.3	6	3.0	1.0		
	9400 TKYW	5	0151	0151.2	1	2.0	1.0		
	9400 TKYW	5	0325	0326.2	3	5.0	2.0		
	3750 TKYW	5	0325	0326.4	4	5.0	2.0		
	9400 TKYW	5	0350.5	0351	9	13.0	3.0		
	3750 TKYW	5	0350.5	0351.2	9	4.0	1.0		
	9400 TKYW	5	0447	0447.7	3	12.0	3.0		
	9400 TKYW	5	0510	0510.7	2	4.0	2.0		
	221 ABST		0600	0654.4	180	35.0			
	100 GORK	44	0630		330 D		25.0		
	100 GORK	24	0645	0752.8	120	2000.0			
	100 GORK	48	0657.8	0659.4	2.6	2500.0D			
	100 GORK		0657.8	0659.9U		2500.0D			
	200 HIRA	45	0658	0659.8	2	230.0	45.0		
111 POTS	45	0658	0659.9	2.9	4400.0	150.0			
100 HIRA	45	0658	0659	3	340.0D	60.0D			

SOLAR RADIO EMISSION OUTSTANDING OCCURRENCES

MARCH 1970

MAR 1970	FREQUENCY STATION	TYPE	STARTING TIME	TIME OF MAXIMUM	DURATION	FLUX DENSITY $10^{22} \text{ Wm}^{-2} \text{ Hz}^{-1}$		INT	REMARKS
			UT	UT	MINUTES	PEAK	MEAN		
8	23 POTS	45	0658.9	0659.9	2.3	10000.0U	1000.0U		
	950 GORK	1	0659.6	0700	1.2	8.8	3.0		
	650 GORK	3	0659.6	0700	1.3	9.3			
	606 MANI	4	0659.1	0700	3.4	11.6	5.3		
	600 UCCL	1	0659.5	0659.7	.6	10.0	5.0		
	500 HIRA	45	0659.7	0659.7	.3	70.0			
	237 TRST	42	0659.3	0700.2	5.5	2030.0			
	234 POTS	45	0659.8	0659.8	.2	1200.0	250.0		
	200 NERA	45	0659.3	0659.9	1.5	250.0	85.0		
	4995 MANI	3	0659.1	0700	2.9	9.5	3.2		
	3750 TKYW	5	0659.8	0700	.6	10.0	3.0		
	2950 GORK	3	0659.8	0700	.6	14.0	6.3		
	2695 MANI	3	0659.1	0700	2.9	17.0	6.4		
	2000 TKYW	5	0659.8	0700.1	.6	6.0	2.0		
	1415 MANI	1	0659.1	0700	2.9	6.6	2.6		
	1000 TKYW	5	0659.8	0700.1	.6	9.0	3.0		
	204 KIEV	44	0700 E	0730 U	410	44.0	19.0		
	200 HIRA	45	0702.5	0703.5	2	50.0	15.0		
	100 HIRA	45	0702.5		2	330.0D	110.0D		
	950 GORK	1	0703	0703.4	.9	1.3	0.6		
	650 GORK	3	0703.3	0703.6	1.4	9.0			
	600 UCCL	1	0703.4	0703.6	.7	10.0	5.0		
	500 HIRA	45	0703.5	0703.6	2	20.0	5.0		
	2950 GORK	1	0703.3		2.7	3.2	2.5		
	2950 GORK	1	0708.3	0708.9	2.1	4.4	2.2		
	9400 TKYW	5	0716	0716.5	2	15.0	3.0		
	9100 GORK	1	0716.2	0716.7	1.8	23.0	9.0		
	8800 MANI	4	0716	0716.6	3.7	7.9	3.9		
	4995 MANI	3	0716	0716.6	3.7	25.4	9.5		
	3750 TKYW	5	0716	0716.7	2	75.0	20.0		
	3000 NERA	5	0716.2	0716.5	.8	18.0	9.0		
	2950 GORK	3	0716.2	0716.6	1.2	26.0	6.3		
	2695 MANI	4	0716	0716.6	3.7	8.2	4.1		
	111 POTS	40	1028.2	1028.2	8.9	200.0	2.0		
	111 POTS	45	1121.4	1121.8	.3	200.0	30.0		
	23 POTS	45	1240.8	1240.9	.4	2000.0	500.0		
	600 UCCL	1	1309.8		.3	20.0	4.0		
	111 POTS	45	1309.8	1310	.3	4000.0	500.0		
	23 POTS	45	1309.9	1310.1	.5	4000.0	1000.0		
	23 POTS	40	1334	1334.9	1.7	3500.0	400.0		
	245 SGMR	6	1412	1438.3	60.9	36.1	16.8		
	606 SGMR	22	1422.7	1435.2	71.4	14.1	6.4		
	600 UCCL	22	1422.5	1435	70	16.0			
	2800 OTTA	20	1428	1500	70	5.4	2.7		
	808 ONDR	45	1429	1430	3.5	3.0			
	2800 OTTA	20	1550	1620	120	4.8	2.4		
	2700 PENN	24	1924	2109.3		7.6			
	2695 PENT	2	2003.5	2004.5	1.5	3.2	1.6		
	2700 PENN	8	2004.5	2004.5	.4	57.1			
	9	3750 TKYW	5	0020	0104	80	7.0	3.0	
9400 TKYW		5	0240	0243.5	10	4.0	2.0		
612 TOKO		45	0340.2	0340.4	.6	81.0			
606 MANI		3	0340	0340.6	2.5	104.0	32.7		
500 HIRA		45	0340	0340.5	1	540.0	240.0		
200 HIRA		45	0340.2	0340.5	.7	60.0	20.0		
100 HIRA		45	0340	0340.4	1	340.0D	100.0D		
4995 MANI		1	0340	0340.4	2.5	5.8	2.9		
3750 TKYW		5	0340	0340.6	2	7.0	2.0		
2695 MANI		3	0340	0340.8	2.5	9.9	3.9		
2000 TKYW		5	0340	0340.8	3	12.0	3.0		
1415 MANI		1	0340	0340.7	2.5	5.6	2.8		
1000 TKYW		5	0340	0340.5	1.5	15.0	5.0		
2000 TKYW		5	0415	0421	45	7.0	2.0		
9400 TKYW		5	0416	0423	55	4.0	2.0		
3750 TKYW		5	0416	0423	35	3.0	1.0		
200 HIRA		45	0526.5	0526.5	.5	300.0	90.0		
100 GORK		6	0526.7	0526.9	.6	30.0D			
9400 TKYW		45	0530	0540	40	5.0	3.0		
3750 TKYW		5	0530	0537	40	4.0	2.0		
2000 TKYW		5	0530	0537	40	7.0	2.0		
100 GORK		6	0532.8	0532.9	.7	20.0			
100 GORK		6	0554.1	0554.4U	.8	30.0D			
221 ABST			0652.3	0655.4	6	25.0	5.0		
200 HIRA		45	0658	0701	10	350.0	5.0		
100 GORK		6	0658.1	0701.5	5.6	30.0D			
9500 BERL		3	0733.2E	0733.2		15.0			
204 KIEV		48	0827.9	0829.7	3.2	90.0D			
204 KIEV		6	0911.9	0912.6	.7	90.0D			
260 ONDR		45	0930	0933	5	100.0			
536 ONDR		5	0933	0933	1	95.0			
100 GORK		6	1024.4	1025	1	20.0			
100 GORK		6	1218.3	1218.5	.5	30.0D			
4995 SGMR		3	1300.5	1301.6	4.3	34.3	11.4		
3000 NERA		5	1300	1301.6	3.4	14.0	6.0		
2800 OTTA		3	1300	1301.5	3	10.0	4.8		
2695 SGMR		3	1300.5	1301.6	4.3	7.5	2.8		
9500 BERL		21	1301.5E	1301.5		6.2			
9100 GORK		1	1301.1	1301.9	1.7	13.0	4.0		
8800 SGMR		1	1301.4	1301.6	3.9	4.4	1.5		

SOLAR RADIO EMISSION SPECTRAL OBSERVATIONS

MARCH 1970

MAR 1970	TIMES OF OBSERVATION		STATION	EVENTS									SPECTRAL TYPE							
				DECIMETRIC BAND			METRIC BAND			DEKAMETRIC BAND										
	START UT	END UT		INT.	START UT	END UT	INT.	START UT	END UT	INT.										
05	0000	0029	HARV				0000	0029	1									I		
		0817	CULG				0000	0723	1									I		
			CULG				0000	0813.5	1									IIIN		
			HARV				0026	0027	1									IIIG		
			CULG				0026	0535	1									IIIG,N,W		
			HARV	0028	0029	1	0028	0029	2									IIIGG		
			CULG				0149		1									IIIB,U		
			CULG				0549		1									IIIB,U		
			WEIS				0827.6	0827.8	1									IIIB		
		0945	1633	WEIS			1024.7	1024.9	1									IIIB		
				WEIS			1038	1505	1									IS		
				WEIS			1159.8	1208.4	2									IIIG,DP		
				WEIS			1209.7	1210.3	1									IIIG		
		1330	2400	HARV	1350	1351	1	1342	1448	1								I		
				WEIS				1350.3	1350.8	1									IIIG,DP,RS	
				HARV				1448	1520	1								IN		
				HARV				1625	1626	3	1625	1626	3					IIIG		
				WEIS				1625.6	1625.8	3								IIIB		
		1100	2315	SGMR							1625.6	1626.3						IIIB		
				HARV				1800	2400	1								IN		
				HARV				1803	1911	1								IIIN		
				SGMR										1909.9	1911.8			IIIG		
				HARV				1918	1920	1								IIIG		
		1712	2400	BOUL										2014.7	2015	1		III		
				BOUL										2057.3	2058	1		III		
		1948	2220	CULG				2127.5	2359	1								IIIG,N		
				HARV				2128	2129	1								IIIG		
				BOUL										2128.4	2128.9	1		III		
				BOUL										2155.9	2156.3	1		III		
				HARV				2156	2329	1								IIIN		
				BOUL				2200.5	2201.7	3	2200.5	2201.7	3					IIIG		
				HARV				2201	2202	2								IIIG		
				BOUL				2220.8	2221.3	1	2220.8	2221.3	1					III		
		2225	2400	CULG																
				BOUL				2256.8	2313	1	2256.8	2313	1					CONT		
				BOUL				2300.2	2302.4	3	2300.2	2302.4	3					IIIG		
				HARV	2302		1	2300	2302	2								IIIGG		
				BOUL				2309	2312.3	3	2309	2312.3	3					IIIG		
				BOUL				2327.1	2327.6	3	2327.1	2327.6	3					III		
				BOUL				2358	2358.3	1	2358	2358.3	1					III		
	06	0000	0817	CULG				0007	0815	1									IIIN	
			0030	HARV				0010	0023	1									IN	
				CULG				0013	0759.5	1									IIIG,N	
				HARV				0014	0018	2									IIIGG	
			0000	0104	BOUL			0015.1	0023.9	2	0015.1	0023.9	2						IIIG	
					CULG				0138	0138.5	1									IIIG,V,U
					CULG				0644	0647	1									IIIG,U
			0634	1639	WEIS				0644	0644.5	1									UNCLF
				WEIS				0717.2	0717.6	1									IIIG	
				WEIS				0758	1545	1									IS	
				WEIS				0758.5	0759.5	1									IIIG,DP	
				WEIS				0820.2	0821	2									UNCLF	
				WEIS				0838.2	0838.5	1									IIIB	
				WEIS				0844.8	0845.5	1									IIIG	
				WEIS				0856.4	0858	2									IIIG	
				WEIS				0931.5	0932.5	2									IIIG	
				WEIS				0931.5	0955	2									UNCLF	
				WEIS				1007.3	1007.7	1									IIIG	
				WEIS				1014	1020	1									IIIGG	
		1100	2315	SGMR										1220	1222.2				IIIG	
				WEIS				1247.8	1249	2									IIIG	
				SGMR										1248	1249.3				IIIG	
				WEIS				1258.4	1258.6	2									IIIB	
		1332	0057	BOUL				1337 E	1500	2				1337 E	1500	2			CONT	
				SGMR										1338	1338.6				IIIB	
				SGMR										1338.6	1530				CONT	
		1330	2400	HARV				1355	1415	2									IV	
				HARV				1356	1357	1									IIIG	
				WEIS										1437	1437.8				IIIB	
				BOUL				1438	1514	1									III,GG	
				BOUL				1438.2	1441.4	3	1438.2	1441.4	3						IIIG	
				SGMR										1439	1440.3				IIIB	
				HARV				1440	1441	2									IIIG	
				WEIS				1440.6	1441.3	3									IIIG,DP	
				HARV	1442	1542	1	1400	2246	1									IN	
				SGMR										1448.9	1451				IIIG	
				HARV	1449	1450	1	1449	1451	2	1449	1450	2						IIIG	
				WEIS				1449	1450	3									IIIG,DP	
				BOUL				1449.1	1451.2	3	1449.1	1451.2	3						IIIG	
				HARV				1454	1458	1									IIIGG	
				BOUL				1512.6	1514	1	1512.6	1514	1						IIIG	
				SGMR							1512.6	1514	1						IIIB	
				BOUL				1617.7	1618.8	2	1617.7	1618.8	2						IIIG	
				BOUL				1618		2	1618		2						IIIG	
				HARV				1653	2246	2									IIIN	
				BOUL							1836.2	1841.2	2						IIIG	
				SGMR							1836.6	1837.5	2						IIIB	
				HARV	1837		1	1836	1841	2									IIIGG	

SOLAR RADIO EMISSION SPECTRAL OBSERVATIONS

MARCH 1970

MAR 1970	TIMES OF OBSERVATION		STATION	EVENTS									SPECTRAL TYPE				
				DECIMETRIC BAND			METRIC BAND			DEKAMETRIC BAND							
	START UT	END UT		INT.	START UT	END UT	INT.	START UT	END UT	INT.							
06	1948	2400	SGMR							1840.6	1841.6		IIIB				
			SGMR							1934.3	1934.9		IIIB				
			SGMR							1946	1946.5		IIIB				
			CULG				2040	2331	1					IIIG,N			
			HARV				2057	2059	2					UNCLF			
			HARV	2110	2111	1	2110	2117	2	2110	2114	2		IIIG			
			CULG				2110	2115	2					IIIG			
			BOUL				2110.3	2114.1	3	2110.3	2114.1	3		IIIG			
			SGMR							2110.4	2111.6			IIIB			
			SGMR							2113.4	2114			IIIB			
			CULG											I			
			BOUL				2141	2245	1					I			
			HARV				2210.9	2219	3	2210.9	2219	3		IIIG			
			HARV	2218		2	2213	2219	2	2218		1		IIIGG			
			CULG	2218	2219	1								IIIG,U			
			HARV				2232	2233	1					U			
			BOUL				2232.3	2232.7	2	2232.3	2232.7	2		III			
			CULG				2245	2400	2					I			
			BOUL				2245.6	2246.2	2	2245.6	2246.2	2		III			
			HARV				2246	2400	2					I,DC			
			BOUL				2313	0000	D 1					CONT			
			07	0000 0000	0031 0802	HARV				0000	0029	1				I,DC	
						CULG				0000	0613	1				I	
						CULG				0000	0817.5	1				IIIN	
						HARV				0015	0016	1				IIIG	
						CULG				0015	0817.5	1				IIIG,N	
						HARV				0019	0023	1				IIIGG	
						CULG				0115	0122	1				IIIG	
						CULG	0144	0145	1	0139	0148	1	0140	0146	1		IIIGG
						CULG				0146	0150	1					II
						CULG				0156	0158	1					IIIG,V
						CULG				0224	0303	1					I
						CULG	0536	0537	1								IIIG
CULG	0551.5	0553				1								IIIG			
0630	1638	WEIS							0634	1446	2				IS		
		WEIS							0656	0700	1				IIIGG,DP		
		WEIS							0707.5	0708	2				IIIG		
		WEIS							0720.2	0725	3				IIIGG,DP		
		CULG				0723.5	0724	1	0720	0725	1				IIIGG,V		
		WEIS							0816	0819	2				IIIGG,DP		
		WEIS							0825.8	0826.4	3				III		
		WEIS							0833.5	0841	2				IIIGG,RS		
		WEIS							0953	0954	2				IIIG		
		SGMR										1152	1154			IIIG	
		SGMR										1217.2	1217.7			IIIB	
		1330				2400	HARV				1336	1440	1				I
							HARV	1349	1350	1	1349	1350	1				IIIGG
							WEIS				1349.2	1349.8	1				IIIG
		SGMR										1349.2	1350			IIIB	
SGMR										1433.2	1433.8			IIIB			
WEIS							1433.3	1434	1					IIIG			
1318	0058	BOUL							1433.4	1433.7	1	1433.4	1433.7	1		III	
		HARV							1440	1620	1				IN		
		HARV				1604	1608	1							I		
		HARV	1652	1653	1	1651	1656	2	1654		2	IIIGG					
		BOUL				1653.5	1654.1	2	1653.5	1654.1	2		III				
		SGMR							1653.7	1654.5			IIIB				
HARV	1700	1701	1	1659	1703	2					IIIG						
HARV				1724	1819	1					IN						
1948	2400	BOUL							1732.3	1733.2	1		IIIG				
		CULG				2032.5	2346	1				IIIN					
		HARV				2249	2250	2	2249	2250	2		IIIG				
		CULG				2249	2250	2					IIIG				
		BOUL				2249.3	2249.6	2	2249.3	2249.6	2		III				
		BOUL				2345.1	2345.3	1					III				
08	0000 0000 0628	0032 0816 1600	HARV				0008	0815	1				IIIN,W				
			CULG				0633	1530	1				IN				
			WEIS				0655	0803	1				IW				
			WEIS				0658	0704.3	3				IIIGG				
			CULG	0659	0700	1	0653	0706	1				IIIGG				
			SGMR							1309.7	1310.8			IIIB			
			WEIS				1309.8	1310.4	3					IIIG,RS			
			WEIS				1333.9	1335.3	2					IIIGG			
			SGMR							1334	1336			IIIG			
			SGMR							1420	1700			IV			
			1330	2400	HARV				1427	1600	2				I		
					HARV	1434	1506	1							I		
					BOUL				1434	1800	D 2	1434	1800	D 2		CONT	
			HARV				1557	1558	2	1557	1558	1		IIIG			
			HARV				1600	1700	1					I			
			HARV				1642	2021	1					IIIN			
			BOUL				1646.4	1648	3	1646.4	1648	3		IIIG			
			SGMR							1646.7	1648.3			IIIB			
			HARV				1647	1648	2	1647	1648	2		IIIG,V			
			1948	2400	HARV				1700	1939	1	1726	1740	1		IN	
					CULG				2021.5		1				IIIB,W		
					CULG				2152	2345	1				I		

SOLAR RADIO EMISSION SPECTRAL OBSERVATIONS

MARCH 1970

MAR 1970	TIMES OF OBSERVATION		STATION	EVENTS									SPECTRAL TYPE			
				DECIMETRIC BAND			METRIC BAND			DEKAMETRIC BAND						
	START UT	END UT		START UT	END UT	INT.	START UT	END UT	INT.	START UT	END UT	INT.				
08	2052	0000	HARV	2204		2	2204		1					IIIG		
			CULG	2204	2205	1	2201	2400	1					IIIN		
			CULG				2210	2300	1					IIIGG		
			HARV				2215	2216	2					IIIG		
			HARV				2223	2258	2					I		
			BOUL				2235	2305	D 1					CONT		
			CLRO				2242	2259	1					CONT		
			HARV				2253	2258	2					IIIGG		
			BOUL				2254.1	2256.9	2	2254.1	2256.9	2			IIIG	
			CLRO				2254.3	2255	2	2254.3	2255	2			IIIG	
HARV				2302		2						IIIG				
09	0000 0000	0033 0802	HARV				0007.5	0718	1					IIIN		
			CULG				0129	0130	1					IIIG		
			CULG	0129	0130	1	0340	0341	1	0340.5	0341	1		IIIG		
			CULG	0339	0341	1	0448	0502	1	0449.5	0550	1		IIIGG		
			CULG	0526.5	0527	1	0526.5	0527	1	0526.5	0527	1		IIIG		
			WEIS				0659.8	0702	1						IIIG	
			CLRO													
			BOUL							1748.7	1749.1	2	1748.7	1749.1	2	III
			SGMR							1748.8	1749.4	2	1748.8	1749.4	2	IIIB
			BOUL							1754.6	1755.5	2	1754.6	1755.5	2	III
10	0000 0000 0625	0034 0815 1644	HARV													
			CULG				0222.5	0810.5	1					IIIG,N		
			WEIS				0810.2	0810.6	1					IIIB		
			WEIS				0820.8	0821.5	1					IIIG		
			WEIS				0837	0842	2					IIIGG		
			WEIS				0912	0912.7	1					IIIG,DP		
			WEIS				0918.2	0938	2					IIIGG		
			WEIS				1002	1004.5	1					IIIG		
			WEIS				1101.6	1114.5	1					IIIGG		
			HARV	1330	2400	1340	1	1338	1340	1					IIIGG	
HARV					1346	1347	2					IIIGG				
WEIS					1346.2	1347.3	1					IIIG				
SGMR								1346.6	1347.6			IIIB				
HARV					1407	1408	1					IIIG				
HARV					1411	1412	1					U				
WEIS	0625	1644			1411.3	1411.5	1					UNCLF				
HARV					1440	1441	1					U				
HARV					1455	1456	2					IIIG				
SGMR								1455.8	1456.4			IIIB				
HARV					1459	1500	2					IIIG				
HARV					1516	1931	1	1652	1921	1		IIIN				
SGMR								1516	1516.8			IIIB				
BOUL	1318	0100			1651.6	1651.9	2	1651.6	1651.9	2		III				
SGMR								1651.6	1652.2			IIIB				
CLRO	1605	0000			1651.8	1652.2	2	1651.8	1652.2	2		III				
SGMR								1704.3	1705			IIIB				
BOUL					1704.4	1708	2	1704.4	1708	2		IIIG				
HARV					1707	1708	2	1707	1708	2		IIIG				
SGMR								1707.4	1708			IIIB				
BOUL								1740	1835	1		CONT				
HARV				1742	1748	1	1742	1800	2	1744	1758	2	IIIGG			
SGMR								1743.2	1744			IIIB				
BOUL								1746.8	1748.1	2		III				
SGMR								1747	1749			IIIG				
CLRO								1747.5	1749	2		III				
CLRO								1751	1759	1		IIIG				
SGMR								1751.2	1752			IIIB				
SGMR								1757.2	1758			IIIB				
BOUL								1757.3	1758.5	2		IIIG				
HARV												IIIG				
HARV								1815	1820	1		IIIGG				
SGMR								1829	1832	1		IIIGG				
SGMR												IIIB				
HARV				1933	1935	1	1934	1935	1	1830.8	1831.5		IIIB			
SGMR										1920	1920.5		IIIB			
BOUL										1934	1935	1	IIIG			
HARV										1933.5	1934		IIIB			
BOUL										1933.9	1934.9	1	III			
HARV													IIIGG			
CULG	1951	2400											IIIG,N			
HARV													IIIG			
HARV													IIIGG			
HARV													IIIG			
CULG													IIIGG			
HARV				2146	2147	1	2153.5	2211.5	2				IIIG			
CULG							2153	2211	2	2158	2211	2	IIIGG			
HARV							2154	2212	2	2154	2212	2	IIIGG			
CLRO							2154	2211	2	2154	2211	2	CONT			
BOUL													CONT			
HARV				2308	2309	1							IIIG			
CULG							2353		1				IIIB,W			

"Type I Noise Active Regions and Energetic Electrons from 1 to 10 March 1970"

by

Kunitomo Sakurai*
Radio Astronomy Branch
Laboratory for Extraterrestrial Physics
NASA/Goddard Space Flight Center
Greenbelt, Maryland 20771

ABSTRACT

Type I noise activity and its relation to energetic electrons from 1 to 10 March, 1970 are discussed by using the observational data on type I noise storms, flare occurrence and solar cosmic rays. During the period mentioned above, there were two typical type I active regions which were located above the active regions McMath Nos. 10607 and 10618 (or 10614), respectively. The interplanetary space, especially the near-by space of the sun, was immersed by solar cosmic ray protons which were seemingly generated by four proton flares which successively occurred on 6 and 7 March.

It seems that two typical coronal magnetic streamers extended upward from the two type I noise active regions mentioned above. It is estimated that enormous numbers of energetic electrons were trapped along such streamers and were closely connected to the origin of highly polarized visible continuum observed at the total eclipse on 7 March. Discussion is given on a possibility of the generation of relativistic electrons within coronal streamers.

Introduction

From 1 to 10 March, 1970 there were two type I noise active regions associated with the active regions McMath Nos. 10607 and 10618 (or 10614). This type I noise activity suggests that enormous numbers of energetic electrons of kinetic energy $10 - 10^2$ keV are generated within such type I noise active regions [e.g., Takakura, 1963; Kundu, 1965; Sakurai, 1970]. These energetic electrons are thought of as being responsible for the emission of type I noise storms. In the period from 1 to 10 March, 1970 it seemed that many energetic electrons therefore, existed within the active regions McMath Nos. 10607 and 10618 (or 10614).

On 6 and 7 March, 1970 solar proton flares occurred three or four times over the visible hemisphere of the sun since the increase of solar cosmic ray flux (5 - 100 MeV) was observed by the ATS-1 satellite and the riometer (30 MHz) at Thule from 6 to 10 March [Solar-Geophysical Data, April, 1970].

The total eclipse of the sun on 7 March really occurred under such a situation as mentioned above. The data on polarization observation at visible continuum [Saito, 1970] show that, in general, highly polarized continuum is emitted from somewhere along the two streamers or more extending into the outer corona as shown in Fig. 1 and these streamers seem to be associated with the type I noise active regions mentioned above. This polarized continuum may be interpreted as being emitted by relativistic electrons. If this is the case, high energy electrons of wide energy range from 10 keV to 10 BeV would be required to be ambient in the outer solar corona, especially along the coronal streamers extending from somewhere above type I noise active regions.

In this paper, we will first consider some characteristics of type I noise activity associated with the active regions McMath Nos. 10607, 10614 and 10618. Consideration will then be given on the high energy particles in the solar outer corona and possibility of generation of relativistic electrons and their contribution to visible polarized continuum.

Characteristics of Type I and Other Activities Associated with the Active Regions McMath Nos. 10607 and 10618

Around 7 March, there were five large active regions as seen on the solar disk. The active regions McMath Nos. 10607 and 10618 and/or 10614 were associated with type I noise activity. The former and the latter were located in the northern and the southern hemisphere, respectively, as shown in Fig. 1. The result from the Nançay interferometric observation at 169 and 408 MHz is shown in Fig. 2. It is clear from this figure that, at the frequency 169 MHz, the type I noise activity of the region McMath No. 10607 is much higher than that of the region McMath No. 10618.

The radio data at 200 MHz (Hiraiso, Japan) and at 245 MHz (AFRL, Sagamore Hill, U.S.A.) show that the daily mean flux at metric frequency range decreased from 1 to 10 March. This result is shown in Fig. 3 together with the daily occurrence number of solar flares, irrespective of importance, associated with the active region McMath No. 10607. The radio flux at metric frequency tends to decrease with the decrease of flare occurrence at the region McMath No. 10607. This result

* NASA Associate at University of Maryland

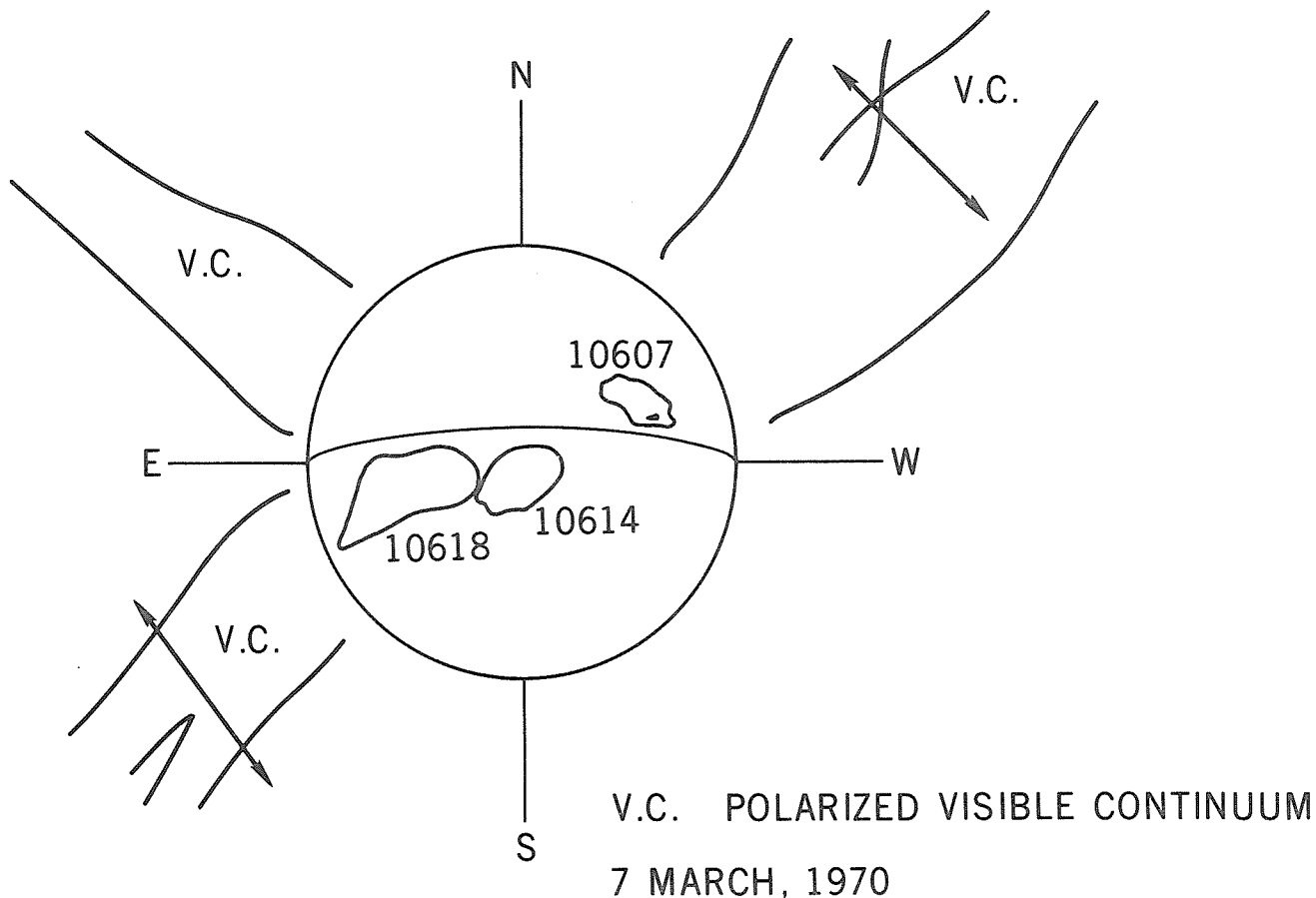


Fig. 1. The location of the active regions McMath Nos. 10607 and 10618 and their relation to the coronal streamers. The direction of E-vector of visible continuum at the total eclipse on 7 March, 1970 is shown.

suggests that main contribution on type I radio emission at metric frequency comes from the active region McMath No. 10607 since most solar flares are followed by type I noise storm emission [e.g., Dodson, 1958; Le Sequeren, 1963].

In relation to radio continuum emission at decametric frequency range, we have analyzed the data obtained by the Clark Lake Observatory, but unfortunately we are not able to say anything about the position and the frequency range on the radio activity at decametric frequencies from 3 to 7 March on account of the malfunction of the observing apparatus. However, it is certain that there appeared radio continuum active regions at decametric frequencies if we refer to the observational data on 1 - 2 and 8 - 10, March. This radio activity seems to be associated with the two type I noise active regions as shown in Fig. 2. According to our preliminary estimation, the positions of those radio active regions at decametric frequencies are located, high above those at metric frequencies. The height of the one of these radio active regions is about two solar radii above the active regions McMath Nos. 10607 and 10614, in association with the activity of these active regions. It must be remarked that type III radio bursts were often observed.

If we take account of these observational results, we can build a picture on the position and structure of those type I noise active regions and their relation to the plage and sunspot active regions. This picture thus derived is shown in Fig. 4. The one type I noise active region is located above the region McMath No. 10607, whereas the other is over the regions McMath Nos. 10614 and 10618. The active region McMath No. 10614 also seems to be responsible for the formation of the latter radio active region because its flare activity is much higher than that for the region McMath No. 10618.

As is seen in Fig. 5, from 1 to 10, March, many solar flares occurred in association with the passage of the active regions mentioned above on the solar disk. On the middle of 7th March, the active regions McMath Nos. 10607, 10614 and 10618 were respectively located around 30°- 40°W, around the central meridian and 40° to 50°E in heliographic longitude. The patterns of their magnetic configuration were of $\alpha\beta$, $\beta\beta$ and $\beta\beta$ (or $\beta\alpha$), respectively. In this figure, four plausible

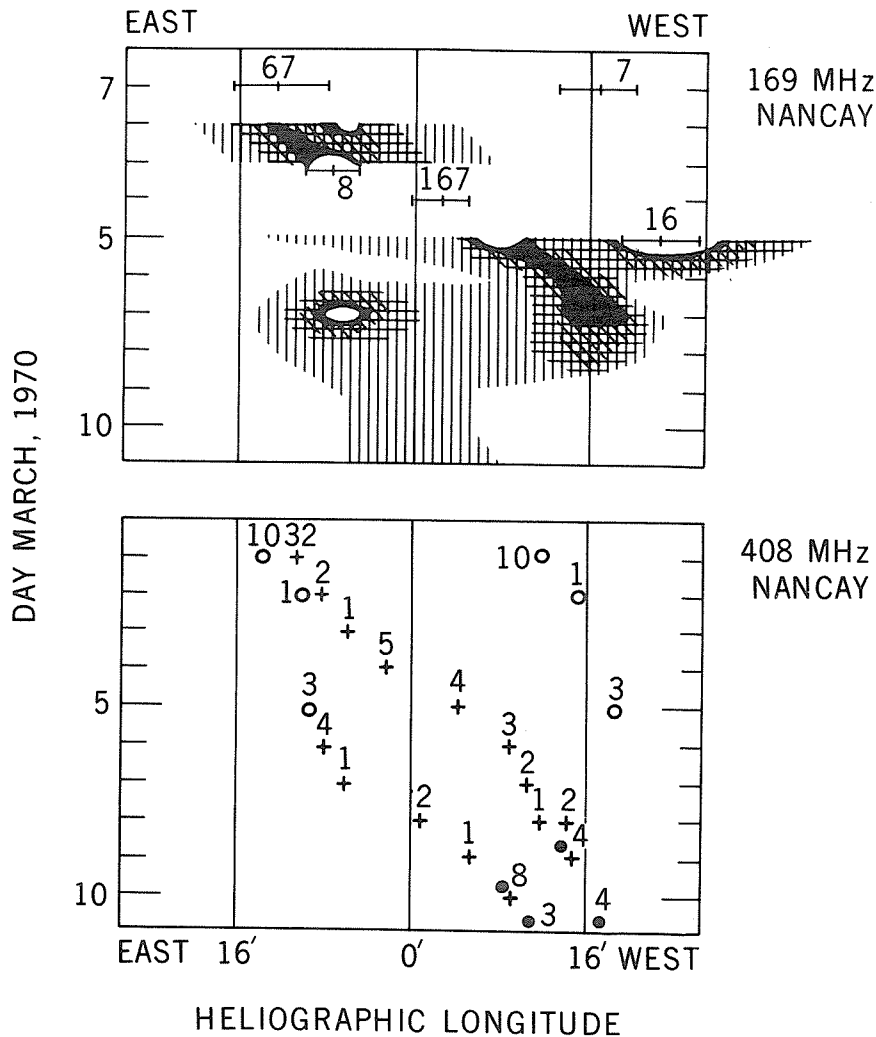


Fig. 2. Type I noise activity at metric frequencies (169 and 408 MHz) observed by Nançay interferometer [Solar-Geophysical Data, April 1970].

proton flares are shown by open circles. These flares seem to have generated solar cosmic rays as observed by the earth's satellite ATS-1 on 6 - 10, March.

As has been discussed earlier [Kai 1970; Sakurai, 1970], the coronal magnetic streamers are usually formed high above the type I noise active regions. If this relation is applied to the case which we are considering, such streamers are perhaps formed above the two type I noise active regions over the active regions McMath Nos. 10607 and 10614 - 10618, extending into the outer corona and further into the interplanetary space. It seems that enormous numbers of energetic electrons are guided outward along such streamers from type I noise active regions. Hence, the radio continuum emission at decametric frequencies described above seems to be generated by such electrons.

The observational result on the visible continuum at the time of total eclipse [Saito, 1970] shows that this emission is highly polarized in the plane perpendicular to the coronal streamers as mentioned earlier. By drawing a schematical picture on the relation between such polarized visible continuum sources and the type I noise active regions, we obtain the following view. The former sources are mainly located above the latter and along the coronal magnetic streamers which are indicated in Fig. 4. This result suggests that the emission mechanism of such polarized visible continuum is closely connected with that of Type I noise storms at both metric and decametric frequencies.

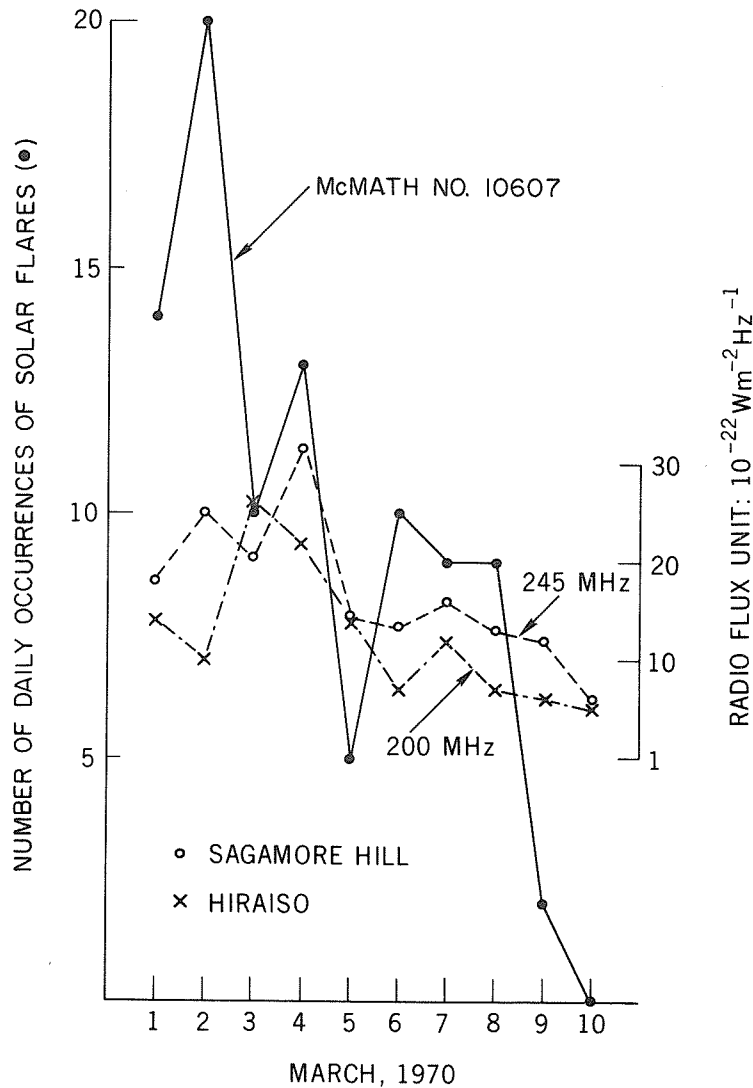


Fig. 3. Variation of the daily average flux of metric radio emission (200 and 245 MHz) and the number of solar flares from 1 to 10 March, 1970.

Solar Cosmic Rays and Energetic Electrons in the Coronal Regions

As has been described above, several proton flares occurred during the period from 1 to 10 March, 1970. They are estimated as tabulated in Table 1 with their characteristics.

Table 1 - Solar Proton Flares on 6 and 7, March 1970

Time	UT	Position	Imp.	McMath No.
March 6	1318	S12 E50	2N	10618
March 7	0143	S11 E09	2B	10614
	0721	N04 W35	1B	10607
	0837	S06 E04	1B	10614

As is shown in Fig. 6, the data obtained by the ATS-1 satellite [Solar-Geophysical Data, April 1970] show that the intensity of solar cosmic rays of Mev-energy began to increase around 1400 UT on 6 March and the excess intensity was continuously observed until the early morning on 10 March. Around 1040 UT on 7 March, the start of riometer absorption increase at 30 MHz was observed at Thule. Due to the lack of observational data by ATS-1 satellite, we can not examine the time variation of solar proton flux on 7 March in detail, but it seems that the sharp decrease of the flux of energy 5 - 21 Mev started after the onset of the SSC geomagnetic storm which occurred at 1417 UT on 8 March. The proton flux near the earth was about 6.8×10^4 particles $\text{cm}^{-2} \text{sec}^{-1}$ on that day before

MARCH 7, 1970

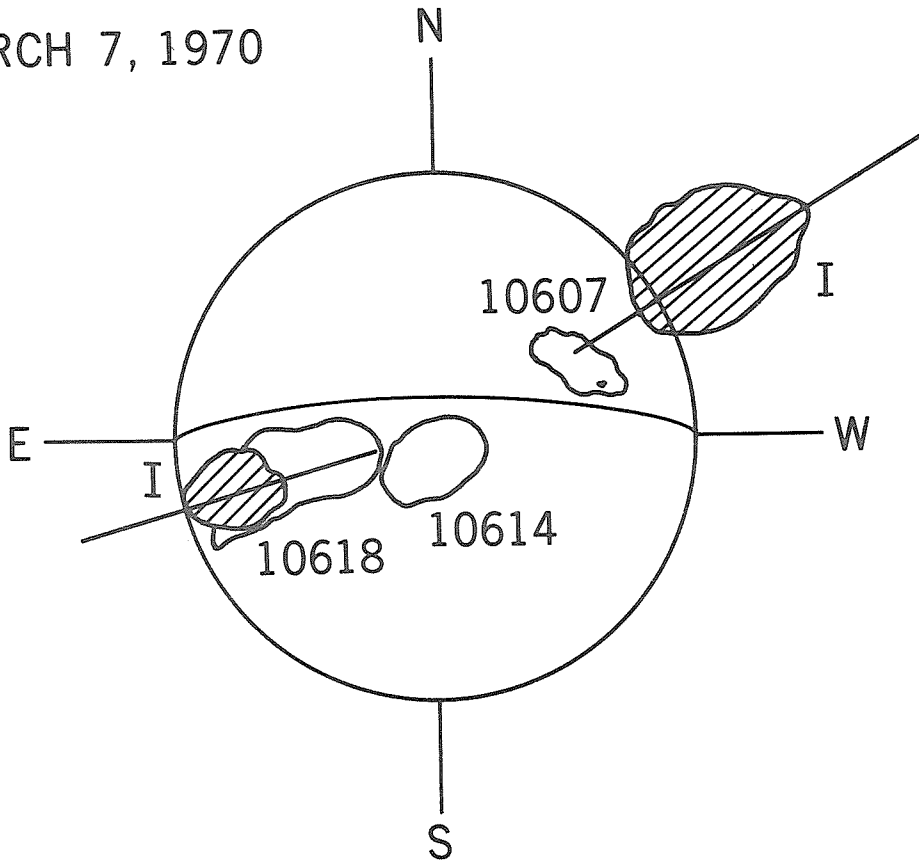


Fig. 4. The location of two type I noise active sources and their relation to the active regions McMath Nos. 10607, 10614 and 10618.

the onset of this geomagnetic storm. This suggests that in association with its passage, the storm plasma cloud responsible for the geomagnetic storm just mentioned took a sweeping action for solar proton particles of Mev-energy ambient in the solar neighborhood and interplanetary space according to the mechanism as discussed by Obayashi [1962; 1964].

On account of successive occurrence of solar proton flares, solar protons and other particles, including electrons, were generated from the sun on 6 and 7 March and so some of them might be trapped near the sun by the magnetic field lines extending from the active regions and their neighborhood in the outer solar corona and interplanetary space. Furthermore, there might exist disturbed magnetic regions within 10 solar radii which played an important role on scattering and trapping of solar protons and other particles [e.g., Lüst and Simpson, 1957; Sakurai and Maeda, 1961; Reid, 1964]. When the total eclipse occurred at 1743 UT on 7 March, the space near the sun seemed to be immersed by solar cosmic ray particles.

As is shown in Fig. 4, there were two type I noise active regions on 7 March. This means that enormous numbers of energetic electrons of kev energy were ambient in these active regions. It seems that many energetic electrons were trapped along the coronal magnetic streamers extending from such active regions into the interplanetary space. Some fraction of those electrons were seemingly ejected outward either continuously or intermittently under the guidance of the magnetic field lines along the coronal streamers.

Since type I noise storms are, in general, generated by the energetic electrons of kinetic energy $10 - 10^2$ kev [e.g., Takakura, 1963; Sakurai, 1970], it is concluded that such energetic electrons were continuously accelerated due to some instability such as flares within or near the type I noise active regions from 1 to 10 March. The acceleration process of those electrons may be related to solar flares because they seemed to occur four times (Table 1). There might be a possibility that some solar flares generated relativistic electrons of Mev and, occasionally, Bev energy.

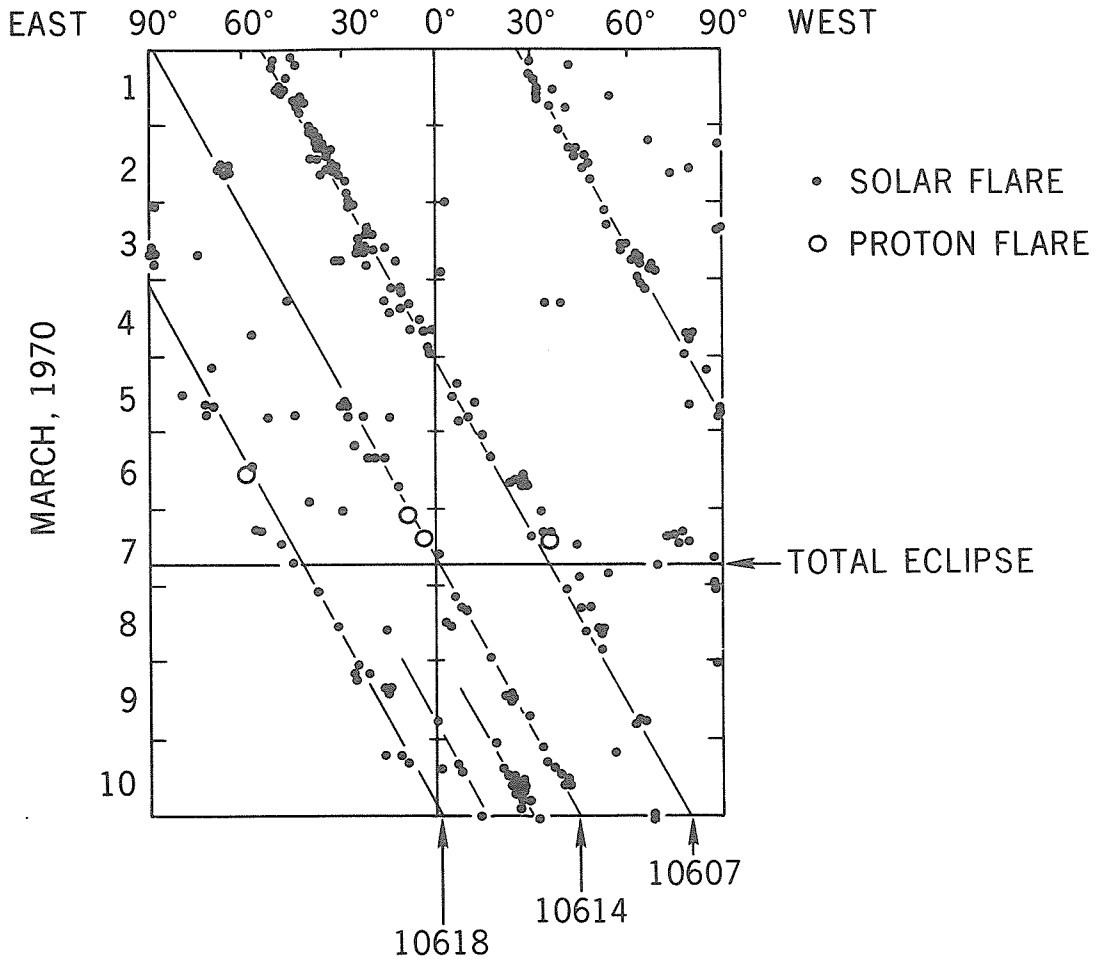


Fig. 5. The passage of the active regions McMath Nos. 10607, 10614 and 10618 over the solar disk and their flare activity. Four white circles indicate possible solar proton flares (see Table 1).

A Possibility of Generation of Relativistic Electrons in the Coronal Streamers

It has been estimated in the last section that many energetic electrons and, perhaps, protons were trapped along the magnetic field lines within the coronal streamers. Since electrically neutral layers are possibly formed within the coronal streamers some instabilities would probably occur along such layers [e.g., Farth, Killeen and Rosenbluth, 1963; Sturrock, 1966]. Triggering process for such instabilities seems to be mainly associated with the onset of solar flares which occur within the sunspot active regions located beneath the base of coronal streamers.

Energetic particles in such neutral layers would be accelerated to higher energy with the growth of instability related to neutral layers. It is estimated that energy range of energetic electrons responsible for type I noise bursts is $10 - 10^2$ kev [e.g., Takakura, 1963]. These energetic electrons seem to be generated almost continuously below and near the type I noise active regions. If a solar flare occurs, these electrons would, therefore, be accelerated to higher energy as Mev range or more and then would be ejected into the coronal magnetic streamers.

These high energy electrons may be, furthermore, accelerated in association with some instability connected with neutral layers within the coronal magnetic streamers. A minor part of those electrons may be accelerated to 100 Mev or more. The generation of these high energy electrons would have been much more efficient in case of solar proton flares.

Consequently, such electrons would have been temporarily trapped within the coronal magnetic streamers over both of the active regions McMath Nos. 10607 and 10614 - 10618.

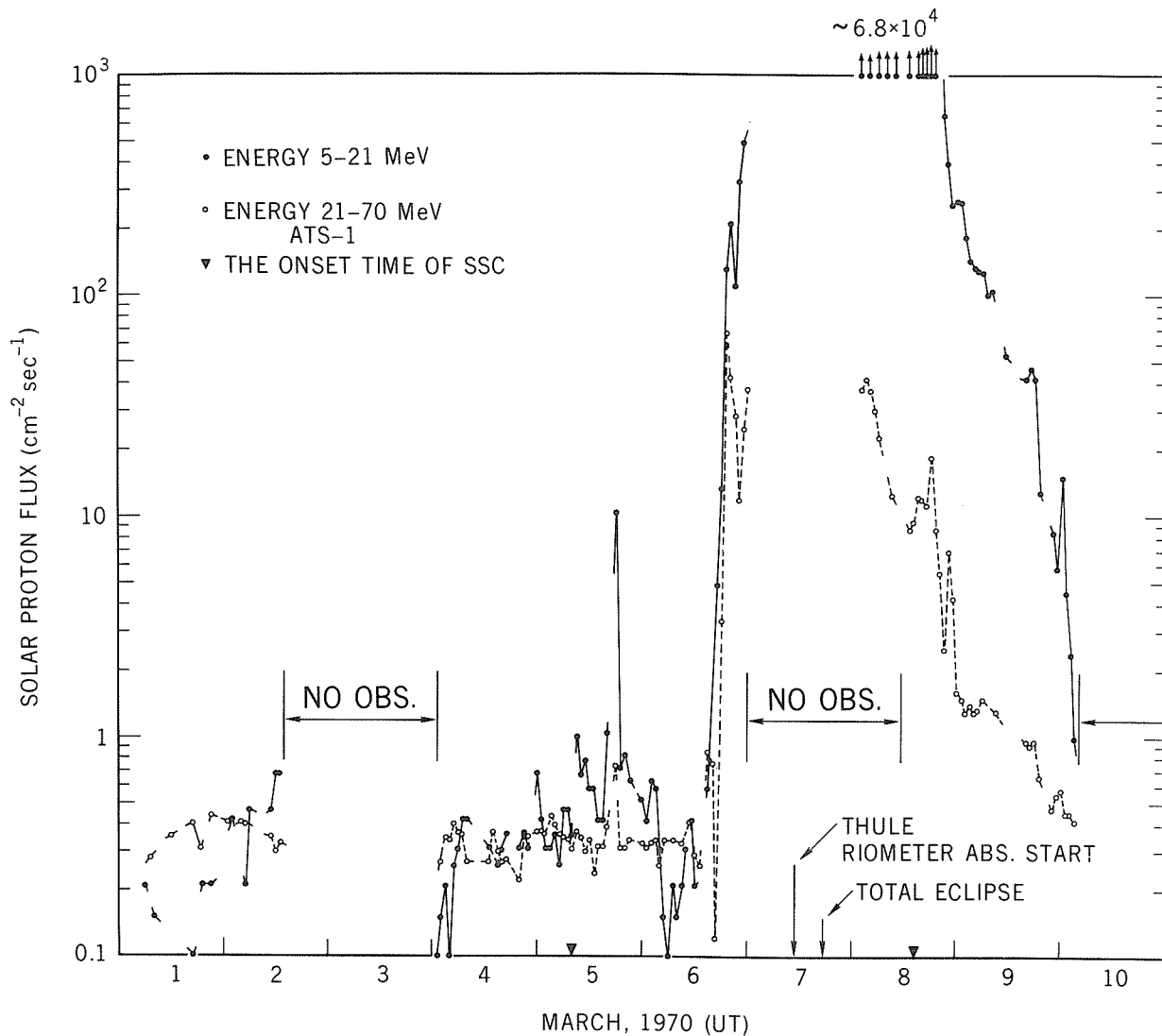
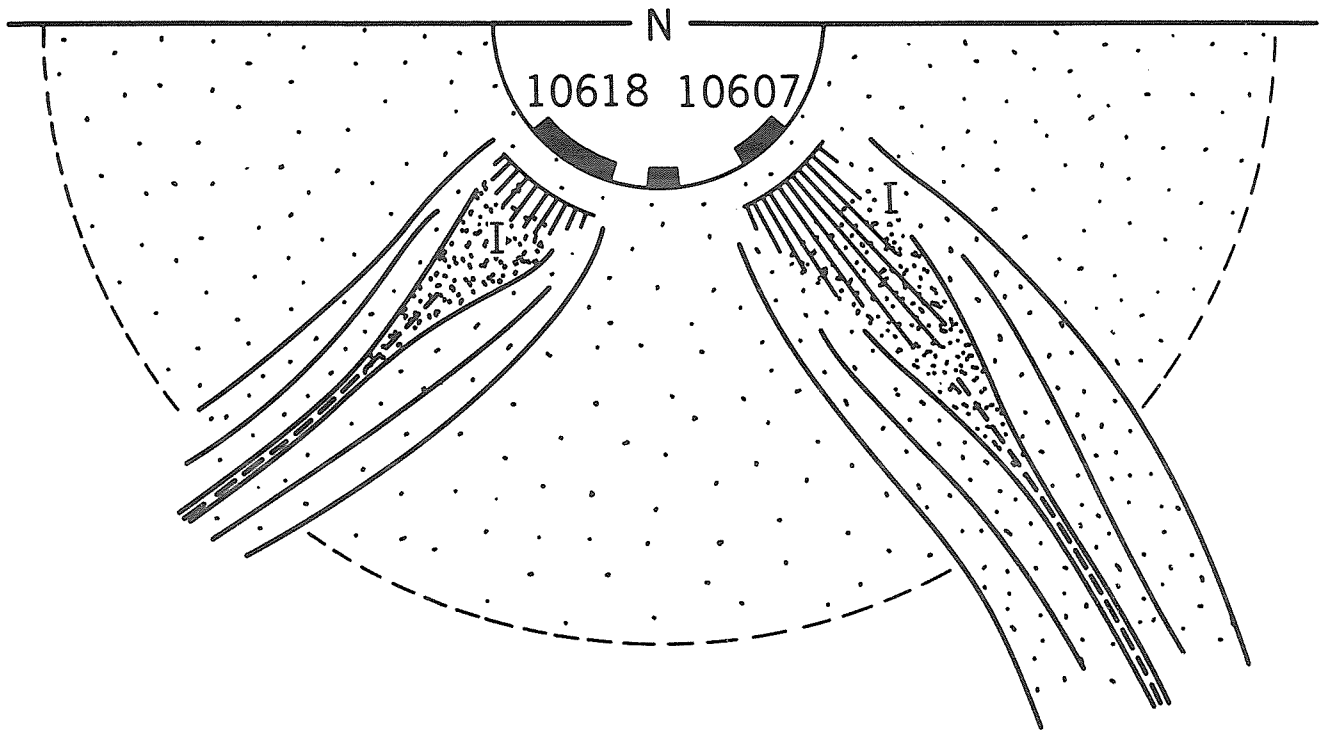


Fig. 6. Solar proton flux observed by the ATS-1 satellite from 1 to 10 March, 1970.

The observational data on optically visible continuum show that this continuum was highly polarized perpendicular to the direction of these two coronal streamers, as indicated in Fig. 1 [e.g., Saito, 1970]. At present, synchrotron radiation mechanism has been used to interpret such polarized visible continuum [e.g., Kellogg and Ney, 1959; Ney *et. al.*, 1961]. Since relativistic electrons would be produced along the coronal streamers as discussed before, there may be a possibility that such continuum is emitted due to the synchrotron radiation by relativistic electrons.

Concluding Remarks

On March 6-7 solar cosmic ray protons of Mev energy were generated by four solar flares intermittently (see Table 1) and were occupying the space near the sun as diffusing gradually outward. Enormous numbers of energetic electrons were also generated and mainly trapped within the coronal magnetic streamers. At the base of such streamers, there were type I noise active regions where electrons of kev kinetic energy were being continuously generated. Thus, we obtain a model as shown in Fig. 7 as regard to the active region and its connection to the coronal magnetic streamers. At the time of total eclipse on 7 March, solar cosmic rays and energetic electrons from kev to Mev or more were existent near the sun. It seems that such a situation as observed on 7 March is rarely realized in the sun's neighborhood and its cause is closely related to successive occurrence of solar proton flares before the total eclipse.



7 MARCH, 1970

I
 TYPE I NOISE SOURCE
 ----- NEUTRAL LAYER

Fig. 7. A model of the coronal streamers and associated active regions over the visible hemisphere at the time of the total eclipse on 7 March.

REFERENCES

DODSON, H. W.	1958	<u>Proc. IRE</u> , <u>46</u> , 149.
FARTH, H. P., KILLEEN, J. and ROSENBLUTH, M. N.	1963	<u>Phys. Fluids</u> , <u>6</u> , 459.
KAI, K.	1970	<u>Solar Phys.</u> , <u>11</u> , 456
KELLOGG, P. J. and NEY, E. P.	1959	<u>Nature</u> , <u>183</u> , 1297.
KUNDU, M. R.	1965	<u>Solar Radio Astronomy</u> , Intersci, New York.
LE SQUEREN, A. M.	1963	<u>Ann. d'Astrophys.</u> , <u>26</u> , 97.
LÜST, R. and SIMPSON, J. A.	1957	<u>Phys. Rev.</u> , <u>108</u> , 1563

NEY, E. P., HUCH, W. F., KELLOGG, P. J., STEIN, W. and GILLET, F.	1961	<u>Ap. J.</u> , <u>133</u> , 616.
OBAYASHI, T.	1962	<u>J. Geophys. Res.</u> , <u>67</u> , 1717.
OBAYASHI, T.	1964	<u>Space Sci. Rev.</u> , <u>3</u> , 79.
REID, G. C.	1964	<u>J. Geophys. Res.</u> , <u>69</u> , 2659.
SAITO, K.	1970	<u>Sky and Telescope</u> , <u>80</u> , and <u>Astronomical Herald</u> , <u>63</u> , 140.
SAKURAI, K.	1970	NASA, <u>GSFC Rep. X-693-70-252</u> .
SAKURAI, K. and MAEDA, H.	1961	<u>J. Geophys. Res.</u> , <u>66</u> , 1966.
	1970	" <u>Solar-Geophysical Data</u> ", <u>IER-FB 308</u> , April 1970.
STURROCK, P. A.	1966	<u>Nature</u> , <u>211</u> , 695.
TAKAKURA	1963	<u>Pub. Astron. Soc. Japan</u> , <u>15</u> , 462.

"Solar Radio Emission for March 6-10, 1970"

by

H. Tanaka
Toyokawa Observatory, Nagoya University, Japan

[The compilers have prepared the following paragraph and illustrations from notes provided by H. Tanaka.]

The following figures illustrate the solar radio emission as observed at Toyokawa during the period March 6-10, 1970. In all cases, noise outside the observable special frequencies is rejected. Figure 1 shows radioheliograms on 3.2 cm for March 7-10, respectively (March 6 was not available). To these the following comments apply:

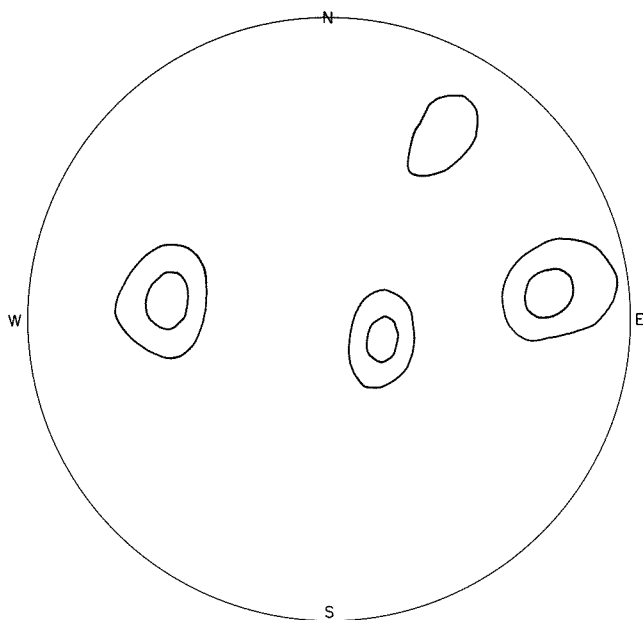
- (1) Half-power beam width after smoothing (negative side lobes < -20 dB)
East-West - 2.25', and North-South - 2.9' (on March 10).
- (2) Unit of apparent brightness temperature is 22,000°K.
- (3) The number of samples is 4095 for 40x40 cos Z square arc minutes, where Z is zenith distance.
- (4) Observed at 0305 - 0326 UT (March 7 - 10).
- (5) Reference: H. Tanaka et al., 3-cm Radioheliograph, Proc. Res. Inst. Atmospheric, Nagoya Univ., 17 (1970).

Figure 2 shows East-West Scans on 3.2 and 8 cm using the 32-element grating. The observations were at about 0301 UT daily. For these:

- (1) Half-power beam width is 1.1', and the number of samples is 256 in 40 min. of arc.
- (2) Normalized so that one square division corresponds to 50 and 25 Flux Units for 3.2 and 8 cm, respectively.
- (3) The radius of optical solar disk is 2.048 divisions.
- (4) The center of drift curves should be shifted by 0.016 and 0.038 divisions to the East for 3.2 and 8 cm, respectively.

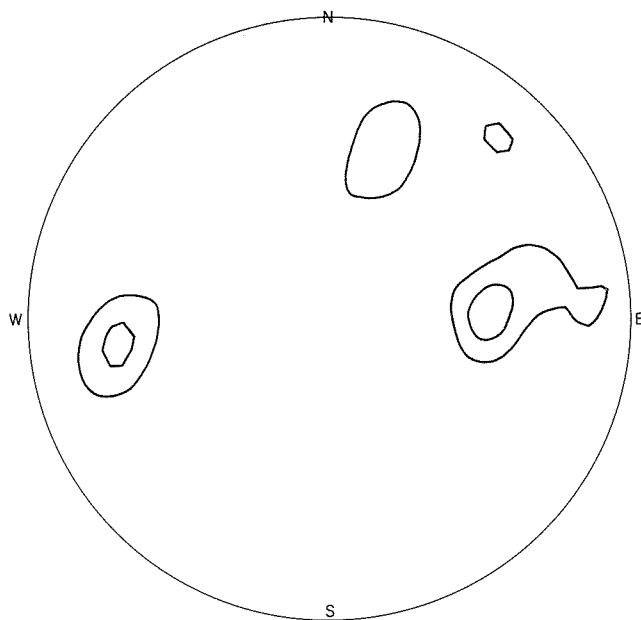
Figure 3 shows East-West Scans on 8 cm using the (32+2)-Element Compound. Data for 3.2 cm are not available. Observations were at about 0301 UT daily.

- (1) Half-power beam widths are 0.38' for the unsmoothed upper curves and 0.57' for the smoothed lower curves (negative side lobes < -20 dB). The number of samples is 256 in 40 min. of arc.
- (2) Normalized so that one square division corresponds to 50 Flux Units.
- (3) The radius of optical solar disk is 2.048 divisions.
- (4) The center of drift curves should be shifted by 0.068 divisions to the East.
- (5) Reference: H. Tanaka et al., A High-Resolution Quick-Scan Interferometer for Solar Studies at 3.75 GHz.



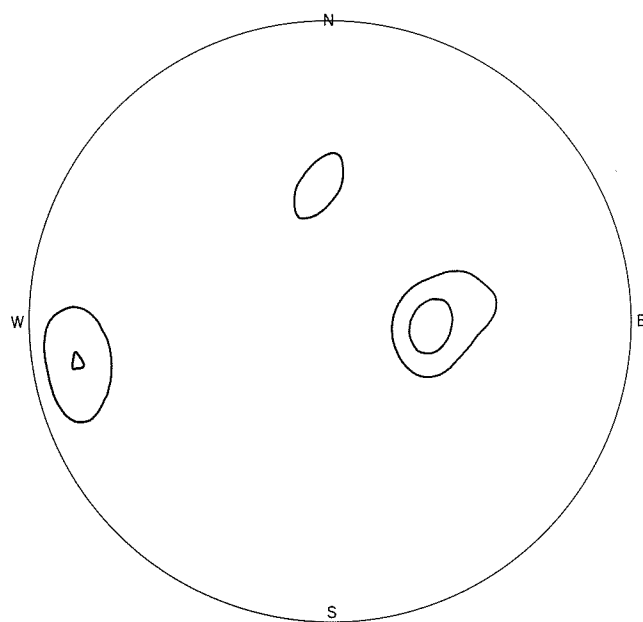
March 7, 1970

P=0.9998599
Z=3.



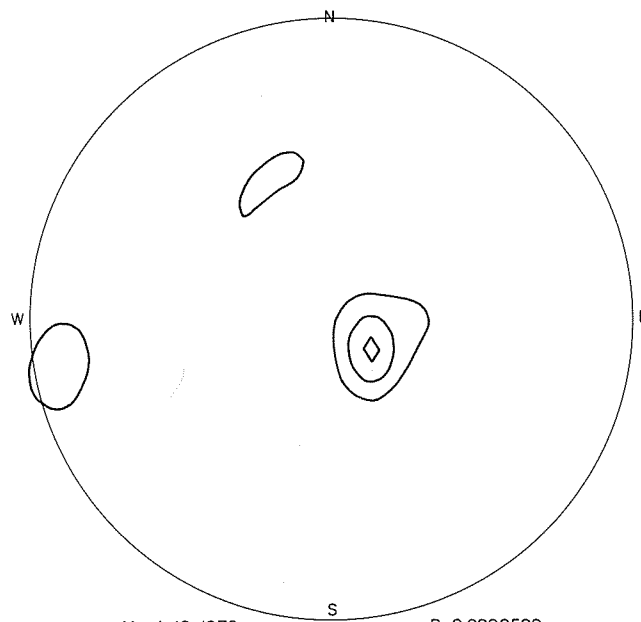
March 8, 1970

P=0.9998599
Z=3.



March 9, 1970

P=0.9998599
Z=3.



March 10, 1970

P=0.9998599
Z=3.

Fig. 1 Radioheliograms on 3.2 cm, Toyokawa, March 7-10, 1970.

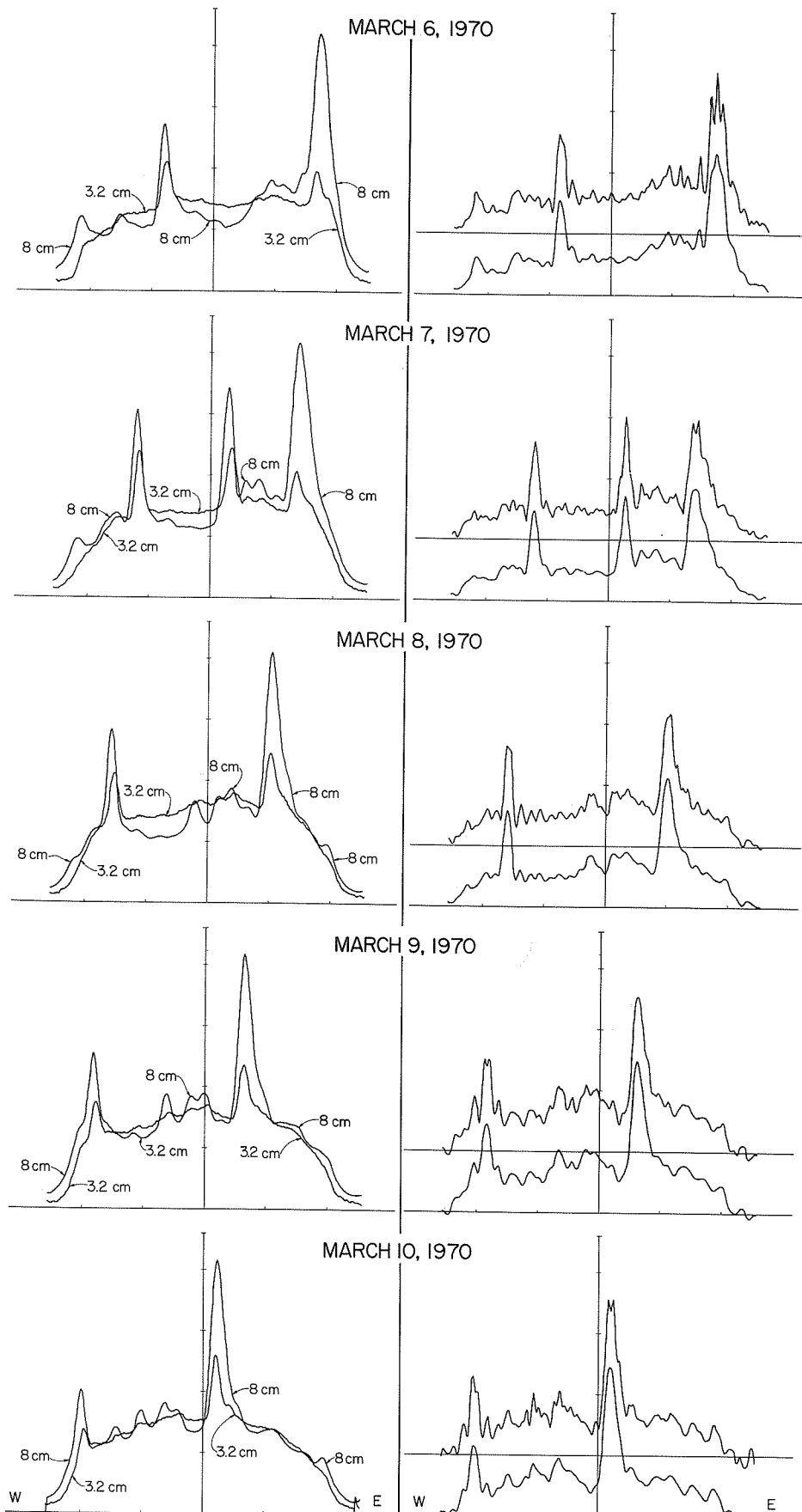


Fig. 2 East-West Scans of 3.2 and 8 cm, 32 element gratings, March 6-10, 1970.

Fig. 3 East-West Scans on 8 cm, (32+2) element compound, March 6-10, 1970.

"The Microwave Spectroheliograms of March 6 - 10, 1970"

by

J. S. Deuter and R. N. Bracewell
Radio Astronomy Institute
Stanford University
Stanford, California

Special spectroheliograms were prepared for March 6-10, 1970, the days around the eclipse of March 7, 1970, from observations made at a wavelength of 9.1 cm with the microwave spectroheliograph at Stanford University [Bracewell, 1961; Descriptive Text, Solar-Geophysical Data].

The outermost contour corresponds to 20,000 K and the contour interval is 20,000 K. The contours, which are intended as a visual aid to interpretation of the numerical values, were prepared in the same way as the 50,000 and 100,000 K contours that are published in Solar-Geophysical Data, i.e., the contours refer to a smoothed map in which each reading is replaced by the mean of the nine values centered on it.

Each reading occupies three spaces, and refers to a point on the sun centrally between the units and tens digits. The horizontal spacing of adjacent readings was 1.64 and the vertical spacing was 1.82 minutes of arc. The brightness temperature unit is 5000 K.

The response of the instrument to a point source has four spikes resembling those seen on some photographs of bright stars, and this effect is a noticeable accompaniment of the brightest region. The position of these effects is geographic north-south and east-west, and so rotated 23 degrees anticlockwise from the axes of the page, since the sun's rotation axis is shown vertical.

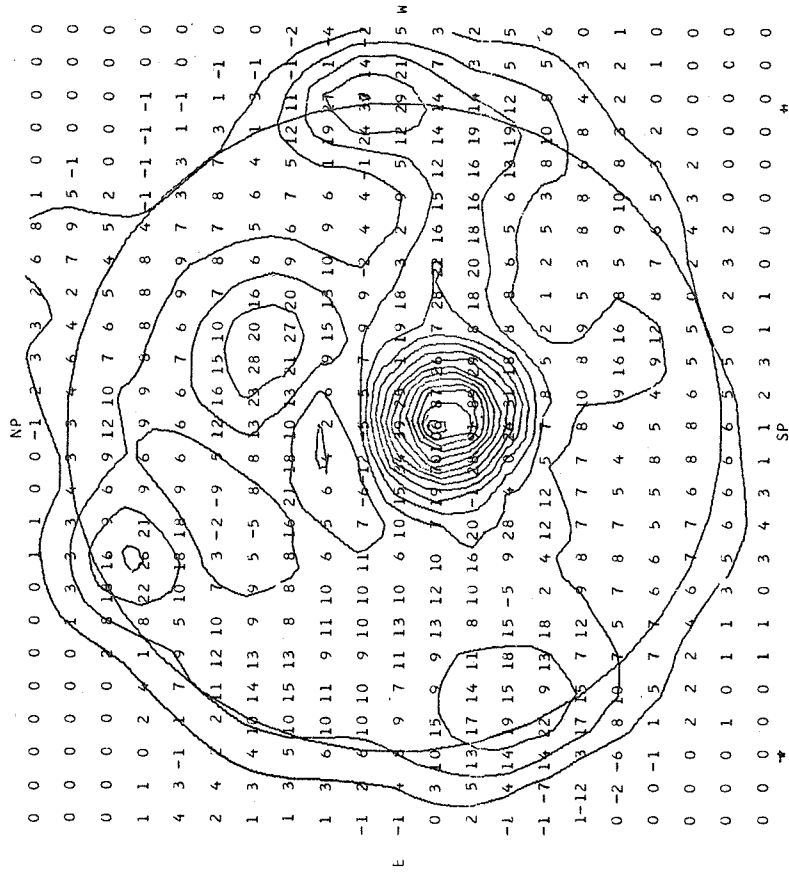
The observations were supported by the Environmental Science Services Administration under contract E22-26-67(N) and the preparation of the special spectroheliograms by the Air Force Office of Scientific Research under contract F44620-70-C-0076.

REFERENCES

BRACEWELL, R. N. and 1961
G. SWARUP

The Stanford Microwave Spectroheliograph Antenna, a Microsteradian Pencil Beam Interferometer, Trans. I.R.E., Vol. AP-9, 22-30

Solar-Geophysical Data, Descriptive Text, Number 306 (Supplement), 19-20, February 1970, U. S. Department of Commerce, Boulder, Colorado



STANFORD, 10 MAR 1970 9.1 CM SPECTROHELIOGRAM 20-21 HOURS UT. S = 160 BRIGHTNESS UNIT = 5000 K

10 MARCH 1970

"Solar Emission at 8.3 mm on March 6 - 12, 1970"

by

G. Feix

Department of Physics and Astronomy
Ruhr-University Bochum, G.F.R.

Flux density measurements of local active regions with absolute accuracies of 2% of the quiet sun level or $0.8 \times 10^{-22} \text{Wm}^{-2}\text{Hz}^{-1}$ respectively are made on a daily basis at Stockert Radio Observatory, Germany.

The general solar situation as observed at mm-wavelengths in the interval March 6 - 12 appears to have produced only minor events. The flux densities of the associated plages were of the order of 2 to $4 \times 10^{-22} \text{Wm}^{-2}\text{Hz}^{-1}$. The greatest change in intensity observed occurred in plage McMath No. 10618 on March 7 with flux rising gradually from about 4 to $9.4 \times 10^{-22} \text{Wm}^{-2}\text{Hz}^{-1}$ and lasting from 1126 to 1300 UT; the peak mm-flux appeared at 1202 UT. The time of the onset of this "sub"-burst coincides fairly well with the record of a cm-burst as reported by Solar Radio Data, Slough, [March 1970]; maxima of $8 \times 10^{-22} \text{Wm}^{-2}\text{Hz}^{-1}$ at 1129 UT and $34 \times 10^{-22} \text{Wm}^{-2}\text{Hz}^{-1}$ at 1126 UT were observed at 9.4 GHz by the RSRS-Observatory, Slough, England. Fig. 1 shows the scan-profile at mm-wavelengths (36 GHz) observed at Stockert Radio Observatory at the same time. This burst was accompanied by a flare of the importance 1B to 2N with a high velocity dark surge; published in Solar-Geophysical Data, [April 1970]. Maximal phases have been observed at 1125, 1127 and 1130 UT.

Out of all plages observed, the daily flux of four plages have been plotted in Fig. 2. Also indicated in this plot is the daily flux at 9.1 cm taken from solar maps of Stanford University, U.S.A., as issued by the Solar-Geophysical Data, [May 1970]; finally, area- and brightness-Ca data furnished by McMath-Hulbert Observatory to the bulletin mentioned have been used to derive an integrated brightness factor for these plages. As can be seen in Fig. 2, the flux sequence of the mm-radio emission does not correspond with the sequence of the 9.1 cm emission. This result appears to be consistent with a model of different layers for the slowly varying component depending upon the wavelength. On the other hand the trace of the normalized Ca-brightness is nearly in accordance with mm-intensities and almost constant for the whole period observed. However, for the purpose of comparison a larger period should be taken into account; recently, more statistical material has been applied to this problem over a period of five to six months [Feix, 1969].

Conclusion

Summarizing, we can judge, on the basis of the data obtained, that this observation period was of a very low activity at mm-wavelengths.

Acknowledgement

The mm -data were kindly supplied by E. Furst, MPI for Radioastronomy, Bonn Germany.

REFERENCES

- | | |
|----------|--|
| 1970 | "Solar-Geophysical Data", Boulder, Colorado U.S.A.
<u>No. 308</u> - Part I, April
<u>No. 309</u> - Part I, May |
| FEIX, G. | 1969 <u>Solar Physics</u> , <u>10</u> , 184. |
| RSRS | 1970 Solar Radio Data, Slough, England. |

March 7, 1970

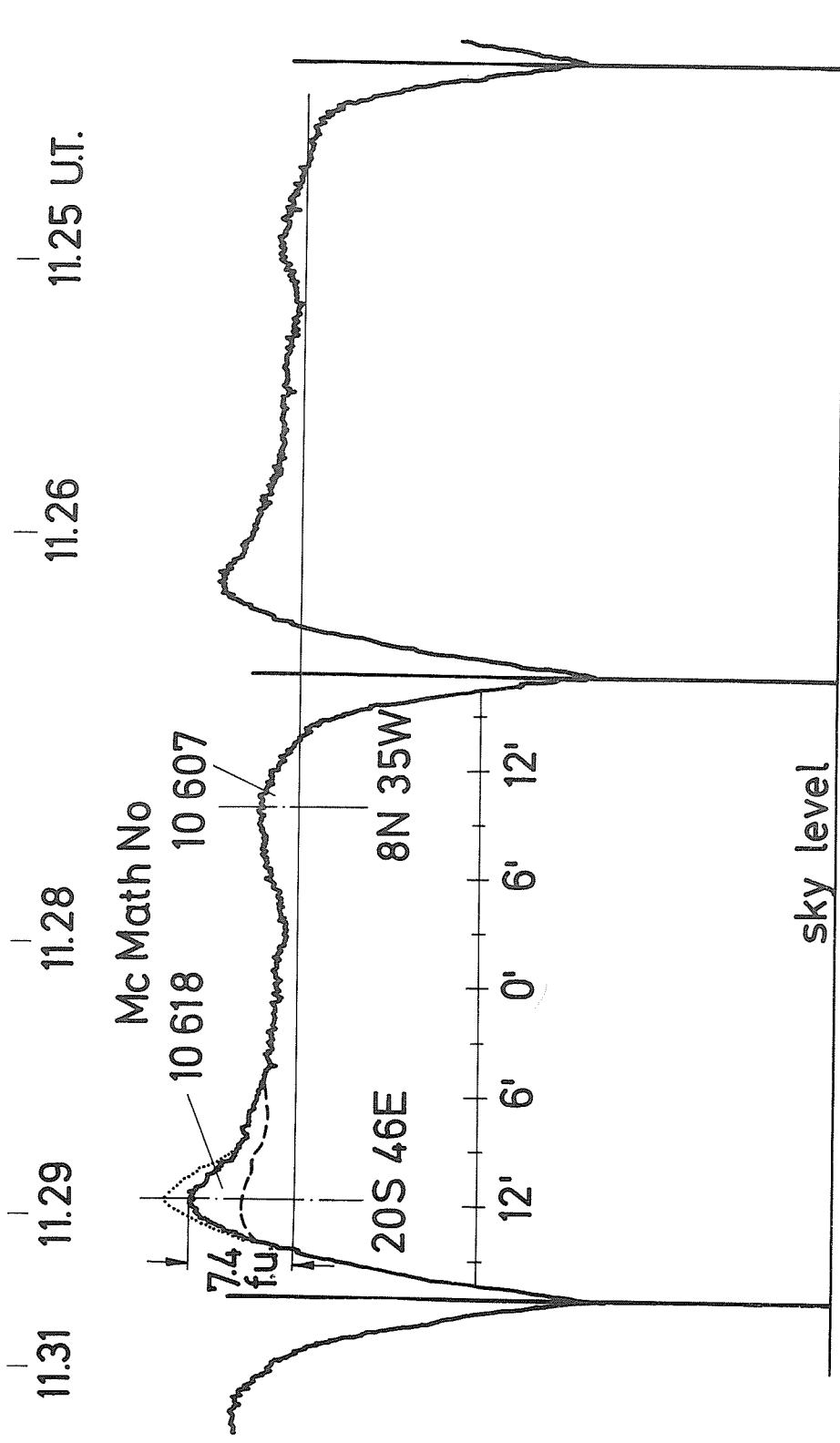


Fig. 1. Solar Scan at 36 GHz on March 7, 1970.
..... superposed trace of the maximum at 1202 UT.
----- superposed trace for reference, March 6, 1970, 0900 UT.
Right hand scan: beam aligned 1.6' south from center of plage No. 10816.

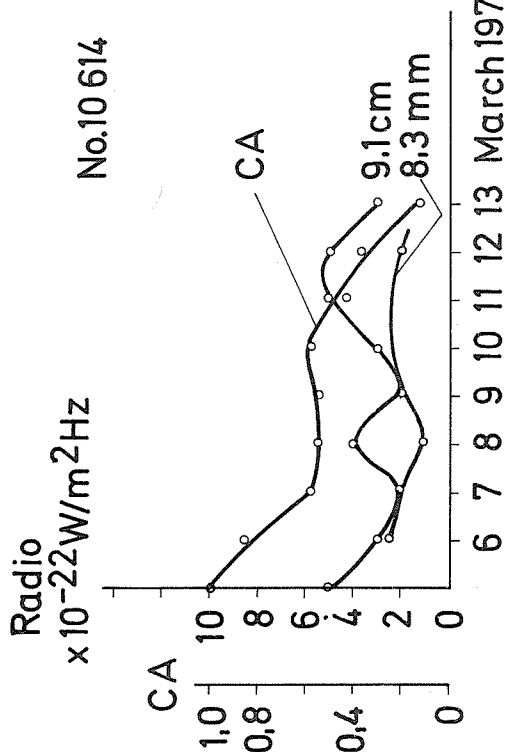
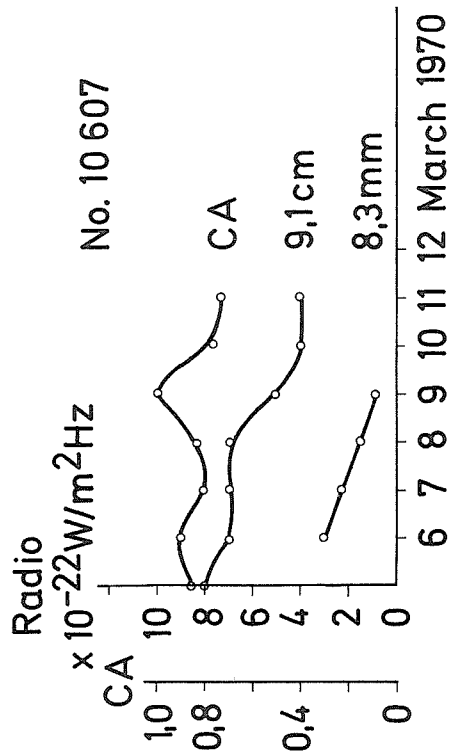
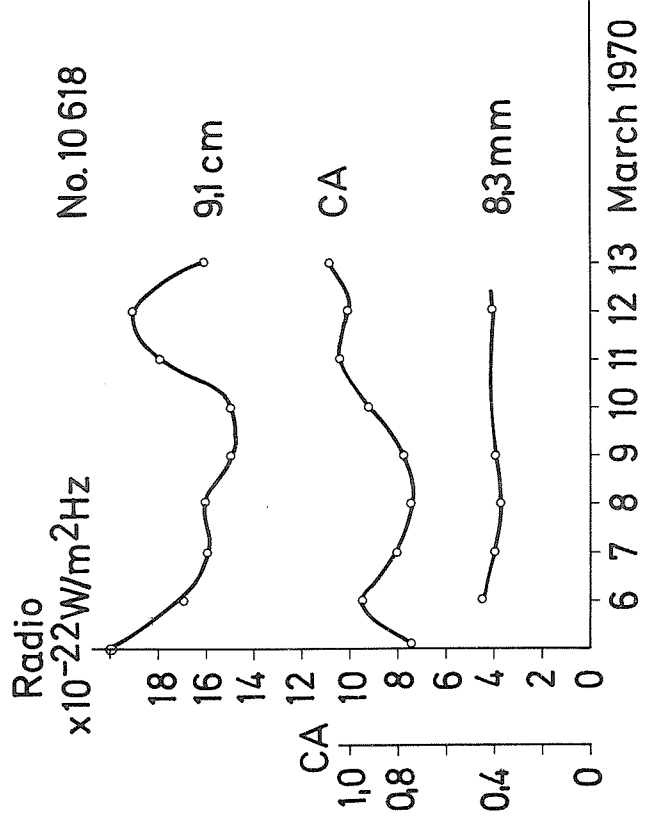
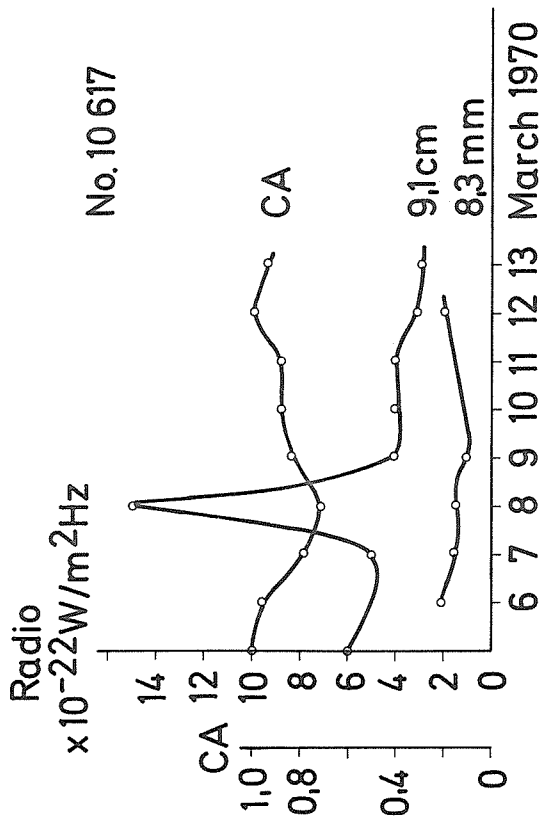


Fig. 2 History of Active Plages During March 5-13, 1970.

Notice: CA-scale of McMath region No. 10617 compared to No. 10618 is reduced by a factor of 0.67; correspondingly No. 10614 by 0.36, and No. 10607 by 0.29.

"Characteristics of Noise Storms and the S-Component of Solar Radio Emission in March, 1970"

by

A. Bohme and A. Krüger
 German Academy of Sciences
 Central Institute for Solar-Terrestrial Physics
 (Heinrich-Hertz-Institute)
 Berlin-Adlershof, GDR

The first decade of March, 1970 was characterized by enhanced components of the slowly varying centimetric radiation and noise storm emission. Table 1 shows the observed daily means of solar flux density at different frequencies measured at the Heinrich-Hertz-Institute. As is well known, in the centimetric region these data refer to the action of the S-component and in the metric region to the noise storm emission, respectively.

Dynamic spectra of these components deduced from single frequency observations are represented in Figures 1 and 2. For comparison, for each day the existing spot groups are introduced into Figure 1 taken from the Maps of the Sun of the Fraunhofer Institute, Freiburg. In this way, representative global information about three distinct levels of the solar atmosphere are available. As indicated by Figure 1, during the period under consideration, especially, two centres of activity were dominating, one in the northern solar hemisphere, the other in the southern. But it must be supposed, considering both, that the S-component and the noise storm radiation came from the northern group which was associated with McMath Plage No. 10607. This region was very active also some days before the time interval here under consideration.

Table 1
 Daily means of solar flux density
 during the period 1970, March 1 - 20 from HHI observations

Date 1970	s-component (+ basic component)				Noise storm					Remarks
	9500	2000	1490	510	234	111	64	40	23	
	MHz				MHz					
1	336	-	121	40	140	186	702	<125	<100	
2	329	-	122	35	28	59	≤313	≤126	<100	
3	330	-	122	35	18	25	<25	<50	<100	9500 MHz values
4	327	-	130	48	56	125	≤64	≤116	<100	according to
5	329	-	128	35	14	43	≤56	≤203	<100	latest absolute
6	331	-	126	35	13	29	≤64	≤263	<100	calibration
7	324	-	129	35	20	31	≤54	≤253	<100	2290 MHz
8	315	-	132	39	13	30	≤50	≤216	<100	equipment
9	320	131:	131	35	9	<8	<25	<50	<100	under recon-
10	316	129:	132	35	9	<8	<25	<50	<100	struction
11	311	-	126	35	10	<8	<25	<50	<100	
12	314	-	128	35	9	<8	<25	<50	<100	2000 MHz level
13	306	-	120	35	8	<8	<25	<50	<100	according to
14	302	123	113	35	8	<8	<25	<50	<100	Nagoya absolute
15	299	122	112	35	8	<8	<25	<50	<100	calibration
16	298	121	113	35	9	<8	<25	<50	<100	
17	299	117	105	35	10	<8	<25	<50	<100	
18	299	117	104	35	11	<8	<25	<50	<100	
19	296	118	103	32	9	<8	<25	<50	<100	
20	302	124	109	32	9	<8	<25	<50	<100	

As a remarkable feature, the radiation of the S-component exhibited relatively high fluxes in the 3 cm-range during the first six days of March, 1970. This fact reflects processes of a storage of energy in deeper levels of the solar atmosphere (i.e. near the transition region chromosphere-corona which is believed to be responsible for the production of energetic flare-burst events [Krüger, 1969, 1971]). However, these processes are more or less loosely connected with the formation of noise storms demonstrated by Figure 2. This storm must be regarded as indicative of a separated heating process taking place in coronal heights of, say, about 0.2 - 1.0 solar radii above the photosphere. Sometimes, such centres of storm radiation have been supposed to be stores

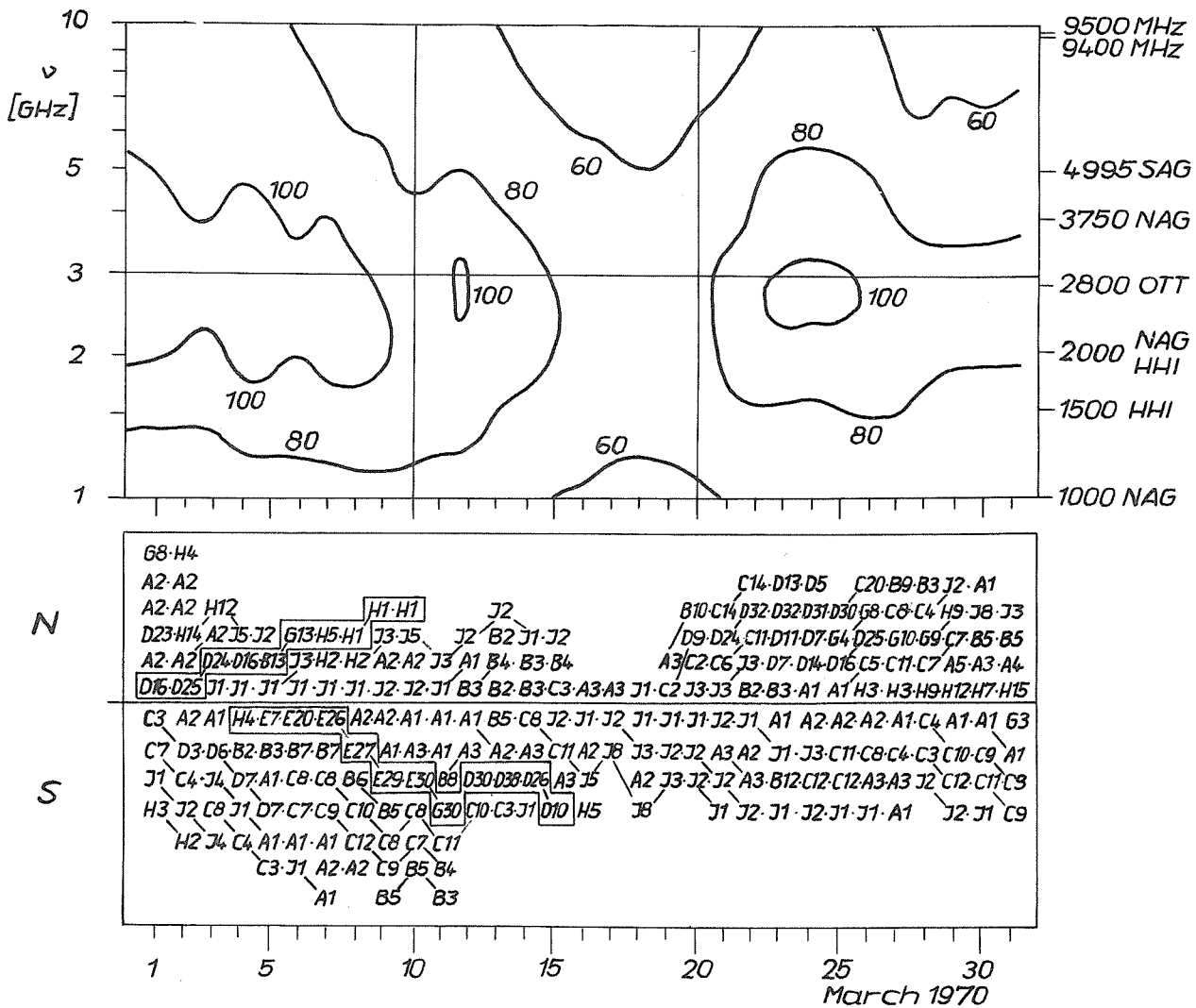


Fig. 1. Plot of dynamical spectra of the S-component in comparison with spot groups in March 1970.

for protons of low energy escaping and coming to the earth, producing auroral phenomena, geomagnetic storms, etc. [Fan, et al., 1968; Denisse, 1952; Pick, 1970].

Figure 2 demonstrated very nicely indeed the close connection between the spectrum of the noise storm emission and the arrival of low-energy protons near the earth. The latter data have been deduced from IMPG (EXP 41) measurements as published in the ESSA Solar-Geophysical Data [1970]. About two days after the maximum of the storm radiation on March 6 on 40 MHz the peak of the proton emission arrived at the vicinity of the earth. A comparison with Table 2 compiling the major type IV bursts in March, 1970 shows, that no type IV event was detected which could be connected with the onset of the particle event. Thus, no explosive solar process may be responsible for the expellation of the particle emission in the range <10 Mev at least for the first phase of the event.

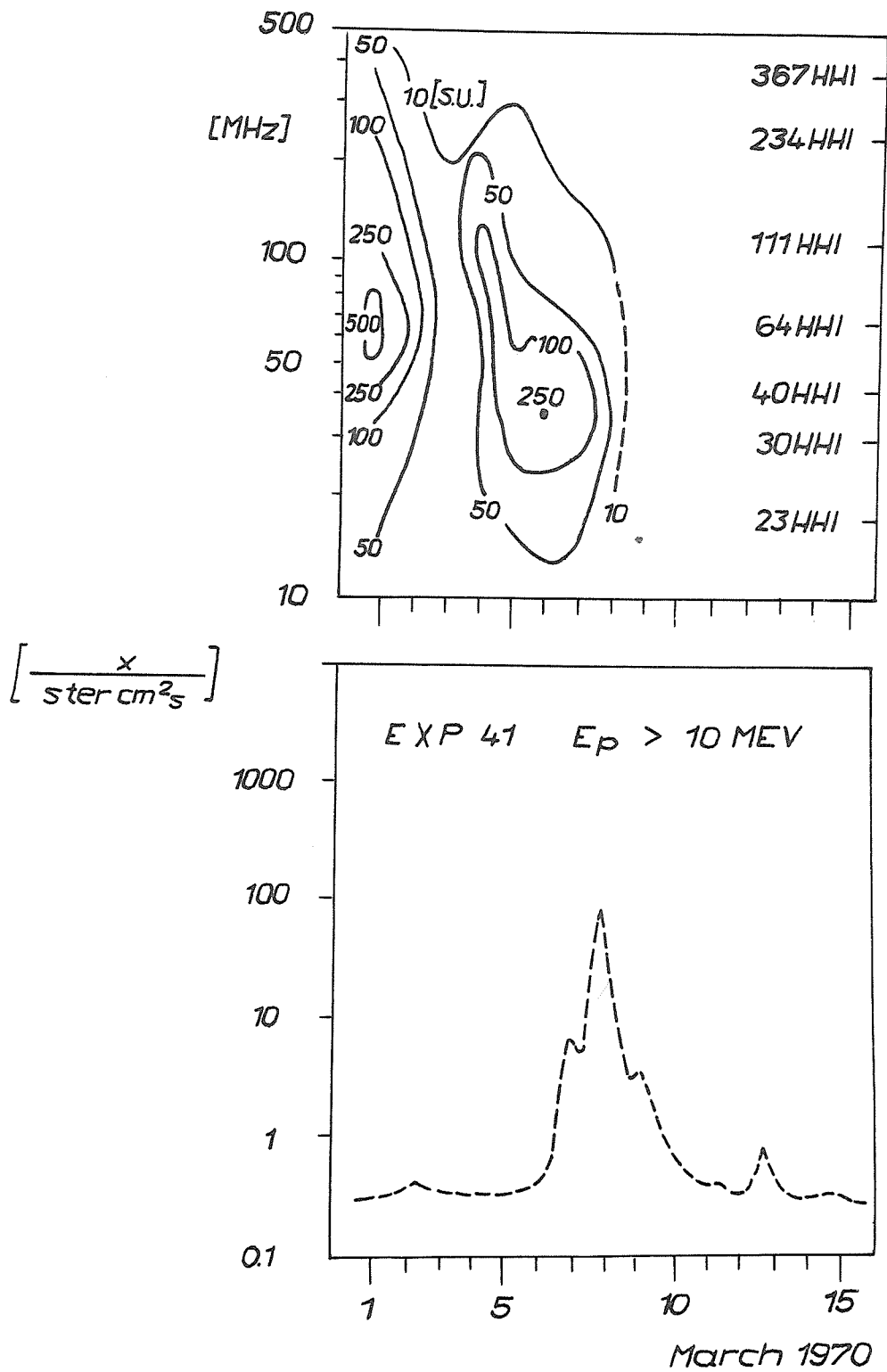


Fig. 2. Dynamical spectrum of the noise storm emission in comparison with the IMP-G solar proton observations.

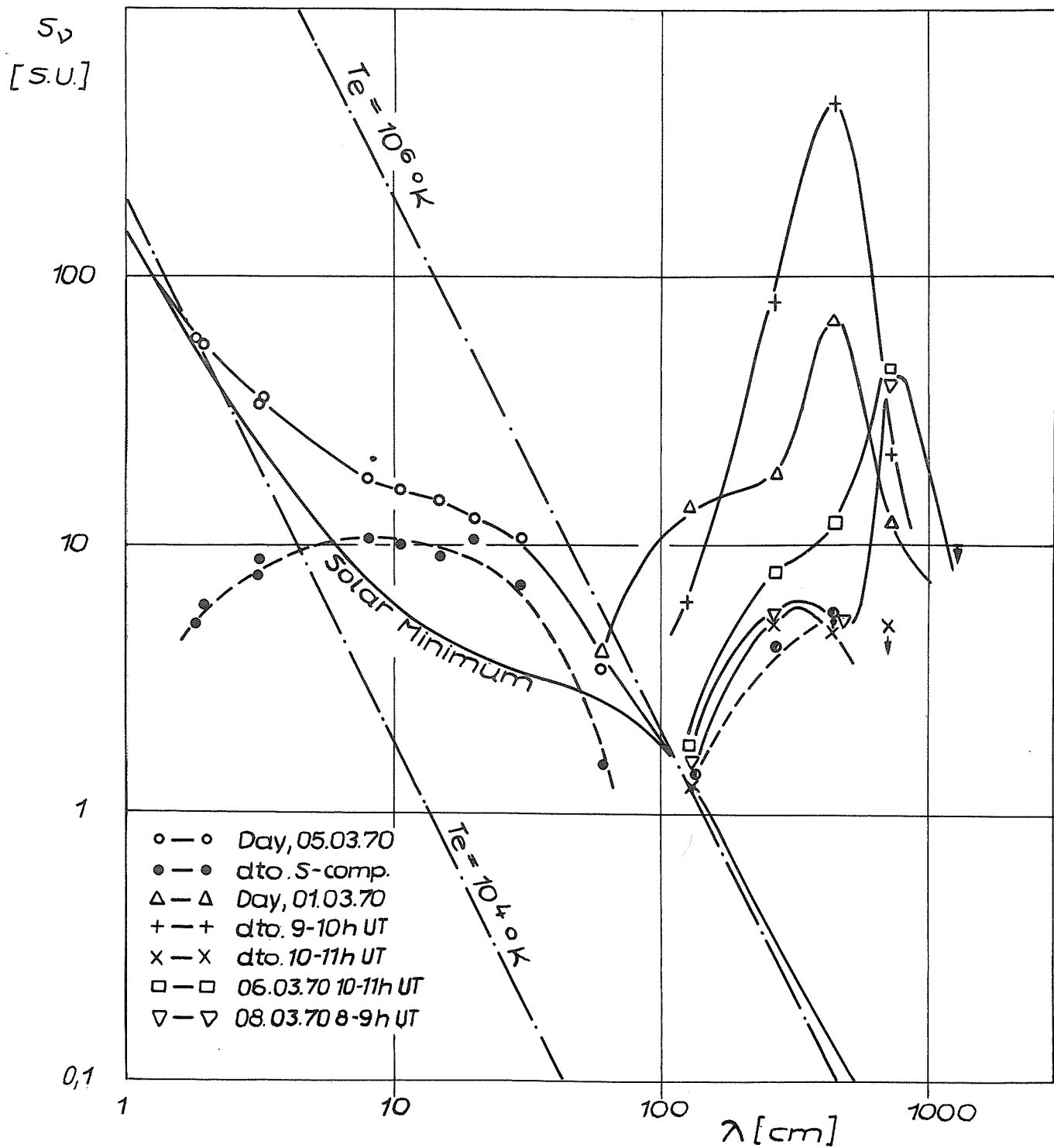


Fig. 3. Spectra of the S-component and noise storm emission.

Table 2

List of type IV bursts during 1970, March 1 - 15

Date Mar.	B u r s t				F l a r e			
	Start UT	Dur. min.	3 cm-flux s.u.	Freq. Range MHz	Start UT	Position	Imp.	Plage Reg.
01	05 00	80	550	100-17000	05 00	N06 E52	-B	10607
01	09 15	75	1250	23-19000	09 36	N05 E48	1B	10607
01	11 05	130	930	23-19000	{11 01 {11 43	N07 E50 N14 W33	1N 2N	10607 10595
01	13 00	60	190	23-19000	(13 58	N23 W57	-N	10592)
02	13 03	300	61	23-15400	13 17	N06 E32	-B	10607
07	01 39	135	60	100- 9400	01 38	S12 E10	2B	10614

It should be noted (Figure 3), that the spectrum of the noise storm shifted from shorter towards longer wavelengths so that accordingly a displacement of the source region into greater coronal heights can be assumed.

Summarizing the observational results of the March 1970 event it can be stated, that

- there is an evidence of a strong association between the complex of the noise storm emission and the occurrence of the particle event, and
- there appears a confirmation of the suggestion of a general dependency of the average energy of solar particle emission on the level of its origin inside the solar atmosphere in such a sense that the harder the emission, the deeper the level of origin.

REFERENCES

- KRÜGER, A. 1969 Remarks on the Slowly Varying Component of Solar Radio Emission during the Proton Flare Period of July 1966, Annals of the IQSY, 3, 70, MIT Press.
- KRÜGER, A. 1971 Physics of Solar Continuum Radio Bursts, Akademie-Verlag Berlin, to be published.
- FAN, C. Y., M. PICK, R. PYLE, J. A. SIMPSON, and D. R. SMITH 1968 Proton Associated with Centers of Solar Activity and their Propagation in Interplanetary Magnetic Field Region Corotating with the Sun, J. Geophys. Res., 73, 1555.
- DENISSE, J. F. 1952 Relation entre l'activité geomagnetique et l'activité radioelectrique solaire, Ann. Geophys. 8, 55.
- PICK, M. 1970 Permanent Sources of Particle Emission from the Sun, Invited Review, STP-Symposium, Leningrad.

"Radioheliograph Observations of Harmonic Type III Bursts"

by

D. J. McLean
Division of Radiophysics, C.S.I.R.O.
Sydney, N.S.W.

[Permission has been received to reprint this article from the Australian Journal of Physics, 24 (2), 1971.]

ABSTRACT

Observations have been made with the Culgoora radioheliograph and spectrograph of type III bursts which show clear fundamental and harmonic components. The significance of these observations is discussed.

Introduction

Smerd, Wild, and Sheridan [1962] have shown that observations of the relative positions of fundamental and harmonic components of type III bursts are important for an understanding of the process of emission of these bursts. In 2½ years of observations with a two-element interferometer they recorded only eight clearly identified harmonic bursts (of which three occurred on one day). It is highly fortunate therefore that on 1970 March 7, in one day's observation with the Culgoora radioheliograph, we observed sixteen clearly recognizable harmonic type III bursts and recorded 80 MHz images of both fundamental and harmonic components. In this paper we shall describe the observational records of these bursts.

Observations

Four distinct groups of type III bursts are included in the observations. Other type III groups also occurred on the same day but either contained no recognizable harmonic bursts, or took place outside the heliograph observing period.

A type I storm was in progress from March 6, 1970, 2141 UT (before the start of heliograph observations) to about 0100 UT on March 7. Figure 1(a) shows the source of this storm as it appeared at 80 MHz just prior to the first group of harmonic type III bursts. From the position and starting time of the type I storm, we can safely relate it to an importance 3 bright spray observed at N15° on the west limb at 1838 UT and associated with a centre of activity some 10° behind the west limb.

The first group of harmonic type III bursts started at 0026:20 UT. No chromospheric flare was observed near this time; it is likely that the ejections responsible for these bursts came from the centre of activity behind the west limb which was responsible for the type I storm. This deduction is based on the close proximity of the two sources at 80 MHz and on the high loop activity of this centre observed optically during the previous few hours. It is also consistent with Kai's [1970] observation that type I and type III bursts from the same centre of activity occupied different positions.

The dynamic radio spectrum of the type III group appears in Figure 2(a). Eight clear harmonic type III bursts are marked on this spectrum with the letters b, --- i. From their remarkable similarity these events may be considered homologous. The bursts of the subsequent groups (Figures 2(b), 2(c), 2(d)) are quite different in appearance from the first group, although some of them also form homologous sequences.

Figure 1 shows contour plots taken from the 80 MHz radioheliograms for the type I storm, event a, and for the type III events, b, --- i. In each case the fundamental source is shown by full contour lines and the harmonic source is shown dotted. The events are identified by the same letters in Figures 1 and 2(a). For events shown in Figures 1(b), 1(f), and 1(i) the type I storm was comparable in brightness with the type III burst, and so is clearly visible in the contour plots. In our discussion we shall ignore the contribution from the type I source. The other five type III bursts in Figure 1 were more intense and the type I source does not appear. Figures 2(b), 2(c), and 2(d) show the spectra of the three other groups to be considered here. The heliograph data for the eight harmonic type III bursts labelled j, --- q are plotted in Figure 3 and identified by the same letters.

Both the third (m,n) and fourth (o,p,q) groups of harmonic type III's can be associated with a subflare at N11° W33°, which started at 0115 UT. If, therefore, our assumption about the origin of the first group is correct, these later bursts originated in a different centre of activity. No flare was observed at the time of the second group but the 80 MHz positions suggest the same origin as for the third and fourth groups.

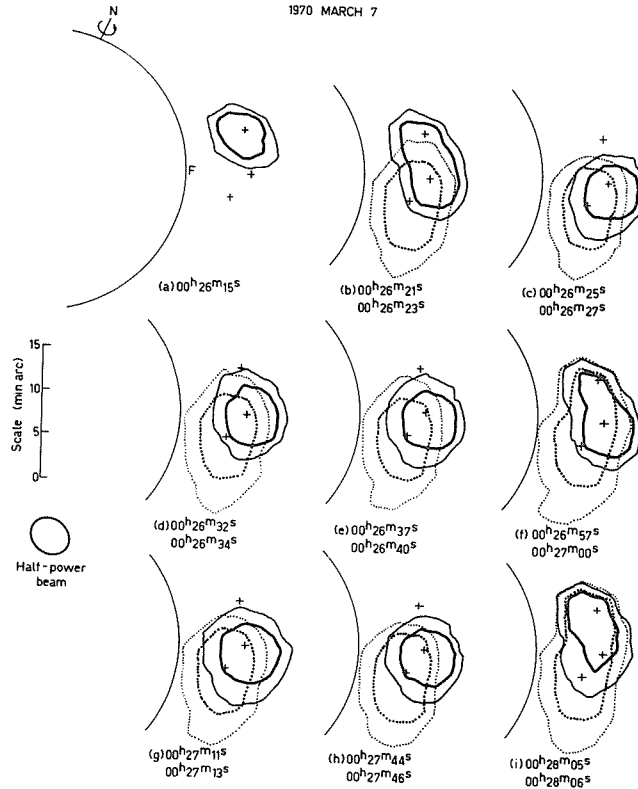


Fig. 1. Contour plots, from radioheliograms of a type I storm (a) and harmonic type III bursts (b, --- i). The heavy contours are at half-power and the light contours at quarter-power. For each of the harmonic type III bursts, the first time corresponds to the fundamental component of the burst (full-line contours) and the second time to the harmonic component (dotted). All the type III bursts on this figure occurred in a single group; the spectrum is shown in Figure 2(a). The positions marked by a + are the average positions of the centroids of the three sources. They are the same for all nine parts of the diagram. In (a), F indicates the presumed position of the related flare.

The degree of polarization of all these bursts is interesting. The type I storm centre showed about 70% right-handed circular polarization. The fundamental components of the first group of harmonic type III bursts were also polarized in right-handed sense, about 50% if we assume that there was no linear polarization, but the harmonic components showed no circular polarization.

None of the type III bursts in any of the other groups showed such strong circular polarization. However, with the possible exception of one burst, the fundamental components do appear to show a systematic 10% of right-handed circular polarization while the harmonic components are unpolarized. The exceptional case at 0033:50 UT (event j) does not appear to have been polarized at all. There is no sign of bi-polar structure in either the type I source or the various type III bursts. All the contour plots in Figures 1 and 3 were made from observations in the right-handed circular sense of polarization.

Discussion

The data presented here are of particular interest for a number of reasons.

(a) Homology. As mentioned earlier, the type III bursts of Figure 2(a) are strikingly alike, and different from those in the other groups discussed here and also from other groups on the same day. It is also evident from Figure 1 that the positions, sizes, and shapes of each harmonic pair in the first group are remarkably similar. However, the second and third groups of type III's (Figures 2(b), 2(c)) are also reasonable examples of homologous spectra, yet here the heliograph observations, although similar for bursts f, k, and l are not so for bursts m and n.

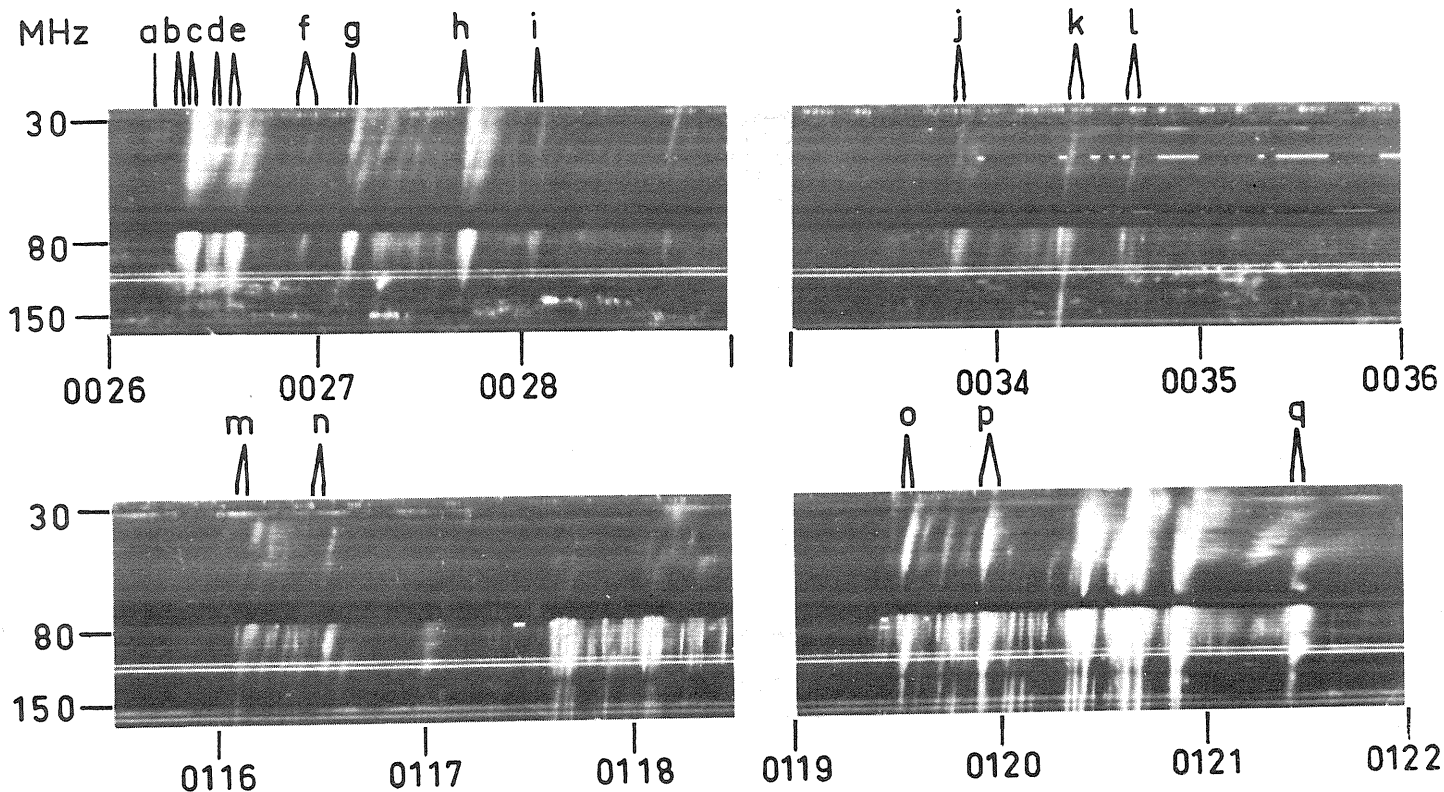


Fig. 2. Dynamic spectra of the harmonic type III bursts studied in this paper. Time increases along the abscissa, wavelength increases along the ordinate; the intensity of solar radio emission at each point is represented by the brightness of the spectrum at that point. Narrow horizontal bright lines are due to man-made interference. The times corresponding to the 80 MHz radioheliograms in Figures 1 and 3 are indicated by the letters a, --- q.

(b) Limb Events. Wild, Sheridan, and Neylan [1959] found that harmonic type III bursts are more commonly observed near the limb than near the centre of the disk. Their observations and the heliograph observations presented here, disagree with the simple theory based on refraction in a smooth corona, which predicts that the fundamental component will only be observable from the centre of the solar disk. A number of authors [Roberts 1959; Wild, Sheridan, and Neylan 1959; Shain and Higgins 1959] have discussed the effect of scattering on small-scale irregularities to explain this discrepancy, and Fokker [1965] has performed calculations which confirm this hypothesis for 200 MHz sources and give plausible sizes for sources. Similar calculations have not yet been performed for 80 MHz fundamental emission nor has any attempt been made to calculate the effect of scattering on the appearance of harmonic sources.

(c) Relative Position of Fundamental and Harmonic Bursts. Smerd, Wild, and Sheridan's [1962] observations of harmonic type III bursts were inconclusive in that they did not fit either of the proposed interpretations. It was predicted that the position of the harmonic component of a burst near the limb would fall several minutes of arc outside the position of the fundamental, if seen directly, or several minutes of arc inside the fundamental, if seen after reflection by the corona. However, as these authors point out, their observations with a two-element interferometer left open the possibility that the harmonic components of type III bursts were observed at the Earth both directly (due to forward emission) and after reflection on the corona (due to backward emission) with comparable intensities. Figures 1 and 3 show that all the sources on March 7, 1970, were simple (except for the peculiar feature near the centre of the Sun in Figure 3(k)). This does not mean that the sources were not double; in that case, however, the brightness of the second component must have been less than about 10% of that of the main component. (Labrum [1971] has observed one case where the source is indeed double, and he is able to draw some interesting conclusions from this observation.)

1970 MARCH 7

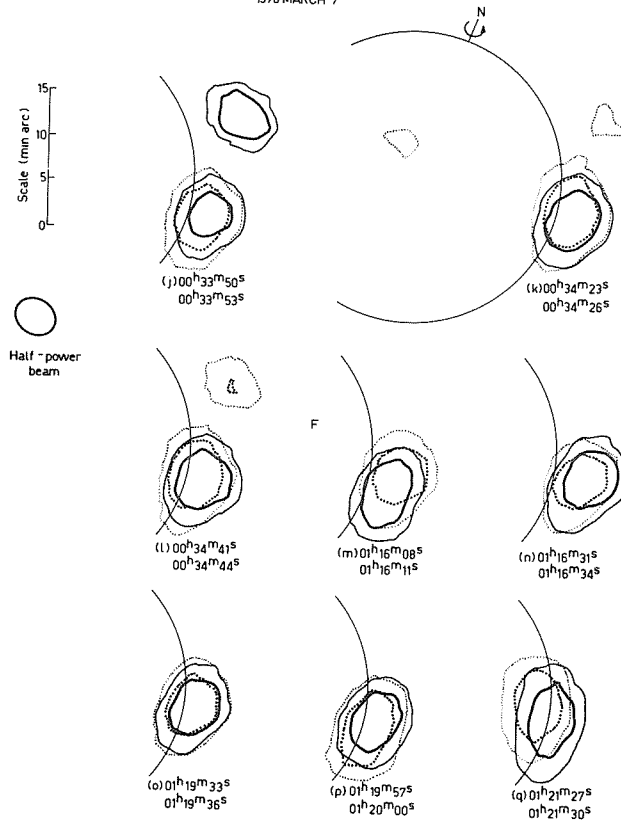


Fig. 3. Contour plots from radioheliograms of the fundamental (full-line contours) and harmonic (dotted) components of harmonic type III bursts. The bursts (j), (k), and (l) occurred in the second group (Fig. 2(b)), (m) and (n) in the third (Fig. 2(c)), and (o), (p), and (q) in the fourth (Fig. 2(d)). In (m) F indicates the observed position of the related flare.

Although we cannot yet explain why the position of the harmonic was so close to that of the fundamental, it would seem that in the present sample the harmonic components were seen after reflection by the corona, not directly. However, Morimoto [1964] has suggested that type III sources appear to come from above the plasma level deduced from optical data, because of the effects of coronal irregularities near the plasma level. Presumably the second harmonic emission coming from much higher in the corona, would not be affected in the same way. The apparent position of the fundamental would consequently lie much higher, and closer to the true position of the harmonic source than for the simple model used by Smerd, Wild, and Sheridan [1962]. This might suggest that for the present observations the harmonics were seen directly, except that they actually lie inside the positions of the fundamentals. At the same time Morimoto's [1964] argument makes the discrepancy between these observations and the simple model (assuming that the harmonic radiation is seen by reflection) still more difficult to explain. We conclude that a careful study, based on a realistic model, of the effects of propagation through the corona is needed before we can interpret these and similar observations successfully.

A further unpredicted feature is the tangential shift to the harmonic source relative to the fundamental. However, this is not surprising if one takes into account the large departures from spherical symmetry apparent in optical observations of the solar corona.

(d) Polarization. Type III bursts rarely show such strong polarization as was observed in the first of the groups described above. The contrast with the three later groups suggests that the extreme solar longitude of the first group may be a significant clue to the cause of this strong polarization. Once again we are faced with the need to consider in detail the effects of propagation through the corona from the source to the observer.

REFERENCES

- | | | |
|--|------|---|
| FOKKER, A. D. | 1965 | <u>Bull. Astr. Insts. Neth.</u> , <u>18</u> , 111 |
| KAI, K. | 1970 | <u>Solar Phys.</u> , <u>11</u> , 456 |
| LABRUM, N. R. | 1971 | <u>Aust. J. Phys.</u> (This volume.) * |
| MORIMOTO, M. | 1964 | <u>Publs. Astr. Soc. Japan</u> , <u>16</u> , 163 |
| ROBERTS, J. A. | 1959 | <u>Aust. J. Phys.</u> , <u>12</u> , 327 |
| SHAIN, C. A. and
C. S. HIGGINS | 1959 | <u>Aust. J. Phys.</u> , <u>12</u> , 357 |
| SMERD, S. F.,
J. P. WILD and
K. V. SHERIDAN | 1962 | <u>Aust. J. Phys.</u> , <u>15</u> , 180 |
| WILD, J. P.,
K. V. SHERIDAN and
A. A. NEYLAN | 1959 | <u>Aust. J. Phys.</u> , <u>12</u> , 369 |

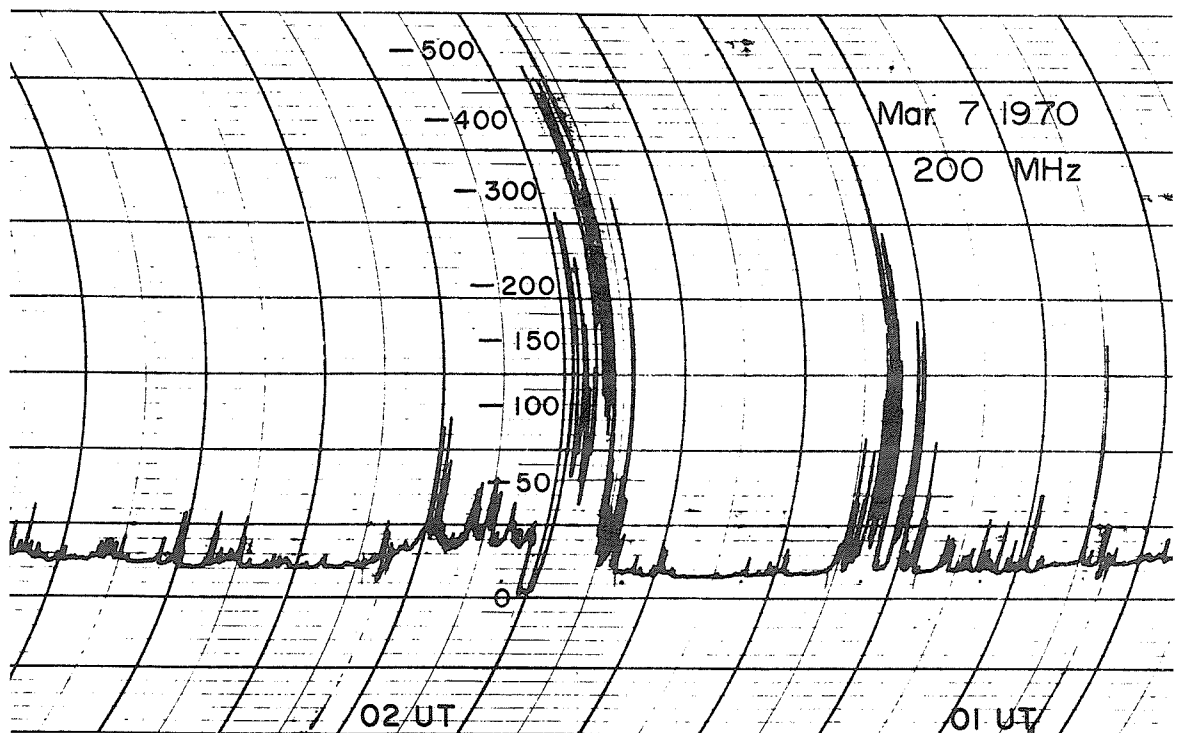
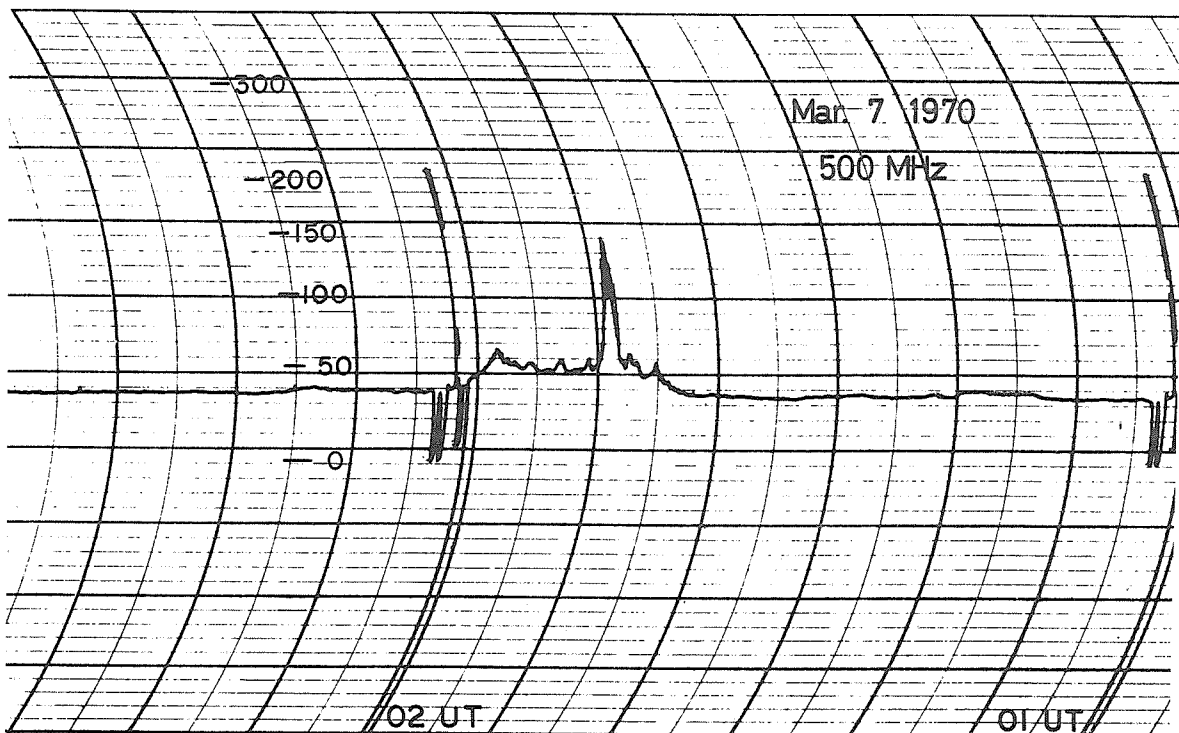
* Article in same issue as McLean's paper.

"Solar Radio Emission, Hiraizo, Japan"

by

F. Yamashita
Solar Radio Research Section
Radio Research Laboratories
Nakaminato-shi, 311-12
Ibaraki-ken, Japan

Copies of original records for several dates at the beginning of March 1970 were sent to WDC-A, Upper Atmosphere Geophysics. Reproduced below are the bursts on 200 MHz and 500 MHz associated with the importance 2B flare, which began at 0138 UT March 7. The flux unit is $10^{-22} \text{Wm}^{-2} \text{Hz}^{-1}$, and the calibrations are shown on the records,



"The Type IV Event on 6 March, 1970"

by

L. Fritzo~~va~~-Svestkova and J. Olmr
Astronomical Institute of the Czechoslovak Academy of Sciences
Ondrejov, Czechoslovakia

This contribution contains some conclusions deduced from the radio observations made at Ondrejov during the critical period from 6 to 10 March 1970. Because of bad weather conditions, there were only short periods of optical observations, for several hours on 7, 8 and 10 March. During this time two flares with importance 2, and seven flares with importance ≤ 1 were observed, but none of them had any connection with radio events registered at Ondrejov. In opposition to the incomplete visual observations the radio measurements were made every day continuously from about 0730 to 1530 UT on three frequencies: 808, 536 and 260 MHz. Table I contains data about all outstanding occurrences during the mentioned period: date, beginning, duration, type and intensity (expressed in the units $10^{-22} \text{Wm}^{-2} \text{Hz}^{-1}$ for frequencies 536 and 260 MHz and in the relative units of the base level for frequency 808 MHz).

Table I

Date Mar.1970	Beg. UT	Dur. Min.	Type	Peak Flux	Freq. MHz
8	1429	3.5	CD	3	808
6	1205	22	CD	120	536
9	0933	1	SD	95	"
6	1220	60	M(CD)	60	260
	1358	21.5	CD	45	"
9	0930	5	ECD	100	"
	1319	15.5	ECD	>110	"

From all our material only one event seems to be of actual interest. It is the radio outburst on 6 March registered at our observatory on 260 MHz (Figure 1). The record is characteristic for type IV, but surprisingly at the same time no increase was recorded on the frequencies 808 and 536 MHz. A slight peak on these frequencies can be suspected, but its existence is very problematic, the size being close to the threshold sensitivity. The situation can be understood when comparing registrations on different frequencies obtained at other solar stations. The curve on Figure 2 made from data of maximum flux at single frequencies indicates the U-shaped type IV burst which is characteristic for proton events [Castelli *et al.*, 1967]. But in contradiction to the similar known type IV events the intensity of this event is extremely weak and obviously did not exceed 50 units on 536 and 808 MHz, which is the threshold sensitivity of our device on these frequencies. In spite of it, this flare was the most probable source of energetic particles recorded near the Earth on 6 March at 1410 UT.

Thus, this event leads to an interesting conclusion: It confirms the fact discovered by Castelli *et al.* that a U-shaped type IV burst is usually associated with proton ejections on the Sun, but it contradicts to the other conclusion made by the same authors that at the same time the flux must be very high. The discussed event is one order weaker than the ones mentioned by Castelli *et al.* and in spite of this the flare was a particle source. Another interesting observation concerns the time delay from centimeter to meter wavelengths. The curves on Figure 3 show the delay of the type IV on meter waves which was extraordinarily great in comparison with similar other cases. This seems to confirm the conclusion made by Svestka [1970] that the weaker is the observed event, the greater delay of type IV on meter wavelengths can be expected.

REFERENCES

- CASTELLI, J. P., 1967 J. Geophys. Res., 72, 5491.
AARONS, J. and
MICHAEL, G. A.
SVESTKA, Z. 1970 Solar Phys., 13, 471.

ONDŘEJOV

6 MARCH 1970

260 MHz

$\cdot 10^{-22} \text{ W m}^{-2} \text{ Hz}^{-1}$

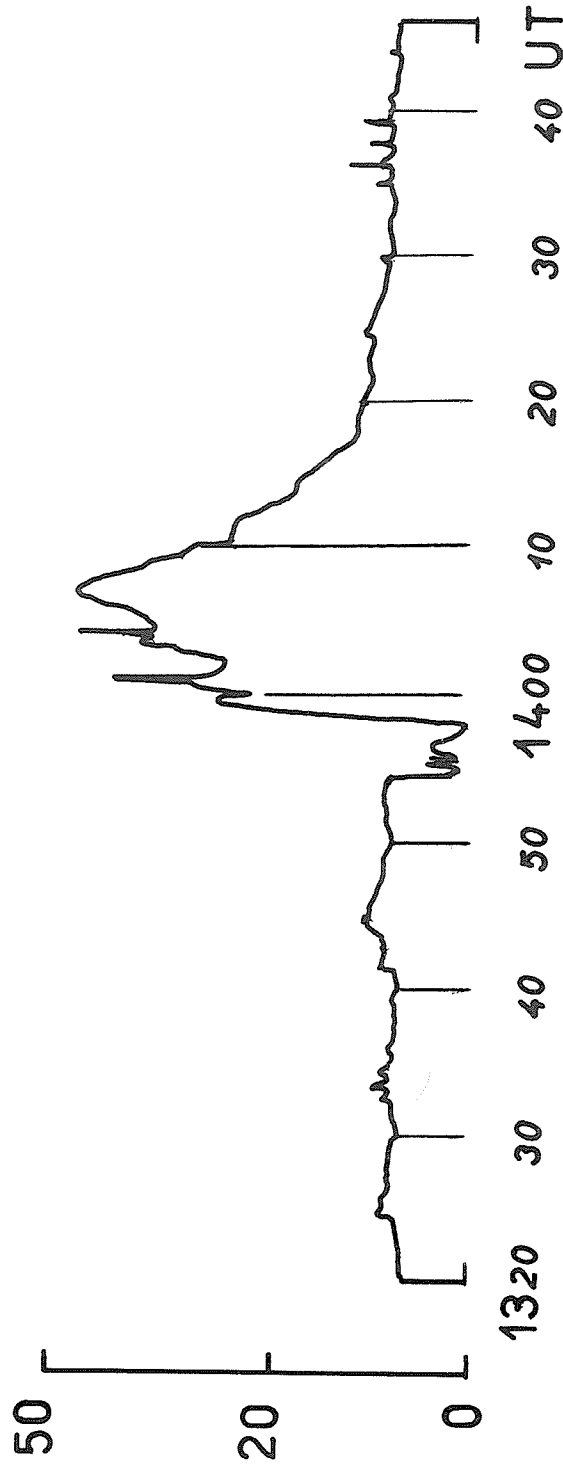


Fig. 1. Radio burst of March 6, 1970, recorded on 260 MHz.

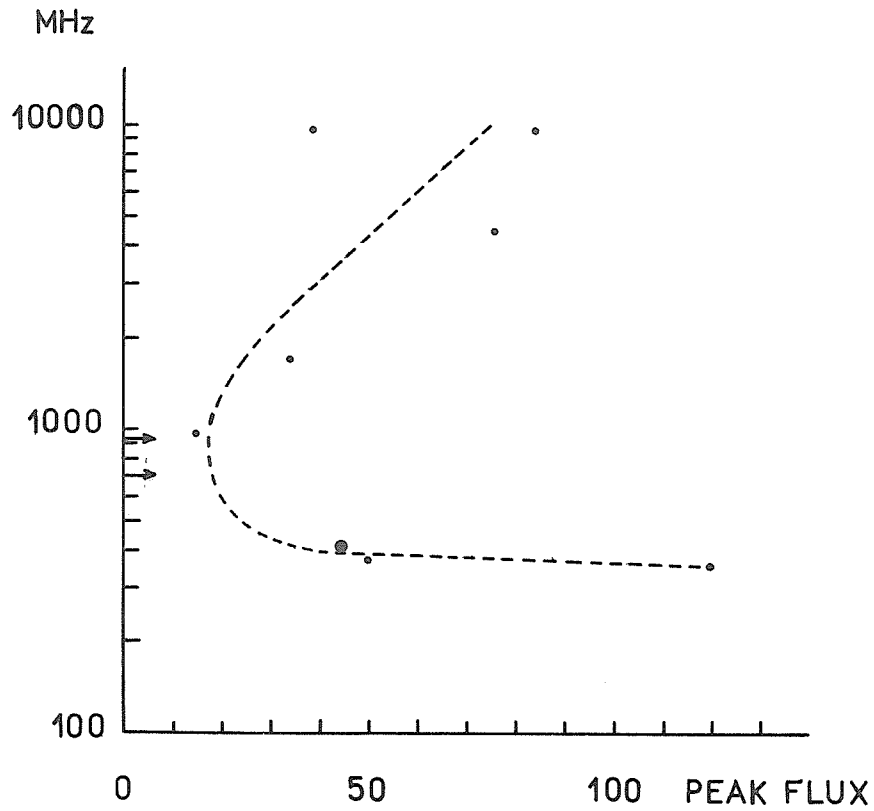


Fig. 2. The arrows indicate the frequencies 808 and 536 MHz on which no effect at Ondrejov was registered. The larger dot corresponds to the Ondrejov measurement on 260 MHz.

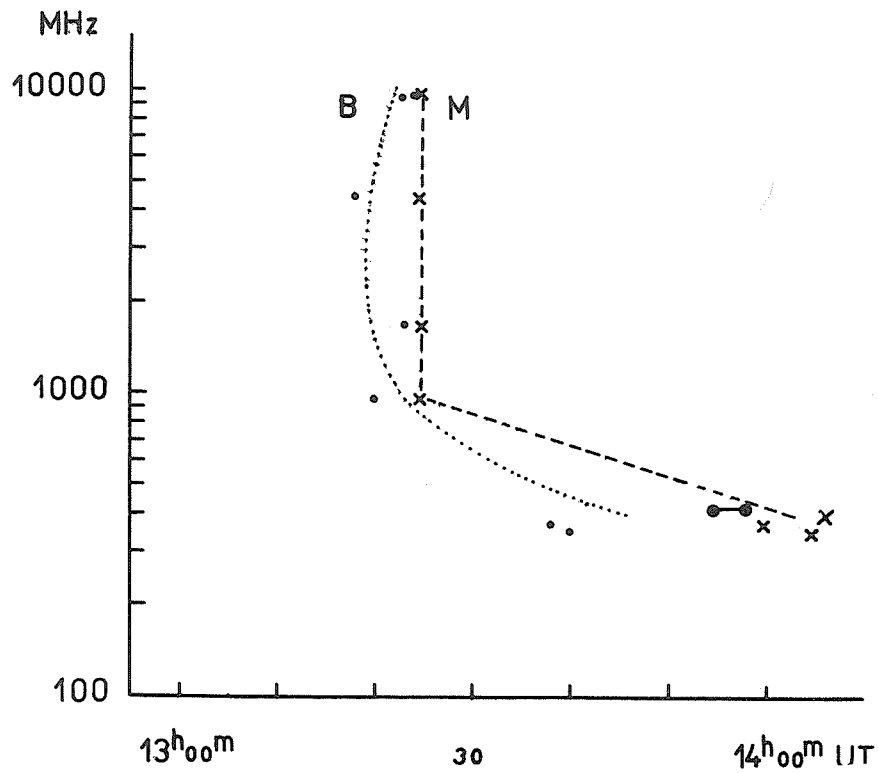


Fig. 3. Curve B is for the onset time, curve M for the time of maximum. Measurements from Ondrejov are indicated in a different way (larger marks).

"Microwave Burst of 6 March 1970 Proton Flare"

by

V. L. Badillo
Manila Observatory
P. O. Box 1231, Manila
Philippines

Events occurring on the invisible side of the sun can have geophysical effects. The PCA of March 6 and the sudden commencements of March 7 and 8, 1970 may be attributed to a proton flare occurring in McMath region 10595 behind the west limb on March 6, 1970 at about 0930 UT. (The time delays for these geophysical effects are about 6, 35 and 53 hours respectively.) The solar microwave burst recorded at this time shows peculiar characteristics which may provide information about the proton flare.

The time evolution and the spectrum of the radio burst are shown in Figures 1 and 2, respectively, while in Table 1 are listed comparative data for three similar proton flares. The duration of the March 6, 1970 burst is very short compared with the other two radio bursts also originating from behind the west limb. An explanation for the brevity of the duration will be proposed below. The bursts in the 4995 and 2695 MHz bands correlate well with each other, but not with the burst in the 1415 MHz band. The peak at 1415 MHz comes 0.1 minute after the peaks in the higher frequencies. Also noteworthy is the narrow bandwidth of the burst compared with bursts associated with proton flares.

Table 1
Burst Data for Proton Events Behind the West Limb

Date	Maximum (UT)	Duration (Min.)	Behind Limb	ssc Delay (Hrs.)	References
4 Nov 1968	0520	20	5°	?	Castelli, <i>et al.</i> (1970) Lafferty, <i>et al.</i> (1970)
30 Mar 1969	0249	105	15°	19	Badillo & Salcedo (1969)
6 Mar 1970	0934	4	10°	35,53	This paper.

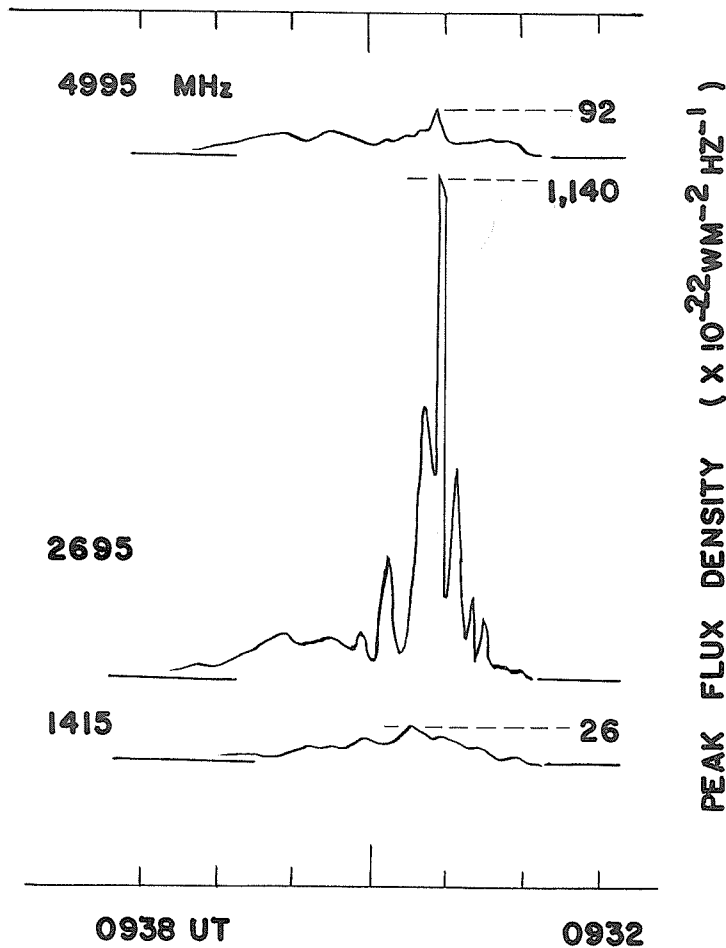


Fig. 1. Burst observed on 6 March, 1970 at Manila Observatory.

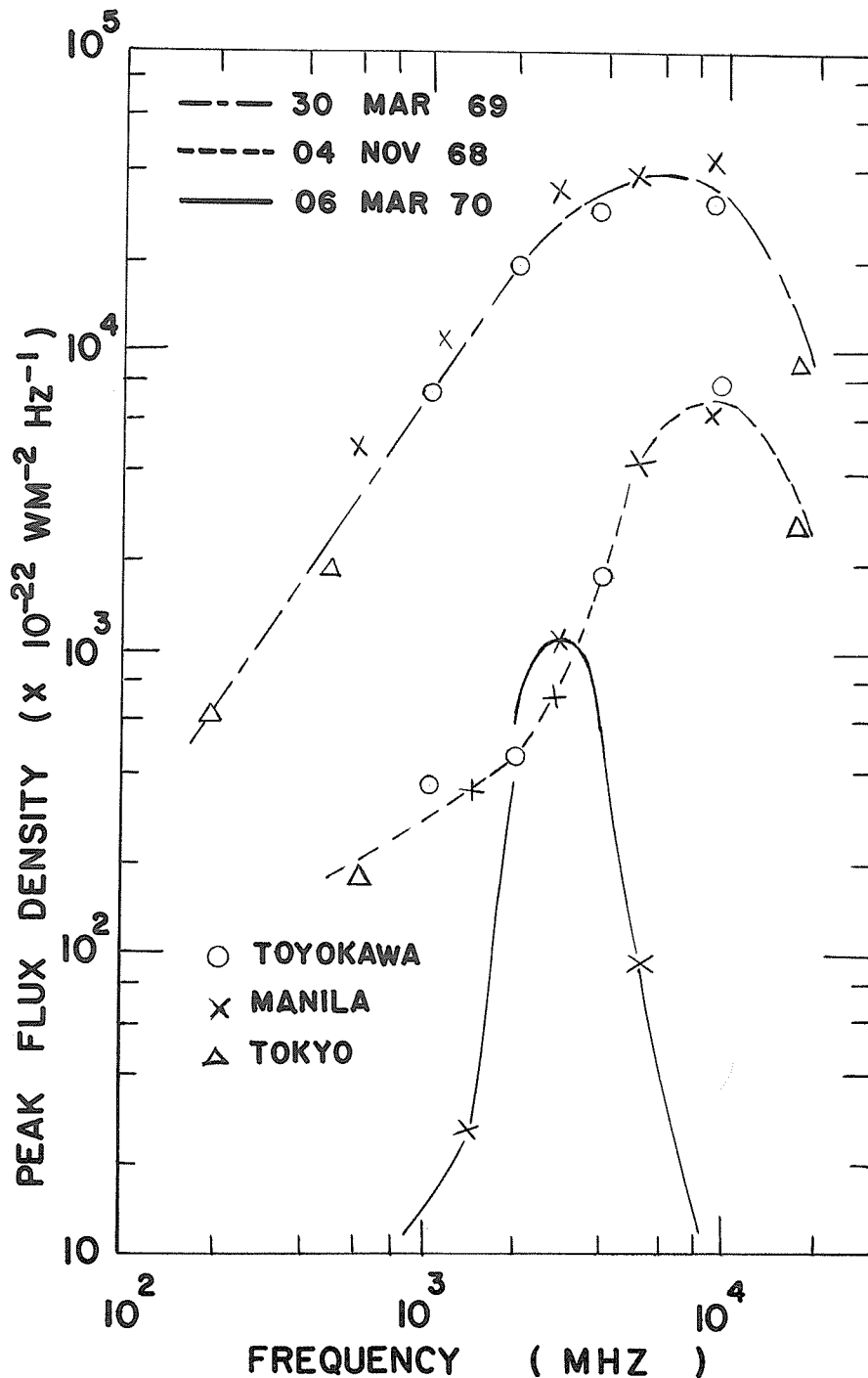


Fig. 2. Spectra of radio bursts from behind-the-limb proton flares.

Nothing measurable was recorded at 606 MHz and lower frequencies for the burst of March 6. The spectra of the three events are similar in the decrease of flux density with decreasing frequency. These spectra differ from the U-shaped spectrum characteristic of proton-producing flares [Castelli *et al.*, 1967]. However the U-shaped spectrum arises from flares on the disk. The spectral index of the March 6, 1970 burst is -6 , while that of the other two is -1.5 . The absorption at lower frequencies of the March 6 burst is stronger than for the other two bursts. But what makes the March 6 burst different from the other two is the absence of radiation at 8800 MHz. In all the radio bursts coming from this region before March 6, radiation at 8800 MHz was never absent. In fact, Sagamore Hill recorded a Great Burst from this region on March first.

Since radiation in the 8800 MHz band is always intense in radio bursts associated with proton flares, some suppression of this radiation must have occurred on March 6, 1970. A mechanism to be considered is occultation by the solar limb of the lower chromosphere, the source of radiation at

the higher frequencies. This mechanism does not seem to have affected the bursts on November 4, 1968 and March 30, 1969. But this mechanism would be enhanced if the electrons and protons were accelerated during the flare not just radially outward but in a decidedly westward direction, that is, in the direction away from the earth. This would explain the suppression of the radiation at the higher frequencies, the brevity of the burst duration and the longer time delay of the sudden commencements. Protons initially accelerated away from the earth could still reach the earth because of the "water hose" effect, but would have longer paths to travel. A longer travel time would allow a more pronounced bunching of protons with different initial velocities.

We are grateful to the following: H. Tanaka for Toyokawa data, T. Takakura for Tokyo data, J. Salcedo for careful measurements at Manila and J. Hennessey for encouragement and use of facilities. This research is funded by Air Force Cambridge Research Laboratories.

REFERENCES

- | | | |
|--|------|--|
| BADILLO, V. and
J. SALCEDO | 1969 | Solar Microwave Burst from Behind-the-Limb Proton Flare, <u>Nature</u> , 224, 503-504. |
| CASTELLI, J. P.,
J. AARONS and
G. A. MICHAEL | 1967 | Flux Density Measurements of Radio Bursts of Proton Producing Flares and Non-proton Flares, <u>J. Geophys. Res.</u> , 72, 5491-5498. |
| CASTELLI, J. P.,
W. CLARK,
W. O'BRIEN and
S. BASU | 1970 | Solar Radio Activity in Plage #9740 22 October-4 November 1968, <u>World Data Center A - Upper Atmosphere Geophysics Report UAG-8</u> , 112-126. |
| LAFFERTY, P. E.,
J. W. SNYDER and
J. H. REID | 1970 | Six Large Solar Events Recorded by NASA Solar Particle Network from October 27 to November 4, 1968, <u>World Data Center A - Upper Atmosphere Geophysics Report UAG-8</u> , 40-47. |

"High-Resolution Observations of a Microwave Burst on March 7, 1970"

by

Shinzo Enomé
The Research Institute of Atmospheric
Nagoya University

Observations

A microwave burst, which took place on March 7, 1970 at 0141 UT near the center of the solar disk [Tanaka, 1970], was one of the most rare events in the sense that there was no S-component before the burst at 3 cm and 8 cm. According to optical observations made at Mitaka and Okayama [Hiei, 1970], the associated flare had the form of a so-called "two ribbon" flare, which appeared just after the sudden disappearance of the overlying dark filament. These facts show that this is a typical "disparition brusque" [Hyder, 1967a, 1967b], but it occurred, unlike the usual case, unaccompanied by a pre-existing coronal condensation.

The single frequency observations (Figures 1a, 1b) show two distinct non-thermal features superposed on a thermal spectrum. The non-thermal spectra at 0145 UT and 0158 UT are plotted in Figure 2, which shows that the peak in the spectrum falls around 2000 MHz at 0145 UT and lower than 1000 MHz at 0158 UT. This, if we take an optically thin model of solar microwave radiation, means sub-relativistic electrons gyrating in a magnetic field of 250 Oersted at 0145 UT and 120 Oersted or less at 0158 UT at the source of the non-thermal components. This suggests that the latter activity occurred higher in the solar atmosphere than the former. The quick-scan record at 8 cm [Tanaka et al., 1969; Tanaka and Enome, 1970] shows no appreciable motion of the source of the burst even during its non-thermal activity. From this we can say that the source of the radio burst did not coincide with the position of the "two bright ribbons", since their separation increased with time [Hyder, 1967a; Hiei, 1970], and further that the position of the non-thermal components cannot be distinguished from that of the thermal, though we have not analyzed yet the absolute position of the source of the burst.

Another character of the non-thermal spectra is that there was a reversal of the sense of the circular polarization with frequency. The reversal frequency was between 2000 MHz and 1000 MHz.

As non-thermal activities ceased around 0200 UT, we can derive from the thermal spectrum at 0210 UT (Figure 3) the emission measure and the electron temperature of the source. N_e^{2V} is 10^{48} cm^{-3} and temperature is about $3 \times 10^6 \text{ }^\circ\text{K}$, if the effect of gyro-resonance absorption is neglected [Kakinuma and Swarup, 1962]. In fact, the thermal source showed the right-handed and left-handed circular polarizations of a few percent in the western and the eastern part of the source, respectively, at 9.4 GHz. This suggests that there was a small thermal component which was due to gyro-resonance absorption and that there was a magnetic field of 1100 Oersted at this thermal component. Comparing with the field-strength at the source of the non-thermal components, it may be that the thermal source was located lower than the non-thermal.

The observed size of the source was 1.4 min. of arc, while the theoretical beam width at the time of observation was 1.3 min. of arc at 9.4 GHz, which reveals that the size of the source was smaller than 1 min. of arc. Thus, the volume of the source may be 10^{28} cm^3 and N_e may be 10^{10} cm^{-3} .

Discussion

Phenomena associated with disparitions brusque have been studied and compactly summarized in papers by Hyder [1967a, 1967b]. The importance of infalling materials has been stressed in his study. An interaction between infalling gas and a coronal condensation, however, must also be taken into consideration. In this context, the March 7 event, although it was not so large in scale, has a significant meaning, since it was not associated with a coronal condensation.

The thermal energy of this event was 3×10^{28} ergs for the electron density of 10^{10} cm^{-3} . The estimation of the non-thermal energy depends much on the model, but it is much smaller than the thermal energy if there was no ejection of a plasma cloud. The gravitational energy of the dark filament has been calculated by Hyder [1967a]. It well covers the thermal energy loss calculated above.

As for the sense reversal of circular polarization with frequency, there are several reports of observations [Kakinuma, 1958; Tanaka and Kakinuma, 1959 and 1962; Tanaka and Enome, 1970]. Recently Ramaty and Holt [1970] have attempted to explain the polarization reversal by gyro-synchrotron self-absorption at the source; namely, with the optically thick model by Holt and Ramaty [1969]. Takakura and Scalise [1970] have criticized the theory of Holt and Ramaty for the following reasons; that their model requires a very efficient acceleration mechanism up to relativistic energies, that relativistic electrons should emit strong radio emission at higher frequencies, or that extremely anisotropic pitch angle distribution is necessary in order to suppress an excess radiation at higher frequencies.

1970 MARCH 7

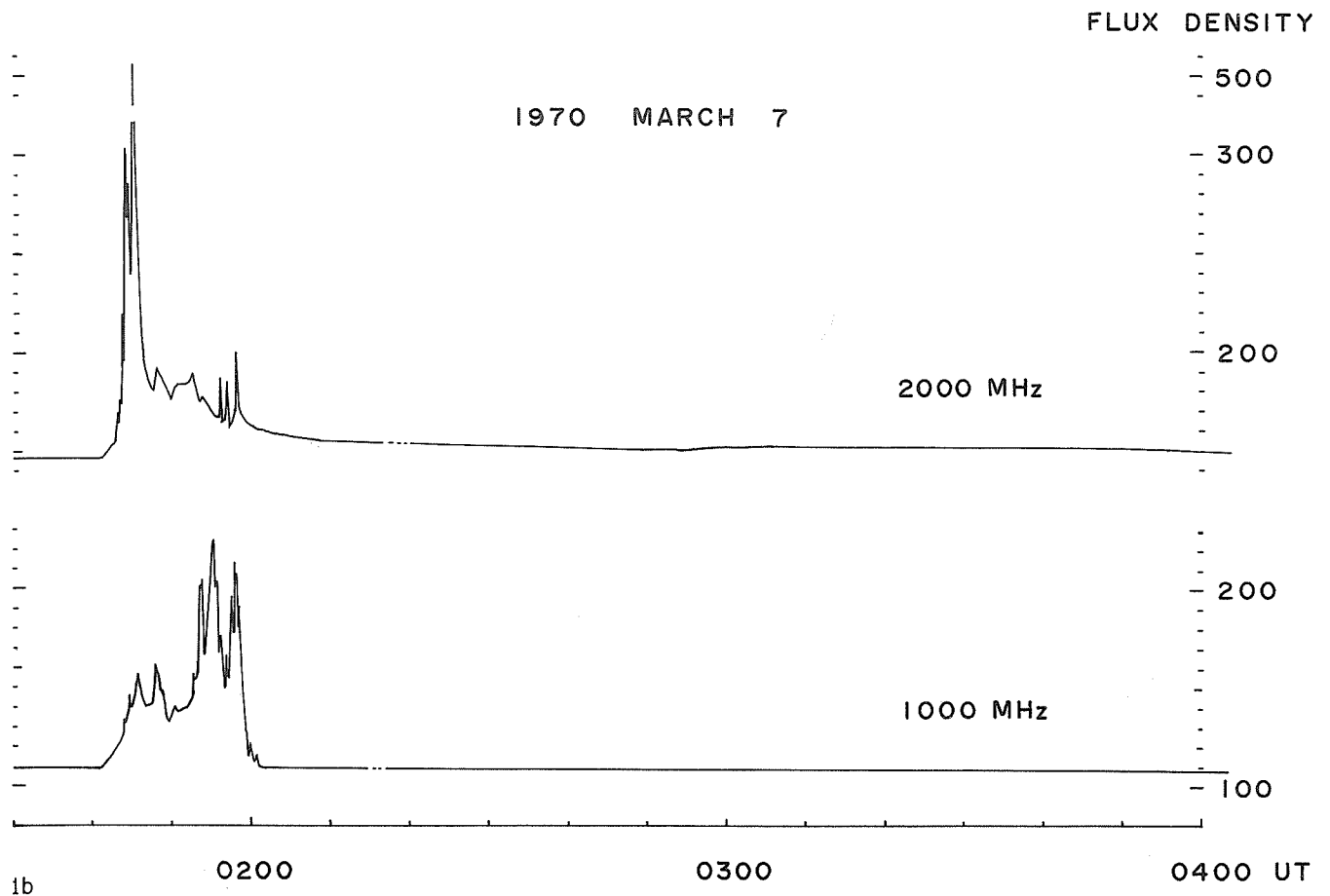
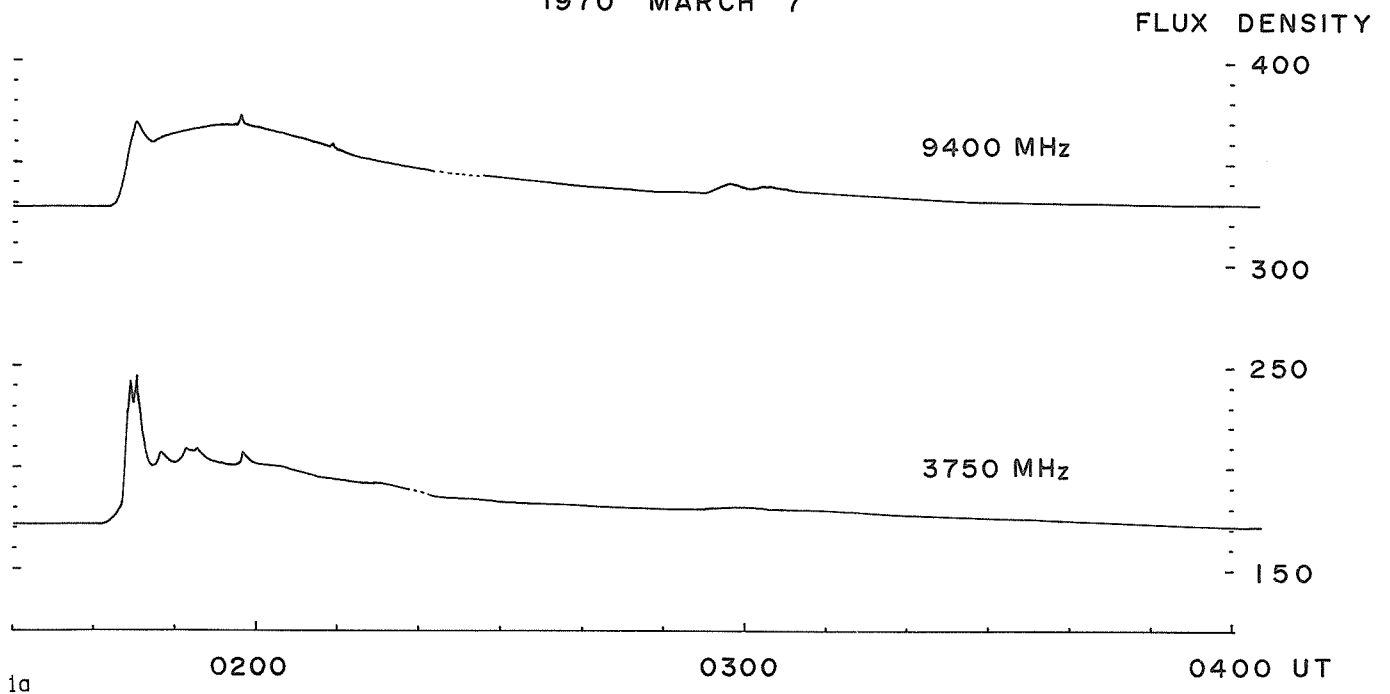


Fig. 1a and 1b. Records of the burst on March 7, 1970 at 9400 and 3750 MHz (Fig. 1a) and at 2000 and 1000 MHz (Fig. 1b). Units are $10^{-22} \text{ W m}^{-2} \text{ Hz}^{-1}$

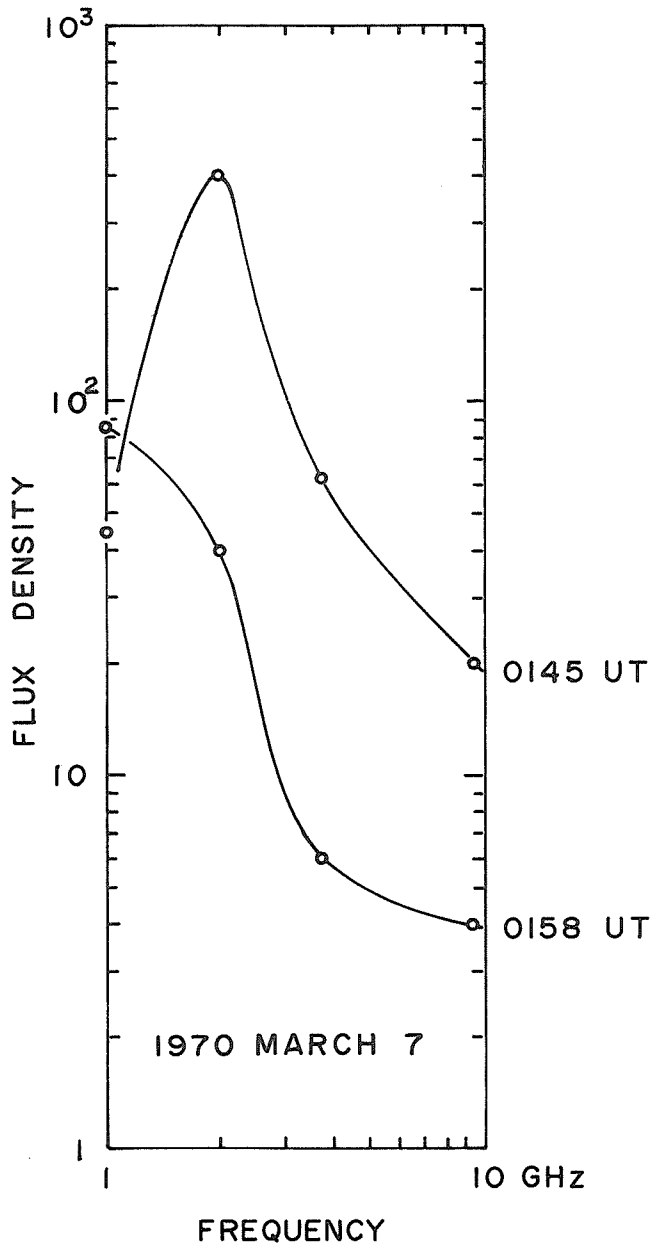


Fig. 2. The spectrum of non-thermal components at 0145 UT and 0158 UT. Flux density is in units of $10^{-22} \text{Wm}^{-2} \text{Hz}^{-1}$.

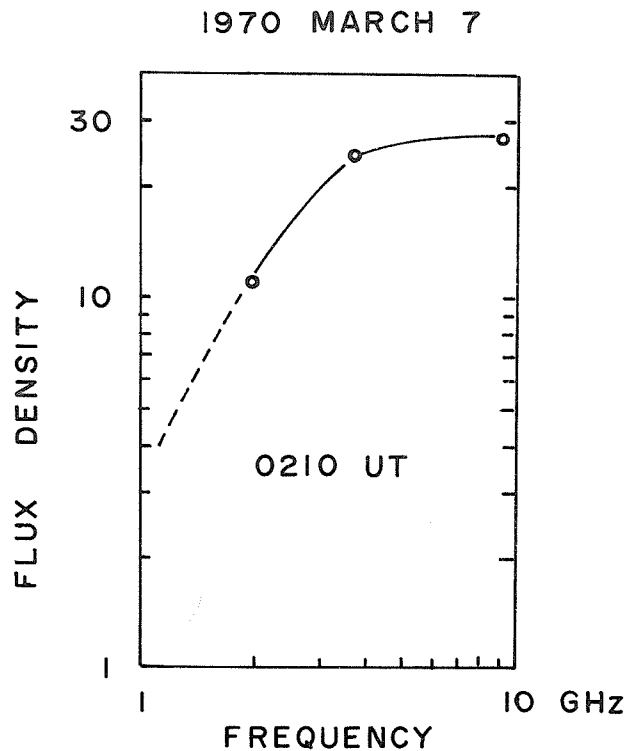


Fig. 3. The spectrum of the thermal component at 0210 UT. Flux density is in units of $10^{-22} \text{Wm}^{-2} \text{Hz}^{-1}$.

Here we would like to present observational facts that are unfavorable to the explanation by Ramaty and Holt [1970]. The reversal frequency falls usually between 3750 MHz and 2000 MHz and it does not depend on the intensity of bursts [Kakinuma, 1958]. The latter fact means that the optical thickness is independent of the intensity of bursts, if we take the viewpoint of Ramaty and Holt. Then the size of the source would be proportional to the square root of the intensity of bursts. The size of sources have been determined observationally to be less than 1 min. of arc and probably 0.5 min. of arc for impulsive bursts of hundreds of flux units [Enome et al., 1969]. In the case of the bursts on September 3 and November 14, 1960 the intensity was as high as 12,000 and 4,300 flux units at 3750 MHz, respectively, and they underwent the reversal of polarization [Tanaka and Kakinuma, 1961]. Thus, the size would have been larger than 5 min. of arc in these cases. Such a large size, however, could be measured even with the interferometers with poor resolution at that time. And from the results of high-resolution observations which have been made in this solar cycle we can hardly believe that.

Finally, we have not yet finished the analysis of data. Determination of the absolute position of the radio source is most important, since it may bring us some new evidence about the relation between optical and radio phenomena or thermal and non-thermal phenomena.

REFERENCES

- ENOME, S.,
T. KAKINUMA and
H. TANAKA 1969 High-Resolution Observations of Solar Radio Bursts with Multi-Element Compound Interferometers at 3.75 and 9.4 GHz, Solar Physics, 6, 428.
- HIEI, E. 1970 Private communication
- HOLT, S. S. and
R. RAMATY 1969 Microwave and Hard X-ray Bursts from Solar Flares, Solar Physics, 8, 119
- HYDER, C. L. 1967a A Phenomenological Model for "Disparitions Brusques" followed by Flarelike Chromospheric Brightenings I: The Model, its Consequences, and Observations in Quiet Solar Regions, Solar Physics, 2, 49
- HYDER, C. L. 1967b A Phenomenological Model for "Disparitions Brusques" followed by Flarelike Chromospheric Brightenings II: Observations in Active Regions, Solar Physics, 2, 267.
- KAKINUMA, T. 1958 Polarization of Solar Radio Bursts at Microwave Frequencies I, Proc. Res. Inst. Atmospheric, Nagoya Univ., 5, 71.
- KAKINUMA, T. and
G. SWARUP 1962 A Model for the Sources of the Slowly Varying Component of Microwave Solar Radiation, Astrophysical Journal, 136, 975
- RAMATY, R. and
S. S. HOLT 1970 Polarization Reversal of Solar Microwave Bursts, Nature, 226, 68
- TAKAKURA, T. and
E. SCALISE, JR 1970 Gyro-Synchrotron Emission in a Magnetic Dipole Field for the Application to the Center-to-Limb Variation of Microwave Impulsive Bursts, Solar Physics, 11, 434
- TANAKA, H. 1971 In this issue, pp. 61-64
- TANAKA, H. and
ENOME, S. 1970 High Resolution Observations of Solar Microwave Bursts, Nature, 225, 435
- TANAKA, H. and
T. KAKINUMA 1959 Polarization of Bursts of Solar Radio Emission at Microwave Frequencies, Paris Symposium on Radio Astronomy, ed. Bracewell, R. N. (Stanford Univ. Press), p. 215
- TANAKA, H. and
T. KAKINUMA 1962 Some Comments on Type IV Bursts, Intern. Conf. Cosmic Rays and Earth Storm, J. Phys. Soc. Japan, 17, Suppl. A-II, 211
- TANAKA, H.,
T. KAKINUMA,
S. ENOME,
C. TORII,
Y. TSUKIJI and
S. KOBAYASHI 1969 A High-Resolution Quick Scan Interferometer for Solar Studies at 3.75 GHz, Proc. Res. Inst. Atmospheric, Nagoya Univ., 16, 113

"Data submitted by Ahmedabad, India for the period March 2 - 10, 1970"

[Editor's Note: The compilers have prepared the following paragraph from correspondence from Dr. K. R. Ramanathan.]

The following data tabulations and copies of recordings were submitted by Dr. K. R. Ramanathan, Physical Research Laboratory, Ahmedabad, India. They detail the solar radio spectral events (Table 1 and Figure 1, prepared by R. V. Bhonsle), riometer SCNA events (Table 2 and Figure 2, prepared by S. S. Degaonkar), and 164 kHz, Tashkent to Ahmedabad, field-strength (SES) events (Table 3 and Figure 3, prepared by R. G. Rastogi) as recorded at Ahmedabad. Included in the tabulation of radio spectral events (Table 1) are also events reported by Weissenau, Germany and Culgoora, Australia. Table 4 (prepared by R. G. Rastogi and S. C. Chakarvarti) gives solar x-ray events from Explorer 37 which correspond to those recorded on the 164 kHz field-strength monitor.

The following data, tabulations and graphs, recorded at Ahmedabad have been submitted:

Table 1

Solar Radio Bursts (Frequency Range: 40-240 MHz)
recorded at Ahmedabad from 2 - 10 March, 1970

March 1970	Time of Observation		Station		Metric Band			Spectral Type
	Start UT	End UT			Start UT	End UT	Int	
02	0330	1130	A'bad		0335:00	0335:10	1	III B
			"		0337:20	0337:45	2	III
			"		0339:40	0340:10	1	III G
			"		0342:30	0344:30	1	III G
			"		0406:40	0407:30	1	III
			"		0418:40	0419:05	2	III G
			"		0430:30	0440:20	2	III G DP
			"		0505:50	0506:30	2	III G
			"		0523:10	0523:20	2	III B
			"		0600:40	0601:15	2	III
			"		0632:40	0633:30	2	III G
			"		0639:20	0641:45	2	III G
			"	Weis	0719:20	0720:50	2	III G
			"	"	0803:45	0804:30	2	III G
			"	"	0815:30	0815:35	1	III B
			"	"	0827:40	0828:00	1	III
			"	"	0903:10	0903:20	1	III
"	Weis	0921:40	0921:50	2	III B			
"	"	1025:50	1036:30	3	III GG			
03	0330	1130	A'bad	Culg	0628:30	0629:30	1	III G
			"	"	0630:30	0632:30	1	III G
			"	Culg	0638:10	0646:50	1	II, III G
			"	"	0944:40	0945:00	1	III G
			"	"	0950:20	0951:10	2	III G
			"	Weis	0954:30	0955:10	1	III G
04	0330	1130	"		0510:00	0516:00	2	III G
			"		0601:45	0602:00	1	III
			"	Weis	0659:20	0700:00	2	III
			"	"	0739:05	0739:20	1	III B
			"	"	0910:00	0910:10	2	III B
			"	"	0929:00	0944:00	3	III GG DP
"	"	0955:30	0956:25	2	III G			
05	0330	1130	"		0949:20	0949:40	1	U
06	0330	1130	"	Weis	0644:10	0645:00	1	III W
			"	"	0717:25	0717:45	1	III G
			"	"	0758:40	0759:40	1	III G DP
			"	"	0838:30	0838:35	1	III B W
			"	"	0844:50	0845:50	1	III G W
			"	"	0856:40	0858:00	1	III G W
			"	"	0931:40	0937:30	1	UNCLF W
			"	"	0952:40	0954:20	1	UNCLF W

Table 1 (continued)
 Solar Radio Bursts (Frequency Range: 40-240 MHz)
 recorded at Ahmedabad from 2 - 10 March, 1970

March 1970	Time of Observation		Station		Metric Band			Spectral Type
	Start UT	End UT			Start UT	End UT	Int	
06			A'bad		1017:00	1017:40	1	III W
			"		1047:00	1047:40	1	UNCLF
07	0330	1130	"	Weis	0656:50	0659:20	1	III G W
			"	"	0707:40	0708:00	1	III
			"	"	0720:30	0725:30	3	III GG DP
			"	"	0816:30	0819:30	2	III GG DP
			"	"	0826:20	0826:40	2	III B
			"	Weis	0834:30	0841:00	2	III G
08	0330	1130	"	"	0659:15	0735:50	3	III GG
09	0330	1130	"	Culg	0340:10	0341:40	1	III G W
			"	"	0343:30	0345:50	1	III G
			"	"	0346:36	0349:20	1	III G W
			"	Culg	0526:50	0527:00	1	III B
10	0330	1130	"		0412:20	0412:45	1	III G
			"		0417:20	0417:45	1	III G W
			"		0528:30	0528:45	1	III B
			"		0602:40	0602:50	1	III B
			"	Weis	0838:40	0840:10	2	III G
			"	"	0918:40	0920:30	2	III GG
			"	"	1002:20	1003:00	1	III G
			"	"	1102:00	1104:00	1	III G

A'bad - Ahmedabad (INDIA)
 Weis - Weissenau (GERMANY)
 Culg - Culgoora (AUSTRALIA)

The symbols used in connection with the spectral type in describing the important bursts are as follows:

B - Single burst
 G - Small group (<10) of bursts
 GG - Large group (>10) of bursts
 DP - Drifting pairs
 W - Weak
 UNCLF - Unclassified activity
 U - U-shaped burst of type III

Details of solar radio spectrograph at Ahmedabad:

1. Frequency range - 40-240 MHz
2. Sweep rate - twice per second
3. Frequency resolution - 300 kHz
4. Operation time - 0330 to 1130 UT on all days
5. Antenna - Three rhombic antennae
6. Antenna mounting - Steerable equatorial

DYNAMIC SPECTRA OF TYPE II AND III
SOLAR RADIO BURSTS AT AHMEDABAD

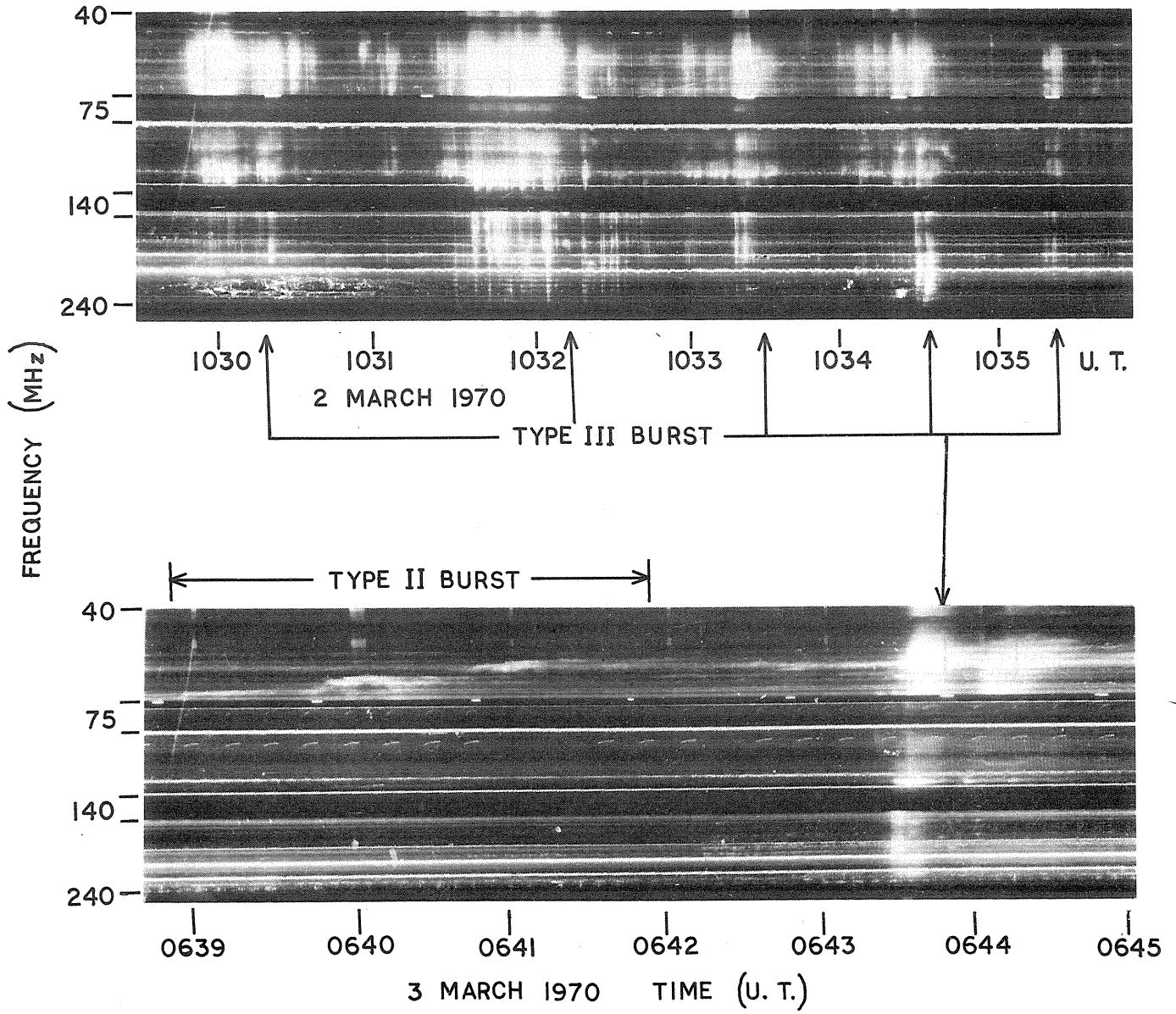


Fig. 1.

Table 2

Details of the sudden cosmic noise absorption recorded at 21.3 MHz at Ahmedabad

Date March 1970	Start Time	End Time	Max. Time	Maximum Absorption dB	Remarks
05	0432	0515	0500	1.0	Gradual; no sharp maximum
06	0932	0955	0937	1.9	"

RIOMETRIC RECORDING ON 21.3 MHz AT AHMEDABAD

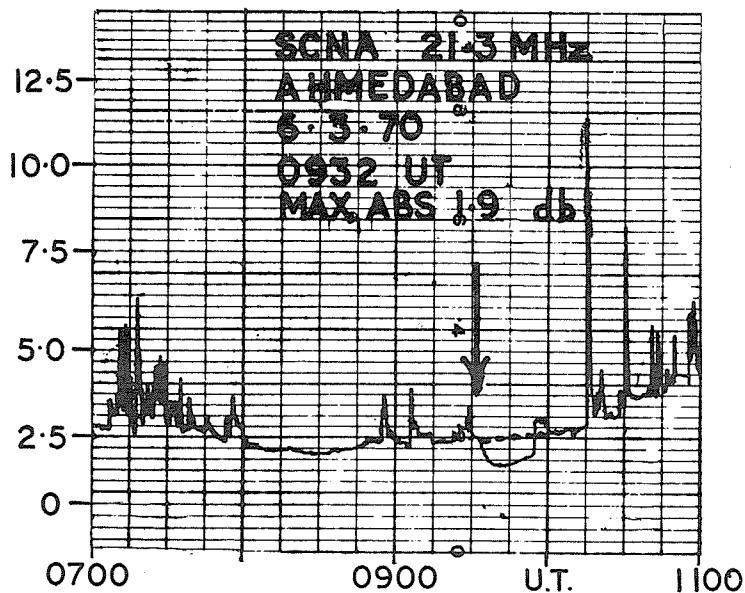
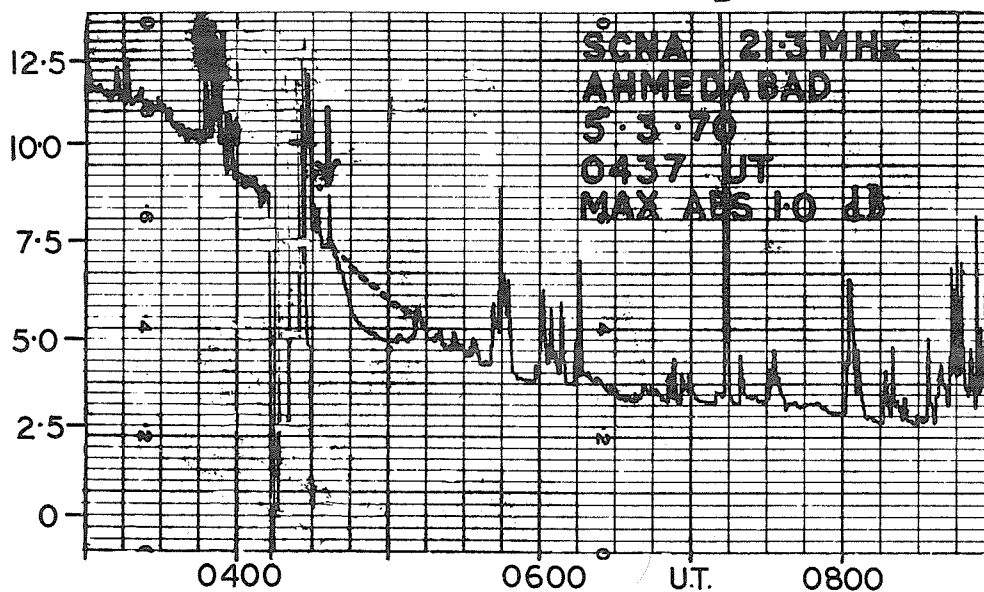


Table 3

Details of timings of the flare effect observed in
the field-strength records of 164 kHz radio waves

Tashkent to Ahmedabad

Date March 1970	Start Time	End Time	Peak Time	Remarks
02	0415 0714 0910	0430 0724 1030	0716 0925	Small Small Fairly big
03	0629 0841	0745 0925	0656 0852	Fairly big Fairly big
04	0603	0630	0615	Small
05	0415 1155	0620 1223	0446 1207	Big Small
06	0932	1058	0940	Big
10	0652	0852	0735	Fairly big

Table 4

X-ray flare events (Explorer 37, *1-8Å) corresponding
to those recorded on 164 kHz field-strength

Date March 1970	Start Time	End Time	Peak Time
02	0417 0910 1007	0430 0930 1108	0428 0929 1034
03	0630 0905	0649D 0916	0649 0905
05	0418 1200	0801 1240	0444 1207
06	0934	1105	0940
10	0700	0857	0746

* from Solar-Geophysical Data, 309 Part I, 80-81, May 1970,
U.S. Department of Commerce, (Boulder, Colorado, U.S.A. 80302).

FIELD STRENGTH RECORDINGS

TASHKENT 164 KHz. TRANSMISSIONS - AHMEDABAD

FIELD STRENGTH - ARBITRARY UNITS

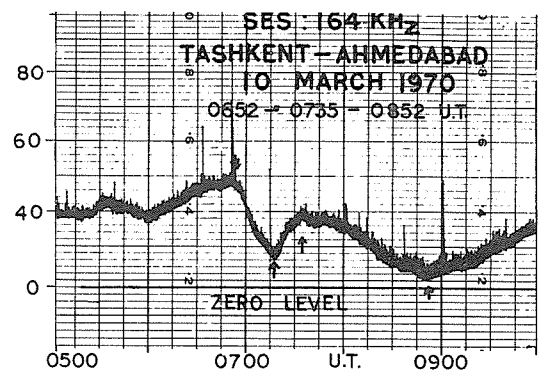
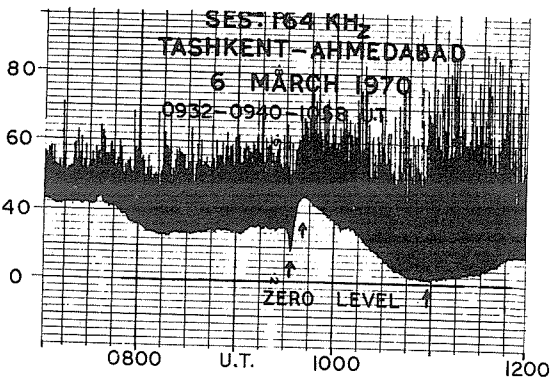
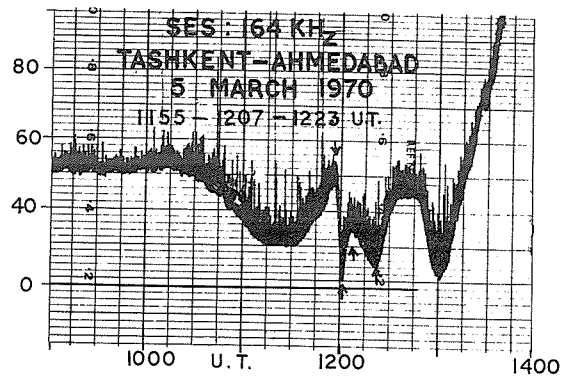
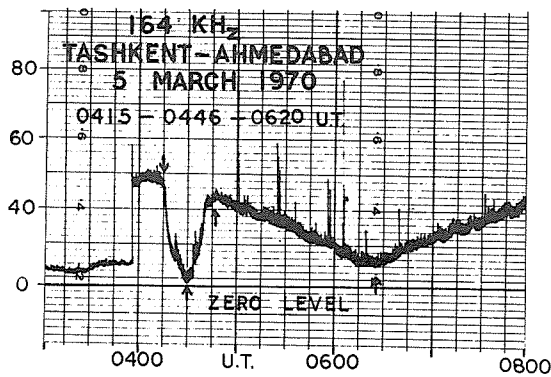
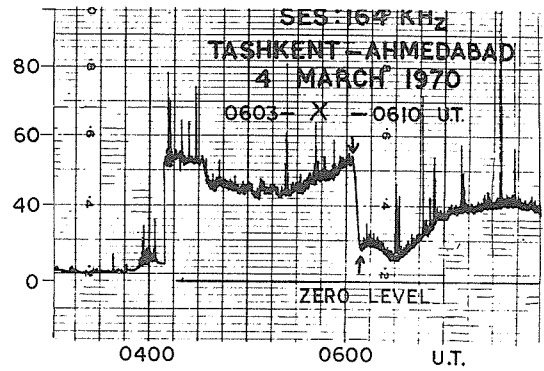
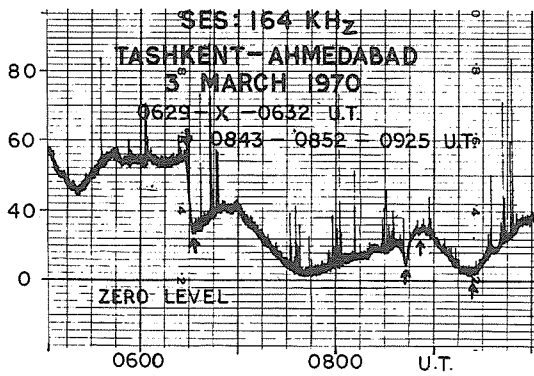
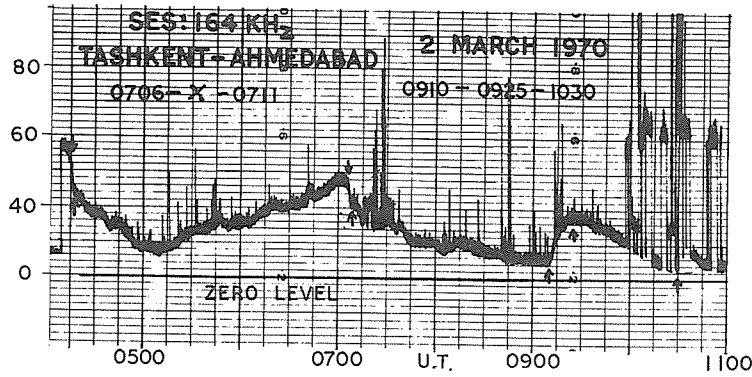


Fig. 3.

4. SOLAR X-RAYS

"Solar Activity and Earth Atmospheric Densities in March, 1970"

by

D. E. Knight, R. J. Uribe and B. E. Woodgate
Mullard Space Science Laboratory
Holmbury St. Mary
Dorking, Surrey, England

The OSO-6 satellite was launched on August 9, 1969 into a 500 km high circular orbit of inclination 33° to the equator. Its orbital period is 96 minutes. Its operation has continued beyond March, 1970.

On board is an experiment from University College, London. It is a grazing incidence grating spectrometer which measures the EUV flux from the whole Sun in several spectral lines every 4 seconds.

Figure 1 shows relative daily average fluxes in the lines tabulated for the period February 19 to March 26, 1970.

Wavelength	Resolution	Contributing Ions	Ionization Potential	Log. Temp. of max. abundance of ion*
304Å	5Å	HeII, SiXI	54.4 eV, 476 eV	4.9, 6.2
1175Å	3.5Å	CIII	47.9 eV	4.75
584Å	5Å	HeI	24.6 eV	4.5
537Å	1.0Å	HeI	24.6 eV	4.5
180Å	1.0Å	FeXI	290 eV	6.1
256Å	0.5Å	HeII, SiX	54.4 eV, 401 eV	4.9, 6.0
835Å	0.9Å	O II, O III	35.1 eV, 54.9 eV	4.4, 4.8

* Mostly taken from Jordan [1969]

It may be seen that the 304Å line peaks on March 11 and the 1175Å line peaks on March 21. Each of these peaks may be identified as originating from different plages, McMath-Hulbert regions 618 and 641, respectively, by comparing EUV flux variations with X-ray and radio flux variations and positions, and plage and sunspot positions using the ESSA Solar-Geophysical Data [1970]. These two lines are primarily formed at similar temperatures and so would be expected to vary together. However, CIII has triplet and singlet states, and the 1175Å line upper level is populated from the triplet metastable pseudo-ground-state, and has an extra density dependence [Jordan 1971]. It appears that Region 641 is denser than Region 618 at their times of maximum activity.

Earth's Upper Atmosphere

By monitoring the HeII 304Å line at satellite dawn and dusk, profiles of transmitted flux versus probing point height were obtained. (The Probing point is defined as the point of minimum height above sea level for the central solar ray to the satellite.)

Theoretical profiles of transmitted 304Å through the upper atmosphere versus probing point height were calculated using the Spring/Fall models from the US66 Standard Atmosphere Supplements, together with the absorption cross sections of molecular oxygen, atomic oxygen and molecular nitrogen to 304Å given by Huffman [1969]. (They are 17, 9 and 12 megabarns, respectively.)

Exospheric Temperature is the parameter used in the US66 Standard Atmosphere Supplements to describe the height density relation of the model composition. The observed profile was referenced to the theoretical profiles and hence, an exospheric temperature and standard deviation were derived. The referencing of the observed to theoretical profiles was restricted to the regions of .3 and .8 transmitted relative intensity and thus to a height range of approximately 300 km to 400 km.

Figure 2 shows exospheric temperatures at satellite dawn and dusk computed in the above manner for time period of February 28 until March 16, 1970. The $\pm \sigma$ levels for each exospheric temperature point are included. The latitudes of the probing points for sunrise and sunset are shown and for comparison purposes the 3 hour Kp indices are plotted.

REFERENCES

- | | | |
|----------------|------|---|
| HUFFMAN, R. E. | 1969 | <u>Can. J. Chem.</u> , <u>47</u> , 1823. |
| JORDAN, CAROLE | 1969 | <u>Mon. Not. R. Astr. Soc.</u> , <u>142</u> , 501. |
| JORDAN, CAROLE | 1971 | to be published in ' <u>Highlights of Astronomy</u> ' |

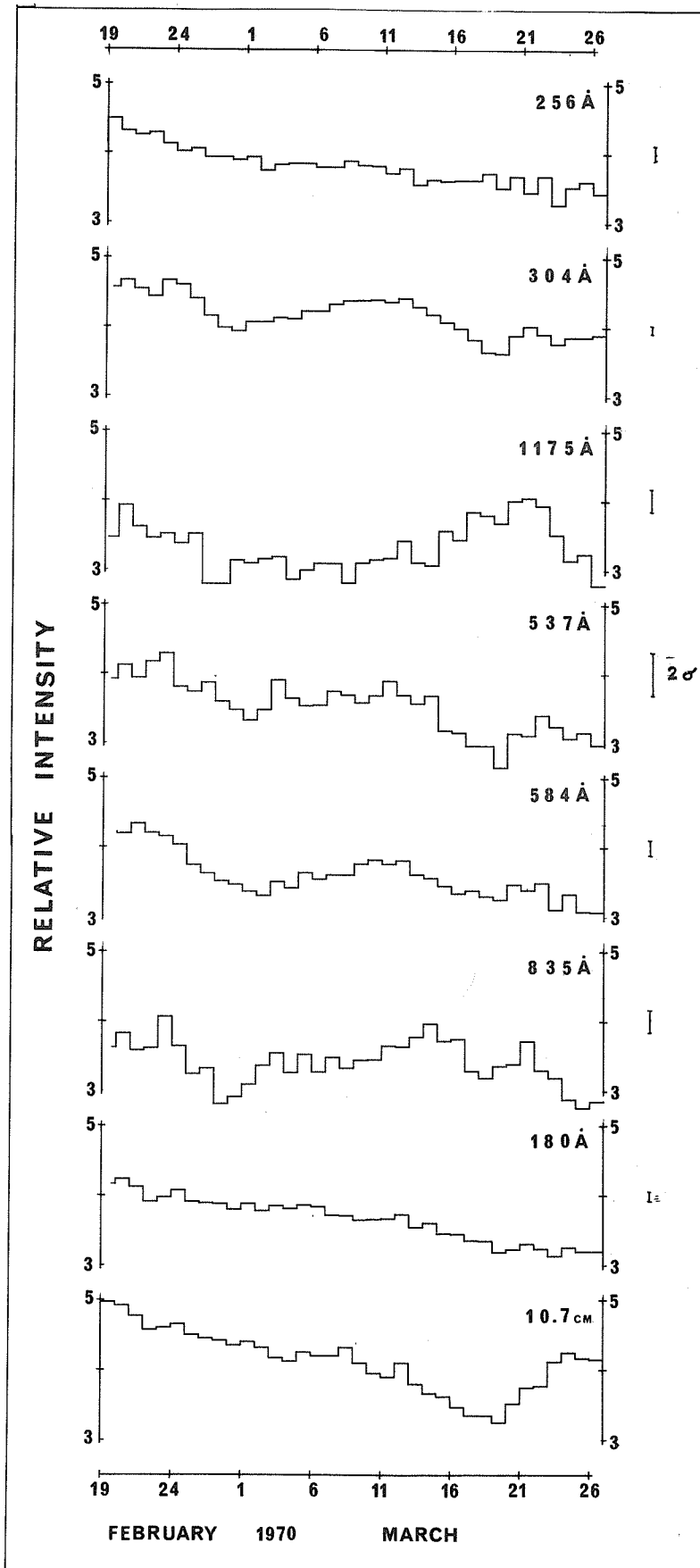


Fig. 1. Relative daily average fluxes for the lines indicated, for February 19 - March 26, 1970.

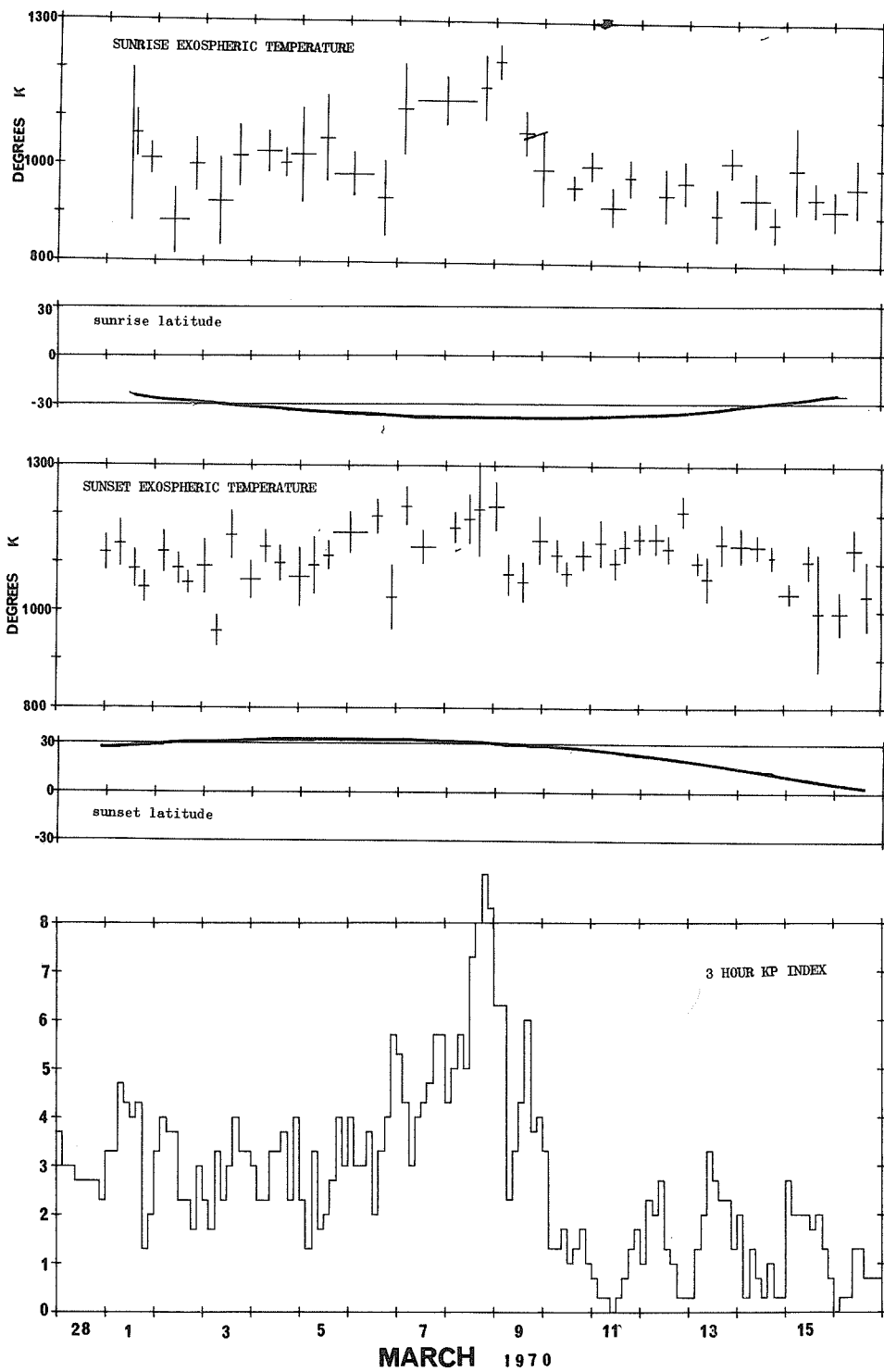


Fig. 2. Exospheric temperatures at satellite dawn and dusk, latitude of probing point and Kp, February 28 - March 16, 1970.

"Physical Models of Two Plage - Associated X-ray
Emitting Regions during the Period March 1 to 14, 1970"

by

P. R. Sengupta
Department of Electronics
I.I.T., Kharapur, India

A large number of X-ray flares were associated with the McMath plage regions 10607 and 10618 during the period March 1 to March 14, 1970.

Physical data of the 0-20Å X-ray emitting regions associated with these two plage regions calculated from the daily 9.1 cm. Radio-Spectroheliograms made by Stanford University, Radio Astronomy Laboratory, and published in Solar-Geophysical Data, NOAA, Boulder [Number 309, Part I, 1970], employing the empirical relation developed by the author [Sengupta, P. R., 1970] are listed in the first three columns of Tables 1 and 2. $T_{i,max}$ is the maximum emission temperature, $n_{e,max}$ the maximum electron density and 'y' the total emission measure of the region. The decay of the active region associated with McMath region 10607 and growth and decay of the active region associated with McMath region 10618 are evident from the calculated data. In column 4 are listed the total 0-20Å flare energy, $E(0-20\text{\AA})$, emitted from the region during the day. $I(0-20\text{\AA})$ listed in column 5 are the emitted flare energy per unit emission measure. The daily $E(0-20\text{\AA})$ values and the ratio of the 0.5-3Å and 1-8Å flux, $F(0.5-3\text{\AA})/F(1-8\text{\AA})$ are obtained from the reported X-ray flux values from the NRL experiment on SOLRAD 9. In some cases extrapolation became necessary for computing $E(0-20\text{\AA})$ as the data are not always continuous for all the flares. The X-ray flares associated with the regions are identified from their coincidence with the optical flares from the regions. The daily flux ratio listed in the tables is for the hardest flare of the day. The $F(1-8\text{\AA})$ values used are corrected for the spectral distribution.

Table 1

Calculated and Observed Physical Data for 0-20Å
Emitting Region Associated with McMath Region 10607

Date Mar.	$T_{i,max}$ (10^6 °K)	$n_{e,max}$ ($10^9/cm^3$)	y (10^{48})	$E(0-20\text{\AA})$ (10^{30} erg)	$I(0-20\text{\AA})$ (10^{-19})	$\frac{F(0.5-3\text{\AA})}{F(1-8\text{\AA})} \times 100$
1	2.0	4	5	4.2	8.4	10
2	2.0	4	7	5.9	8.4	10
3	1.9	3	4	2.8	7.0	8
4	1.8	2	2.5	1.4	6.0	6
5	1.8	2	1.5	0.85	5.8	8
6	1.8	2	1.3	0.76	6.1	-
7	1.7	1.5	1.0	0.50	5.0	5
8	1.6	1.0	1.0	0.42	4.2	5
9	1.6	1.0	0.5	0.22	4.4	-

The flare X-ray emission is seen to be closely related to the calculated physical data of the emitting regions. This agreement is significant. In Figure 1, the daily $I(0-20\text{\AA})$ is seen to be exponentially related to the calculated $T_{i,max}$ and $n_{e,max}$ values in case of both the regions. But the slopes are different for the two regions, as also the $I(0-20\text{\AA})$ from the two regions for a given value of $T_{i,max}$ and $n_{e,max}$. This shows that while for an individual region $\log I(0-20\text{\AA})$ is directly proportional to $T_{i,max}$ or $n_{e,max}$, the quantity of flare energy is also dependent on other parameters like the location of the regions and the associated magnetic fields, etc. It is interesting to note that the non-flare X-ray emission, on the other hand, has been found to be dependent only on T_i and n_e [Sengupta, P. R., 1970].

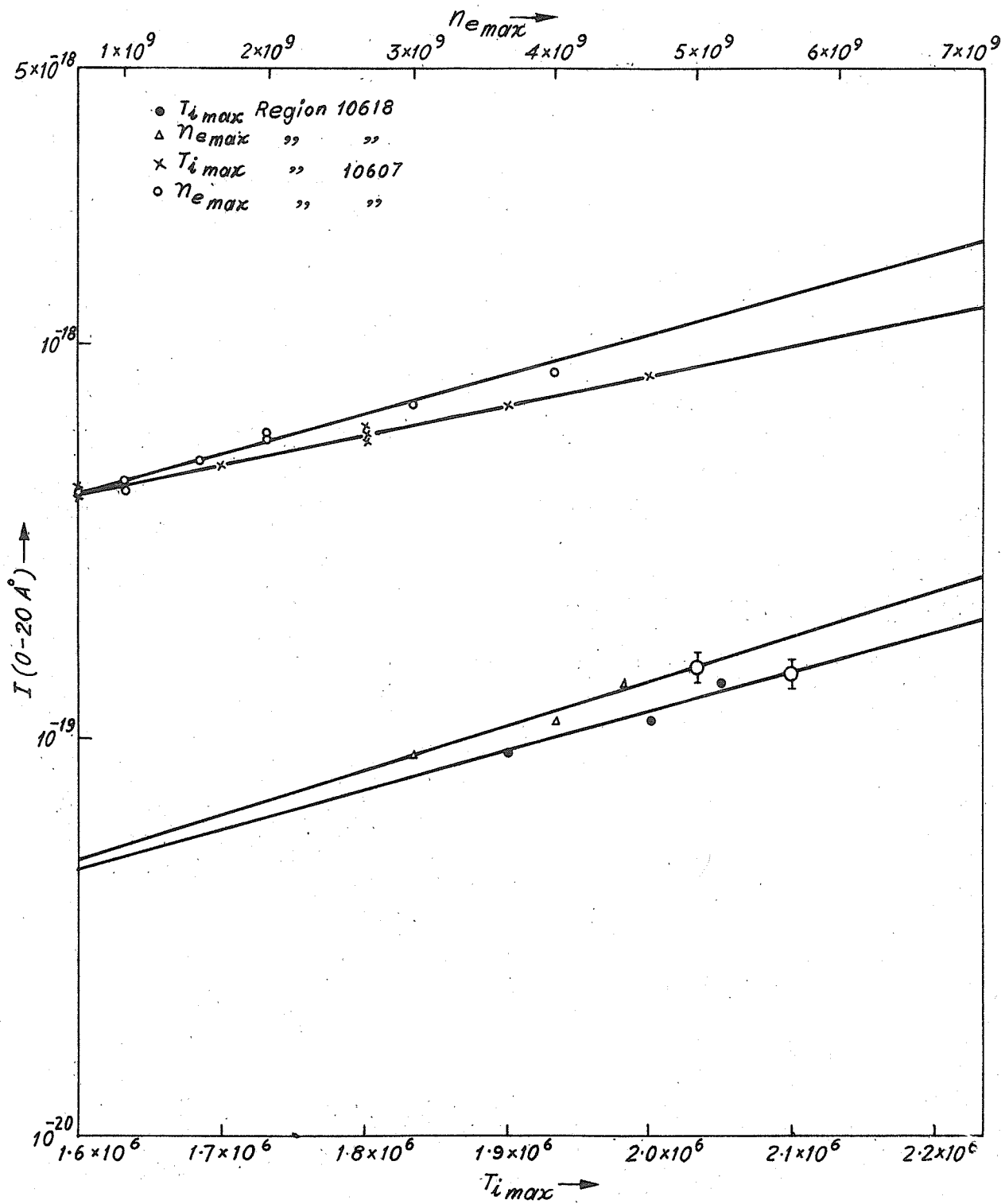


FIG. 1 RELATION BETWEEN $I(0-20 \text{ \AA})$ AND $T_{i,max}$ AND $n_{e,max}$.

MARCH 6, 1970

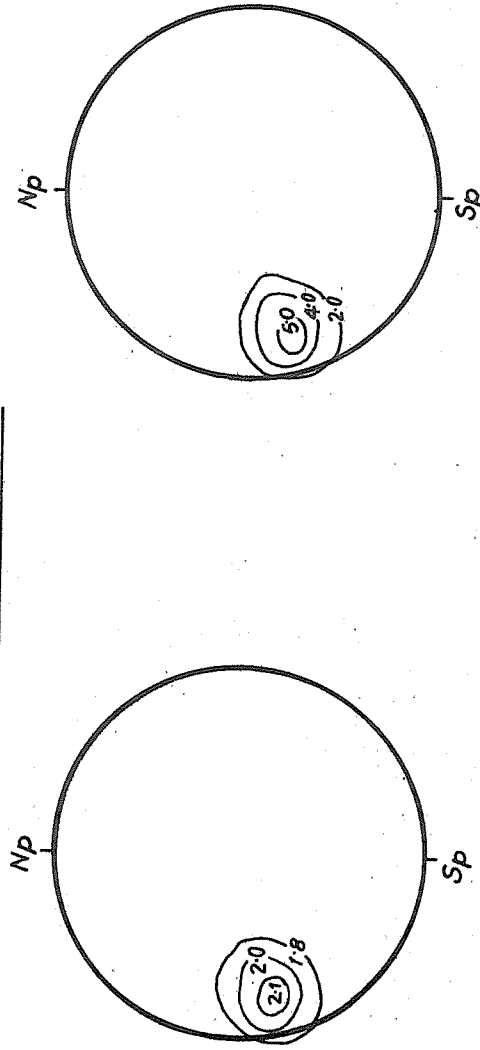


FIG. 2

(i) TEMPERATURE DISTRIBUTION
IN MILLION DEGREE KELVIN IN
THE 0-20Å EMITTING REGION
ASSOCIATED WITH McMath-
REGION 10618

(ii) ELECTRON DENSITY DISTRIBUTION
IN UNITS OF $10^9/\text{cm}^3$ IN THE 0-20Å
EMITTING REGION ASSOCIATED WITH
McMath REGION 10618

Table 2

Calculated and Observed Physical Data for 0-20Å Emitting Region Associated with McMath Region 10618

Date Mar.	$T_{i_{max}}$ (10^6 °K)	$n_{e_{max}}$ ($10^9/cm^3$)	y (10^{+8})	$E(0-20\text{Å})$ (10^{30} erg)	$I(0-20\text{Å})$ (10^{-19})	$\frac{F(0.5 - 3\text{Å})}{F(1 - 8\text{Å})} \times 100$
3	1.9	3	6	0.56	0.91	5
4	2.0	4	12	1.4	1.10	6
5	2.05	4.5	20	2.8	1.40	6
6	2.1	5.0	17	2.7	1.60	6
7	2.1	5.0	16	2.4	1.50	6
8	2.1	5.0	16	2.5	1.55	-
9	2.1	5.9	14.0	2.1	1.50	-
10	2.1	5.0	7.0	1.1	1.56	6
11	2.1	5.0	7.0	1.05	1.43	-
12	2.1	5.0	7.0	0.95	1.40	6
13	2.1	5.0	2.0	0.28	1.40	-
14	2.1	5.0	2.0	0.28	1.40	-

According to existing models the major part of the flare-emission in this wavelength region is thermal emission, i.e. due to flare time heating of the emitting plasma. For a thermal spectrum,

$$I(0-20\text{Å}) \approx C \exp(-7.0/T_{if})$$

The value of constant C depends on the physical property and the volume of the emitting plasma. T_{if} is the flare emission temperature. The exponential relation between $I(0-20\text{Å})$ and $T_{i_{max}}$ or $n_{e_{max}}$ makes T_{if} directly proportional to $T_{i_{max}}$ or $n_{e_{max}}$ of the region.

The temperature and electron density are not uniform over the region. The computed temperature and electron density distribution in the active region associated with McMath region 10618 on March 6 are shown in Figure 2. This was the day of peak activity for the region (see Table 2).

Concluding Remarks

The physical model of the 0-20Å emitting regions derived from the 9.1 cm spectroheliograms using the method developed by the author are consistent with the flare emission from the region.

Acknowledgement

The author is grateful to Dr. R. W. Kreplin of the Naval Research Laboratory and Miss J. Virginia Lincoln of the World Data Center-A, Upper Atmosphere Geophysics, NOAA, Boulder, for the X-ray flux data.

REFERENCE

- SENGUPTA, P. R. 1970 A New Method of Calculating 0-20Å Solar X-ray Flux and its Spectral Distribution using 9.1 cm Spectroheliogram Solar Physics, In press

(The paper was also presented at the International Symposium on Solar-Terrestrial Physics, Leningrad, U.S.S.R., May, 1970)

"Solar X-Ray Emission March 5-10, 1970"

by

D. M. Horan and R. W. Kreplin
E. O. Hulburt Center for Space Research
Naval Research Laboratory
Washington, D. C. 20390

During the period March 5-10, 1970, the Naval Research Laboratory's SOLRAD 9 Satellite (Explorer 37, 1968-17A) provided solar X-ray data which are sufficiently continuous to say that no major solar X-ray event escaped detection. Gaps in the data due to satellite night do not exceed 35 minutes in duration and it is unlikely that a major solar event could completely run its course in so short a time.

Figures 1 through 6 are plots of the solar X-ray energy flux vs. time during the period of interest. In each of the plots the top curve represents the solar X-ray emission in the 8 to 20 Å band, and the next lower curve represents the solar X-ray emission in the 1 to 8 Å band. In both cases a gray body solar emission spectrum with a 2×10^6 K color temperature was assumed in converting from ionization chamber current to energy flux units. The third curve from the top represents emission in the 0.5 to 3 Å band assuming a gray body spectrum with a 10×10^6 K color temperature for the emitting solar region. Since the 0.5 to 3 Å band solar emission is generally below the threshold level of the detector, the curve representing these data will be quite intermittent.

The X-ray emission is plotted in units of ergs/cm²/sec on a logarithmic scale. The abscissa is linear with the integers denoting hours in Universal Time (UT). Charged particle interference with the X-ray detectors, which can cause the plotted flux levels to be higher or lower than the actual flux, is indicated by the lowest data curve. The ionization chamber current caused by the charged particle background is digitized and recorded as a "count." The number of "counts" is linearly related to the current generated in the 0.5 to 3 Å ionization chamber by penetrating charged particles when the detector is facing away from the sun. Counts of 10 to 15 indicate no particle interference with the detectors. Counts of 20 to the maximum value of 127 indicate increasing amounts of particle interference. However, the data processing computer program does not plot data obviously contaminated by particle interference, and this feature causes randomly spaced data gaps of 30 minutes duration or less.

The record of X-ray emission for March 5, Figure 1, shows high background levels in the 1 to 8 Å and 8 to 20 Å band throughout the day and several Class M flares. (NOAA's Space Environment Services Center has defined a flare whose flux in the 1 to 8 Å band exceeds 1×10^{-2} ergs/cm²/sec as a Class M event.) The first Class M event began at about 0417 UT and corresponds to a Class IB H-α flare located at S15 E71.* The second Class M flare, which had the largest peak flux and the longest duration of the day's events, began a few minutes later and corresponds to a Class 1N H-α flare at N15 W86. Other Class M events achieved peak flux levels in the 1 to 8 Å band at 1207, between 1615 and 1655, and at 1914 UT.

The background levels in the 1 to 8 Å and 8 to 20 Å bands remained high throughout March 6, Figure 2. A Class M flare emitted peak flux in the 1 to 8 Å band at 0940 UT, followed by another event which emitted peak 0.5 to 3 Å band flux at 1005 UT. The plot shows that the 1 to 8 Å band flux exceeded 1×10^{-2} ergs/cm²/sec between 1230 and 1430 UT and, although the plot indicates that there were two distinct Class M events, gaps in the data due to satellite night prevent precise identification of starting and peak times.

The data for March 7, Figure 3, also show high background levels throughout the day with several Class M events. The first Class M event emitted peak flux in the 1 to 8 Å band at 0156 UT. Two other events were above the Class M threshold level as the satellite emerged from the Earth's shadow at 1129 and 1625 UT, but their beginning times and peak values do not appear on the plot. The path of SOLRAD 9 never crossed regions of total or partial solar eclipse, and therefore the data were completely unaffected by the eclipse.

Figure 4 shows that the background emission remained at a near high level throughout March 8 with many small events occurring. Only one event, which began at 1930 UT, could be rated as a Class M X-ray flare. The data for March 9, Figure 5, show moderate to low background levels and no significant X-ray events. Moderate to low background levels persisted throughout March 10, Figure 6. A single Class M event occurred with peak flux in the 1 to 8 Å band emitted at about 0740 UT.

In summary, the solar X-ray emission during the period between March 5 and March 10, 1970 was not unusually interesting. About a dozen flares qualified as Class M events, but not one could be considered a major solar event.

* All references to H-α Flare Class and location on solar disk were obtained from "Solar-Geophysical Data", No. 308 Part I, April 1970, U.S. Department of Commerce, Boulder, Colorado, U.S.A. 80302.

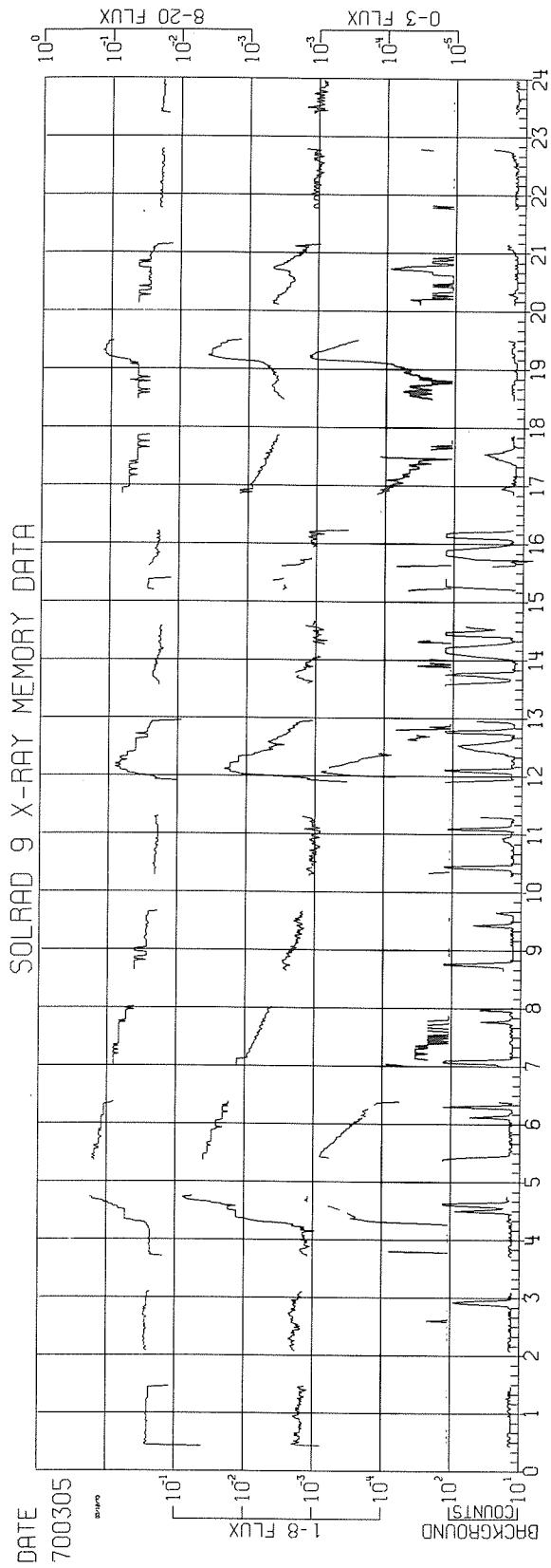


Fig. 1. Solar X-ray emission on March 5, 1970

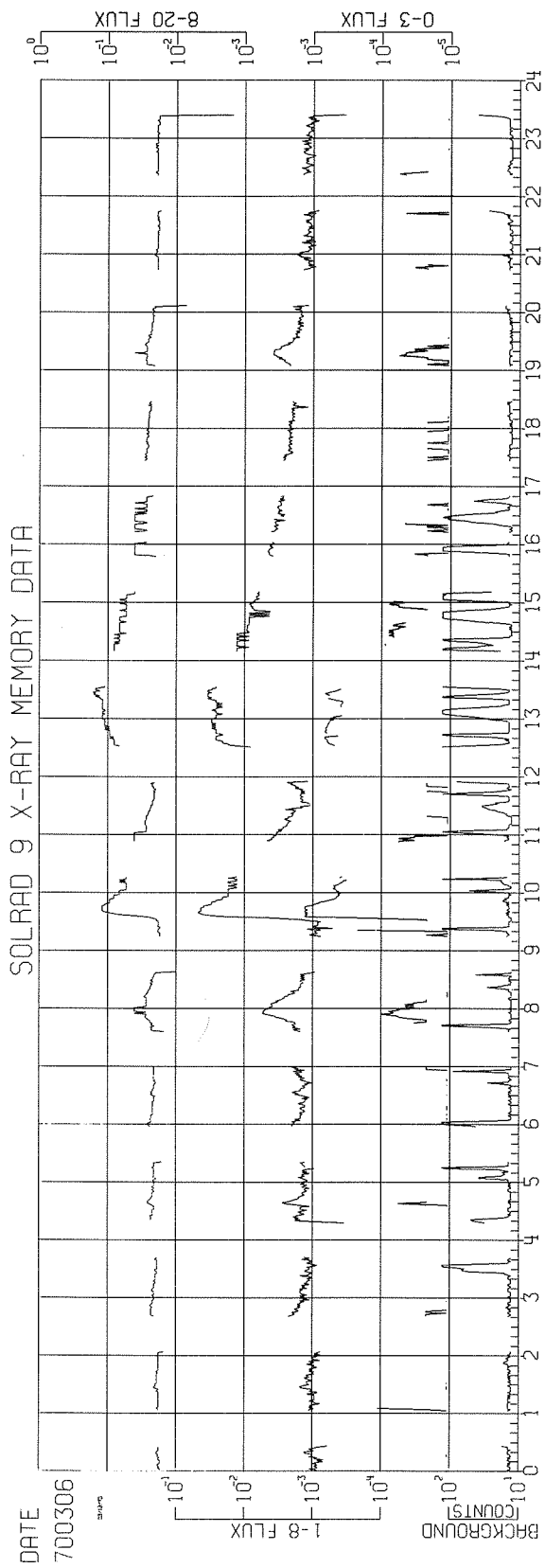
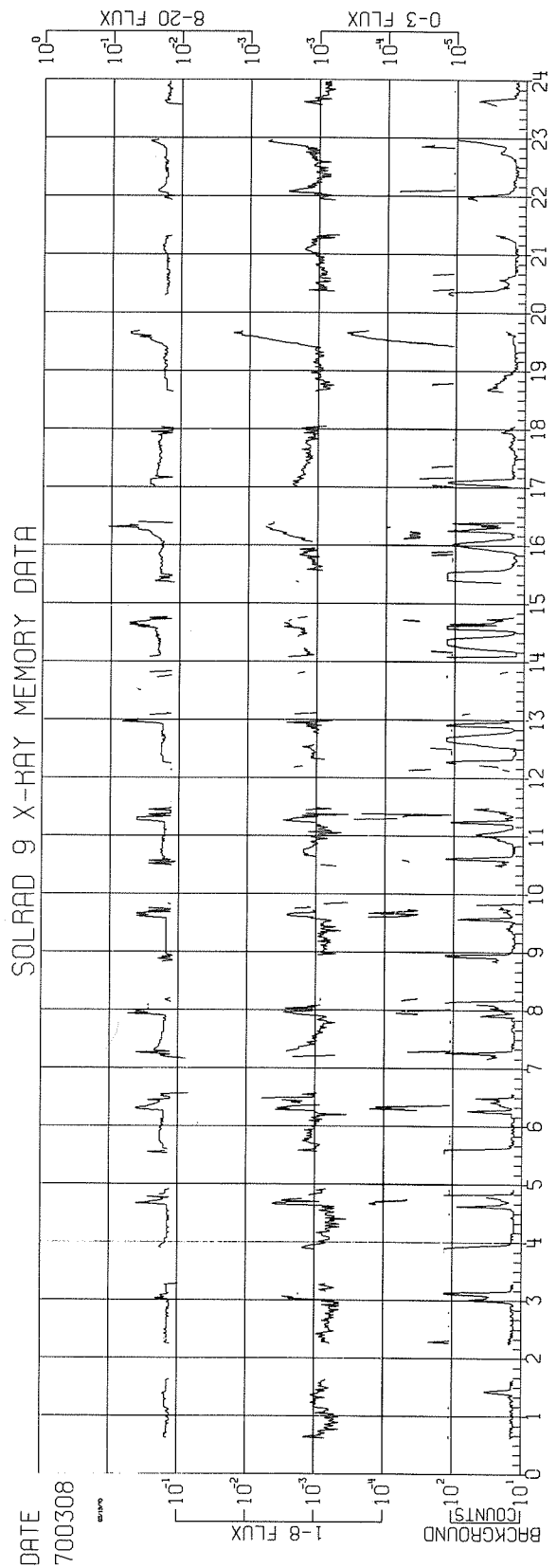
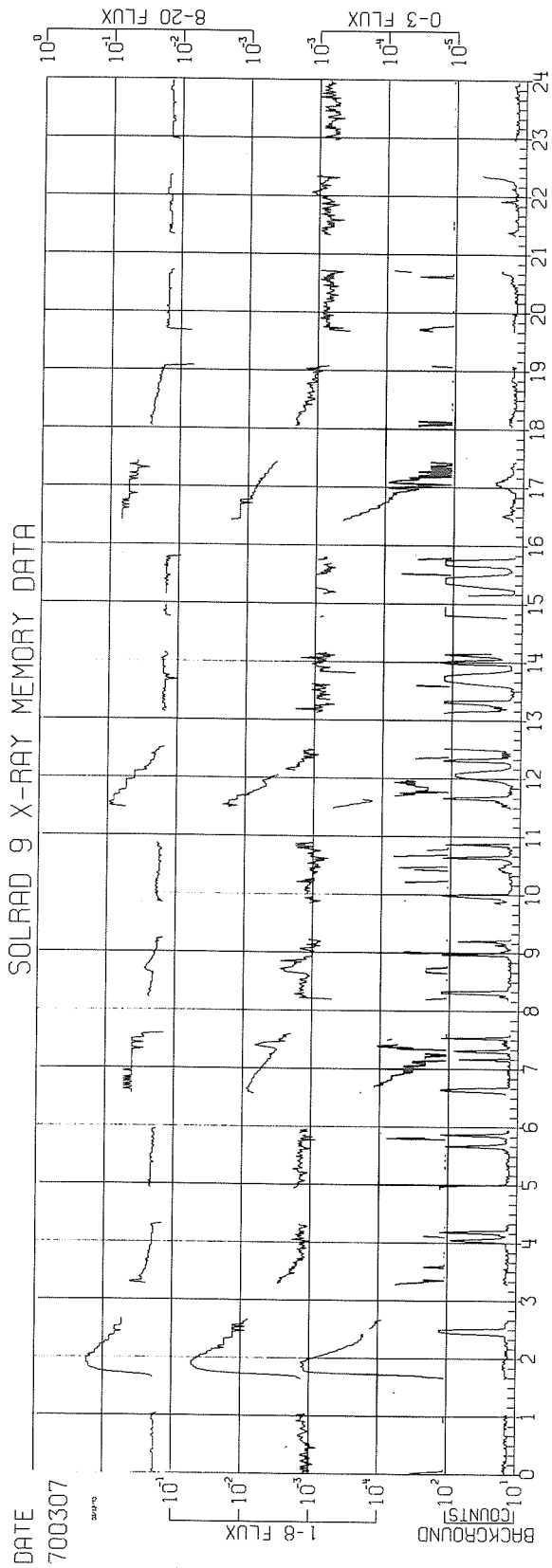


Fig. 2. Solar X-ray emission on March 6, 1970



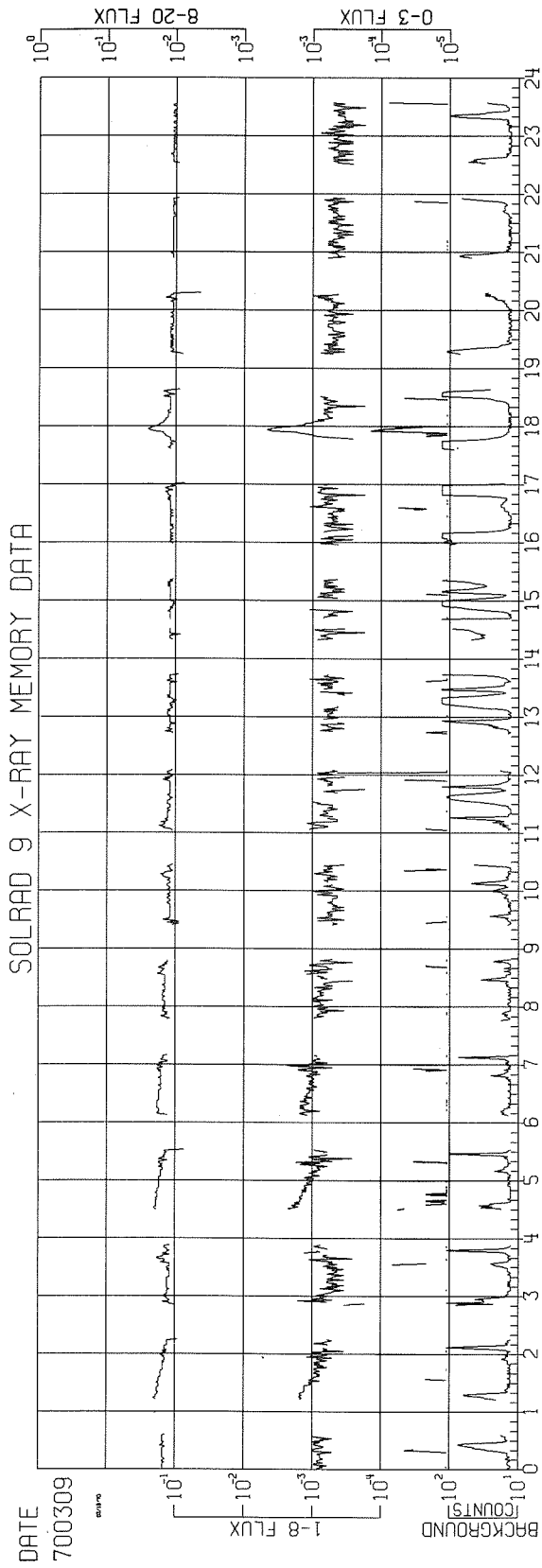


Fig. 5. Solar X-ray emission on March 9, 1970

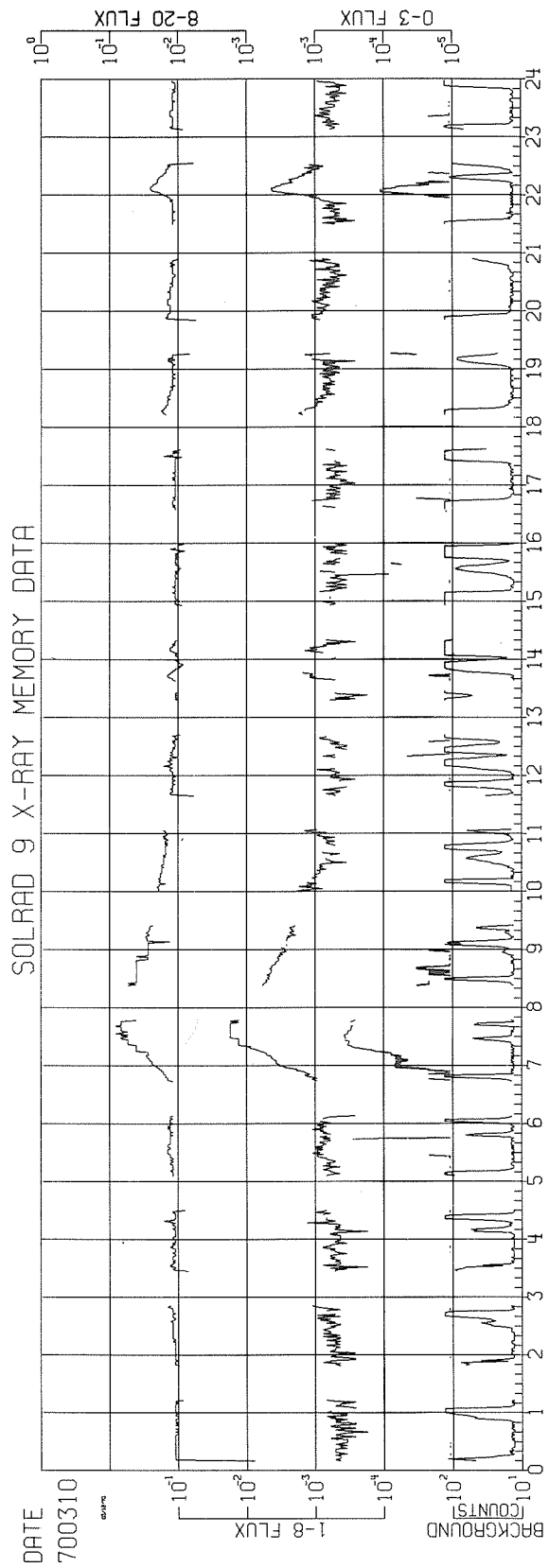


Fig. 6. Solar X-ray emission on March 10, 1970

5. SUDDEN IONOSPHERIC DISTURBANCES

"Sudden Ionospheric Disturbance Summary from WDC-A Archives"

by

J. Virginia Lincoln
Aeronomy and Space Data Center
National Oceanic and Atmospheric Administration, Boulder, Colorado

SID events for March 6 - 8, 1970 as published in "Solar-Geophysical Data" are repeated here for the user's convenience.

Mar. 1970	Universal Time				Wide Spread Index	Number of Station Reports by Type								Known Flare	Region
	Start	End	Max	Imp		SWF	SCNA	SEA	SPA	LF- SPA	SES	SFD			
06	0933	1033	0938	3	5	5	2	7	4		2		0931	x-ray	
06	1144U	1355U	1248	3	3	1		2	2				NF		
07	0145	0202	0158	2	5	2			8	6	6		0140	10614	
07	0620	0724	0645	1	1				1				0625	10618	
07	0633		0635	1	3					2	2		0632	10618	
07	0723	0733	0727	1-	3		1		1				0723E	10607	
07	0841	0852	0844	1	1	1							0840	10614	
07	0918	0933	0924	1	1				1				0917	10607	
07	1123	1208	1133	2	3	5	1	5	3		1		1121	10618	
07	1603	1644	1622	2+	5	3	5	7	1	1			1601	10618	
07	1843	2000	1930	1	1	1							1841	10607	
08	0655	0715	0702	1-	1				1				0657	10614	
08	1609	1658	1625	1-	3				2	1			1607	10618	
08	1930	2220	1943	1	5	3			4	1			1925	10614	
08	1950	2050	2000	1	3				2			1	1952E	10614	
08	2205	2255	2208	1	1				1	1			2203	10607	
08	2254	2312	2300	1	3				2	1			2250E	10614	

"Multi-frequency Radiowave Observations of SID events during 1 - 6 March, 1970"

by

T. B. Jones and R. E. Evans
Physics Department
University of Leicester
United Kingdom

Introduction

Two distinct types of ionospheric disturbance are associated with solar flare activity. The first is produced by an enhancement of solar ionizing radiations and results in a rapid change in the electron density distribution known as a sudden ionospheric disturbance (SID). Some 10 to 20 hours after an SID a further disturbance sometimes occurs as a result of the solar particle emissions during the flare. This second type of event is usually long-lived and often results in ionospheric and magnetic storm activity. Radiowave observations of events of this latter kind during March 1970 are described elsewhere in this report (page 247).

Sudden ionospheric disturbances can influence the propagation characteristics of ionospherically reflected radiowaves throughout the wide frequency range from about 10 kHz (VLF) to 20 MHz (HF). The object of this paper is to present simultaneous observations of the effects on VLF, LF and HF propagation of some of the SID events during 1 - 6 March, 1970.

Radiowave Observations

At VLF the phase and amplitude of signals received over both long and short propagation paths have been recorded at Leicester. Since SID effects can differ on the two types of circuit, the phase records for both the short 16.0 kHz GBR (Rugby) and 19.6 kHz GBZ (Criggion) to Leicester paths are presented together with those for the long 12.0 kHz Trinidad to Leicester circuit.

Measurement of the total field of the LF (272 kHz) transmission from Uherske - Hradiste (Czechoslovakia) indicate that both ground and sky waves are received at Leicester. The effects of SIDs can readily be detected since the changes which occur in the sky wave path produce 'beat-like' oscillations in the received field strength.

Two types of propagation anomaly have been recorded on HF transmissions due to flare enhanced ionization. Increases in the D-region electron density resulting from the enhanced flux of solar x-rays in the wavelength range 1 - 10Å produce attenuation of waves passing through the region to be reflected at higher levels in the E and F layers. On occasions the effect can become so great that the signals are totally absorbed and these events are therefore termed short wave fadeouts (SWF). Changes can also occur in the electron distribution in the E and F regions due to flare increases in long wavelength x-rays and some EUV line emissions. As a consequence, the reflection levels of HF transmission will vary and small 'Doppler' like frequency shifts (SFD) will be observed in the reflected signals. The magnitude of the Doppler shift will depend on the rate of change of the reflection height. Only one SFD was detected during the flare activity of 1 - 6 March, 1970. A summary of the transmissions monitored is presented in Table 1.

Table I

Frequency	Transmitter Location	Path Length km	Parameter Monitored	SID Effects
12.0 kHz	Trinidad	7200	Phase and Amplitude	SPA SES
16.0 kHz	Rugby UK	28	"	" "
19.6 kHz	Criggion UK	130	"	" "
272 kHz	Uherske-Hradiste Czechoslovakia	1400	Total field	Beats
6.09 MHz	Luxembourg	610	Absorption	SWF
7.0 MHz	Weybourne UK	160	Doppler	SFD

Experimental Results

Observations are available throughout the disturbed periods of early March, 1970, and the recordings for three of these days are reproduced as examples of the effects observed. The records for 1, 5 and 6 March have been selected since they illustrate a wide range of SID events.

March 1, 1970

Four large SIDs produced disturbances on all the transmissions monitored as illustrated in Figure 1. The first event commenced at about 0936 UT and SPAs are evident on both long and short path VLF transmissions. An interesting feature is the marked difference in the rate of phase recovery observed on the Trinidad and GBZ paths. At LF the characteristic quasi-sinusoidal beat pattern was observed on the field strength recording. The HF (6.09 MHz) record indicates a typical SWF event with a sudden fall in signal strength, the period of low signal being followed by a rapid recovery to the pre-flare level. This flare was the only one during the 1 - 6 March which produced an SFD and it appears therefore that large enhancements of solar radiations ionizing at E and F region heights occurred only during this flare.

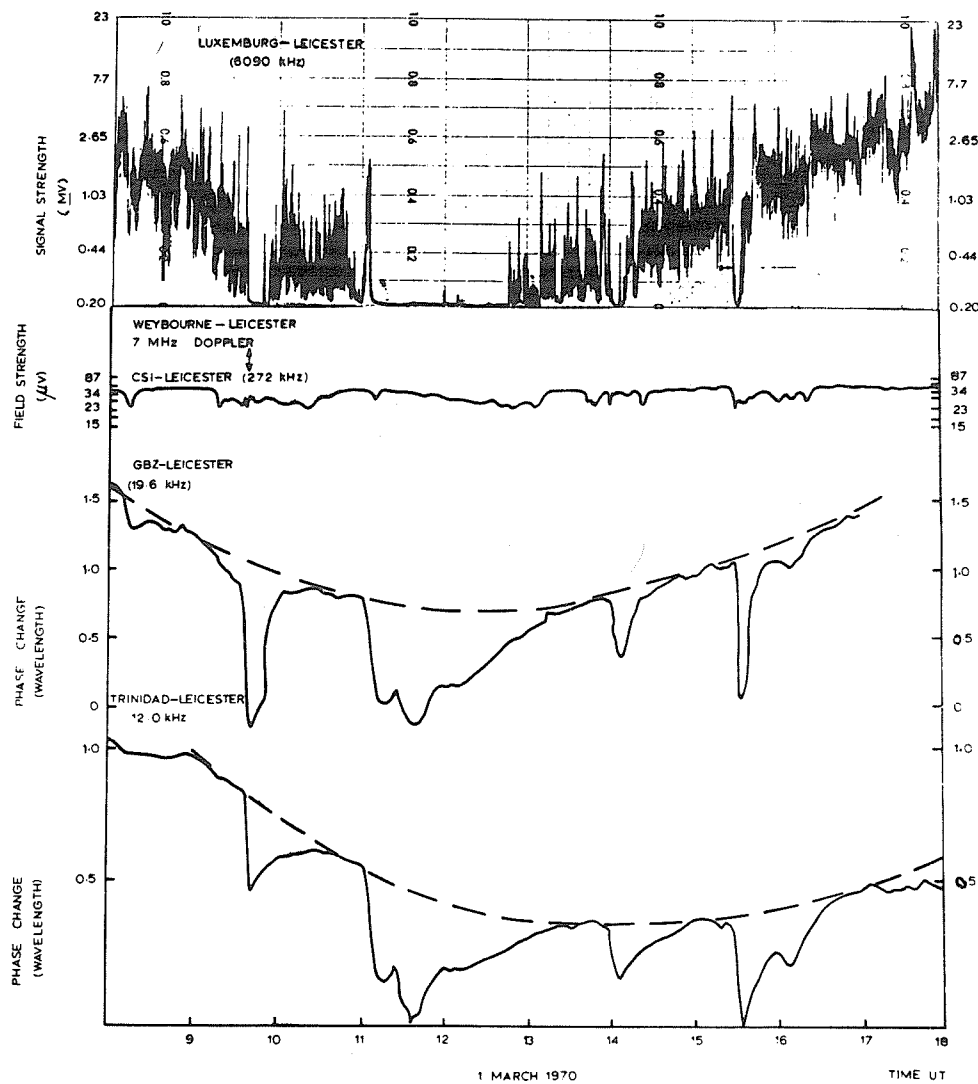


Fig. 1. Multi-frequency radiowave observations of SIDs for March 1, 1970 (broken lines represent normal diurnal variations).

The second SID is a long-lived event starting at 1104 UT. The VLF phase records show that the disturbance persists until about 1350 UT and that marked structure is present with phase minima at 1120 and 1140 UT. In contrast to the first SPA the phase recovery times on both VLF transmissions are identical for the event. The LF recording shows little effect and no SFD was observed. Short wave fadeout conditions persisted from 1100 to 1248 UT. There is an interesting increase in signal level at the start of the HF disturbance between 1100 and 1110 UT.

The SID at 1400 UT is a typical small event and its effects are evident on the 12.0, 19.6, 272 and 6090 kHz transmissions. The final disturbance commenced at 1530 and is similar to the event of 1104 UT. Structure is evident in the SPAs on both VLF frequencies and also to a smaller extent in the SWF event. Maxima in the phase disturbance are evident at 1536 and 1610 UT and the phase of both circuits has returned to its undisturbed level by about 1645 UT. The LF total field strength is disturbed throughout the period 1532 to 1630 UT. The SWF is of considerably shorter duration than the SPAs, and although there appears to be a secondary minimum at 1540, normal conditions have returned by 1545 UT.

March 5, 1970

During this day two SID events were observed, as shown in Figure 2, but neither produced SFDs. The SID commencing at 1200 is a typical small disturbance and has no special features apart from the different recovery times of the long and short path SPAs.

The second SID which starts at 1618 UT is a large event, the VLF phase anomaly persisting until about 1840 UT on the Trinidad transmission. Events of this duration (140 mins.) are rather uncommon. The SWF event is again characterized by a rapid fall in signal strength to a fairly constant level which is maintained throughout the main phase of the flare. There follows an extremely fast recovery to the normal undisturbed signal level at 1645 UT. Once again the SWF event is considerably shorter than the VLF phase anomalies.

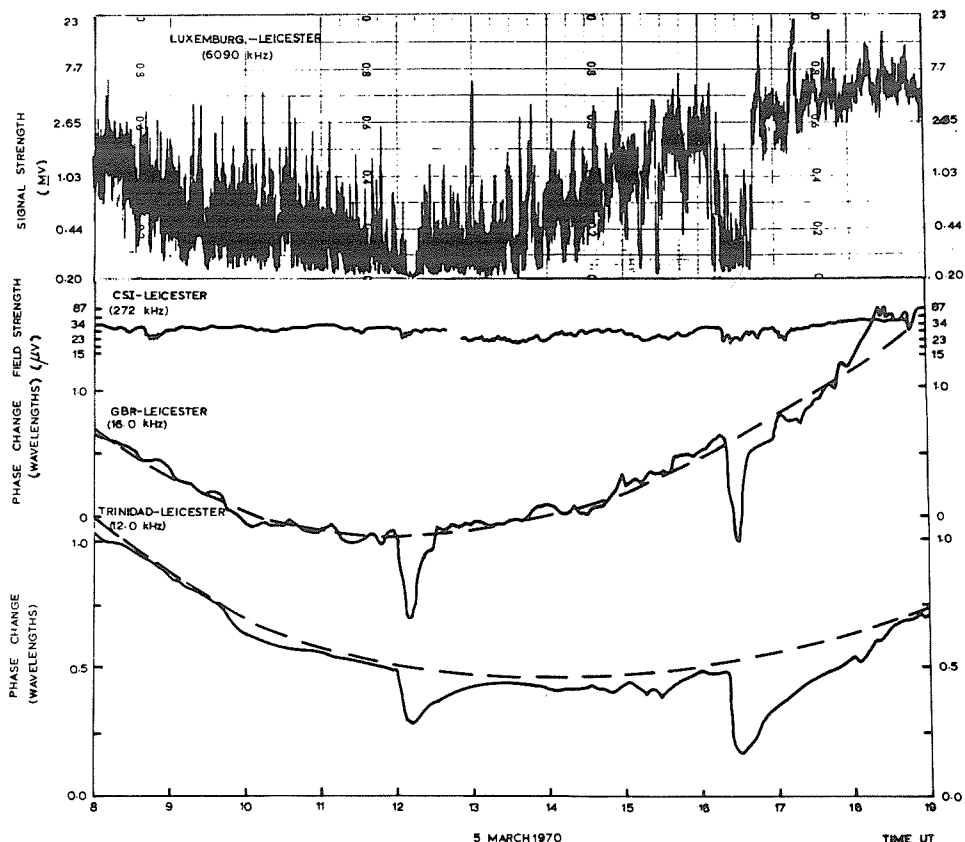


Fig. 2. Multi-frequency radiowave observations of SIDs for March 5, 1970 (broken lines represent normal diurnal variations).

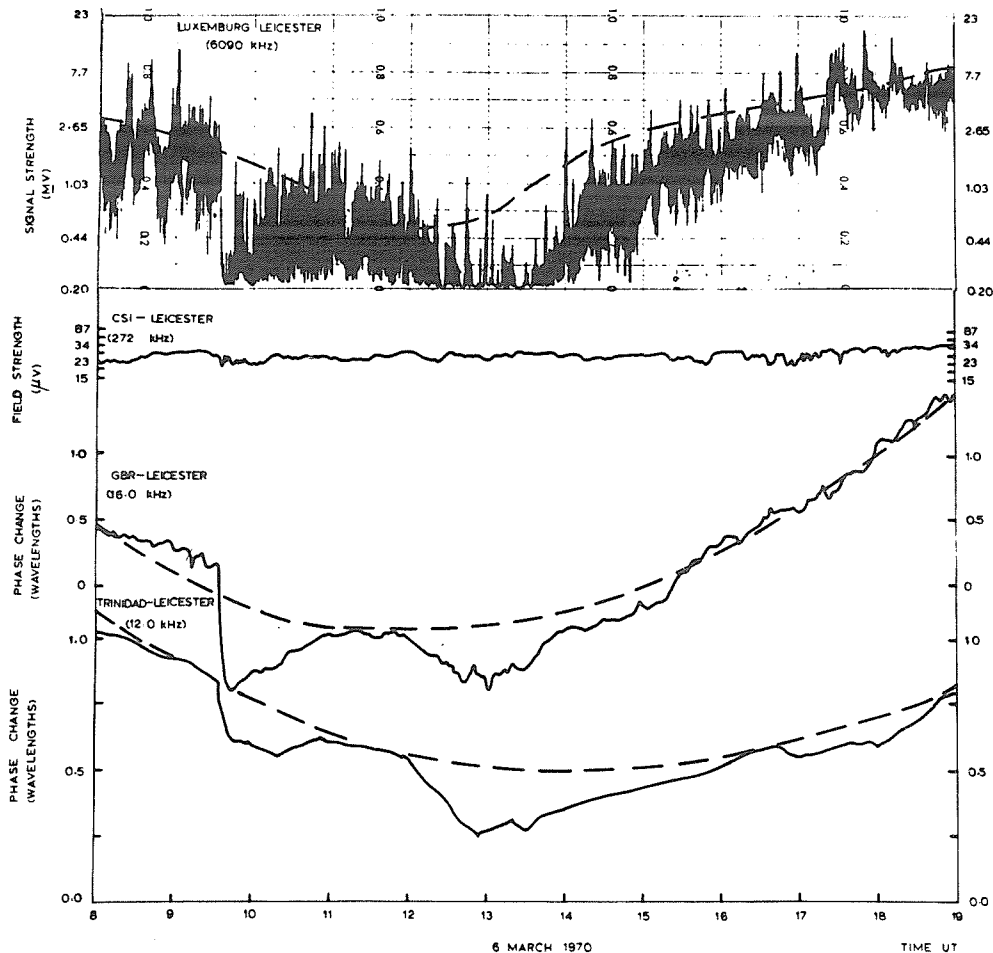


Fig. 3. Multi-frequency radiowave observations of SIDs for March 6, 1970 (broken lines represent normal diurnal variations).

March 6, 1970

The experimental observations are reproduced in Figure 3 and this day is of particular interest since a rather rare type of SID was recorded. The first event at 0934 UT is a typical SID and has no unusual features apart from the second minimum in the HF signal strength recorded at 0958 UT. The second event starting at 1158 UT is however of considerable interest. The VLF observations indicate a very slow phase advance in contrast to the rapid onset usually associated with SPAs. The minimum phase is reached at 1254 UT, i.e. about 50 mins. after the start of the disturbance. There is some indication of a second maximum at 1330 UT on the 12.0 kHz transmission, but this is not clearly defined on the GBZ record. The phase recovers to its undisturbed value at about 1540 and 1610 UT for the 16.0 and 12.0 kHz transmissions, respectively. Thus, the phase disturbances produced by this SID last for over four hours. No LF or SFD effects were detected which is consistent with the absence of a sudden change in the electron density profile. The slow rate of phase change indicates a slow rate of enhancement of the solar x-ray spectrum, although this cannot be confirmed as direct observations of the solar x-ray flux have not yet been published. The HF amplitude decrease is again of much shorter duration than the VLF phase anomalies. For comparison the average diurnal amplitude variation for early March is superimposed on the HF signal strength record (dashed curve in Figure 3). The signal starts to decrease at 1200 UT and very low levels are recorded from 1224 until 1334 UT. In contrast to the other SWFs reported in this paper a gradual increase in signal strength takes place from 1334 until 1417 UT when the signal returns to its undisturbed level. This result suggests that the flare enhancement of the solar radiations which ionize at heights where the absorption of the HF signals occurs does not persist as long as the enhancement of penetrating x-radiations which ionize at the reflection levels of the VLF waves. Alternatively, the recombination coefficients at the respective levels could differ considerably giving a slower recovery of the enhanced ionization at low levels in the D-region. This seems rather unlikely, but more definite conclusions will have to await the publication of direct observations of the flux changes in the solar ionizing radiations.

Conclusions

Ground based observations of SID events have been made simultaneously using a wide range of frequencies (VLF to HF). The data indicate the different responses of the various types of propagation to the flare enhanced ionization and emphasize the importance of multi-frequency experiments for studies of SIDs.

Three flare active days are discussed during which some typical and one rather rare type of SID events were observed. No attempt has been made to interpret the disturbances quantitatively in terms of electron density variations, but this will be undertaken as soon as the relevant solar x-ray data become available.

"On the SID Activity of early March 1970"

by

P. Triska and J. Lastovicka
Geophysical Institute
Czechoslovak Academy of Sciences
Prague, Czechoslovak

A high SID activity was observed during early March 1970 according to the data from Panska Ves Observatory (50°32'N, 14°34'E) of the Geophysical Institute, Prague. Except March 4, at least one SID event per day occurred from 1 to 7 March. The following types of SID's have been monitored:

SWF events on field-strength records (A3 method) made at 2614, 2775 and 6090 kHz, the transmitter-receiver distances being about 610, 520 and 610 km, respectively.

SFA events (sudden field anomalies) at 155 and 164 kHz; these are indirect measurements of the phase reflection height recognized from the interference between the ground wave and the one-hop sky wave; the transmitter-receiver distance for both paths is about 1000 km.

SEA and SDA (sudden decrease of atmospheric) events occurring on the integrated atmospheric-noise level at 27 kHz and 5 kHz, respectively. No SDA was detected during the period under consideration, as it is usual for March and April [Triska and Lastovicka].

Table 1 gives a list of all SID events from 1 to 14 March. Table 2 contains some more detailed data on the events from March 6 and 7.

Table 1

Date Mar.	Start UT	Max UT	End UT	Importance
1	0810		0832	1
	0938	0941	1023	3
	1106	1140	1300	2
	1400	1404	1448	2
	1531	1536	1600	2
2	0736		0746	1
	0910		0949	1
	1032	1035	1051	2
	1101		1152	1
	1340	1359	1517	2
3	0847	0856	0909	1
5	1202	1210	1252	2
6	0933	0942	1112	3
	1220		1425	2
7	1123	1133	1223	2
	1607	1622	1654	2
14	1201		1218	1

The sudden ionospheric disturbance which started at 0936 UT on March 6 was one of the strongest events observed during March 1970. Its time development correlates very well with the X-ray flux as measured by the SOLRAD-9 satellite (1 - 8 Å band). This solar flare caused a typical strong SID event (Figures 1 - 4). The SWF at 2775 kHz started suddenly, the field strength went rapidly down to zero (to the receiver noise level, i.e. about 0.5 μ input voltage), the recovery phase being interrupted at 1155 UT by another slowly starting SWF event. Very typical are also the other three events, i.e. SEA at 27 kHz and SFA at 164 and 155 kHz. SFA's were caused mainly by the decrease of the sky wave reflection level, by about 9 km in this case. Figure 5 shows the phase-height daily variation derived from the 164 kHz field-strength record. Finally, Figure 6 shows the diurnal variation of ionospheric absorption (A-3 measurements at 6.09 MHz) with pronounced maxima of the SWF events.

Table 2

Freq. type of SID	Reflec-tion point	6 March						7 March								
		Universal Time			Imp	Universal Time			Imp	Universal Time			Imp			
		Start	Max	End		Start	Max	End		Start	Max	End				
6090 kHz SWF	50°04'N 10°20'E	0936	0942	1036	3	1220	1425	2	1123	1133	1156	1		Q		
2775 kHz SWF	52°27'N 12°27'E	0935		1037	3			E	1123		1145	2		Q		
2614 kHz SWF	52°08'N 11°00'E				C			C	1123		1147	2		Q		
164 kHz SFA	49°00'N 08°01'E	0933		1025	3			Q				C	1605	1628	1	
155 kHz SFA	48°13'N 20°20'E	0933		1021	2			Q	1123		1150	1			N	
27 kHz SEA		0936	0947	1112	2			N	1123	1142	1223	2	1607	1622	1654	2
		$\Delta = 4$ dB							$\Delta = 2.5$ dB				$\Delta = 3$ dB			

Remarks: The time is UT. N - no effect; E - large increase of absorption, time development not clear; Q - small or nearly no effect; C - measurement can not be evaluated for technical reasons.

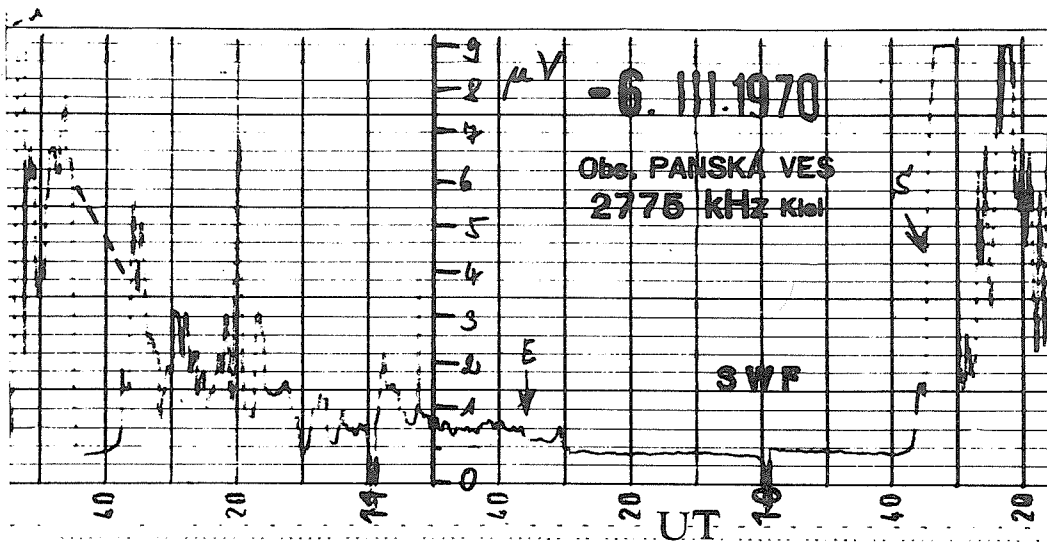


Fig. 1. Shortwave fadeout at 2775 kHz, start 0935 UT on March 6, 1970.

On the contrary, the afternoon effect on 6 March between about 1220 - 1425 UT was a non-typical one, with a slow commencement and of a relatively long duration. The HF absorption on 6.09 MHz as shown in Figure 6 reached again nearly the same maximum value of about 43 dB. However, only a slight effect can be found on LF records of 155 and 164 kHz signals, and also no SEA at 27 kHz was detected. Thus, it can be concluded that this second SID event affected mainly the upper part of the D-region. This seems to correspond to the satellite X-ray data [Solar-Geophysical Data] that show much softer X-ray spectrum for this latter event compared with the former one at 0935 UT.

On March 7, also two SID events were detected at Panska Ves, the principal data of which are given in Table 2 above. The event at 1605 UT occurred at a solar zenith angle of more than 80°

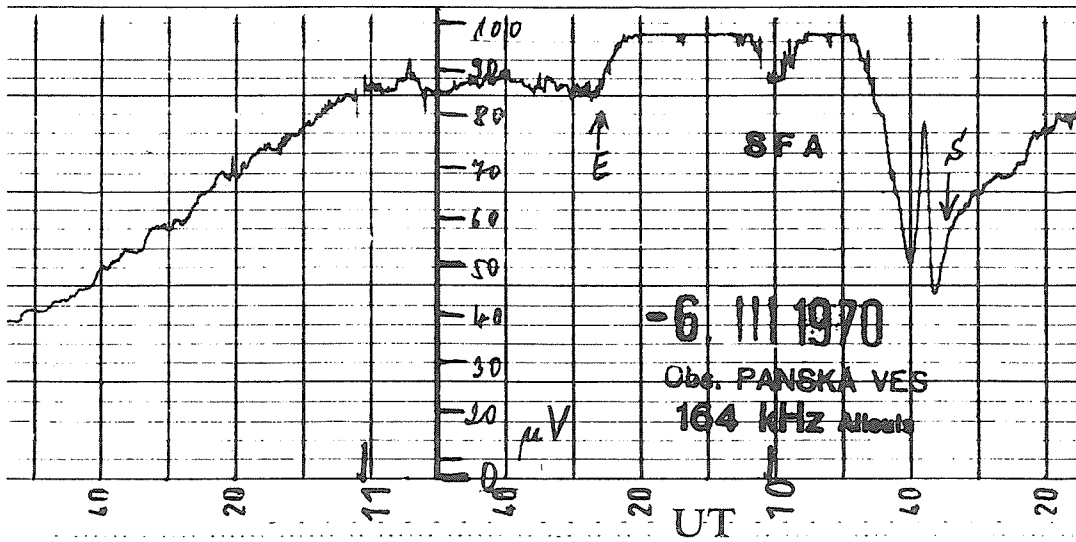


Fig. 2. Sudden field anomaly at 164 kHz, start 0933 UT on March 6, 1970

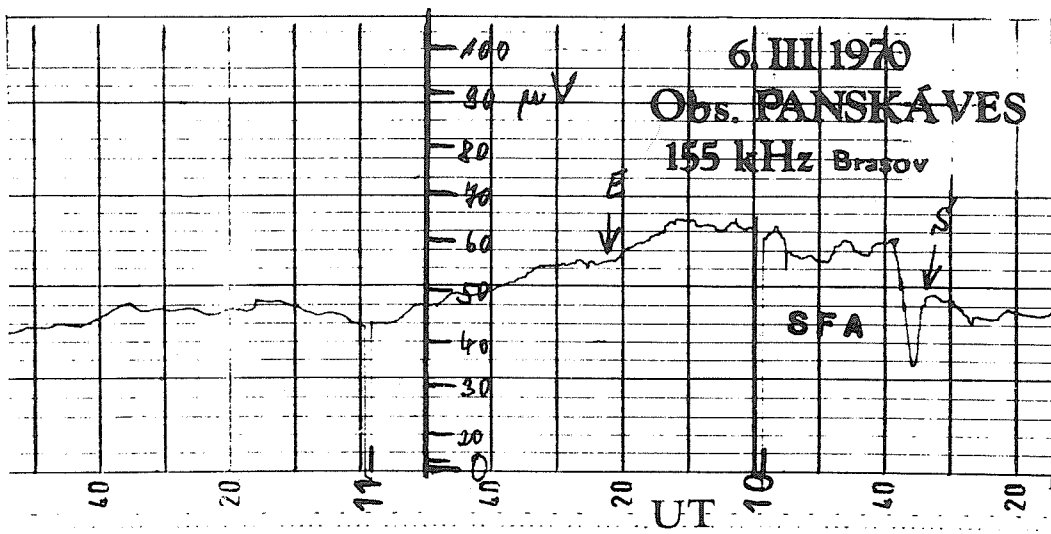


Fig. 3. Sudden field anomaly at 155 kHz, start 0933 UT on March 6, 1970.

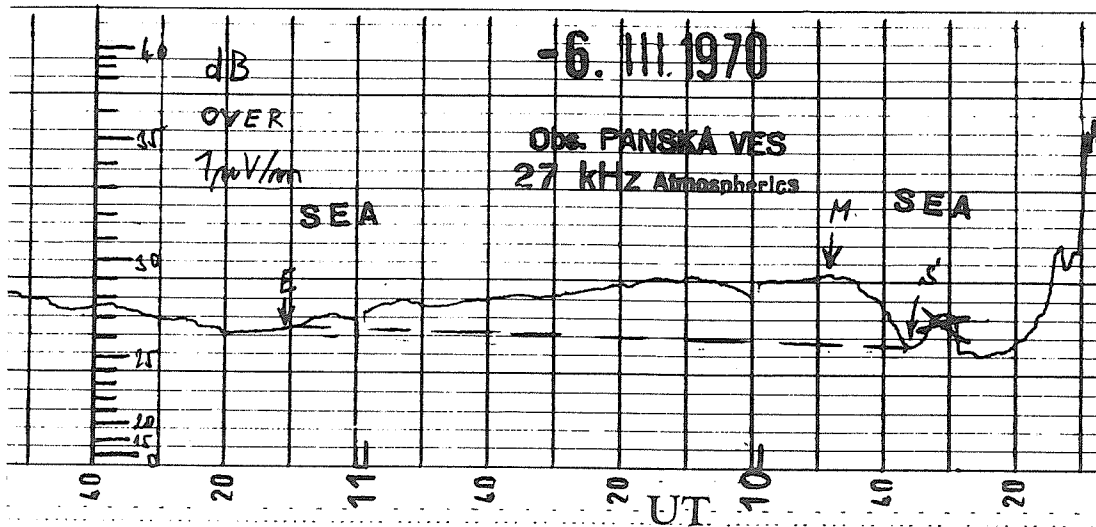


Fig. 4. Sudden enhancement of atmospherics at 27 kHz, start 0936 on March 6, 1970.

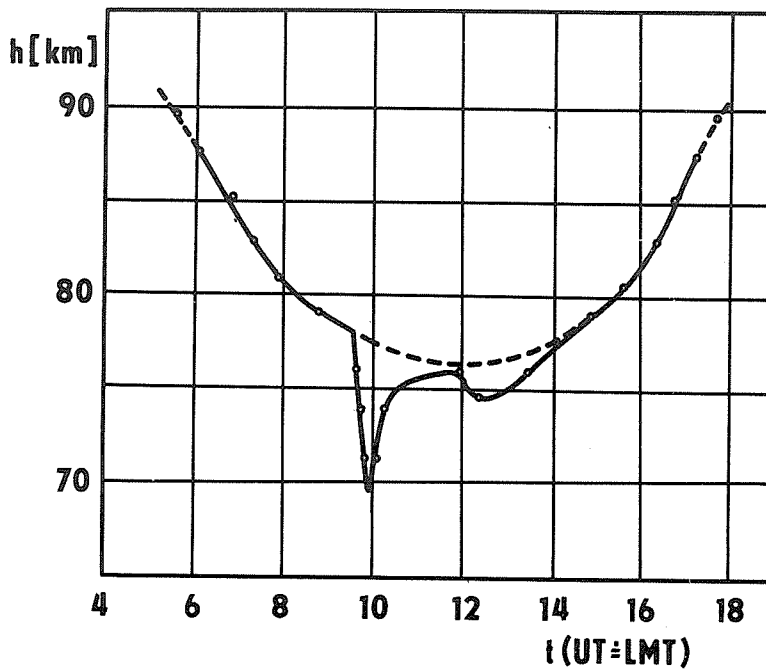


Fig. 5. Phase-height daily variation derived from the 164 kHz field-strength record (indirect phase measurement) on March 6, 1970. Dotted curve denotes the approximate quiet-day variation.

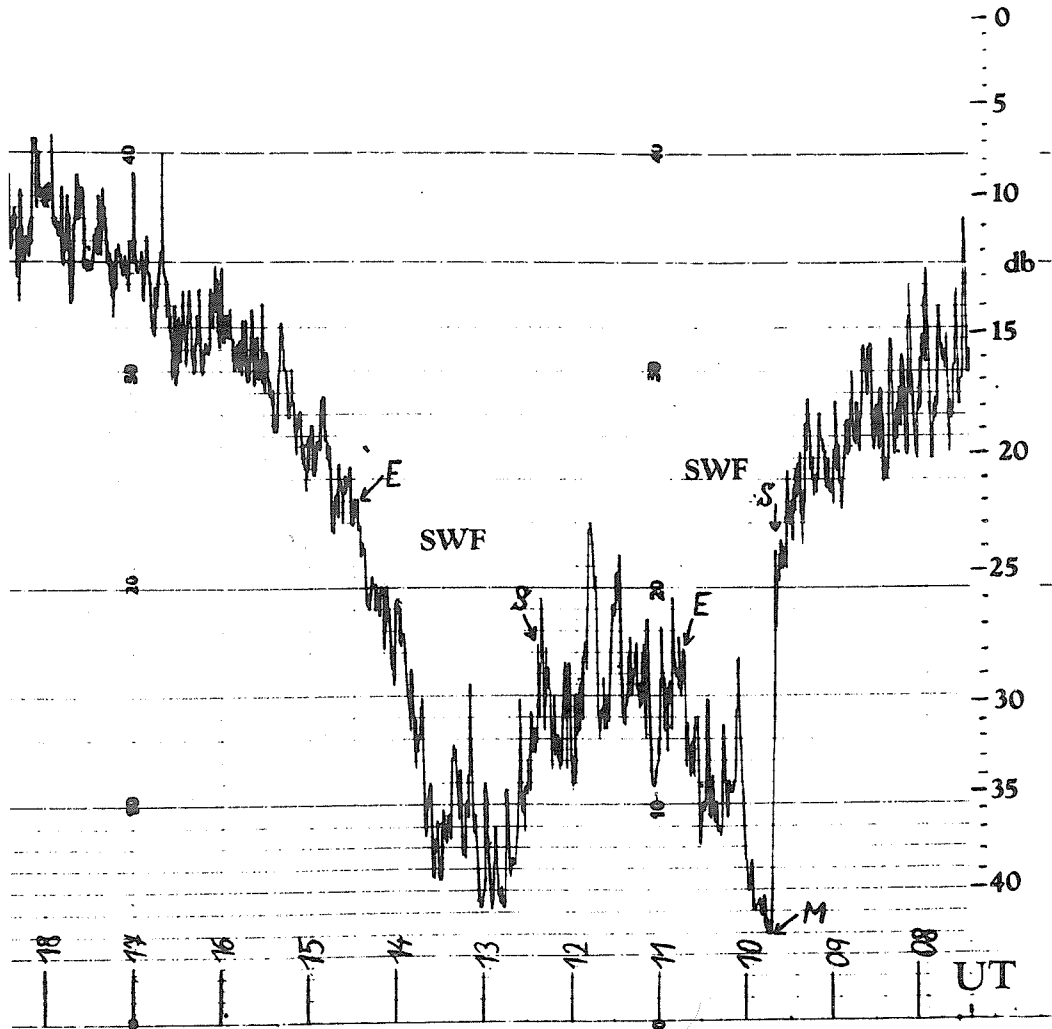


Fig. 6. A3-absorption at 6.09 MHz on March 6, 1970. Shortwave fadeouts started at 0936 UT and 1220 UT. The zero-level of absorption is a provisional reference level only.

for all reflection points of all paths used and therefore it is marked either only slightly or not at all, i.e. at 164 kHz ($\chi = 81^\circ$) SFA could be found whereas the 155 kHz path ($\chi = 86.6^\circ$) was not influenced.

REFERENCES

1970

Solar-Geophysical Data, IER-FB 309, Part I, 78-81, May 1970; IER-FB 313, Part II, 70-87, September 1970, U.S. Department of Commerce, (Boulder, Colo., U.S.A. 80302)

TRISKA, P. and
J. LASTOVICKA

(in print)

On the sudden decrease of atmospheric absorption on 5 kHz. Travaux Inst. Geophys. No. 340, 1970, Academia Praha.

"Atmospherics and SEA during the Period 1970 March 4 - 10"

by

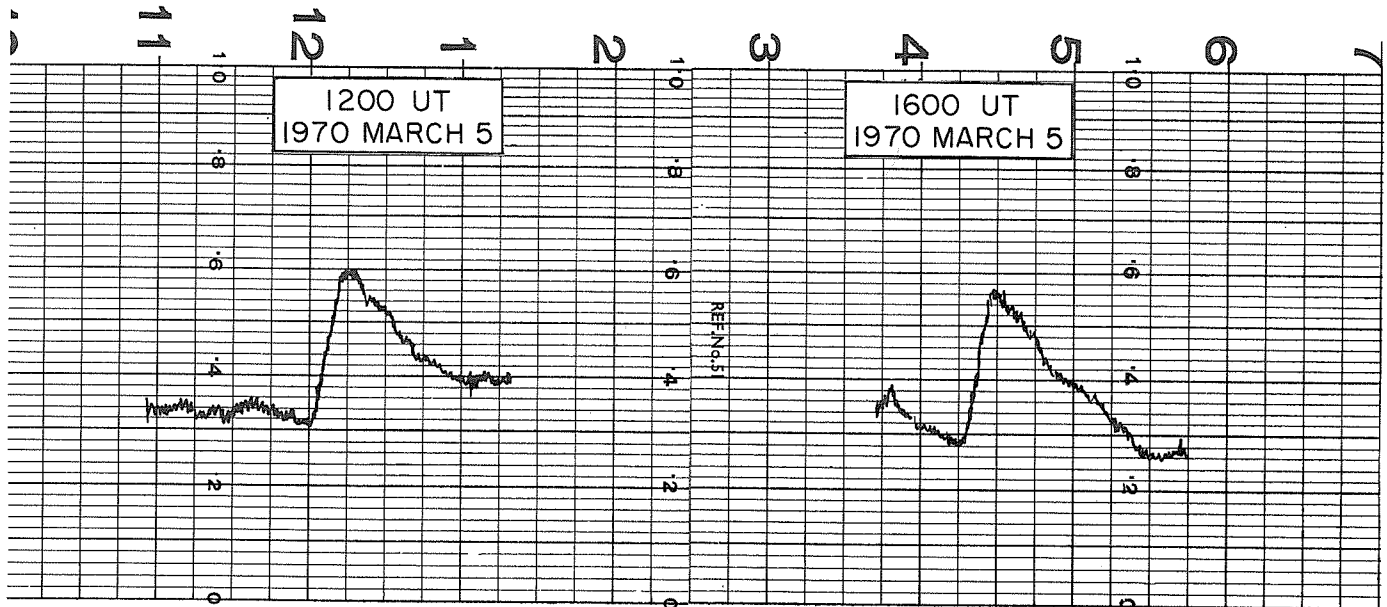
V. Barocas
Wilfred Hall Observatory
Preston, England

At the beginning of the month of March the general level of atmospherics, as recorded at 27 kHz, began to show some signs of increase. The previous two months had been generally quiet with a rather low level of atmospherics and with the occurrence of only 4 SEA, two in each month, none showing an index of importance greater than 1.

In the first two days of March, 3 SEA were recorded and after that, on March 4, the level of atmospherics began to increase and by March 5 had increased by 3.52 dB. During this particular day two SEA were recorded, both having an index of importance 2. These two events were widely recorded as the first was reported by 5 stations and the second by 7 stations.

Following this activity the level of atmospherics remained the same on March 6, but a rather large SEA of importance 3 was recorded by 7 stations. This SEA was not only of high intensity but was also of long duration and appeared to be related to a solar flare observed at the time. Following the decay of the SEA the level of atmospherics remained fairly high for the rest of the day, showing an increase of 4.40 dB on the level before the SEA occurred, and an increase of 7.96 dB on the level measured on March 4, that is at the time before the onset of the increased activity.

By March 7 the level of atmospherics was once again back to the value as on March 4. Nevertheless, on the same day two SEA were recorded, the first was reported by 5 stations and the second by 7 stations. After the events of March 7 the general level of atmospherics decreased and very little activity was detected for several days.



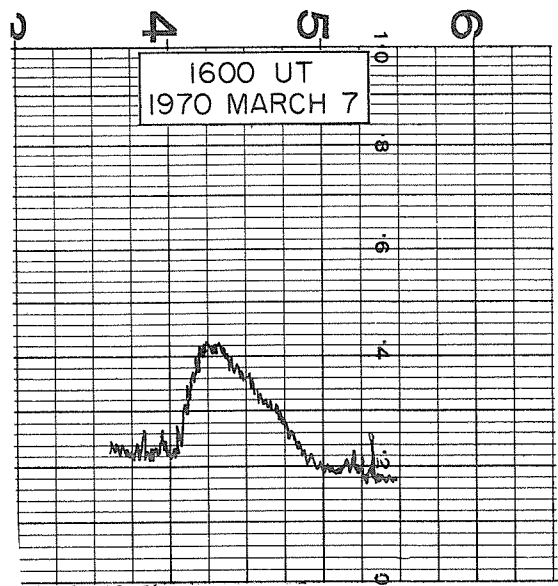
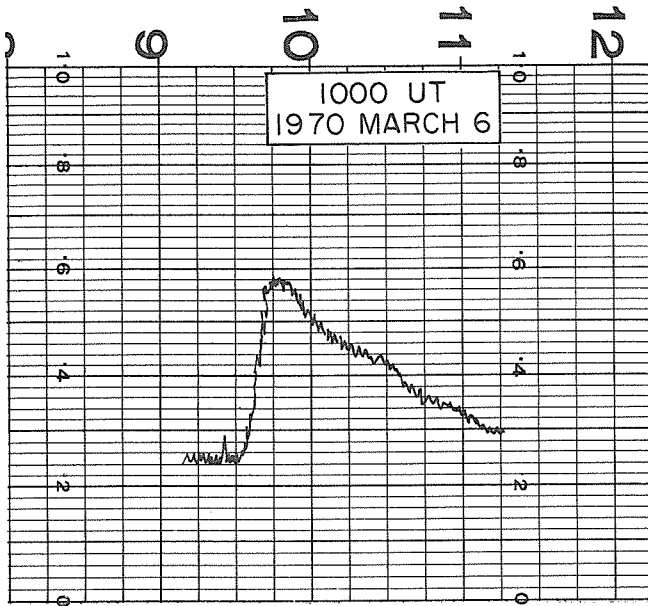


Table I summarizes the data relating to SEA recorded at our station during the period March 5 - 10.

Table 1

Date Mar. 1970	Beg. (UT)	SEA Max. (UT)	End (UT)	Max. (dB)	Imp.	A (dB X t)	Time of known flare (UT)	McMath Plage Region
5	1200	1212	1300	6.15	2	369.0	1157	X - ray
5	1620	1630	1730	6.61	2	462.7	1615	10618
6	0933	0940	1115	8.30	3	846.6	0931	X - ray
7	1124	1135	1215	3.11	2	149.3	1121	10618
7	1610	1618	1720	6.18	2+	432.6	1601	10618

The index of importance of an event is still a very empirical quantity and is subject to the estimate of the observer. In Table I the index of importance quoted is that obtained from the "Solar-Geophysical Data", because these are considered to be much more satisfactory than an individual estimate, since they are based on all the values given by reporting stations.

At our observatory we have been trying for some time to find some less empirical system which could give us more homogeneous results. Bearing in mind that the importance of an SEA depends both on the maximum intensity and on the duration of the event, we have adopted a system of using a value A which is the product of the maximum intensity expressed in dB, relative to daily average value, by the duration in time expressed in minutes. These values A are given in Table I.

One interesting feature of Table I is the evidence of a strong correlation between the solar flares and the SEA over the three days under consideration. From our investigations the correlation is not generally as strong as this, particularly in the case of flares of importance less than 3.

The other point which is worth noting is that the SEA reported in Table I have all been observed by a considerable number of stations. Now from an earlier investigation we carried out a few years ago, it appeared that generally the recording of one particular SEA by several stations occurred only when the SEA was associated with a large solar flare.

6. SOLAR WIND

"Vela 5 Solar Wind Observations during the Geomagnetic Storm of March 8, 1970"

by

Michael D. Montgomery and S. J. Bame
 University of California, Los Alamos Scientific Laboratory
 Los Alamos, New Mexico

Vela 5 solar wind observations during the sudden commencement associated with the large geomagnetic storm of March 8, 1970, showed the passage of an unusually strong interplanetary shock wave. Flow speed, density, and temperature during the time of interest are shown in Figure 1. Since the angle between the satellite spin axis and the sun-satellite line was less than 35° during most of the time interval shown, most of the protons missed the edge of the instrumental acceptance fan before shock arrival preventing reliable determination of proton temperature. The last reliable proton temperature measurements were obtained at 0930 UT when the temperature was 1.5×10^4 °K. Sample error bars appear on those curves where uncertainties are large enough to be shown. The closely spaced points are derived from data transmitted in real time--the widely spaced ones come from data stored on the satellite. Solar ecliptic coordinates of the satellite at the time of the event were: latitude, 19° ; longitude, 340° ; and radial distance, $18.4 R_E$.

The estimated shock velocity, using values of flow speed and density on both sides of the discontinuity of $V_1 = 440 \text{ km sec}^{-1}$, $V_2 = 860 \text{ km sec}^{-1}$, $n_1 = 5.5 \text{ cm}^{-3}$, and $n_2 = 13 \text{ cm}^{-3}$, was 1150 km sec^{-1} . Assuming a preshock proton temperature of 1.5×10^4 °K, the sonic Mach number was 21--almost an order of magnitude higher than typical. The dynamic pressure rise at encounter was very nearly an order of magnitude. An integration of the energy flux excess (above ambient) over time yields a total energy of $\sim 10^{32}$ ergs at 1 AU. This energy is mostly contained in a large, relatively narrow spike thus displaying the characteristics of a blastwave. The event is energetic, but a factor of 3 less so than the most energetic ones analyzed by Hundhausen *et al.*, [1970] using Vela observations from 1965-1967.

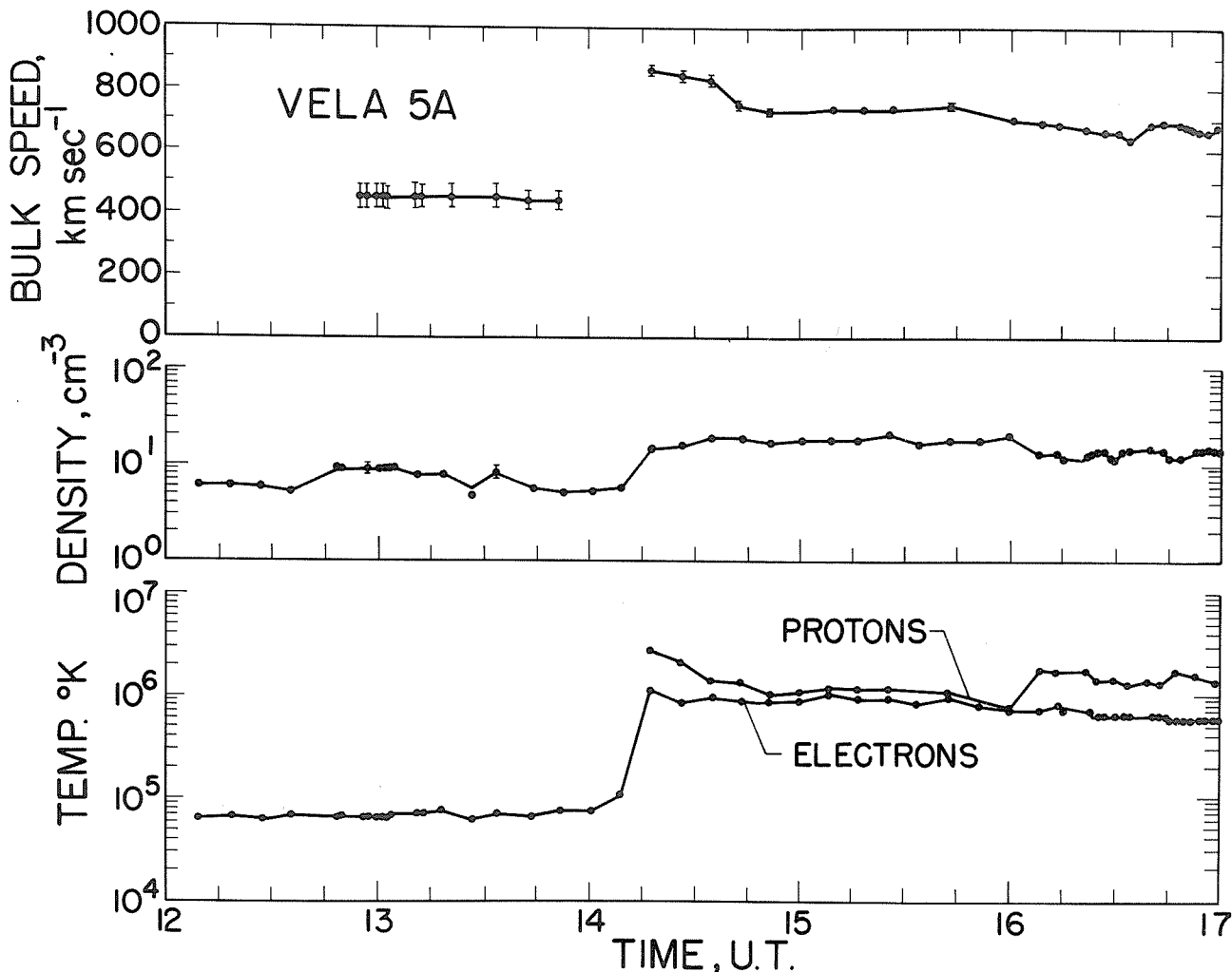


Fig. 1. Vela 5A observations of solar wind bulk velocities, density and temperatures on March 8, 1970.

"Energetic Electrons and Protons Observed on OGO-5, March 6-10, 1970*"

H. I. West, Jr., J. R. Walton and R. M. Buck
Lawrence Radiation Laboratory
University of California
Livermore, California

and

R. G. D'Arcy, Jr.
Bartol Foundation of the Franklin Institute
Swarthmore, Pennsylvania

Introduction

At the start of the March 8 magnetic storm (~ 1418 UT) OGO-5 (1968-14A) had just exited from the magnetosphere. It returned to the magnetosphere about the completion of the storm on March 10; hence, we were unable to observe the main phase effects of the storm. OGO-5 was, however, in a position to observe the accompanying solar particle event and the condition of the magnetosphere at the completion of the storm. In March of 1970 the orbit of OGO-5 was at an inclination of 50.7° (was 31° at launch March 4, 1968) apogee $20.5 R_e$ and perigee $2.58 R_e$. Apogee was on the morning side of the earth at a solar ecliptic azimuth, ϕ_{se} , 311.9° and elevation, λ_{se} , 33.0° . The orbital period was 62.5 hours.

Instrumentation

These data were obtained by the LRL electron and proton spectrometer experiment on OGO-5. The electron analyzer consisted of two magnetic 180° first order focusing spectrometers. Solid state detectors in the focal plane provided both particle detection and secondary energy analysis. Shielded background detectors provided an accurate measure of the background. Data were obtained from energy channels centered at 79, 158, 266, 479, 822, 1530 and 2830 keV. The proton data were obtained from a range energy telescope and single adjacent detector located in line with the aperture of the larger of the electron spectrometer magnets. The energy channels were 0.10 to 0.15 MeV for the single detector and for the telescope 0.23 to 0.57 MeV, 0.57 to 1.35 MeV, 1.35 to 5.4 MeV and 5.6 to 13.3 MeV. An alpha channel derived from the telescope provided a channel at 5.9 to 21.6 MeV. In order to obtain directional information on the earth-sun oriented satellite, the aperture of the spectrometers were scanned relative to the satellite at a rate of $3^\circ/\text{second}$ through an excursion of 230° . The axis of the scan was about the radius vector passing through the center of the earth.

Electron Observations

Figure 1 shows the time history of the lowest energy channel (79 keV) of the electron spectrometer. At the lower counting rates, data were averaged for 9.6 minutes per data point and the backgrounds subtracted. The residual flux observed just prior to the arrival of solar electrons at 1100 UT March 6 is believed to be real. The electron fluxes were low and showed no obvious anisotropy although there may be some evidence of anisotropy in the period 1200 to 2400 on March 6. The counting rates in the other electron channels were too close to background for us to show their time history during the solar particle event. However, data averaging ~ 0000 UT March 7 gave a spectrum $dN/dE = 6 \times 10^6 E^{-(3.0 \pm 0.5)}$ electrons/cm²-keV-sr-sec. The integral above 100 keV is $3.8 \pm 1 \times 10^3$ electrons/cm²-sec.

Magnetospheric entry normally produces a very obvious signature in the data; we find a marked rise in the counting rates and scan modulation in the rates characteristic of trapped radiation. Multiple entry occurred on March 7. In sequence we have entry at 2139 UT ($R = 9.92$, $\lambda_m = -27.7^\circ$, $L = 12.73$, $\phi_{se} = 342.8^\circ$, $\lambda_{se} = -20.0^\circ$) exit at 2149 UT (9.74 , -28.7° , 12.75 , 343.3° , -21.0°) in at 2225 UT (9.07 , -32.5° , 12.85 , 345.2° , -25.1°) and out and in at 2233 UT (8.91 , -33.3° , 12.89 , 345.7° , -25.9°).

Just prior to the start of the storm on March 8, electron fluctuations (momentary gusts of particles above an isotropic level) were observed 1320 to 1403 UT, coordinates (14.33 , 48.9° , 33.27 , 282.6° , 62.39°) to (14.86 , 46.7° , 37.6 , 286.1° , 61.0°). No special effects were observed at the start of the storm at 1418 UT however.

The entry in to the magnetosphere during the late recovery of the storm on March 10 was significant. In Figure 2 we show the details of the entry near the front of the magnetosphere. Here we have picked off the peak fluxes in the scan modulated counting rates. There was a well

* This work was performed under the auspices of the U.S. Atomic Energy Commission and NASA P.O. S-70014G.

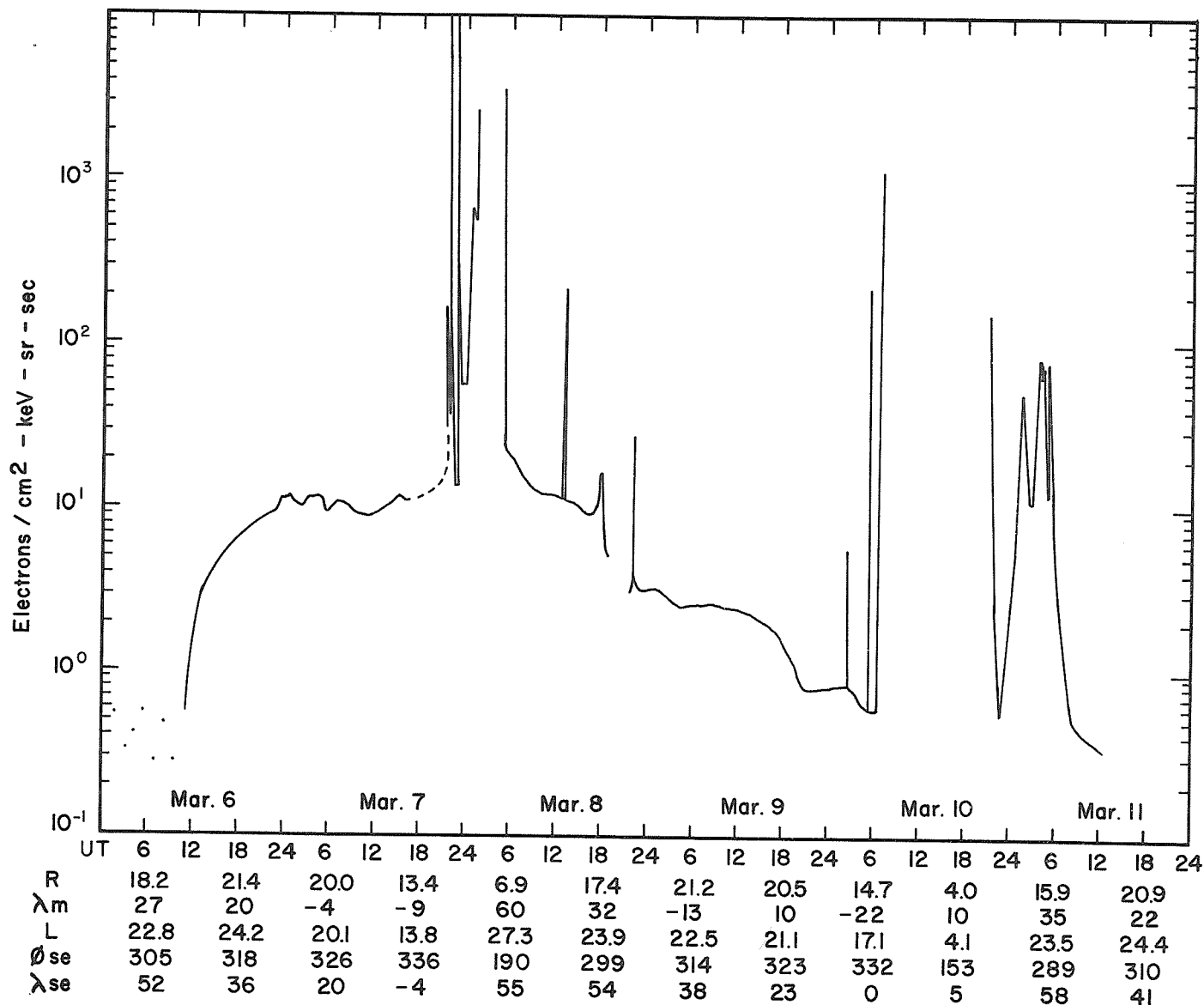


Fig. 1. Observation of electrons in the 79 keV channel March 6-10, 1970. The electron fluxes were averaged over direction.

defined entry at 0644 UT ($R = 14.10$, $\lambda_m = -22.3^\circ$, $L = 16.52$, $\phi_{se} = 334.1^\circ$, $\lambda_{se} = -9.6^\circ$). The counting spikes at 0535 (14.96 , -21.9° , 17.39 , 331.3° , 1.5°) show a signature somewhat similar to the well defined entry at 0644; however interpretation as magnetospheric entry is quite uncertain. There were drop outs in the scan modulated counting rates at 0738 UT (13.36 , -22.5° , 15.74 , 333.6° , -4.5°) and at 0831 UT (12.60 , -22.8° , 14.96 , 334.8° , -7.4°). In previous observations we have been able to show that such drop outs were the result of magnetopause crossings through examination of magnetometer data. Magnetometer data is presently not available to check this point. The observation of the magnetopause at $14.1 R_e$ probably is indicative of a greatly inflated magnetosphere resulting from the enhancement of the trapped fluxes during the magnetic storm. The magnetopause crossing on the next orbit as shown by the electrons was at 0018 UT March 13 at coordinates (11.31 , -32.2° , 15.85 , 334.6° , -13.1°). The outer magnetospheric regions on March 10 showed well developed wave structure in the amplitude of the electron counting rates. The wave structure was also evident on March 13. Electron spectra observed on March 10 are shown in Figure 3.

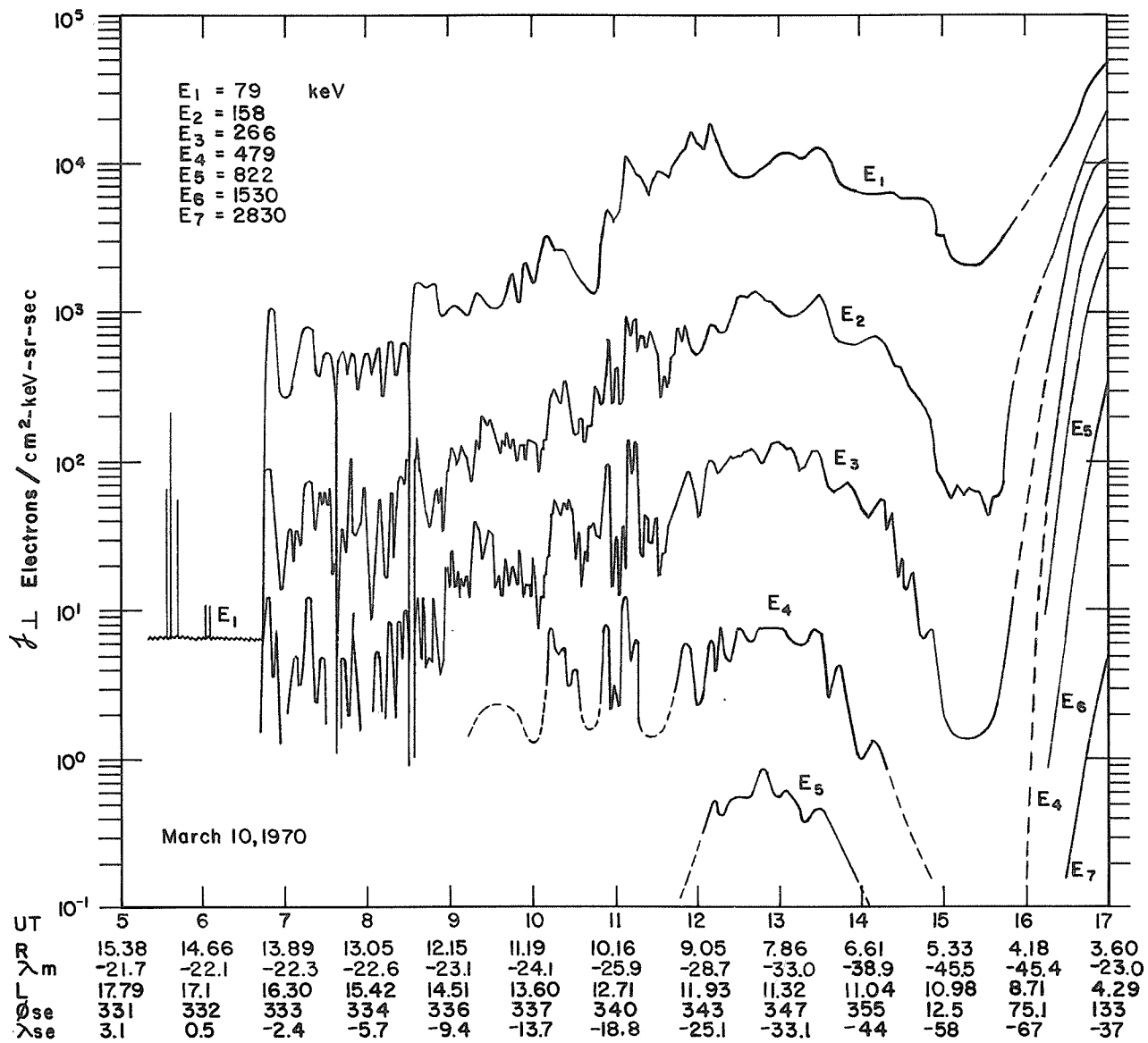


Fig. 2. Electron observations in the magnetosphere on March 10, 1970. The peak observed in the scan modulated counting rates provided j_{\perp} .

Proton Observations

The proton observations are shown in Figure 4. Prior to the start of the solar particle event measurable fluxes of protons were observed in the lowest four energy channels. The fluxes were most obvious in the lowest energy channel (0.10 to 0.15 Mev) showing up as sharply directed fluxes (10 to 20 degrees) coming from approximately the solar direction. Protons associated with the solar particle event were first observed about 1800 March 6. The protons in general (when outside the magnetosphere) showed a great deal of anisotropy. In an effort to show this we have resorted to a bar graph superimposed on the average of the data, the bar showing the maxima and minimum. At the lower counting rates the anisotropies were not particularly easy to observe so that only averages could be obtained. Also, in general the anisotropy decreased at the higher energies. For P5 and the α -channel the fluxes were too low to check on anisotropy except on March 8.

The plane of the aperture scan was inclined at about 40° to the plane of the ecliptic when OGO-5 was near apogee, and deviated from this during the rest of the orbit depending on the elevation of the satellite relative to the plane of the ecliptic. The aperture scan did not always include the solar direction. The angle of closest approach is given by θ_{min} in Figure 4, denoted

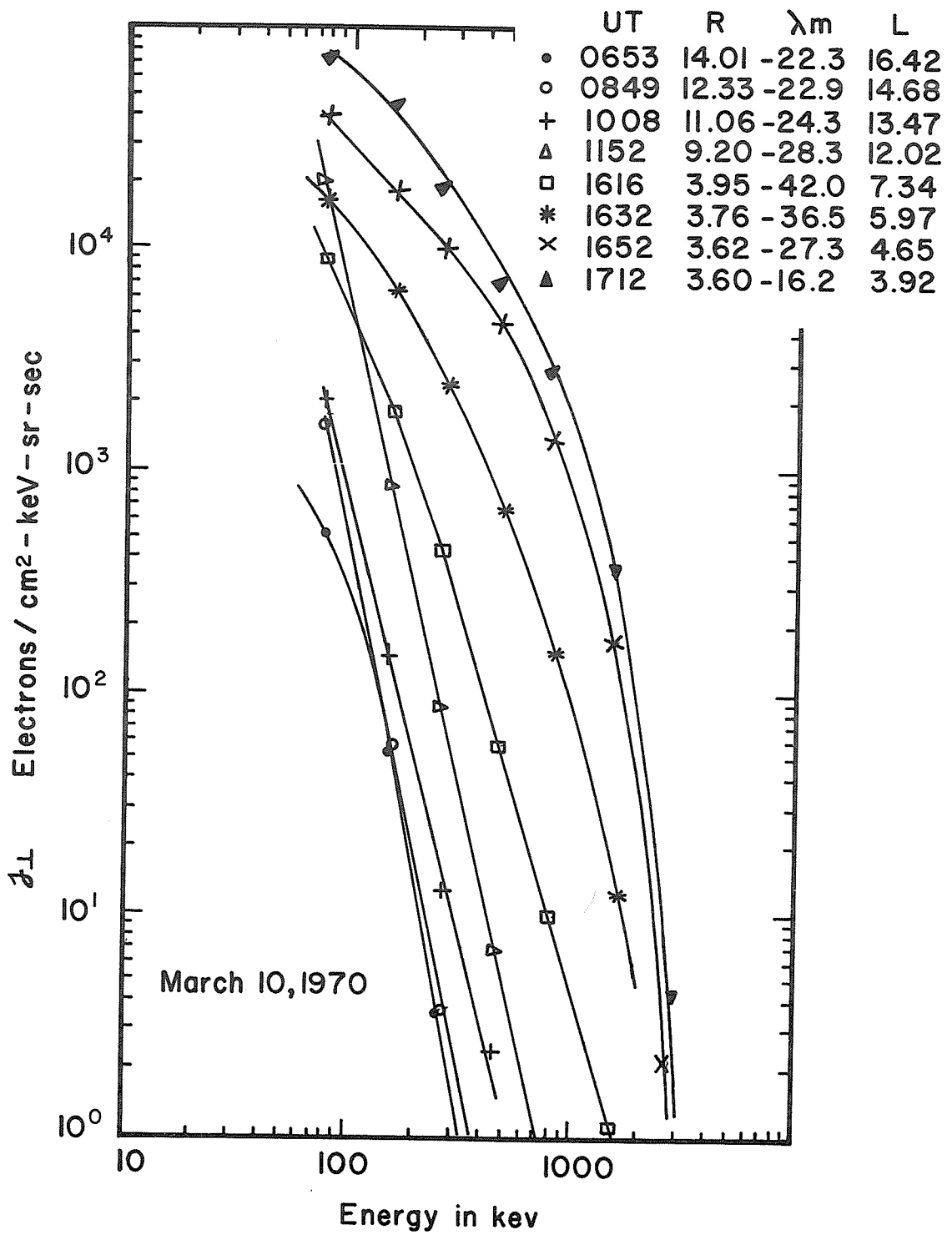


Fig. 3. Electron spectra for the flux profiles of March 10, 1970 as shown in Figure 2.

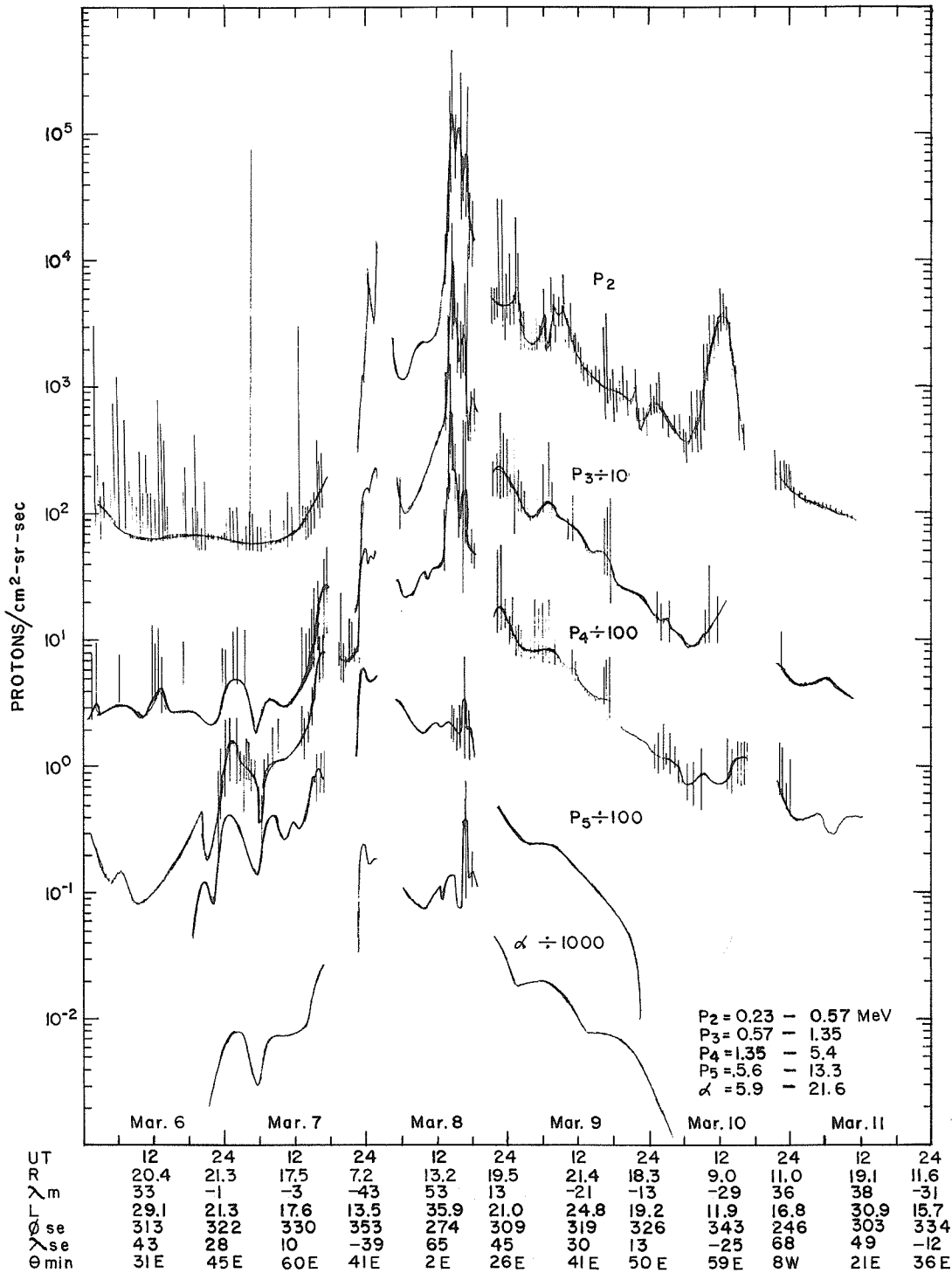


Fig. 4. Proton observations for March 6-10, 1970. The solid line shows the data averaged over direction. Superimposed are bars to represent the maxima and minima when anisotropic fluxes were observed. Because of the great fluctuations observed in the 0.10 - 0.15 Mev channel, these data are not included in the plot.

E or W as to whether the aperture was looking to the east or west at the time of θ min. Fortunately, at the start of the storm the scan came close to including the solar direction. At ~ 1312 UT March 8 the proton fluxes at OGO-5 changed from isotropy to marked anisotropy. Isotropy is usually observed in solar fluxes observed in the magnetosphere. It is not obvious however that 1312 UT, coordinates (14.21, 49.4°, 33.53, 281.8°, 62.5°), was the time of a magnetopause crossing. Over the period of the next hour there was a marked rise in the fluxes and in the anisotropy, this being most marked at the lower energies. A significant jump in the counting rates was observed at ~ 1418 UT the time the magnetic observatories indicate to be the start of the storm.

7. SOLAR ENERGETIC PARTICLES

"HEOS-A1 Solar Proton ($1 \leq E \leq 13$ Mev, $E > 30$ Mev, $E > 360$ Mev) and Interplanetary Magnetic Field Data for March 6-10, 1970"

by

A. Balogh, C. Dyer, A. Engel,
P. Hedgecock, R. Hynds and J. Sear
Physics Department
Imperial College, London

Introduction

The HEOS-A1 satellite (1968-109A) was launched from Cape Kennedy in December, 1968, into a highly eccentric orbit. Apogee is 222,000 km, perigee ~ 1800 km, and the period ~ 106 hours. The inclination of the orbit is 44 degrees. During the period of the observations presented here, the angle between the satellite and the earth-sun was approximately 84 degrees. The satellite spin-axis was tilted at an angle of approximately 25° to the solar ecliptic plane.

The Imperial College Group has 3 experiments on the satellite. A 3-axis, fluxgate, magnetometer, and 2 particle telescopes. The magnetometer has a range of $\pm 64\gamma$, and a sensitivity of 0.5γ per digitization step. Full details are available in Hedgecock [1970].

One of the particle telescopes detects protons of $E > 360$ Mev. It can also make an omni-directional measurement, when protons of $E > 30$ Mev and electrons of $E > 1$ Mev are detected. The telescope, which points radially outward from the satellite spin-axis has a geometric factor $\sim 7\text{cm}^2\text{sterad}$ and a viewing half-angle of ~ 20 degrees. The omni-directional geometrical factor is $\sim 43\text{cm}^2$. The detector and the method of directional measurement are fully described in Engel [1970].

The second telescope is designed to measure protons in a number of energy ranges. The data we present here is for protons of 1 to 13 Mev. This telescope also points radially outwards from the satellite spin-axis. It has a geometric factor of $0.21\text{cm}^2\text{sterad}$ and an effective half-angle of ~ 35 degrees. This experiment is fully discussed in Balogh and Hynds [1970].

Interplanetary Observations

The data presented here cover the period 0000 hours UT on the 6th March to 2400 hours UT on the 10th March 1970. All measurements are presented in the form of hourly mean values except those for protons of $E > 360$ Mev, which are shown as 6-hourly mean values. Representative errors are indicated where appropriate.

The directional particle data is represented by averages of the radial pointing detectors. Data from similar detectors pointing along the anti-spin-axis direction are not given. In the case of protons of $E > 360$ Mev it was not significantly different from that of the radial pointing measurements. For protons in the 1 to 13 Mev range, overflow of the counting system causes the data to be indecipherable.

Figure 1 shows the observations. The energy ranges of the various measurements are indicated. During some parts of the period shown the satellite was inside the magnetospheric bow shock. The crossing points of the bow shock are indicated on the magnetic field data.

Close to the maximum of the particle increase observed for the 1 to 13 Mev protons, some difficulty was experienced due to overflow of some of the data stores. However, by cross-correlation between the 8 radial sector measurements we have confidence that we have correctly interpreted the overflow. The period affected is indicated in Figure 1.

The magnetometer experiment contained a core store device. This showed the shock front observed on the 8th to pass the satellite at $14^{\text{h}}11^{\text{m}}54^{\text{s}}$ UT. The magnetic field strength was observed to increase from 13γ to 33γ in a sampling time of 1.4 seconds. At this time the satellite was at a geocentric distance of 33.74 earth radii.

REFERENCES

- BALOGH, A. and 1970 Intercorrelated Satellite Observations related to Solar
R. J. HYNDS Events; edited by V. Manno and D. E. Page; published by
D. Reidel.
- ENGEL, A. "
- HEDGECOCK, P. C. "

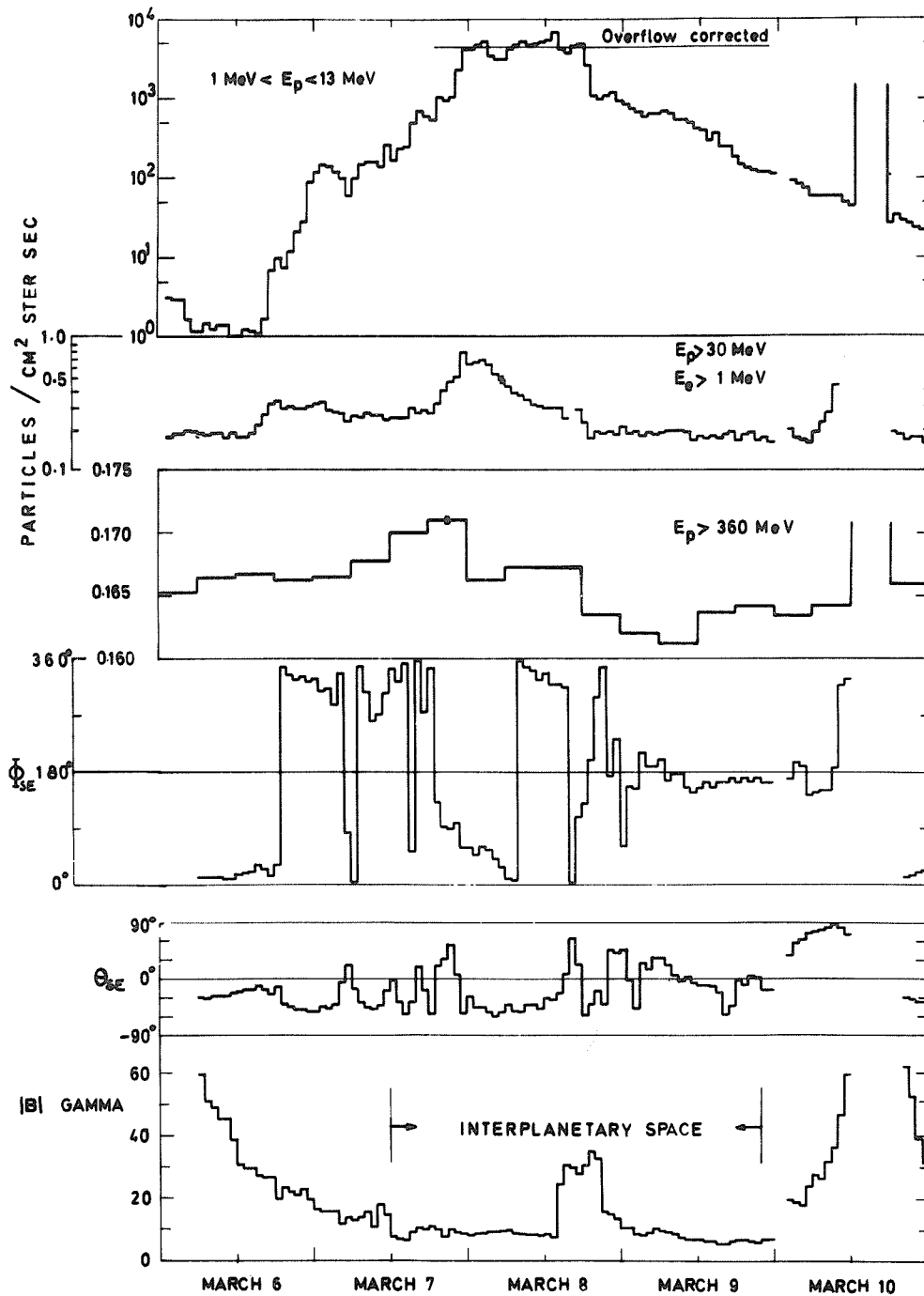


Fig. 1. Energetic particle, and magnetic field, data for the period 6th to 10th March, 1970. The periods in interplanetary space are indicated. Also shown is the period where a correction was necessary to the 1 to 13 Mev proton data because of data storage overflow (see text). The magnetic field data is expressed in solar ecliptic co-ordinates.

"Observation of Energetic Solar Particles during March 6-10, 1970"*

by

R. P. Lin

Space Sciences Laboratory
University of California
Berkeley, California 94720

and

K. A. Anderson
Physics Department and Space Sciences Laboratory
University of California
Berkeley, California 94720

We present here observations of energetic solar electrons and protons for the period March 6-10, 1970. These observations are from the University of California energetic particle experiment aboard IMP-5. Six Geiger-Müller detectors cover four integral energy channels for electrons and three integral channels for protons. In addition, two pairs of identical GM detectors are pointed at 90° to each other to provide some directional information. The energy ranges covered are >18 kev, >45 kev, >80 kev and >120 kev for electrons and >0.25 Mev, >1.5 Mev and >2.3 Mev for protons. Also, 3-20 kev and 1-20 kev solar x-rays are observed by the E1 and E3 counters respectively.

An ionization chamber similar to ones flown on IMP-4, Explorer 33 and 35 completes the detector complement. Table 1 presents the detector characteristics.

The data is presented in Figure 1 in the form of hourly average count rates over the five day period. These can be converted into flux using the geometric factors given in Table 1. Background due to galactic cosmic rays is indicated by a B on each detector count rate scale. Except for the short intervals marked on the figure the fluxes are all solar in origin.

Table 1

IMP-5 Detector Characteristics

Detector Designation	Type of Detector	Window	Sensitivity			Geometry Factor cm ² ster	Look Angle FWHM	Angle to Spin Axis
			Electrons	Protons	X-ray			
P1	LND 705 GM tube	0.5 mg/cm ² mica	>18 kev	>0.25 Mev	None	2.7x10 ⁻²	40°	0°
P2	LND 7041 GM tube in scatter configuration	1.5 mg/cm ² mica	>45 kev	--	None	6.3x10 ⁻²	70°	0°
P3	LND 7041 GM tube with Al foil	3.0 mg/cm ² mica and 4.5 mg/cm ² Al	>80 kev	>1.5 Mev	None	0.75	70°	0°
E1	LND 7041 GM tube, thick window	13 mg/cm ² mica	>120 kev	>2.3 Mev	3-20 kev**	1.03	70°	90°
E2	LND 7041 GM tube in scatter configuration	1.5 mg/cm ² mica	>45 kev	--	None	6.5x10 ⁻²	70°	90°
E3	LND 7041 GM tube with Al foil	2.7 mg/cm ² mica and 4.5 mg/cm ² Al	>80 kev	>1.5 Mev	1-20 kev**	0.86	70°	90°
IC	4" diameter spherical, Neher type integrating ionization	210 mg/cm ² Aluminum skin	>0.7 Mev	>12 Mev maximum sensitivity ~17 Mev	≥20 kev	~80 cm ² omni-directional	--	--

** X-ray range -- 0.1% efficiency points

* This research supported in part by the National Aeronautics and Space Administration under contract NAS 5-9091.

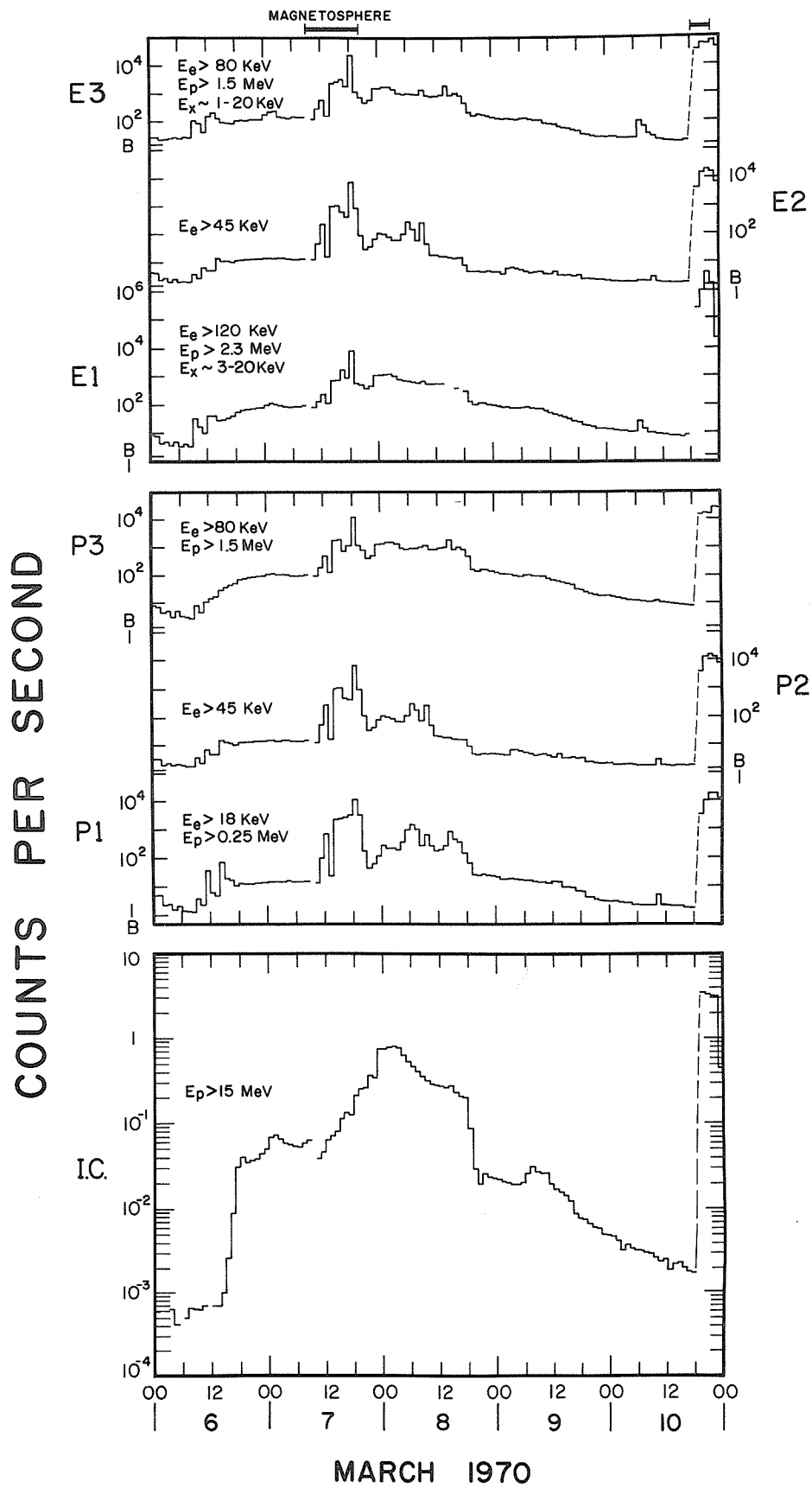


Fig. 1. Hourly average counting rates March 6-10, 1970.

"Solar Protons and Alpha Particles in the March 6-9, 1970 Events"

by

J. C. Armstrong and C. O. Bostrom
The Johns Hopkins University
Applied Physics Laboratory
Silver Spring, Maryland

This note presents proton and alpha particle data measured with solid state detectors aboard the IMP-G (Explorer 41) satellite during the period March 6-9, 1970.

The IMP-G satellite has an apogee of $\approx 28.5 R_e$, perigee of ≈ 250 km, and inclination of 84° . During the period of interest, the local time of apogee was ≈ 2000 UT; magnetospheric coordinates of apogee are $X \approx 12 R_e$, $Y \approx 25 R_e$, $Z \approx 5 R_e$. Thus, the bulk of the data to be presented will represent measurements in the evening sector of the tail and near the ecliptic plane.

Detectors

The portion of the Applied Physics Laboratory's experiment of primary interest here consists of a single, thin (96μ) solid state detector inside a copper housing. The field of view is conical, with half-angle 30° . The detector has a large active area ($\approx 2 \text{ cm}^2$) and a relatively large geometric factor of $\approx 1.7 \text{ cm}^2 \text{ ster}$. There are two discrimination levels, one at 0.9 Mev, the other at 4.14 Mev. From ΔE vs. E curves (and considering the effect of a thin light shield), the data from this detector represent particles with $1 \lesssim E_p \lesssim 10$ Mev (Detector 4A) and $4 \lesssim E_\alpha \lesssim 36$ Mev (Detector 4B), or approximately the same energy/nucleon for both protons and alphas. Each data point to be presented represents an accumulation time of 38.4 seconds (i.e., over ≈ 20 spin periods of the satellite; thus, eliminating any possibility of detecting anisotropies which might be present in the particle fluxes). The statistical uncertainty in individual data points can be found from $(C/38.4)^{1/2}$, where C is the counting rate plotted. For the proton to alpha ratios to be presented, this uncertainty is given by

$$\frac{1}{38.4} \left(\frac{1}{C_p} + \frac{1}{C_\alpha} \right)^{1/2} \text{ times the ratio.}$$

A detailed description of the $E_p \geq 10$, ≥ 30 , and ≥ 60 Mev detectors is given in Solar-Geophysical Data (Descriptive Text), No. 306 (Supplement), February 1970, U.S. Department of Commerce, (Boulder, Colorado, 80302), and will not be repeated here.

We now consider several possible contributors to the background in detector 4B. The two most likely are proton pile-up and penetrating protons which enter the detector edge and have a long path length in the sensitive volume. For proton pile-up to cause counts in detector 4B, one of the following must occur: (i) Two protons with total energy of 4.14 Mev must have exact coincidence (least favorable double coincidence situation), (ii) two protons with total energy greater than 4.14 Mev have coincidence within some time $t < \tau$. τ is a maximum when both protons have $E_p = 3.0$ Mev (maximum energy which a proton can deposit in the detector) and a minimum when the energies are 3.0 and 1.14 or 7.5 Mev. Laboratory measurements with the IMP-G spare package, using a calibrated double pulser with variable time between pulses, give values of τ ranging from 30 nanoseconds for $E_{p1}, E_{p2} = 3.0$ and 1.2 Mev, respectively, to 145 nanoseconds for $E_{p1} = E_{p2} = 3.0$ Mev. These values of τ represent a 50% chance that the proton pile-up pulse will cause a count in detector 4B. The number of counts in 4B due to proton pile-up is, thus, dependent on the proton spectrum to some extent. However, calculations using reasonable proton spectra and various "effective" values of τ indicate an essentially negligible contribution to detector 4B count rates. The actual data taken during this event support this conclusion. Radiation belt measurements with detector 4A count rates of $\approx 40,000$ c/s and detector 4B count rates of ≈ 40 counts/sec (at $L \approx 2.4$, $B \approx 0.09$ gauss) give a proton/alpha ratio of ≈ 1000 , in accord with previous measurements [Krimigis et al., 1968]. If for this case we assume that all the detector 4B counts are due to proton pile-up and use the simple coincidence formula

$$C_{4B} = 2\tau_{\text{eff}} (C_{4A})^2$$

we get

$$\tau_{\text{eff}} \approx 50 \text{ nanoseconds}$$

where we have assumed that half the counts in detector 4A are due to protons which could contribute to pile-up. But even this value of τ must be a considerable over-estimate, else we would not have gotten a proton/alpha ratio in the radiation belts in substantial agreement with previous experiments. Additional evidence comes from observing that at times the count rate of detector 4A is increasing while that of 4B is decreasing even during periods of very high count rates for detector 4B (see, for instance, Figure 4 between 06-14 UT).

The other area which must be investigated before concluding that 4B counts are indeed due to alphas is side penetration of energetic protons with a long pathlength in the detector. Side penetration requires protons with $E_p \geq 30$ Mev. The $E_p \geq 30$ Mev protons show a maximum increase during the events being considered of a factor of 3. For the background rate for $E_p \geq 30$ Mev, detector 4B count rates are ~ 0.1 c/s, and if we attribute this entirely to penetrating protons, it is seen that an increase in $E_p \geq 30$ Mev by a factor of 3 can cause a maximum of ~ 0.3 c/s in detector 4B, which is negligible for data taken during the event. Thus, we conclude that detector 4B is indeed measuring alpha particles.

Data

The higher energy protons will be considered first. Protons with $E_p \geq 60$ Mev showed no discernable change for the period of interest. For $E_p \geq 30$ Mev, there was an increase in c.r. from 0.65 c/s at ~ 1424 UT to 0.96 c/s at ~ 1912 UT on March 6, with a slow decrease to 0.8 c/s at ~ 1800 UT on March 7, at which time there was another increase to 1.6 c/s at ~ 00 UT on March 8, followed by an essentially uneventful decrease to background at ~ 2030 UT on March 8. One-hour averages of these data are published routinely in the Solar-Geophysical Data, U.S. Department of Commerce, (Boulder, Colorado, USA, 80302); in particular, the data for the March 1970 period appears in the September 1970 (No. 313) Part II issue.

A time history of count rates for $E_p \geq 10$ Mev is shown in Figure 1 for the period of interest (these data are also published in Solar-Geophysical Data, but only as 1-hour averages). Certain relevant occurrences, such as boundary crossings, etc., are noted on the Figure. We point out that the occurrence of a sudden commencement had little effect on the $E_p \geq 10$ Mev particles, in contrast to the lower energy particles.

A time history of the protons with $1 \leq E_p \leq 10$ Mev is shown in Figures 2a, 3a, and 4a. The interesting oscillations in intensity from $\sim 01-06$ UT on March 7 are not correlated with large magnetic disturbances on the earth. In contrast, the oscillations from $\sim 1400-1900$ UT on March 8 are closely associated with a sudden commencement and magnetic disturbances which reached a peak amplitude of $\sim 4000\gamma$ at the College, Alaska magnetic observatory.

A time history of alpha particles with $4 \leq E_\alpha \leq 36$ Mev ($1 \leq E_\alpha/\text{nucleon} \leq 9$ Mev) is shown in Figures 2b, 3b, and 4b. Although the general behavior of these particles as a function of time is similar to that of protons with $1 \leq E_p \leq 10$ Mev, there are interesting variations when the two are compared in detail. This is seen in Figures 2c, 3c, and 4c, where we have plotted the ratio $J_p(1 \leq E_p \leq 10 \text{ Mev})/J_\alpha(1 \leq E_\alpha/\text{nucleon} \leq 9 \text{ Mev})$ as a function of time. This ratio ranges from ≈ 30 to ≈ 260 , in general accord with the results of Armstrong and Krimigis [1970]. The maximum occurs with the satellite in the magnetosheath and rather late in the event, in exact coincidence with the arrival of the sudden commencement.

As concluding remarks, we would like to make the following comments for this event:

(i) Protons and alphas with $E \gtrsim 1$ Mev/nucleon might or might not be affected by the boundary between the magnetosphere and the magnetosheath, apparently depending on interplanetary conditions (compare, for instance, the periods 09-11 UT, March 6, and 07-10 UT, March 8, with the period 2000-2230 UT on March 7).

(ii) The plasma (shock) causing the sudden commencement for this event carried with it proportionately more protons than alphas with $1 \lesssim E/\text{nucleon} \lesssim 10$ Mev than were present at other times during the event.

REFERENCES

- | | | |
|---|------------------------|---|
| <p>KRIMIGIS, S. M.,
J. A. VAN ALLEN and
A. L. BURNS</p> | <p>1968 (Abstract)</p> | <p>Mariner 5 Observations of Magnetospheric Protons and Alpha Particles, <u>Trans. Am. Geophys. Union</u>, 49, 268</p> |
| <p>ARMSTRONG, T. P. and
S. M. KRIMIGIS</p> | <p></p> | <p>A Statistical Study of Solar Protons, Alphas, and $Z \geq 3$ Nuclei in 1967-68, <u>APL Preprint</u>, October, 1970 (Submitted to <u>J. Geophys. Res.</u>)</p> |

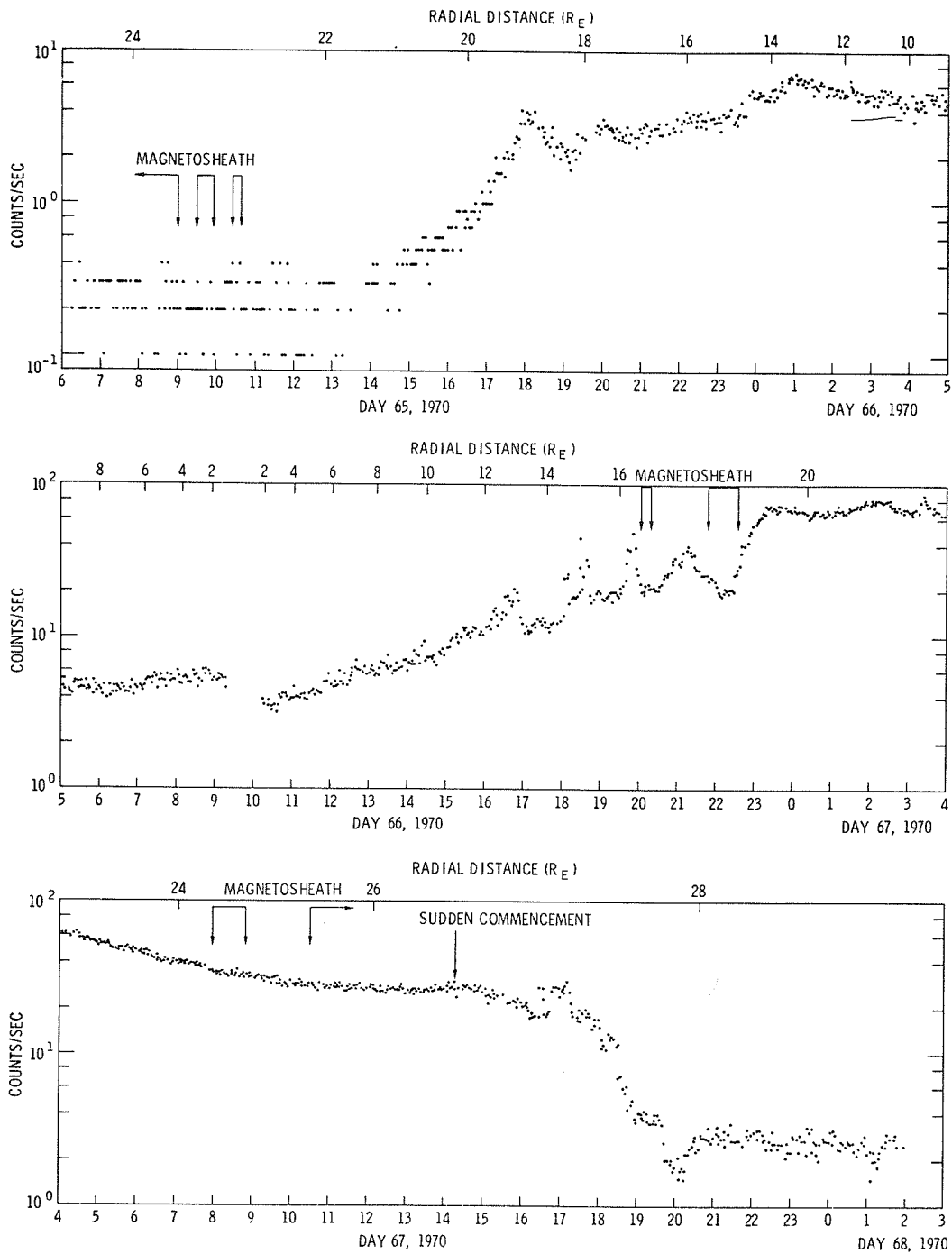


Fig. 1. A time history of solar protons $E_p \geq 10$ MeV from March 6-9, 1970. The boundary crossings between the magnetosheath and magnetosphere at ~ 0900 , ~ 0930 , and ~ 1030 UT are determined from on-board magnetometer data, courtesy of Dr. D. H. Fairfield. The later indications are at times when the satellite is encountering magnetosheath plasma on the outbound portion of the trajectory and are courtesy of Dr. L. A. Frank.

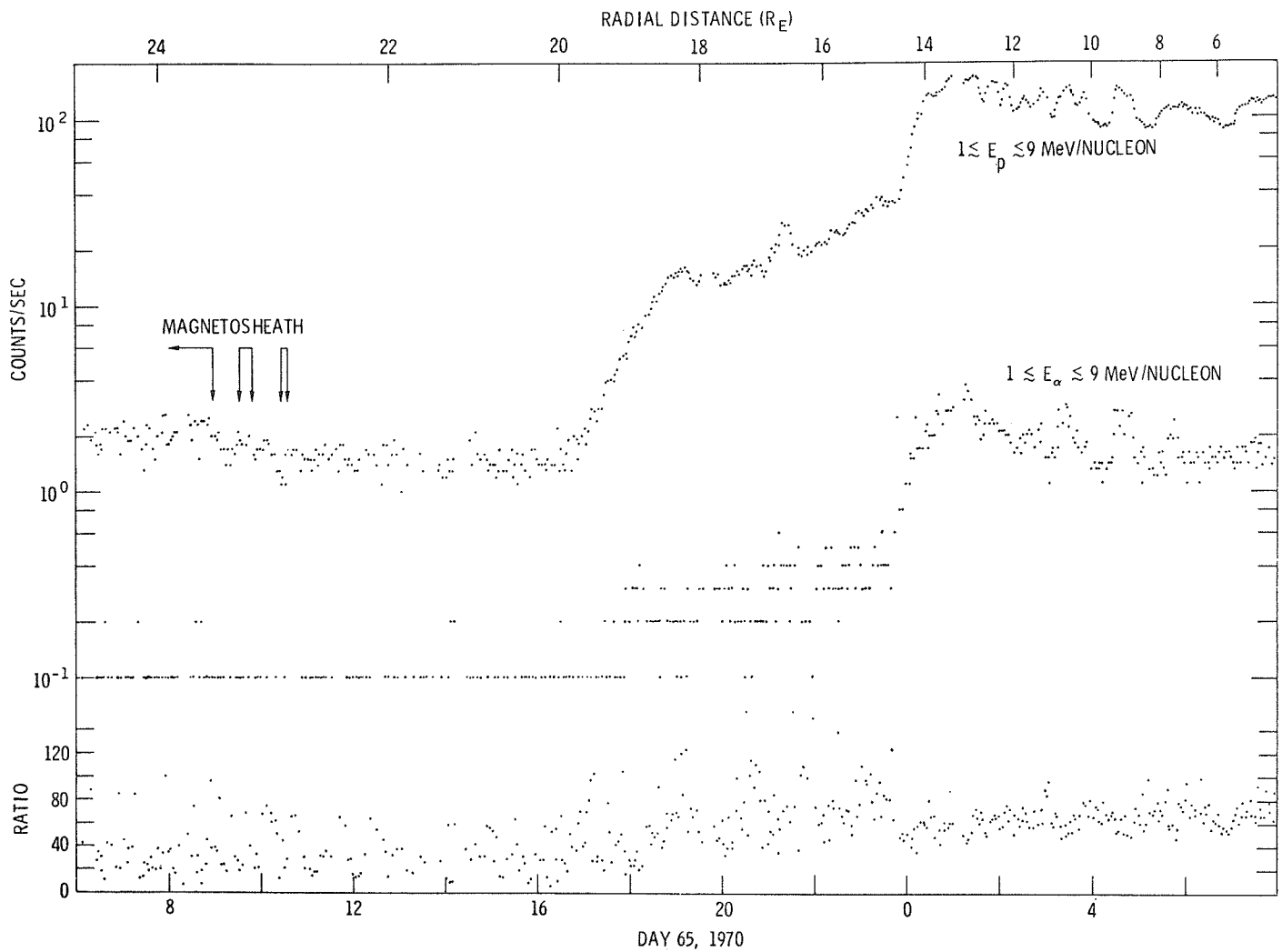
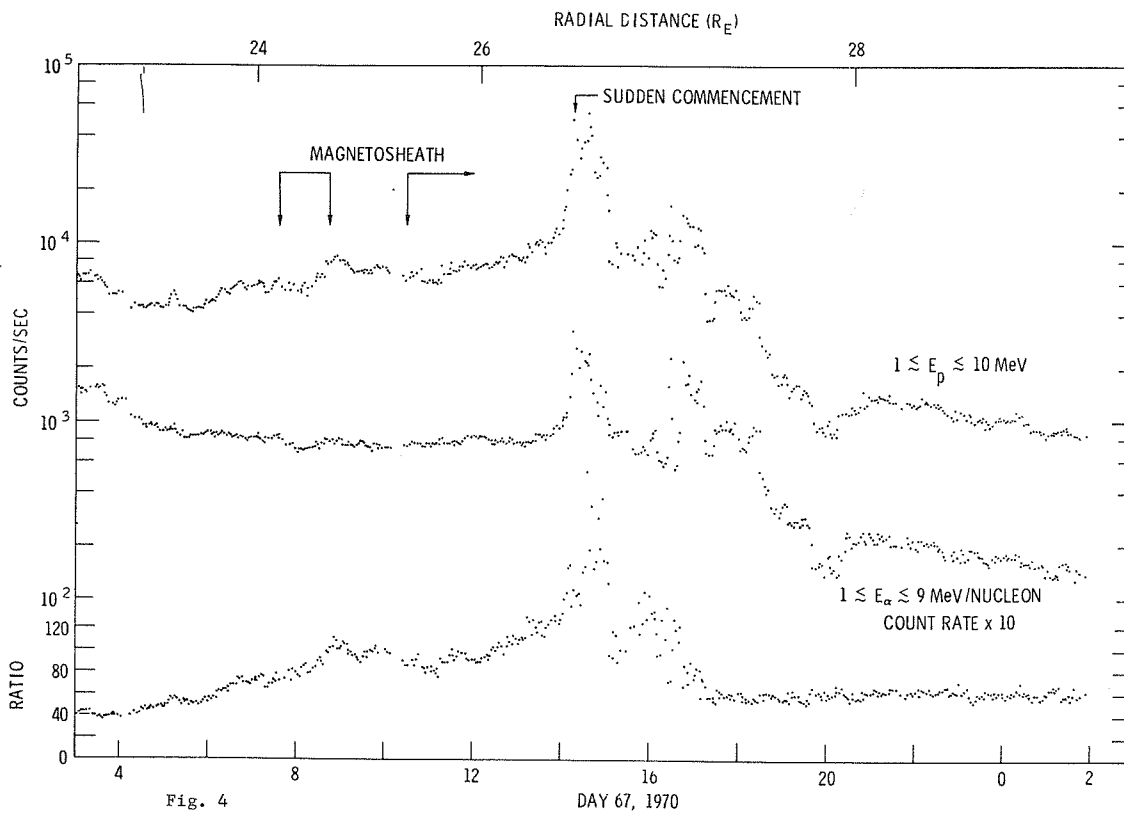
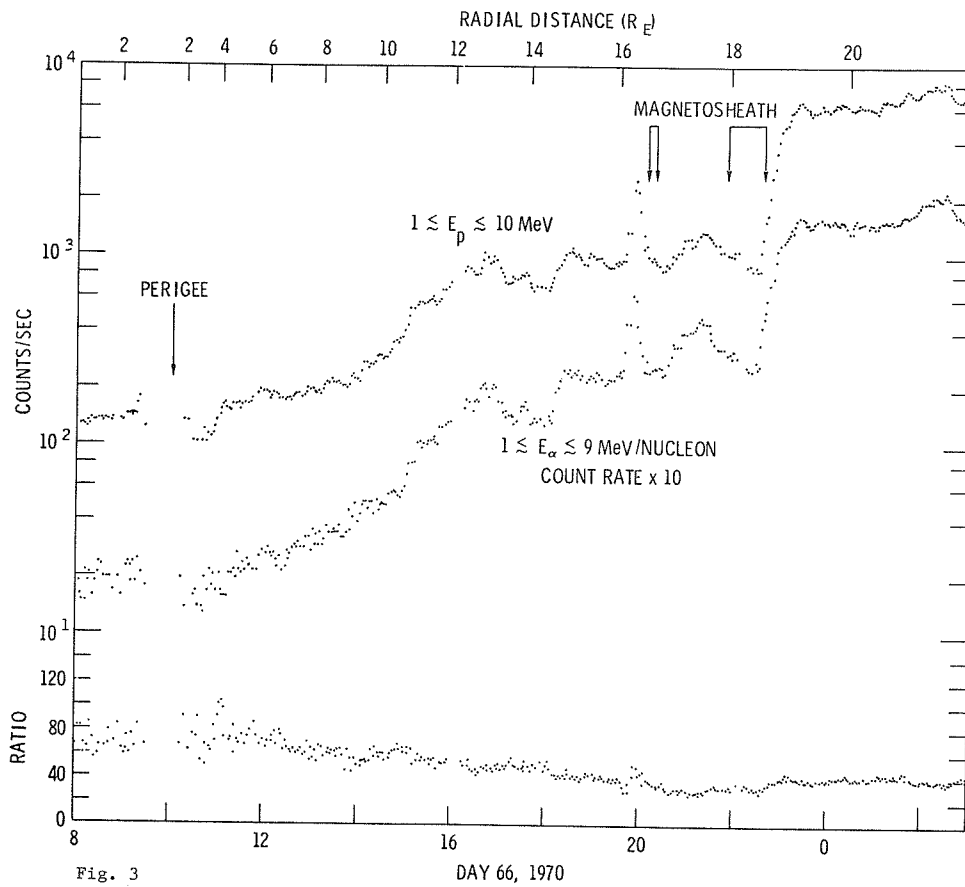


Fig. 2. Solar protons ($1 \lesssim E_p \lesssim 10 \text{ MeV}$), alphas ($1 \lesssim E_\alpha/\text{nucleon} \lesssim 9 \text{ MeV}$), and their ratio as a function of time for the March 6-9, 1970 events.



Figures 3 and 4. Solar protons ($1 \lesssim E_p \lesssim 10$ MeV), alphas ($1 \lesssim E_\alpha/\text{nucleon} \lesssim 9$ MeV), and their ratio as a function of time for the March 6-9, 1970 events.

"Proton, Alpha and Bremsstrahlung Fluxes Measured Aboard OV5-6"

by

G. K. Yates, L. Katz and J. G. Kelley
Air Force Cambridge Research Laboratories
L. G. Hanscom Field, Bedford, Mass.

and

B. Sellers, F. A. Hanser and P. R. Morel
Panametrics, Inc., Waltham, Mass.

Satellite OV5-6 (International designation 1969-046B) measures solar fluxes of protons, alphas and gamma rays. Its ephemeris for one revolution on 6-7 March 1970 is shown in Figure 1. This ephemeris is essentially valid for all revolutions during this event. Its orbital period was 3116.7 min.

The proton-alpha particle detector on OV5-6 consists of two totally depleted silicon surface barrier detectors in a telescope configuration. The detectors each have a 2 cm² area and are separated by 2.54 cm. The outer one is 200 microns thick and the inner one 750 microns. The outer detector is shielded from light by 0.6 mil of aluminum foil. In the coincidence mode of operation, the telescope has a geometric factor of 0.52 cm²-sr, with a detection cone of 30° half angle. The average angle of detection is 17°. A coincidence is set by an energy loss window on the first detector and a threshold on the second detector. The resulting coincidences detect protons and alpha particles (principally) in the following ranges: protons 5.3 to 8 Mev, 8 to 17 Mev, 17 to 40 Mev, and 40 to 100 Mev; alpha-particles 20 to 32 Mev, 32 to 68 Mev, and 68 to 100 Mev. The telescope cycles sequentially through these seven ranges, each range is counted and then read out. The complete cycle is completed in approximately two minutes. The telescope looks in the equatorial plane of the satellite. This plane was inclined about 45° to the earth-sun line during the March 1970 event. Since the spin period during this time was 4.8 seconds, the telescope accumulated counts in a given particle energy range for approximately two satellite rotations.

The telescope also has a calibration mode which allows some lower energy proton data to be obtained during high flux periods. Each coincidence count is followed by a single count from one of the detectors. The differential energy loss is measured in the 200 micron detector, and in the 750 micron detector the integral energy loss is measured. The detectors alternate in readout. Thus, each detector is read out once for each two coincidence count cycles (approximately 4 minutes) and each read out covers seven points. The calibration mode count time is 1.8 seconds, and the detectors sweep out about 130° during the count time. For this mode the 200 micron detector has a geometric factor of 3.2 cm²-sr and provides information on protons in the energy ranges 1.25 to 1.41 Mev, 1.41 to 1.79 Mev, 1.79 to 2.71 Mev, 2.7 to 4.8 Mev, and 4.8 to 5.6 Mev.

Figure 2 shows 50 minute averages of the data from the four coincidence proton channels and the lowest energy alpha particle channel. Fluxes are given in particles /cm²-sec-sr-Mev; most gaps correspond to periods of no telemetry; a few points when the satellite is within the trapped radiation belt are omitted. Figure 3 shows the time structure observed near 2000 UT on March 7. Each point represents one coincidence mode measurement; successive points are about two minutes apart.

Spectra at certain times during the event are shown in Figures 4, 5 and 6. These include the calibration mode proton data averaged over spin to make it comparable to the coincidence mode data. The lower energy data have been corrected for the contribution by high energy protons and for background from a weak alpha source normally used to check the gain of the detector electronics. The energy ranges are shown by horizontal bars, and where significant one sigma statistical uncertainties are shown by vertical bars.

The bremsstrahlung (or X-ray and gamma) detector utilizes a 0.5" dia. x 0.5" long NaI (Tl) scintillator cemented to an RCA C70102M photomultiplier tube using a soft epoxy (Solithane), and the entire unit encased in a machined nylon shell. The shell was cut out, except for three strips, around the sensitive side area of the crystal to permit optimum X-ray transmission. This instrument was furnished by TRW, Inc. The signals from the bremsstrahlung detector were input to a series of four stacked discriminators to provide measurements of photons in the energy intervals 19.4 to 76.5 keV, 76.5 to 232 keV, 232 to 1175 keV, and all photons of energy greater than 1175 keV. The outputs of the discriminators were input to log count rate meters which convert the count rate to an analog voltage for telemetry. The omnidirectional geometrical factor is 1.89 cm². The highest energy channel is also sensitive to electrons of energies greater than 1.83 Mev and protons of energies greater than 17.2 Mev. Figure 7 depicts the observed fluxes in these energy intervals. No attempt has been made to correct for possible contaminations by Van Allen belt particles or high energy protons or electrons, except for the deletion of data points at perigee.

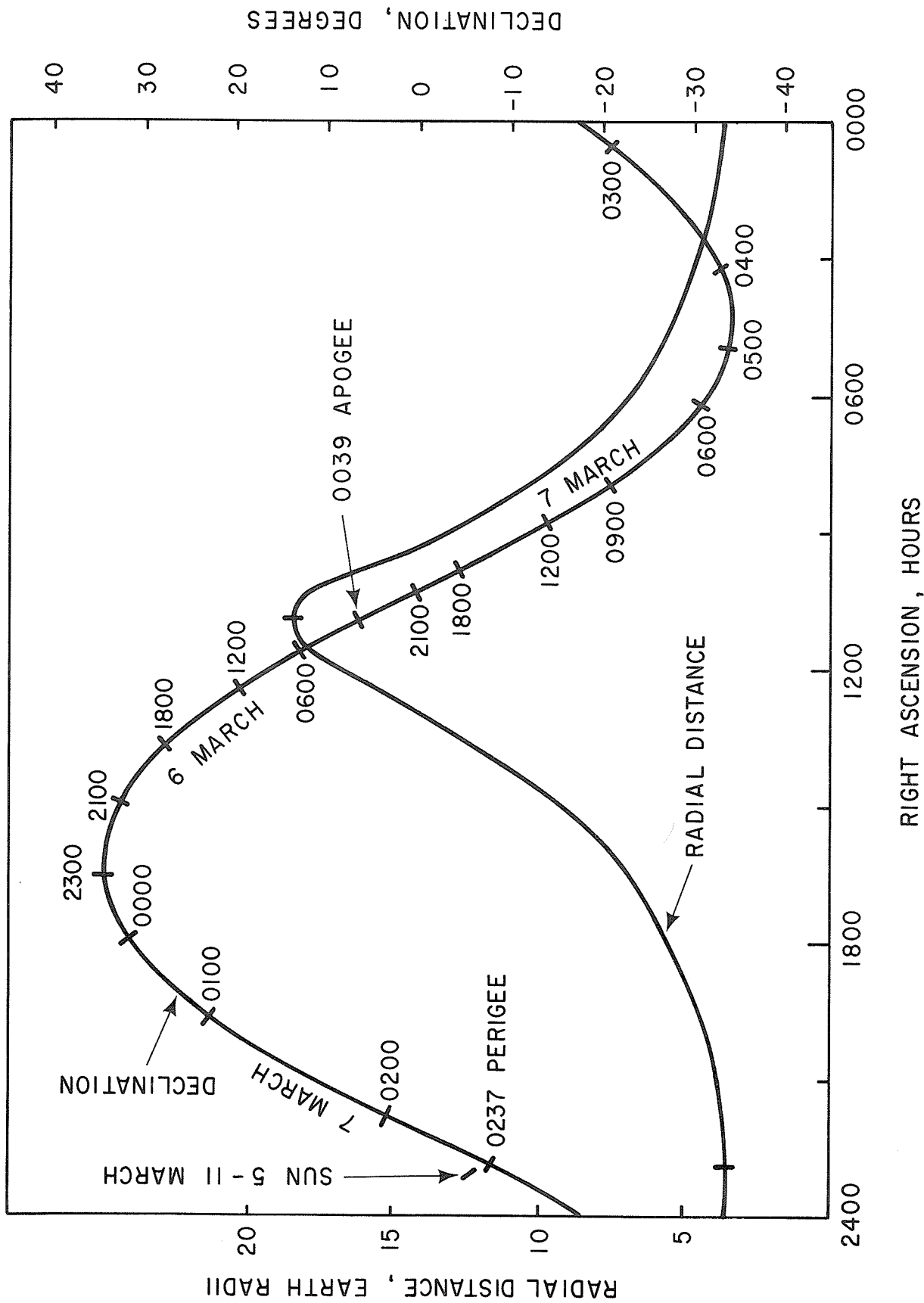


Fig. 1. Celestial coordinates of satellite orbit. Universal time is shown on the declination curve beginning at apogee, 0039 hours, 6 March and ending one period later. The period, which is 51 hours and 56.7 minutes, may be added to these times to determine positions on other dates.

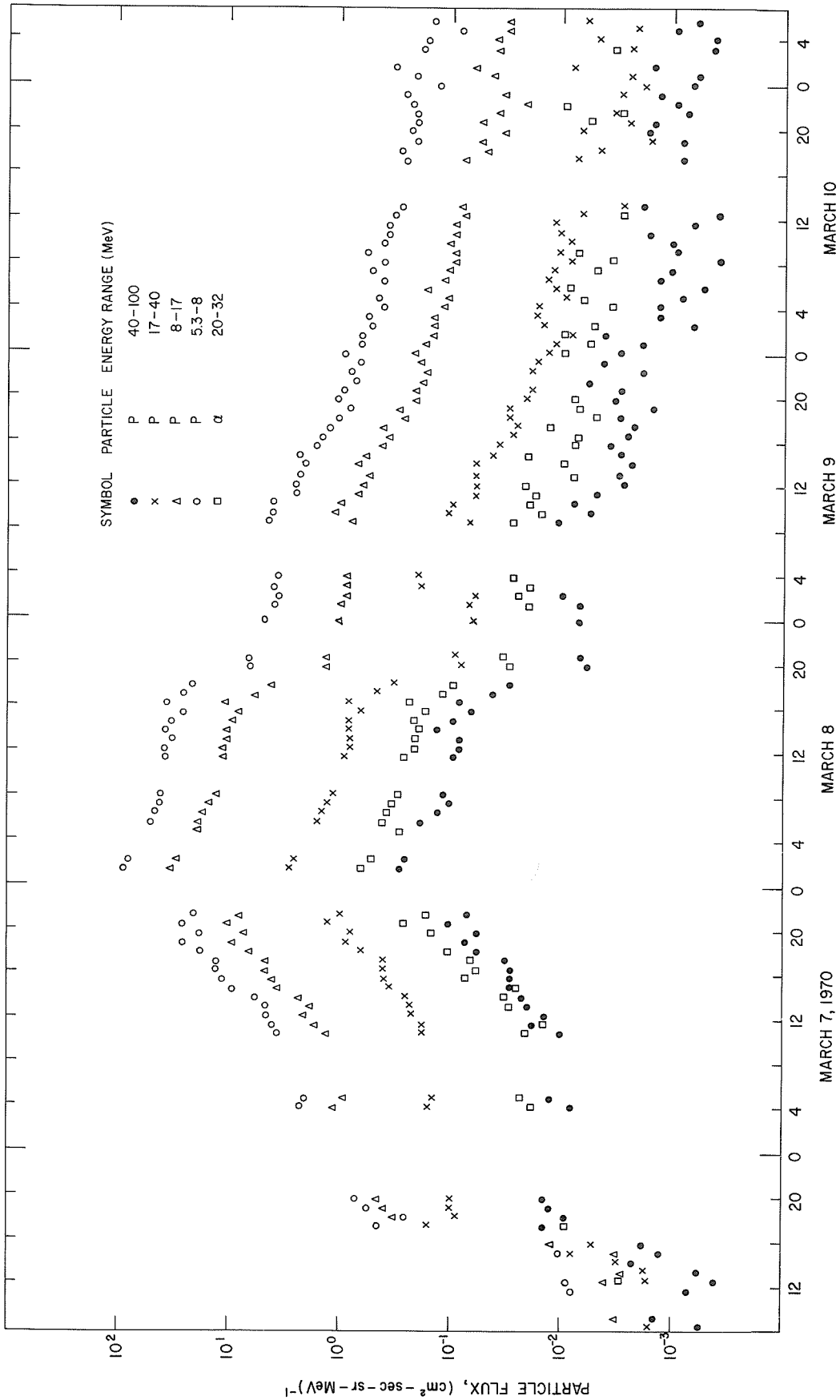


Fig. 2 Time variation of particle fluxes (50 minute averages).

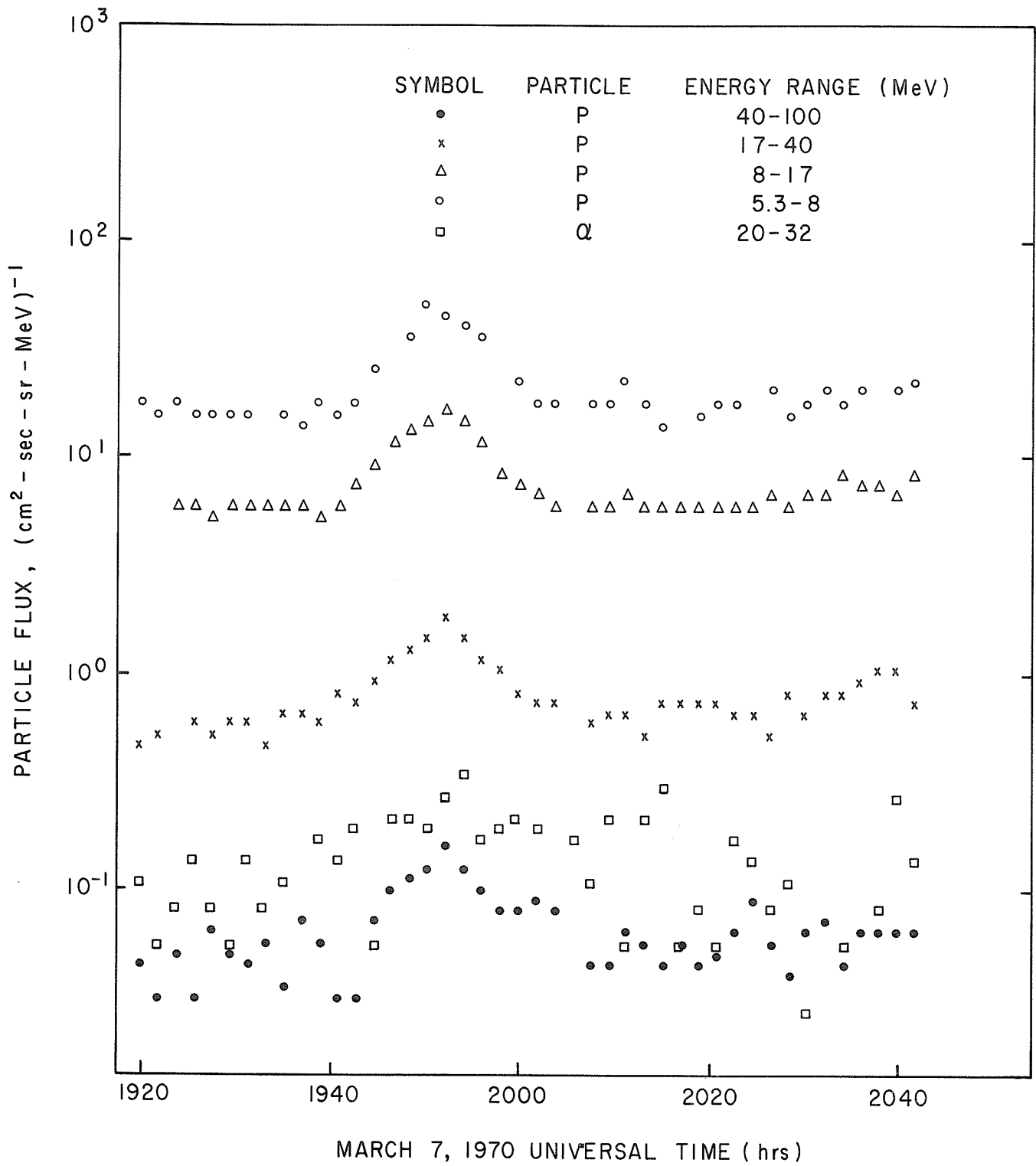


Fig. 3. Time variation of particle fluxes near 2000 UT, 7 March.

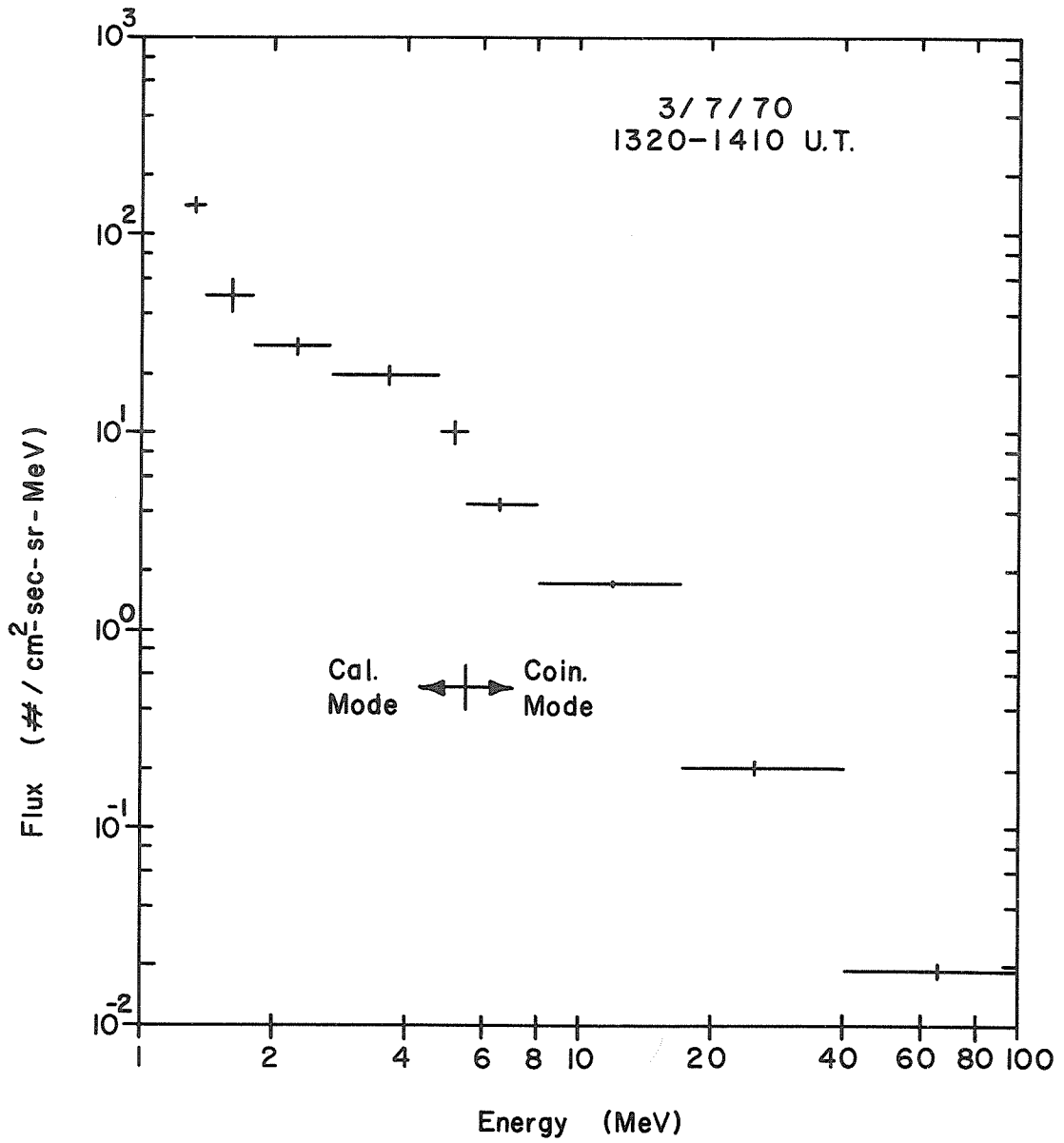


Fig. 4. Proton spectrum in early phase of event.

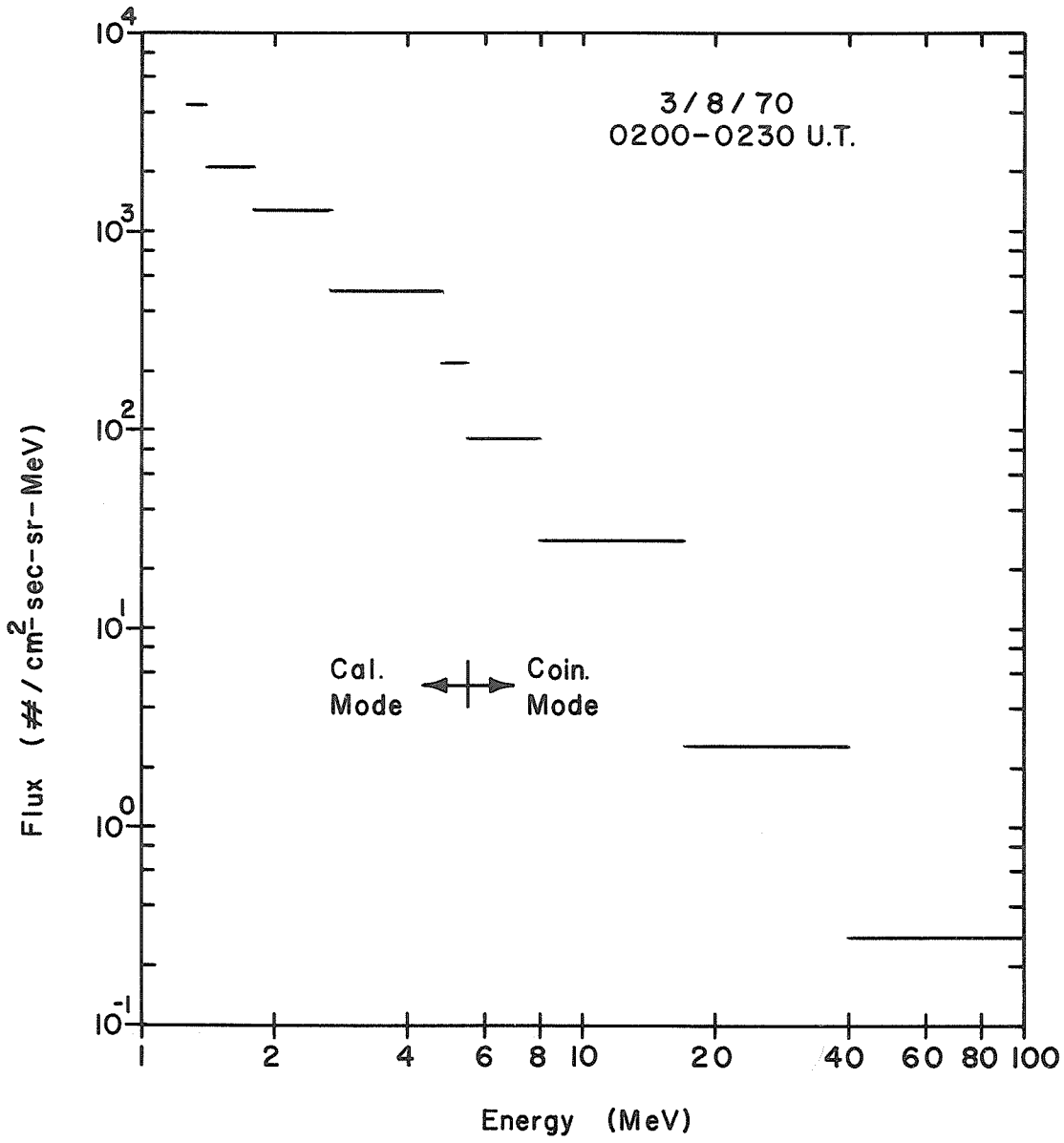


Fig. 5. Proton spectrum near maximum of event.

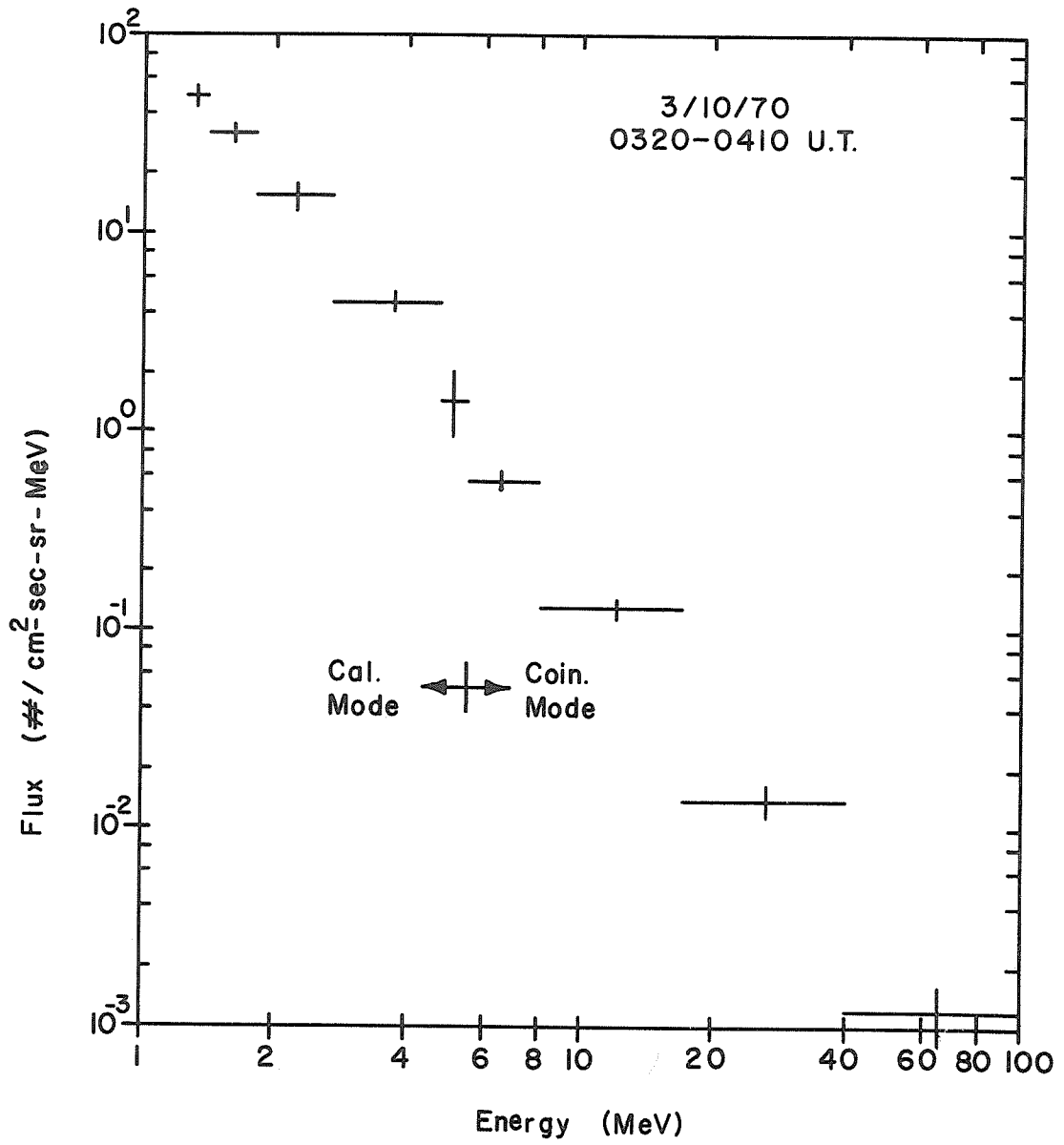


Fig. 6. Proton spectrum in late phase of event.

"Temporal Variations in the 100 kev to 8 Mev Protons Over
the Northern Polar Cap during the March 7, 1970 Event"

by

H. R. Lindalen, K. Aarsnes, R. Amundsen and F. S raas

Department of Physics
University of Bergen
Bergen, Norway

This paper presents preliminary results from the S71C experiment (University of Bergen, Norway, and Danish Space Research Institute, Denmark) for the time period March 7 to March 10, 1970.

The experiment is flown onboard the ESRO IA (Aurorae) satellite launched on October 3, 1968, into a near polar orbit with inclination 94°, apogee 1533 km and perigee 258 km. During the period considered, the satellite passed the northern polar region at an altitude of about 400 km. The satellite is magnetically stabilized.

The S71C experiment employs three totally depleted surface barrier detectors, two unshielded detectors, D1 and D2, and one background detector, D3, shielded by 0.3 mm of aluminum. The detectors D1, D2 and D3 make the following angles with the satellite axis: 0°, 90° and 45°. The orientation of the detectors in the northern hemisphere is such that D1 detects particles that will be absorbed in the atmosphere, whereas D2 detects particles that mirror at the satellite altitude. A collimator restricts the solid angle of each detector to 0.074 sr. and the directional geometric factor is 0.037 cm²sr. Magnets in front of the apertures sweep away electrons with energies less than 500 kev. The detector output is analyzed in a six channel differential pulseheight analyzer.

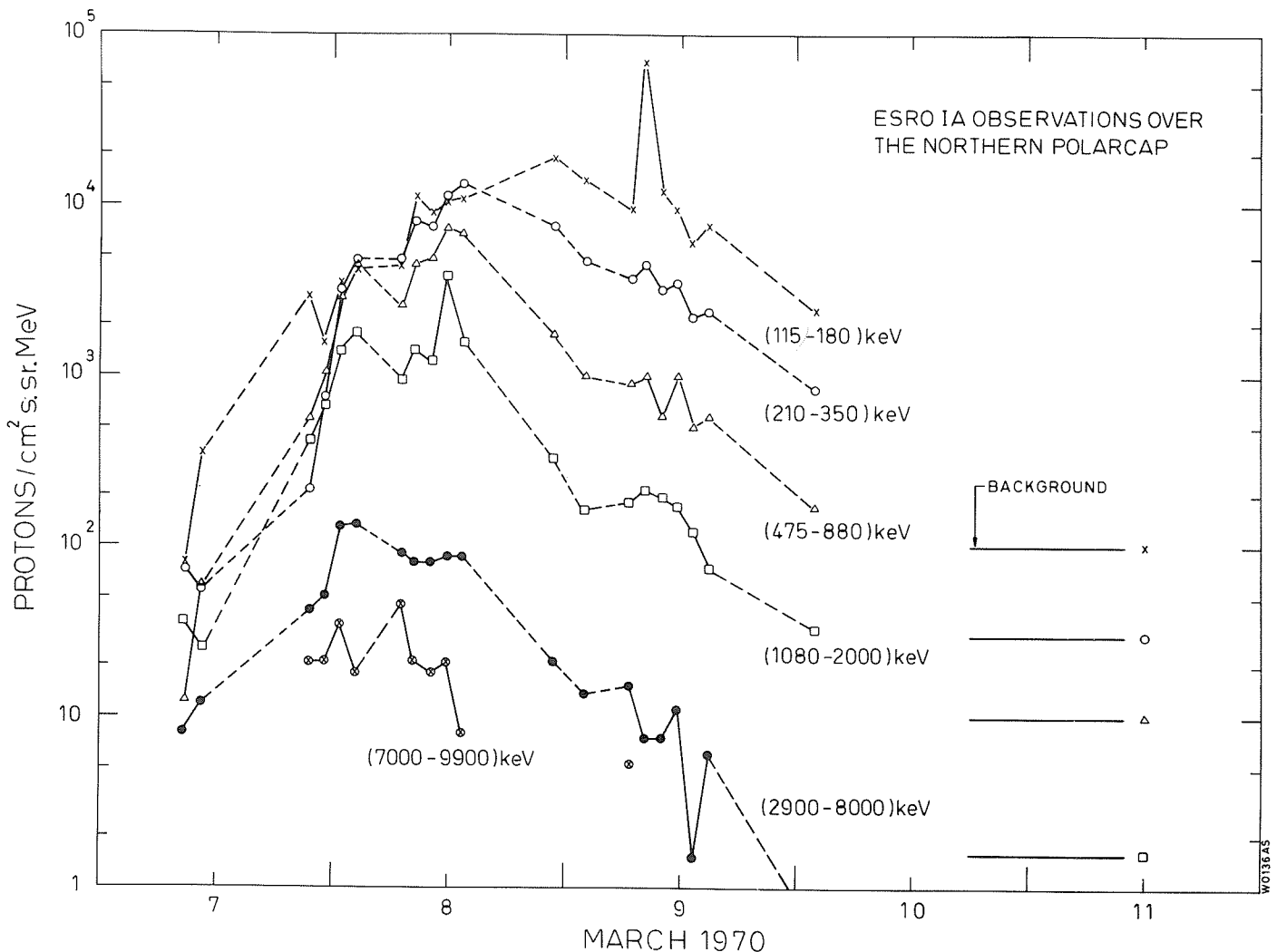


Fig. 1. Average values of intensities of (115-180) kev, (210-350) kev, (475-880) kev, (1080-2000) kev, (2900-8000) kev and (7000-9900) kev protons above invariant latitudes 80° plotted vs. time.

The different energy channels are counted sequentially taking two adjacent channels each time, the counting period being 0.345 seconds. A complete energy spectrum from all three detectors is obtained every 3.6 seconds. A description of the instrument is given by S oraas *et al.* [1969].

In order to study the time history of solar protons, from each satellite pass 10 samples above invariant latitude 80° were averaged. The results are shown in Figure 1, where the directional differential flux of precipitating protons in the following energy channels (115-180) keV, (210-350) keV, (475-880) keV, (1080-2000) keV, (2900-8000) keV, are plotted versus universal time. Also plotted is the (7000-9900) channel from detector D3.

Between 2230 UT and 2400 UT on March 7, there was a sudden increase in the count-rate in all energy channels. The (2900-8000) keV channel reached its maximum count-rate during this time interval. The differential energy spectrum could not be approximated with a simple exponential or power law, as can be seen from Figure 2.

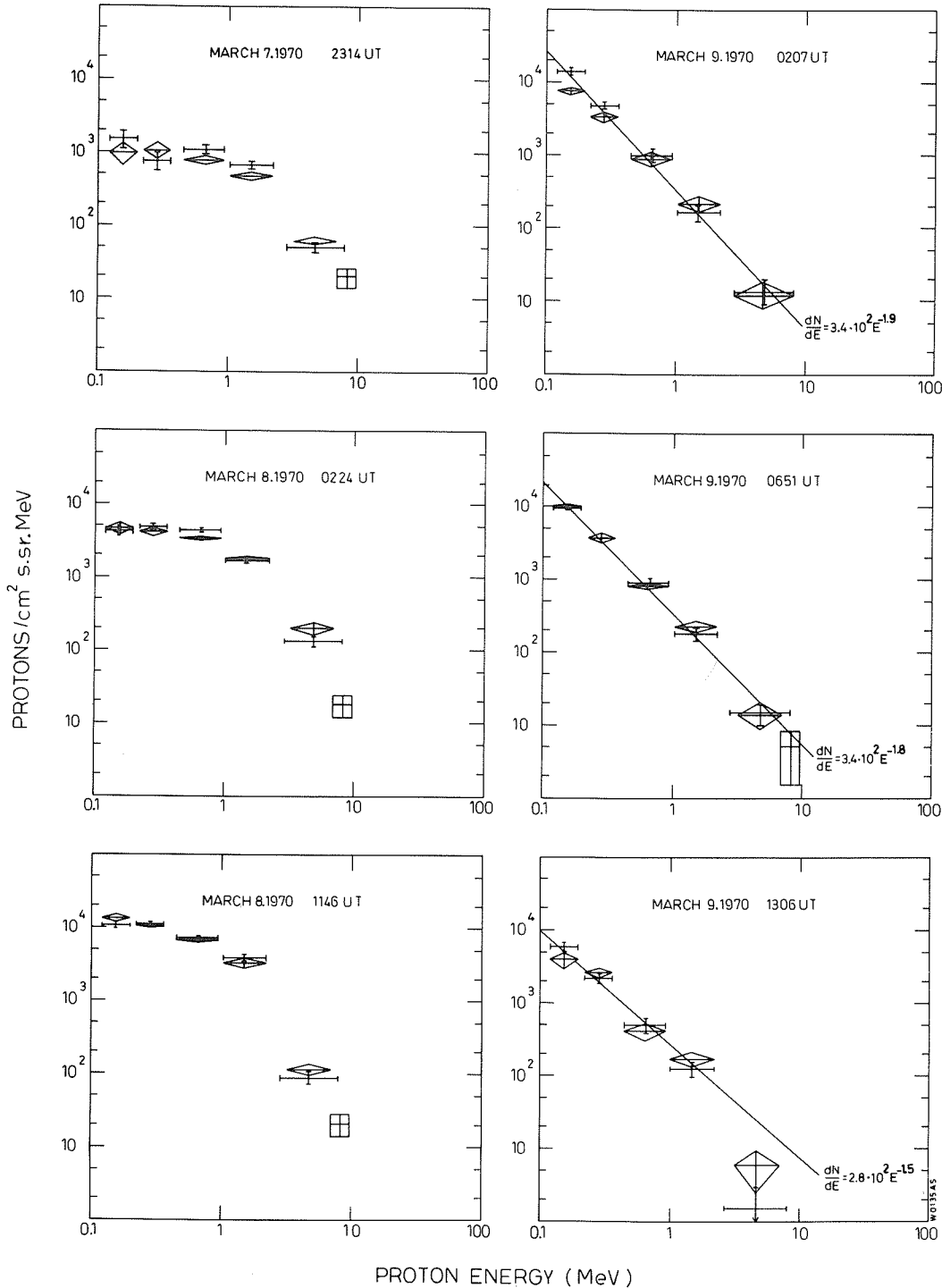


Fig. 2. Differential energy spectra of solar protons over the northern polar cap during March 7 to March 9, 1970. The diamonds refer to detector D1, the crosses to detector D2 and the squares to detector D3.

Protons below 3000 kev continued to rise until noon on March 8. Between 1240 UT and 2325 UT on March 8, we have no available observations. From around midnight March 8 the flux in all energy channels tended to decrease.

Comparing these data with the data referring to locally mirroring protons (D2) and taking into account the statistical uncertainties, the measured pitch angle distribution is consistent with isotropy over the upper hemisphere. This is shown in Figure 2 where data from all three detectors are used to obtain the proton differential energy spectrum referring to different phases of the event. On March 7 and 8, the differential energy spectrum is fairly flat up to around 2 Mev. The intensity versus energy relation could from March 9 be approximated with a simple power law. As time progressed, the intensities decreased slowly, but little change was observed in the spectral slope. The lines in Figure 2 have only been drawn to indicate the spectral form.

REFERENCE

SØRAAS, F.,
K. AARSNES,
H. R. LINDALEN and
M. MØHL MADSEN

A satellite instrument for measuring protons in the energy range 0.1 Mev to 6 Mev, Department of Physics, University of Bergen, Norway, Report No. 8.

"Trapped Particles over the Northern Polar Cap between 6 and 10 March 1970"

by

V. Domingo, D. E. Page and M. L. Shaw
Space Science Department (ESLAB)
European Space Research and Technology Centre
Noordwijk, Holland

The temporal and spatial pattern formed by solar particles across the polar cap now present a rather complicated picture. The observed particle distribution apparently depends not only on time and position but on energy and type of particle and on the direction of pointing and acceptance angle of detectors used. One feature which has been studied is the relationship between the poleward boundary of the Van Allen belts and the low latitude limit of solar particles. Data recorded at high northern latitudes is reported in full here in order to avoid arbitrary or subjective definitions of boundary, etc.

A geiger counter* with a geometric factor of $8.5 \times 10^{-3} \text{ cm}^2 \text{ sterad}$ and an opening angle of about 16° , was located perpendicular to the magnetic field aboard the field-aligned satellite ESRO IA/Aurora. The geiger responded to electrons above 40 kev (defined in the usual way) and to protons above 500 kev. The output of the geiger was handled by a logarithmic rate-meter over the range 4 to 4.7×10^3 counts/sec (saturation). The ratemeter output with a time constant of approximately 3 secs. was sampled by an analogue telemetry channel each 12.8 secs.

The ESRO IA satellite which was launched on 3 October 1968 had at the time of the event an inclination near 94° , apogee of 800 km and perigee of 240 km. The orbital plane was near the dawn-dusk meridian, the satellite passing from approximately 0600 to 1800 LMT (local solar time) over the north pole. Data were recorded in real time from Tromsø, Spitzbergen, Redu, and Fairbanks (the tape recorder lasted for 6 months).

The counting rates from 6 March 1970 at 0000 UT until 10 March 1970 at 1800 UT have been plotted against invariant latitude in Figures 1 through 4. Table 1 gives the height and time of passage of the satellite over the point nearest to the north pole. The northern edge of the radiation belt is generally clearly visible and it can be seen that it suffers large fluctuations during the event.

TABLE I

ORBIT	DAY	UNIVERSAL TIME (hours)	HEIGHT (km)	ORBIT	DAY	UNIVERSAL TIME (hours)	HEIGHT (km)	ORBIT	DAY	UNIVERSAL TIME (hours)	HEIGHT (km)
7515	6 Mar. 70	1.264	687	7539	7 Mar. 70	15.259	655	7563	9 Mar. 70	5.234	624
7516	"	2.847	686	7540	"	16.832	654	7564	"	6.816	622
7517	"	4.429	684	7541	"	18.414	653	7565	"	8.399	621
7518	"	6.012	683	7542	"	19.997	651	7566	"	9.982	620
7519	"	7.595	682	7543	"	21.580	650	7567	"	11.564	618
7520	"	9.178	680	7544	"	23.162	649	7568	"	13.147	617
7521	"	10.760	679	7545	8 Mar. 70	0.745	647	7569	"	14.730	616
7522	"	12.343	678	7546	"	2.328	646	7570	"	16.313	614
7523	"	13.926	676	7547	"	3.910	645	7571	"	17.895	613
7524	"	15.508	675	7548	"	5.493	643	7572	"	19.478	612
7525	"	17.091	674	7549	"	7.076	642	7573	"	21.061	610
7526	"	18.674	672	7550	"	8.659	641	7574	"	22.643	609
7527	"	20.256	671	7551	"	10.241	639	7575	10 Mar. 70	0.226	608
7528	"	21.839	670	7552	"	11.824	638	7576	"	1.809	606
7529	"	23.422	669	7553	"	13.407	637	7577	"	3.391	605
7530	7 Mar. 70	1.005	667	7554	"	14.989	636	7578	"	4.974	604
7531	"	2.587	666	7555	"	16.572	634	7579	"	6.557	603
7532	"	4.170	665	7556	"	18.155	633	7580	"	8.140	601
7533	"	5.753	663	7557	"	19.737	632	7581	"	9.722	600
7534	"	7.335	662	7558	"	21.320	630	7582	"	11.305	599
7535	"	8.918	661	7559	"	22.903	629	7583	"	12.888	597
7536	"	10.501	659	7560	9 Mar. 70	0.486	628	7584	"	14.470	596
7537	"	12.083	658	7561	"	2.068	626	7585	"	16.053	595
7538	"	13.666	657	7562	"	3.651	625	7586	"	17.636	593

* Supplied and calibrated by the Norwegian Defence Research Establishment, Kjeller, Norway, and the Danish Space Research Institute, Lyngby, Denmark.

The normal quiet time count rate over the central polar cap is below 10 per second. In Figure 5 we have plotted the median count rate obtained in the "plateau" region above 75° invariant latitude. The particle flux over the polar cap is visible from 6 March at 1500 UT until 10 March at 1200 UT. On 8 March there is a clear peak at 0200 UT and a dubious peak at 1500 UT. The latter is dubious because at that time the satellite orbit is rather far from the magnetic pole and may therefore be near the "auroral zone enhancements" of solar particle flux. We regard the definition of a "plateau" as not being very meaningful in the light of the present knowledge of structure across the polar cap. However, it is a way of illustrating how the event intensity progressed with time.

Figures 1-4 show counting rate versus invariant latitude. The numbers refer to the pass numbers of the satellite (see Table 1). The curves with an M refer to data measured in the morning side of the pass and those with an A to the afternoon side of the pass over the north pole.

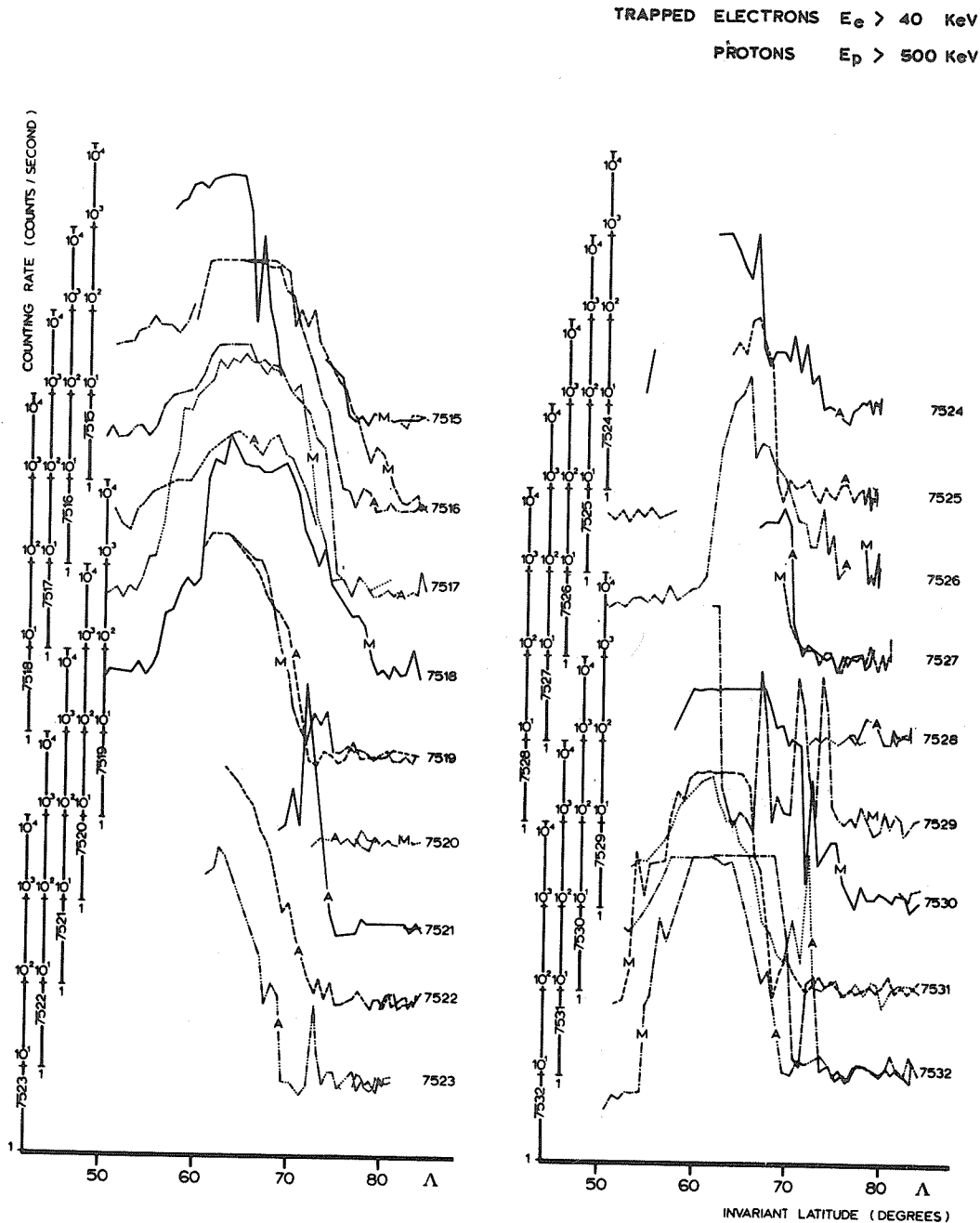


Fig. 1.

TRAPPED ELECTRONS $E_e > 40$ KeV

PROTONS $E_p > 500$ KeV

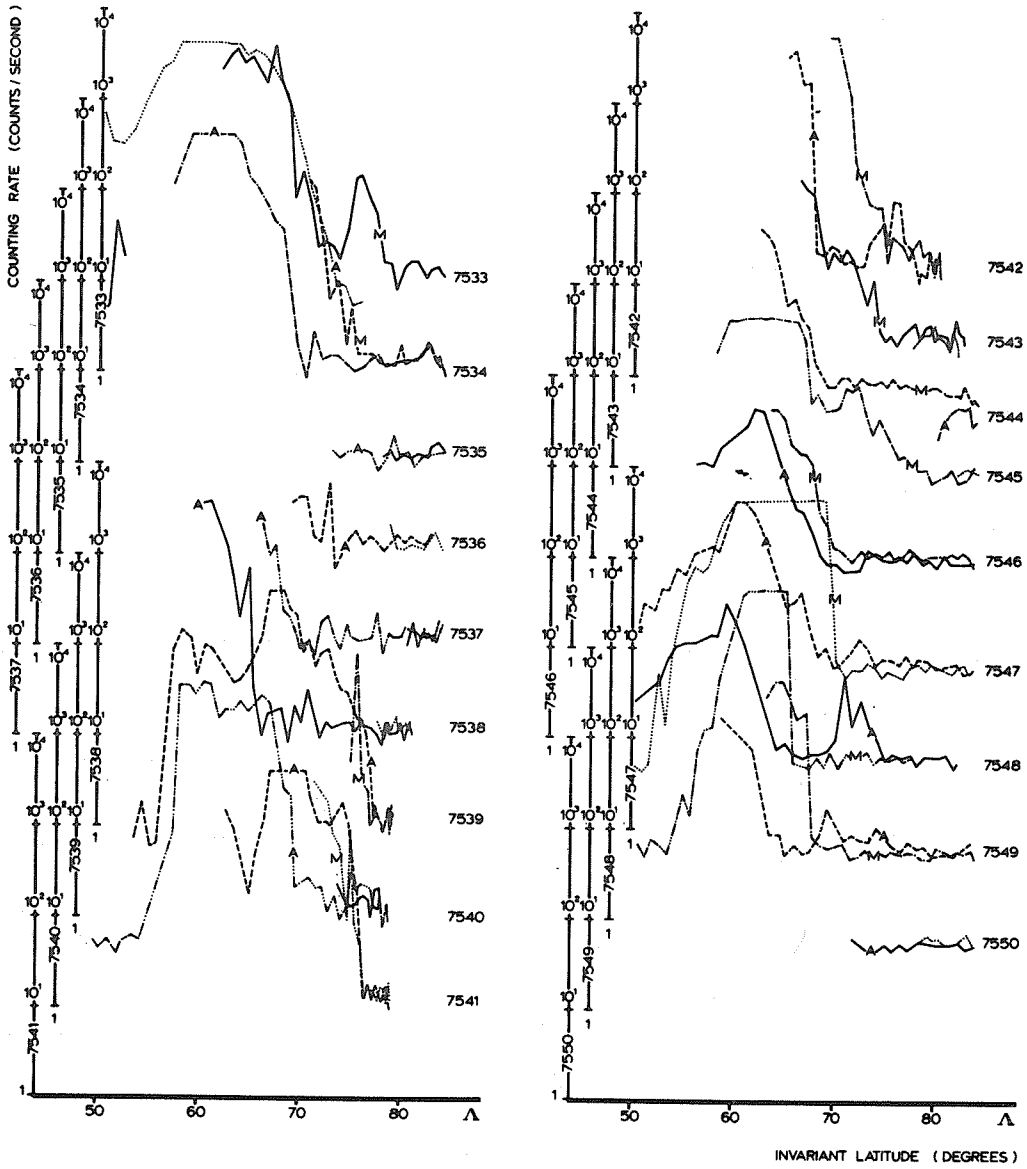


Fig. 2.

TRAPPED ELECTRONS $E_e > 40$ KeV

PROTONS $E_p > 500$ KeV

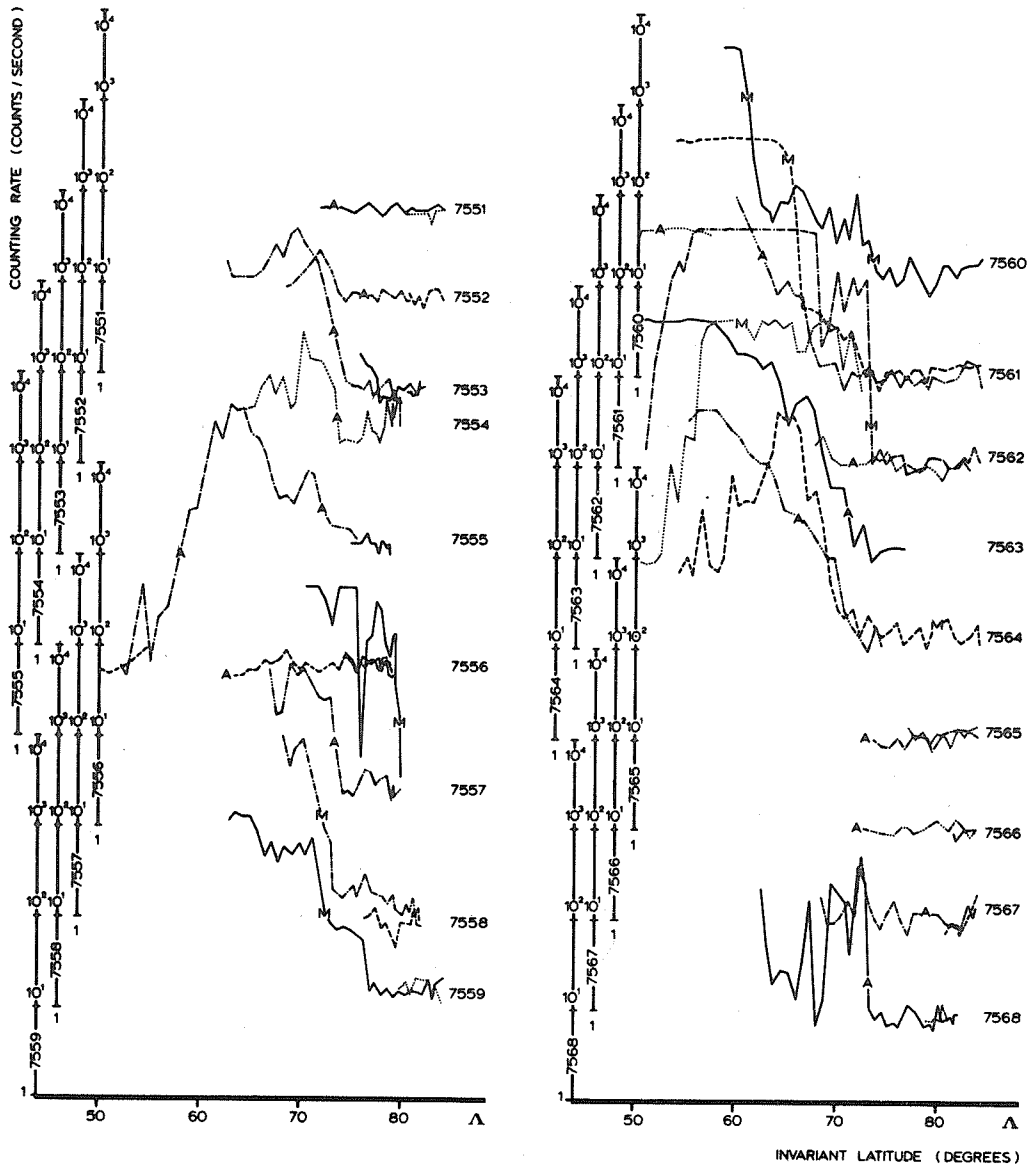


Fig. 3.

TRAPPED ELECTRONS $E_e > 40$ KeV

PROTONS $E_p > 500$ KeV

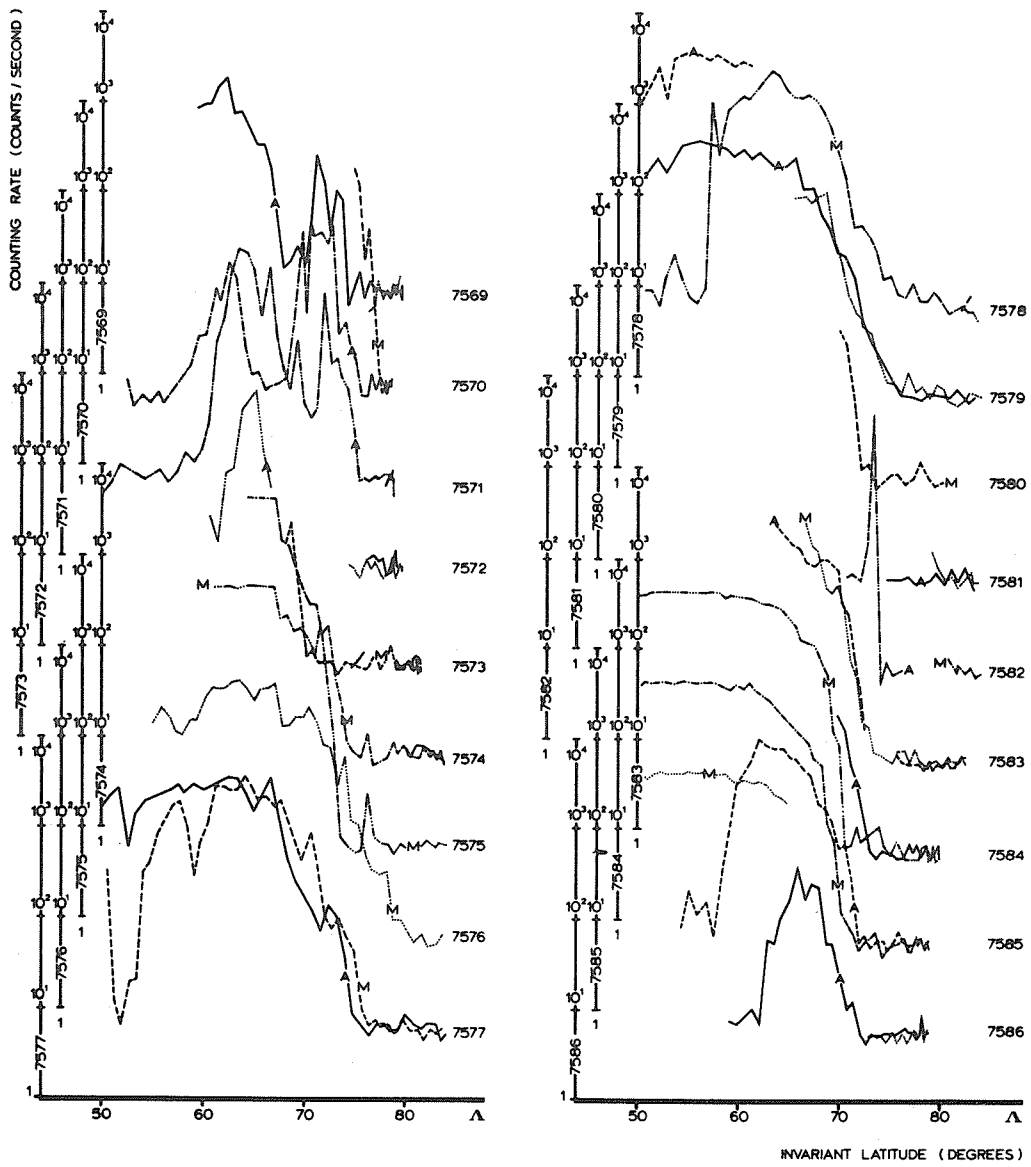


Fig. 4.

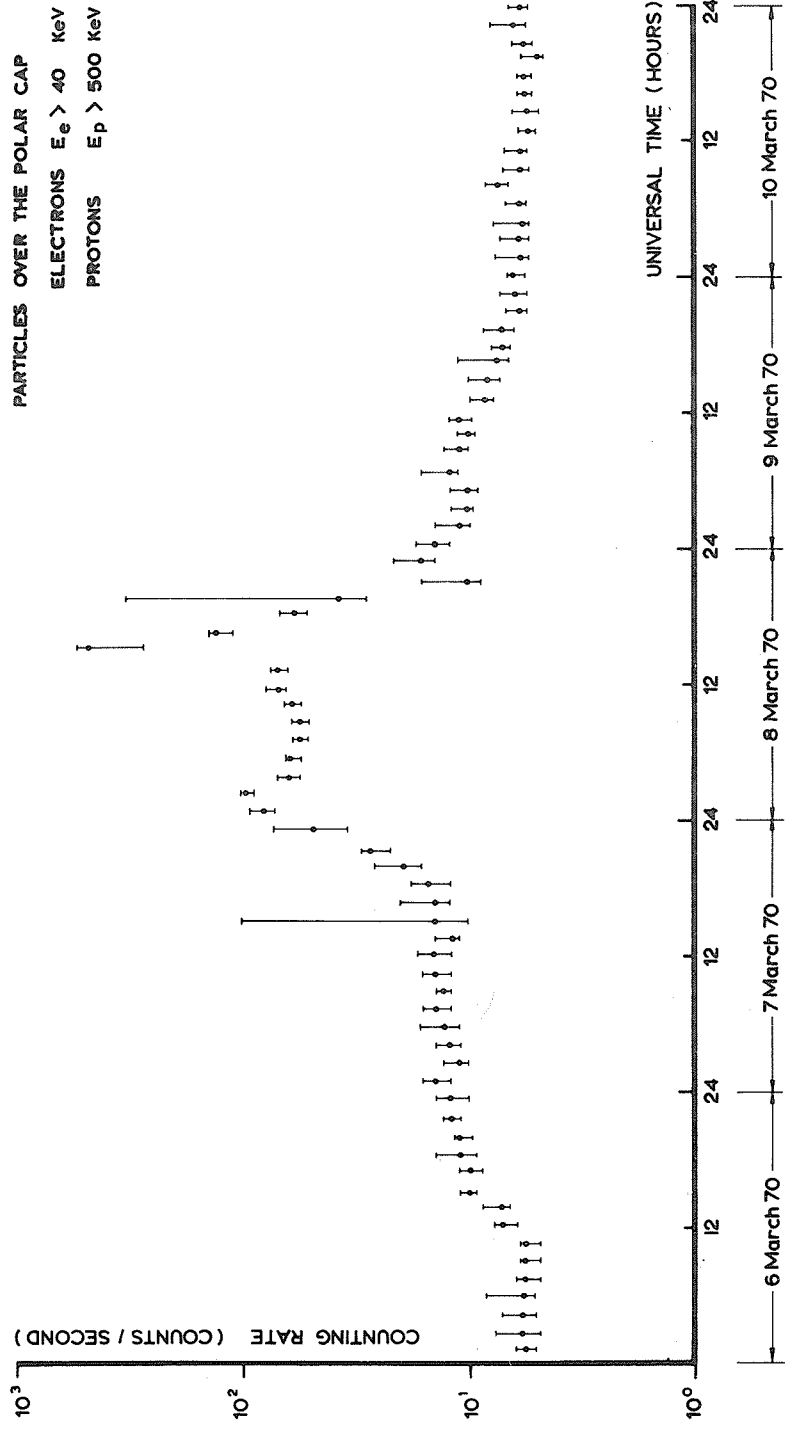


Fig. 5. Median value of the counting rate measured over the north pole (invariant latitude $\Lambda > 75^\circ$) versus time. The bars are such as to leave 50% of the considered counts inside of them, to give an idea of the dispersion of the points considered.

"Redistribution of Trapped Protons following the 8 March 1970 Magnetic Storm"

by

S. M. Krimigis and P. Verzariu
Applied Physics Laboratory
The Johns Hopkins University
Silver Spring, Maryland

D. Venkatesan
Department of Physics
University of Calgary
Calgary, Alberta, Canada

and

B. A. Randall
Department of Physics and Astronomy
University of Iowa, Iowa City, Iowa

Introduction

The period 6 to 13 March 1970 represents a time interval when the interplanetary medium was filled with large fluxes of low energy (<10 Mev) particles [Armstrong and Bostrom, 1970]. On 8 March a magnetic storm occurred at 1417 UT which induced severe disturbances on the trapped energetic particle population in the magnetosphere. In this paper, data are presented which show the redistribution of protons in the energy range $0.3 \leq E \leq 0.45$ Mev. The data were obtained with equipment on the University of Iowa satellite Injun 5^P(1968-066B) which has an apogee of 2525 km, perigee of 644 km and inclination 80.7° . The detector system is described in detail elsewhere [Krimigis and Verzariu, 1970]. Briefly, it consists of a solid state detector telescope with a full angle of $\sim 30^\circ$ and points to within $\pm 10^\circ$ of the normal to the local B vector.

Observations

The onset of solar particles for the period of interest occurred at ~ 1700 UT on 6 March and the intensity of 1-10 Mev protons reach background by the end of 14 March [Armstrong and Bostrom, 1970]. Data coverage with Injun 5 was relatively sparse during the two days prior to the sudden commencement (SC) (1417 UT, 8 March) so that a satellite pass immediately prior to the SC is not available. Judging from magnetic activity before the SC, however, one infers that no significant trapped proton redistribution could have taken place prior to this time.

Figure 1 shows a series of satellite traversals of the radiation belt for the period March 3 to 14, 1970. Note that all of these passes are taken in the early evening to local midnight sector in magnetic local time (MLT) and that the B range covered is approximately the same for all passes. The pass on March 3 (day 62) is believed to be representative of the steady state situation prior to the SC on 8 March. One observes the following:

- (a) The shape of the intensity profile has been severely distorted ~ 50 minutes after the sudden commencement. The peak flux has increased by a factor of ~ 2 and the boundary has apparently moved inward. The intensity below $\sim 55^\circ$ invariant latitude Λ has not changed significantly.
- (b) Further distortion of the intensity profile has not as yet occurred on the following pass two hours later at ~ 1715 UT on the same day.
- (c) The pass at ~ 2115 UT shows additional effects in the intensity profile with such changes extending down to at least 50° . The intensity maximum has moved inward to $\Lambda \sim 52^\circ$ and the peak flux has increased to $\sim 4 \times 10^6$ ($\text{cm}^2 \text{sec sr Mev}^{-1}$), i.e., a factor of 20 higher than the maximum pre-event flux. We note that this pass follows a major recovery in the geomagnetic field at high latitudes, which occurred at ~ 2020 UT. This recovery may be associated with the onset of bay activity.
- (d) Passes on days 69 to 73 (10 to 14 March) show the establishment of a new steady-state distribution with a much sharper peak located at $\Lambda \sim 57^\circ$ ($L \sim 3.4$). The peak intensity is about a factor of 20 greater when compared to that prior to the sudden commencement. One also notes that there is no significant change in the location of the boundary.

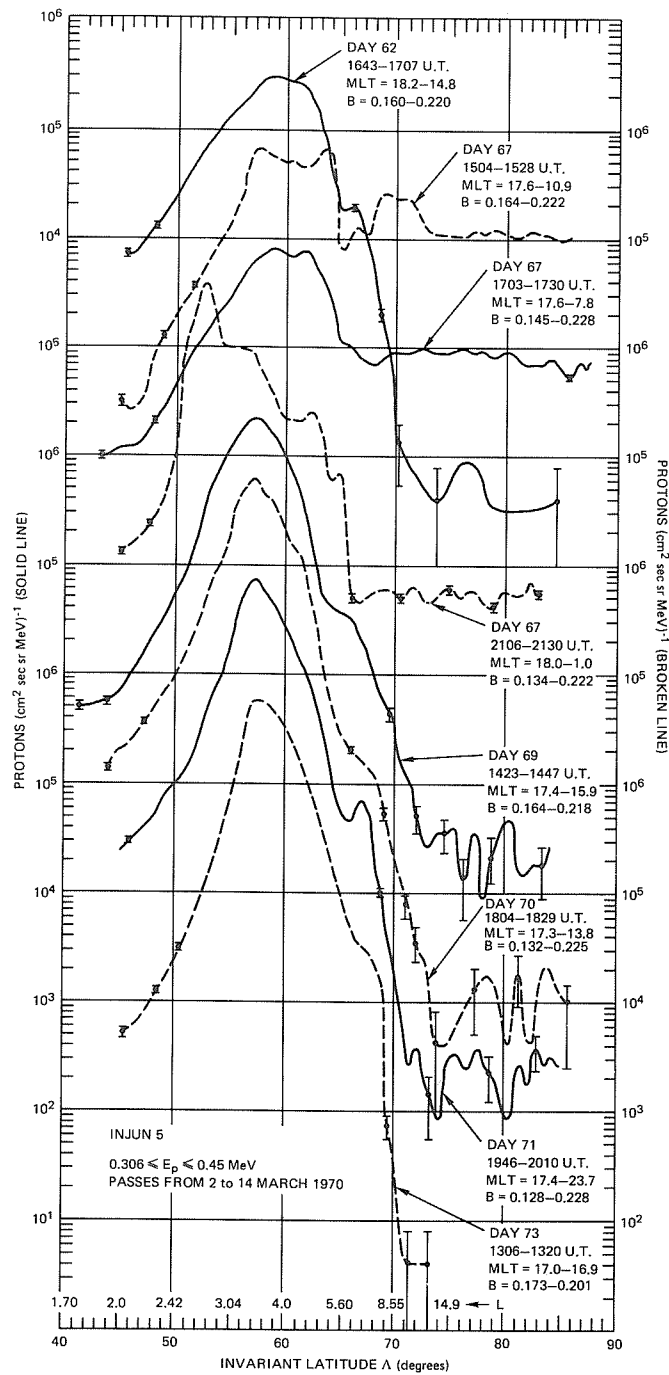


Fig. 1. A plot of the differential proton intensity versus invariant latitude Λ . The corresponding values of L are also shown. Sample error bars are shown whenever the error exceeds the size of the point. The scale on the left-hand ordinate represents the intensity of the solid curve in the decade where the peak intensity occurs. The scale on the right-hand ordinate represents the intensity of the broken curve in the decade where the peak intensity occurs. The MLT and B ranges for $\Lambda \sim 45^\circ$ to $\Lambda \sim 90^\circ$ are shown for each pass.

- (e) The polar plateau intensity profiles are generally similar to those that have been observed in the past. A detailed investigation of these plateaus is beyond the scope of this study.

We note here that intensity changes for higher energies (up to 1.4 Mev) appear to be similar (although less pronounced) to those observed at 0.3 Mev and shown in Figure 1.

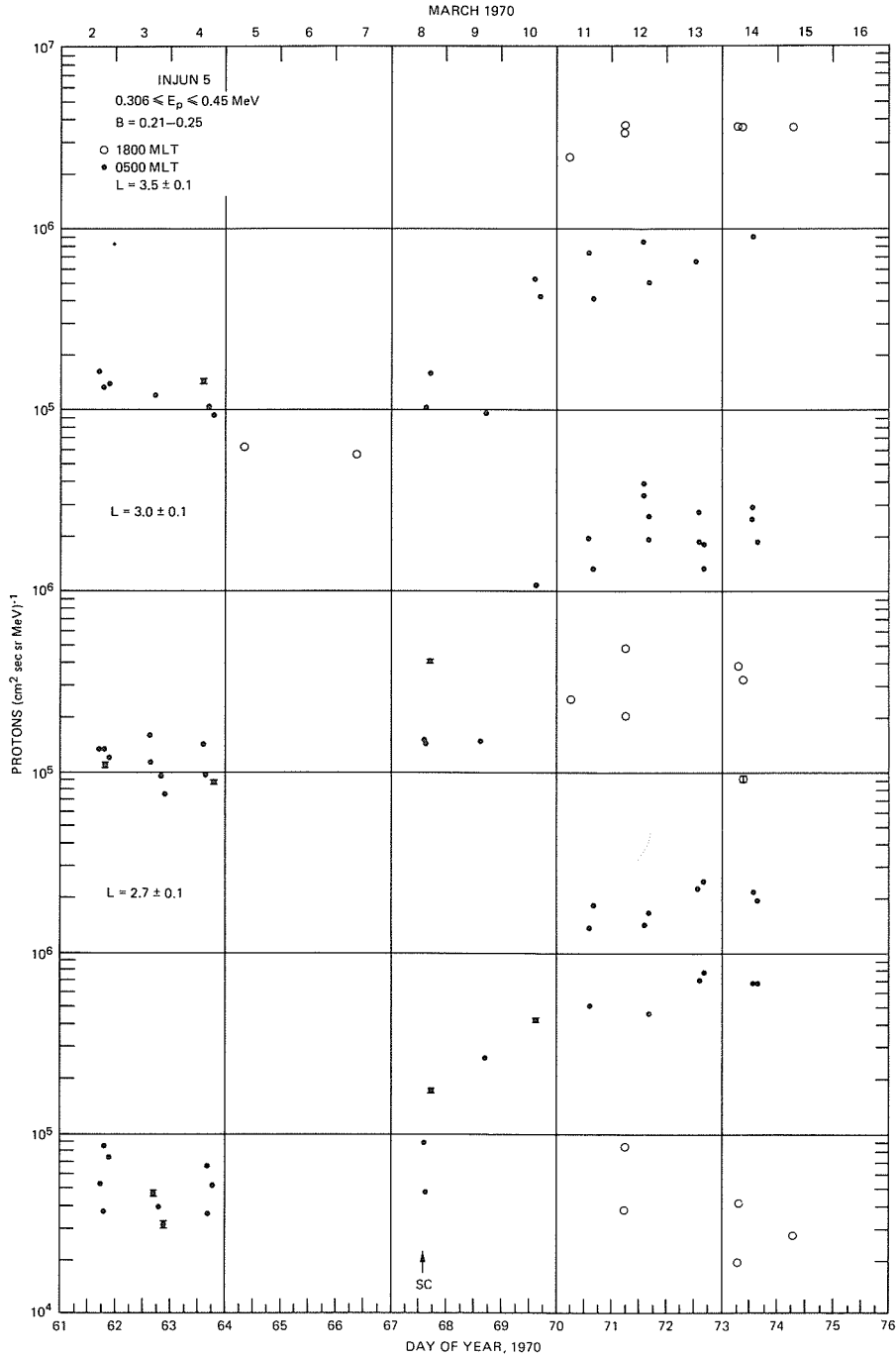


Fig. 2. A plot of the differential proton intensity for three L values and in the indicated B range. Note the local time asymmetry and the reversal in its sign as one progresses from $L \sim 3.5$ to $L \sim 2.7$. The error bars do not exceed the size of the plotted point except where shown.

Figure 2 shows the differential intensity as a function of time for the period 2 to 15 March at L values of 3.5, 3.0, 2.7 and B range 0.21 to 0.25 gauss. The points are coded according to the magnetic local time (MLT) at which the observations were obtained. There are several remarks to be made regarding this figure:

- (a) The intensity began to increase immediately after the sudden commencement and continued to build up until at least day 71 (12 March). The post-storm intensity was at least a factor of 25 higher than the prestorm value.
- (b) There exists a local time asymmetry in the intensity profile for the same values of L and B. Specifically, (1) at $L = 3.5 \pm 0.1$ (top panel) the intensity at ~ 1800 MLT is higher by a factor of 5 than that at ~ 0500 MLT; (2) at $L = 3.0 \pm 0.1$, on the other hand, the converse is true, i.e., the intensity at 0500 MLT exceeds that at 1800 MLT by a factor of ~ 5 ; (3) the same holds true at $L = 2.7 \pm 0.1$ as in (2) but the intensity at 0500 MLT is greater by a factor of ~ 20 than the one at 1800 MLT. The scatter in the data at the two respective local times is probably due to the wide range in B and the sharp gradients in the L profile as seen from Figure 1.

We consider the dawn-dusk asymmetry to be one of the most important observations obtained during the March 1970 magnetic storm.

Summary and Discussion

The results presented in Figures 1 and 2 may be summarized as follows: (1) The peak differential intensity of $0.3 \leq E_p \leq 0.45$ Mev geomagnetically trapped protons increased by a factor of ~ 20 following the 8 March 1970 magnetic storm; (2) there exists a dawn-dusk asymmetry in the intensity increase which is a strong function of L in the range 2.7 to 3.5.

Because of the preliminary nature of the present study, it is not possible to attempt a complete and full interpretation of the data. There are, however, some features that clearly stand out. First, the magnitude of the increase exceeds anything that has been reported so far for protons in this energy range and at L values as low as 2.7 earth radii [for a review see Williams, 1970]. Secondly, the bulk of the increase must be accounted for by locally accelerated particles of either solar wind or exospheric origin rather than direct injection of energetic solar particles into trapped orbits, since the trapped particle intensity far exceeds the solar particle intensity observed over the polar caps. Further, there was a build-up in the intensity over several days, during which the solar particles had decayed to insignificant fluxes (Figure 1). Thirdly, the local time asymmetry and the reversal in its sign in going from $L \sim 3.5$ to $L \sim 3$ suggests a direct connection between the ring current and the energetic particle population. In particular, protons present at 1800 MLT are not able to drift to 0500 MLT at $L \sim 3.5$, while protons at 0500 MLT at $L \sim 2.7$ are not able to drift to 1800 MLT, suggesting that there is a sink of particles at some local time on either side of $L \sim 3.2$. That this effect persists for several days is indeed remarkable, since the ring current must have presumably decayed by this time. We emphasize here the fact that the data are preliminary and stress the tentative nature of the conclusions, pending a more complete study.

Acknowledgements

We thank all those at the University of Iowa and elsewhere whose effort made the Injun 5 satellite a success. The Injun 5 spacecraft was designed and built at the University of Iowa under contract NAS1-2973 with the NASA/Langley Research Center (LRC). Data reduction was supported by LRC under contract NAS1-8141 and by the GSFC under contract NAS5-10625. Analysis and publication at The Johns Hopkins University Applied Physics Laboratory has been supported by NASA/LRC under Task I of contract NOW-62-0604-c.

REFERENCES

- | | | |
|---------------------------------------|------|---|
| ARMSTRONG, J. C. and
C. O. BOSTROM | 1971 | "Solar Protons and Alpha Particles in the March 1970 Events", this report, p. 134. |
| KRIMIGIS, S. M. and
P. VERZARIU | 1971 | "Implications on Particle Storage at the Sun from Observations of Solar Flare Proton Spectrums", <u>J. Geophys. Res.</u> , <u>76</u> , 792-807. |
| WILLIAMS, D. J. | 1970 | "Trapped Protons ≥ 100 kev and Possible Sources", in <u>Particles and Fields in the Magnetosphere</u> , B. M. McCormac (ed.), D. Reidel Pub. Co., Holland, p. 396. |

"Proton and Alpha Particle Measurements Over the Northern Polar Cap with
the Satellite GRS-A/Azur During the March 1970 Solar Proton Event"

by

E. Lammers and J. Moritz
Institut für Reine und Angewandte Kernphysik
Universität Kiel
Germany

Some data taken with the satellite GRS-A/Azur over the northern polar cap during the March 1970 solar proton event are presented.

The satellite GRS-A/Azur was launched November 8, 1969, 0152 UT into a nearly polar sun synchronous dawn-dusk orbit with a perigee of 383.84 km and an apogee of 3,145.43 km. The inclination is 102.975 degrees, the period 121.876 minutes. The satellite is magnetically aligned to the magnetic field lines. During the period from March 2 to 17, the period for which data are given here, the apogee moved from 27° to 50° N on the evening side of the orbit.

The experiment EI-92 of the satellite measures with two solid state detectors the directional intensity perpendicular to the magnetic field lines of protons in the energy range 0.25 to 13.5 MeV and of alpha particles in the energy range 2.0 to 6.4 MeV. The full opening angle of the directionality defining aperture is 20.4 degrees, the geometry factor is 0.0137 cm²sterad. Pulse height discrimination of the detector pulses in combination with coincidence constraints defines 6 separate count rate channels. These channels are sampled every 10 seconds and the data are transmitted in real-time. The 6 channels represent:

Channel 1:	protons in the energy range	1.65	to	13.5	MeV
Channel 2:	protons in the energy range	0.25	to	12.5	MeV
Channel 3:	protons in the energy range	0.25	to	1.65	MeV
Channel 4:	protons in the energy range	0.5	to	1.65	MeV
Channel 5:	protons in the energy range	1.0	to	1.65	MeV
Channel 6:	Alpha particles in the energy range	2.0	to	6.4	MeV

In the process of data evaluation the time-ordered data are supplemented with the magnetic coordinates B, L, and Λ using the GSFC 12/66 model. Multiplication of the count rates per 10 sec with the factor 7.39 leads to particles/cm² sec sterad.

During the March period only passes over the north polar cap have been received and due to the distribution and function of the receiving ground stations not always all of the 12 polar passes per day were covered. Depending on the time of the day the satellite's orbit reaches to different maximal geomagnetic latitudes in respect to invariant latitudes.

Count rate profiles of polar passes are shown in the Figure 1 through 3. They give examples of three different types of profiles to be discerned during the period of enhanced count rate over the polar caps. Figure 1 gives a pass reaching up to 86.61° invariant latitude beginning at 0231 UT on March 8. The total polar cap is filled with protons exhibiting only little structure. There is a small indication of lower intensity on the evening side of the pass, a feature that can be recognized on some of the polar passes with smooth intensity profile. In contrast passes with more structure very often show an enhancement on the evening side.

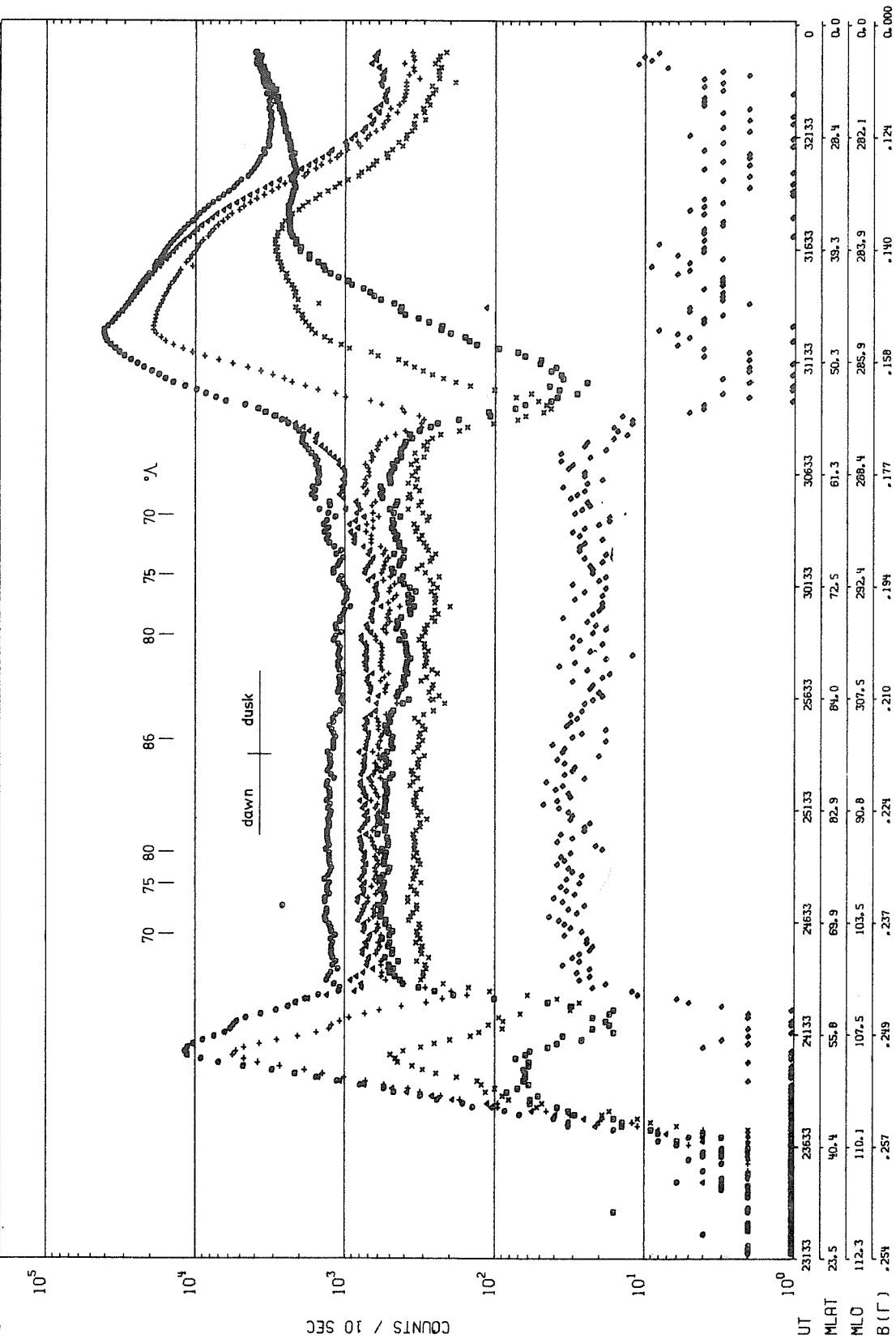
Figure 2 gives one of the two passes following the ssc at 1420 UT that show a completely different appearance of the count rate over the pole than all other passes. These two are a pass at 1506 UT (not shown here) that reaches up to only 70° invariant latitude and the one at 1857 UT shown in Figure 2 reaching to 73.5° invariant latitude. These two passes show very disturbed flux conditions reaching down to 55° invariant latitude, a region normally filled with trapped particles. Another pass from 1705 UT in between the two passes with rapidly varying fluxes shows in contrast a rather smooth flux profile comparable to the one given in Figure 3. This might be an indication of direct particle access to the polar caps if one correlates this to the large negative excursions on the magnetic records of high latitude stations at 14 to 16 and 19 to 21 hours UT, whereas the value goes back to almost normal between 16 and 19 hours UT when a more smooth intensity profile is measured.

Figure 3 gives a pass from early March 9, that shows the typical flux enhancement at auroral latitudes, which seems to be the normal distribution of particles over the polar caps as it is seen in most of our passes.

The time development of the measured intensities of protons and alpha particles for the period March 2 to 17 is given in Figures 4 through 6 for an invariant latitude of 70°. This latitude was chosen as it gives the maximum of contacts well beyond the normally observed trapping boundary which

can be defined, at 68° for the low energy and at 60° invariant latitude for the higher energy protons, as the point where the count rate at magnetically quiet times falls into the normal background rate. The intensity of the 0.25 to 1.65 MeV protons started to rise on February 26, not shown on the plot, and mainly stays over the background intensity for the whole time period. Maximum intensity is observed immediately following the ssc on March 8, 1420 UT. The intensity of the 1.65 to 13.5 MeV protons is not enhanced until March 6, around 18 hours and the onset coincides with the > 10 MeV flux increase observed with IMP G [Solar-Geophysical Data, Number 313 - Part II, U. S. Department of Commerce (Boulder, Colorado U.S.A. 80302)]. Again maximum intensity is observed on the passes following the ssc. As for the low energy protons a second slight intensity increase appears on late March 12. The alpha particles in general exhibit a behavior comparable to the high energy protons.

If the assumption is correct that the passes immediately following the ssc are exempt because of direct particle access to the polar caps an envelope can be drawn to the intensity-time profiles leading to different times of the intensity maximum for different particle energies and a nearly exponential decline from maximum with a time constant of 12 hours which is independent of particle energy. Then the 1.65 to 13.5 MeV protons reach maximum intensity about 8 hours earlier than the 0.25 to 1.65 MeV protons. The maximum for alpha particles lies closer to the maximum of the lower energy protons.



Figures 1 through 3 five the measured count rates of the 6 channels of the experiment plotted against UT for 3 passes that include data from the northern polar cap. In 5 minute intervals information is given on the satellite's location in (from top to bottom) height above ground in km, the magnetic shell parameter L (at the top of the plot), UT in hr. min. sec., the magnetic dipole latitude MLAT, the magnetic dipole longitude MLO and the local magnetic field intensity (GSFC 12/66) B in Gauss (beneath the plot).

GRS-A/AZUR DATE 80370 PLOT 22 ORBIT 1426 E1 S2 CHAN 10 20 30 40 50 60 DAY 432 185722

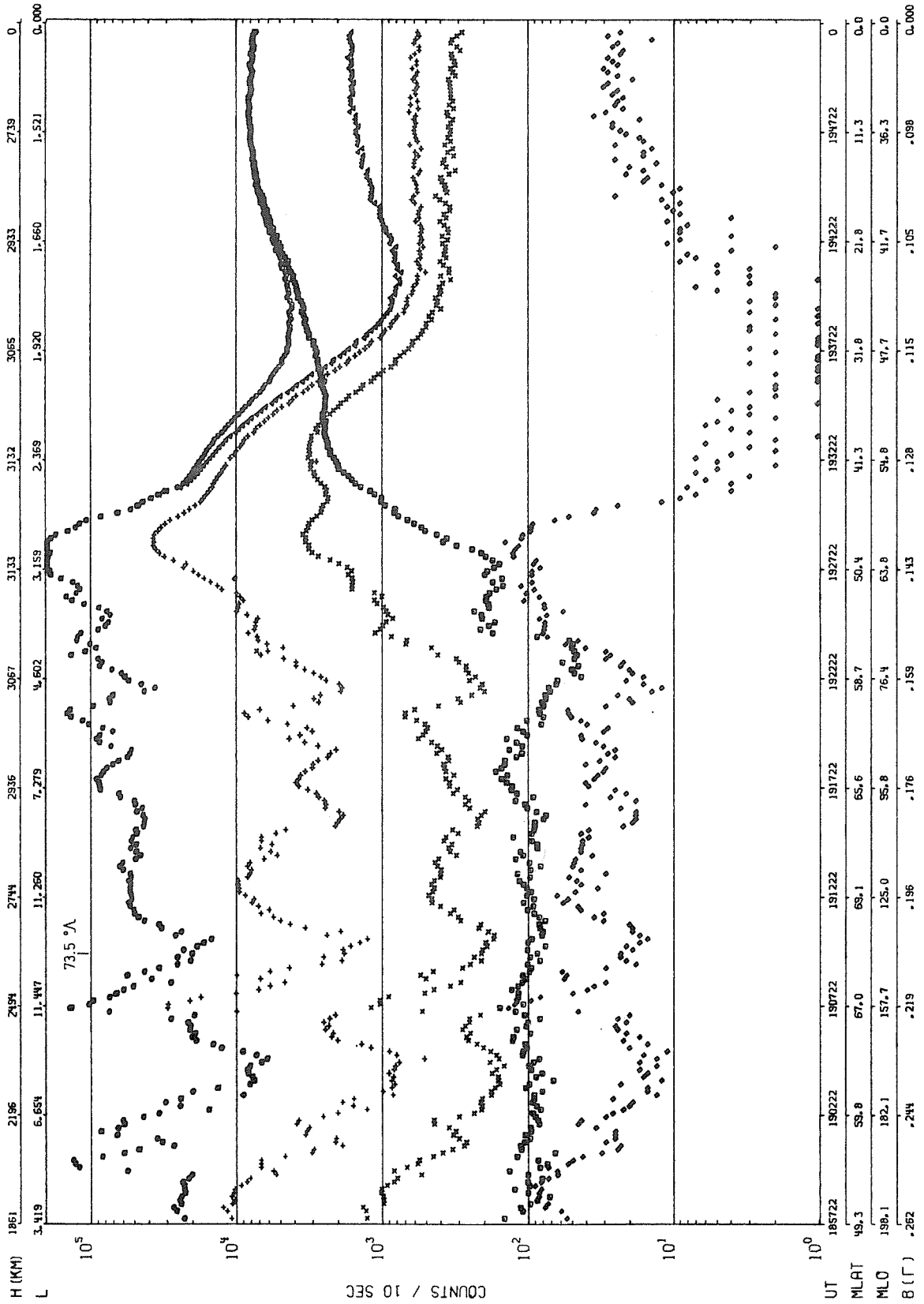
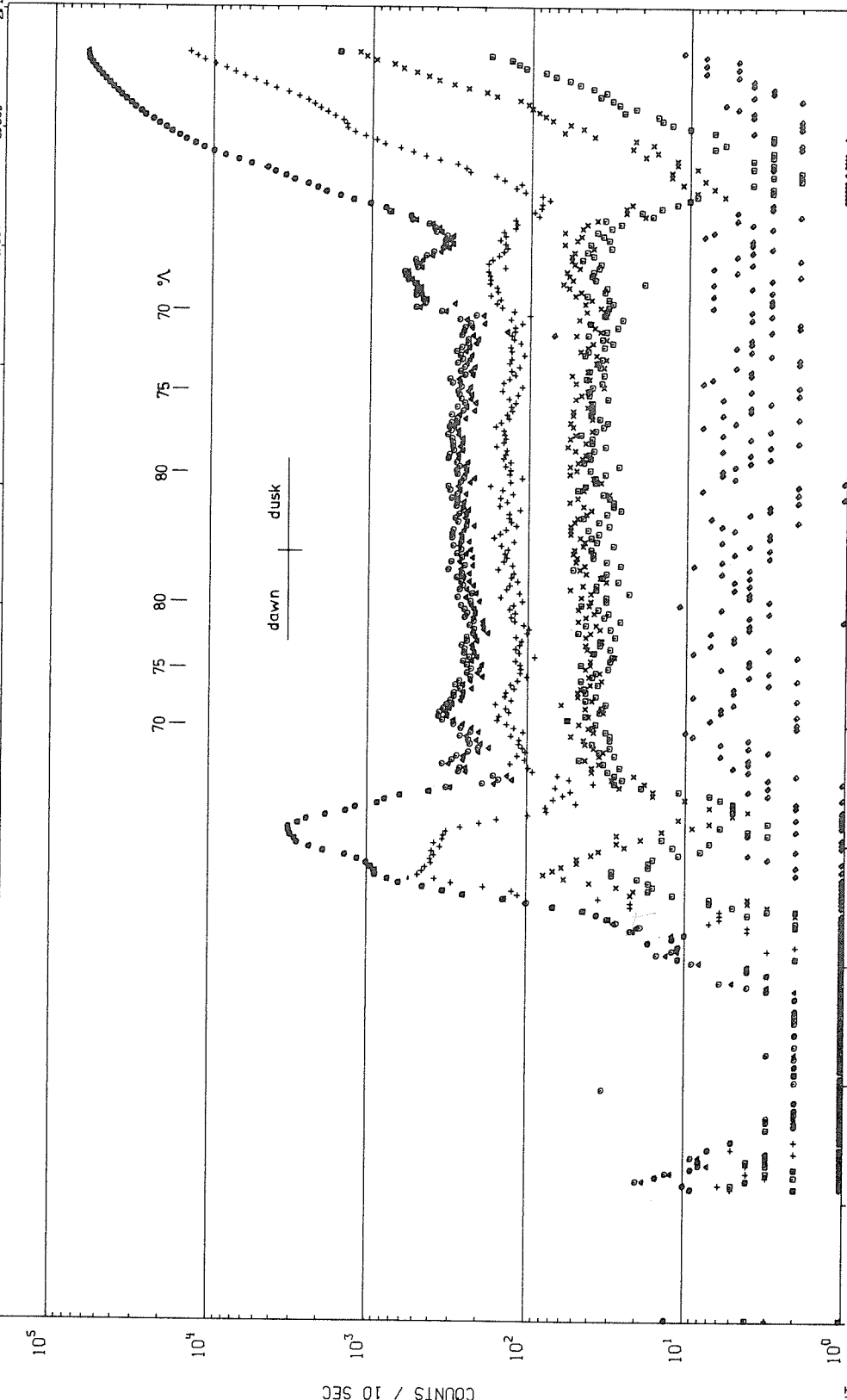


Fig. 2.

1 2 3 4 5 6

H (KM)	411	528	759	1062	1408	1765	2108	2417	2691	2890	3038	3122
L	1.325	1.155	1.308	1.859	3.377	8.377	30.293	37.769	12.720	5.937	3.550	2.471



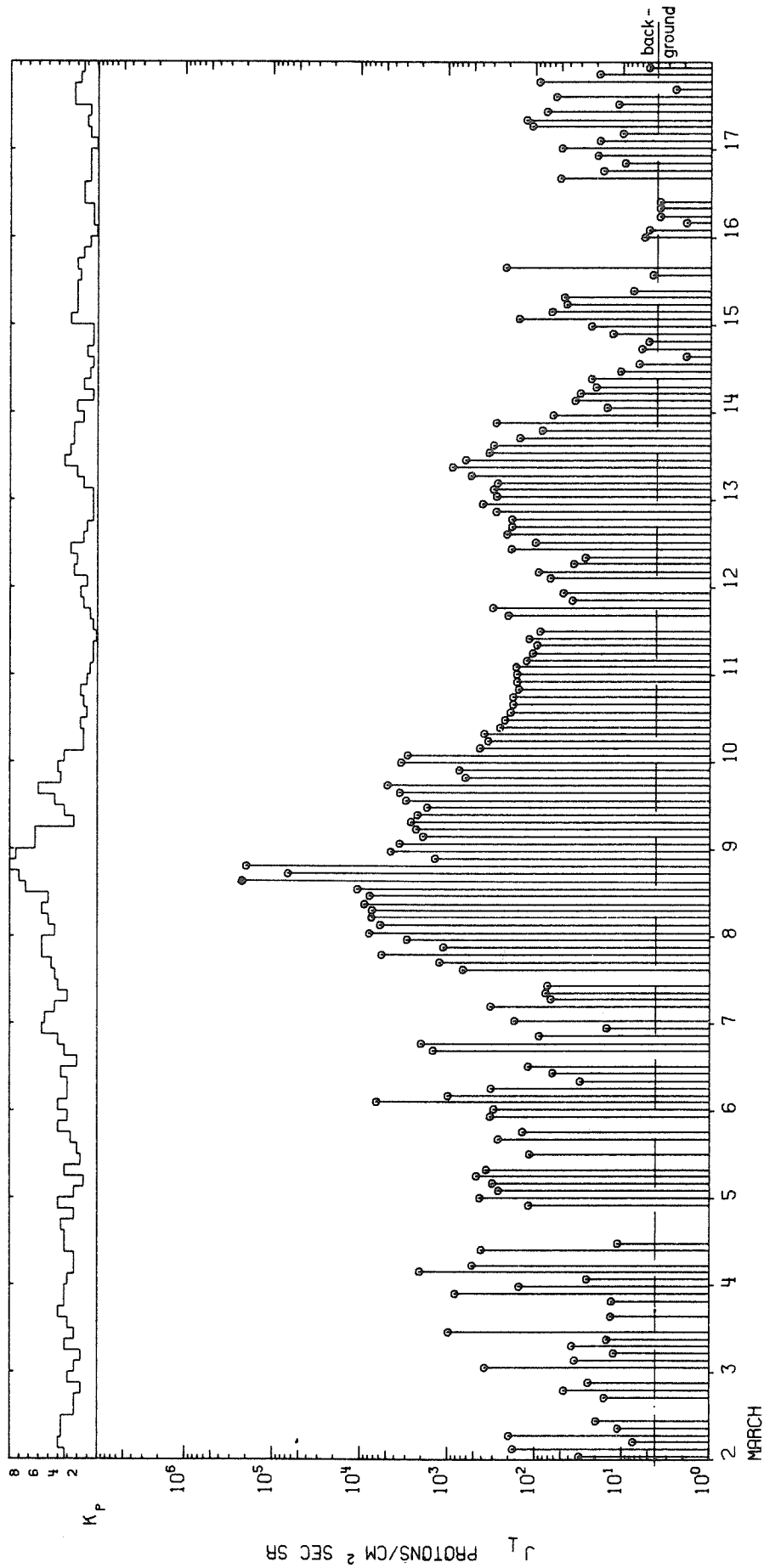
UT	84338	84838	85342	85942	90342	90942	91342	91842	92342	92842	93342	93842
MLAT	-21.9	-1.4	18.3	36.3	52.6	66.9	77.7	78.0	69.0	58.4	47.8	37.3
MLO	26.5	22.0	17.5	12.4	5.4	352.9	320.5	253.8	222.4	210.2	203.3	186.4
B (Γ)	.210	.202	.239	.279	.292	.279	.254	.229	.207	.187	.170	.153

Fig. 3.

GRS-A/AZUR

TIME DEPENDENCE OF PROTONS

PROTON ENERGY 0.25 - 1.65 (MEV)

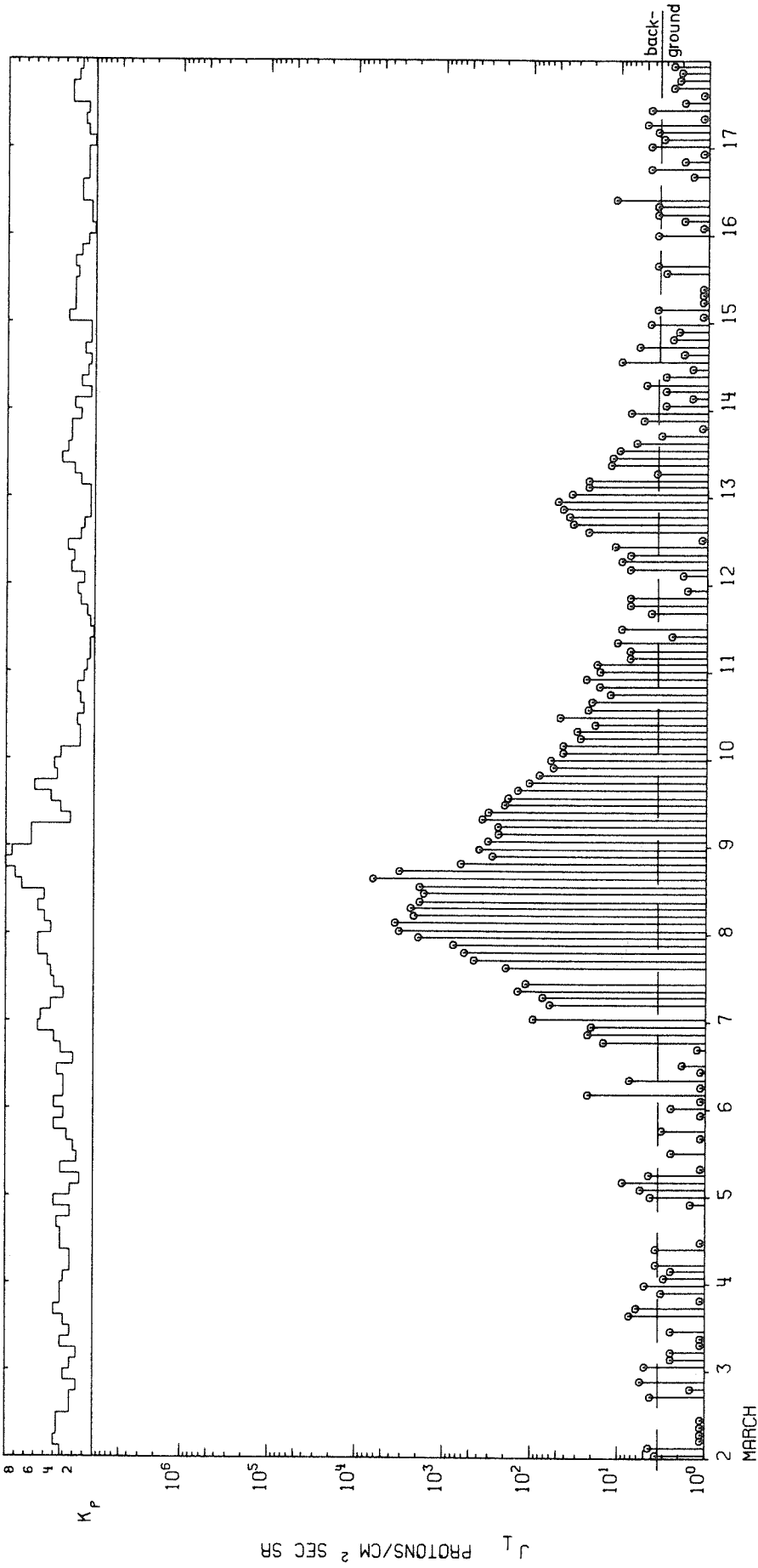


INVARIANT LATITUDE 70 (DEG), NORTH

Fig. 4.

Figures 4 through 6 give the measured intensities per cm^2 sec sr at the invariant latitude 70 ± 0.5 for protons in the two energy intervals 0.25 to 1.65 and 1.65 to 13.5 MeV and for alpha particles with 2.0 to 6.4 MeV for the period March 2 to 17. The lowest real intensity plotted is at $1.2 \text{ */cm}^2 \text{ sec sr}$. All dots placed at the base line signalize available data representing intensities below $1.2 \text{ */cm}^2 \text{ sec sr}$. K_p values are given at the top of the plot.

TIME DEPENDENCE OF PROTONS
PROTON ENERGY 1.65 - 13.50 (MEV)



YEAR 70

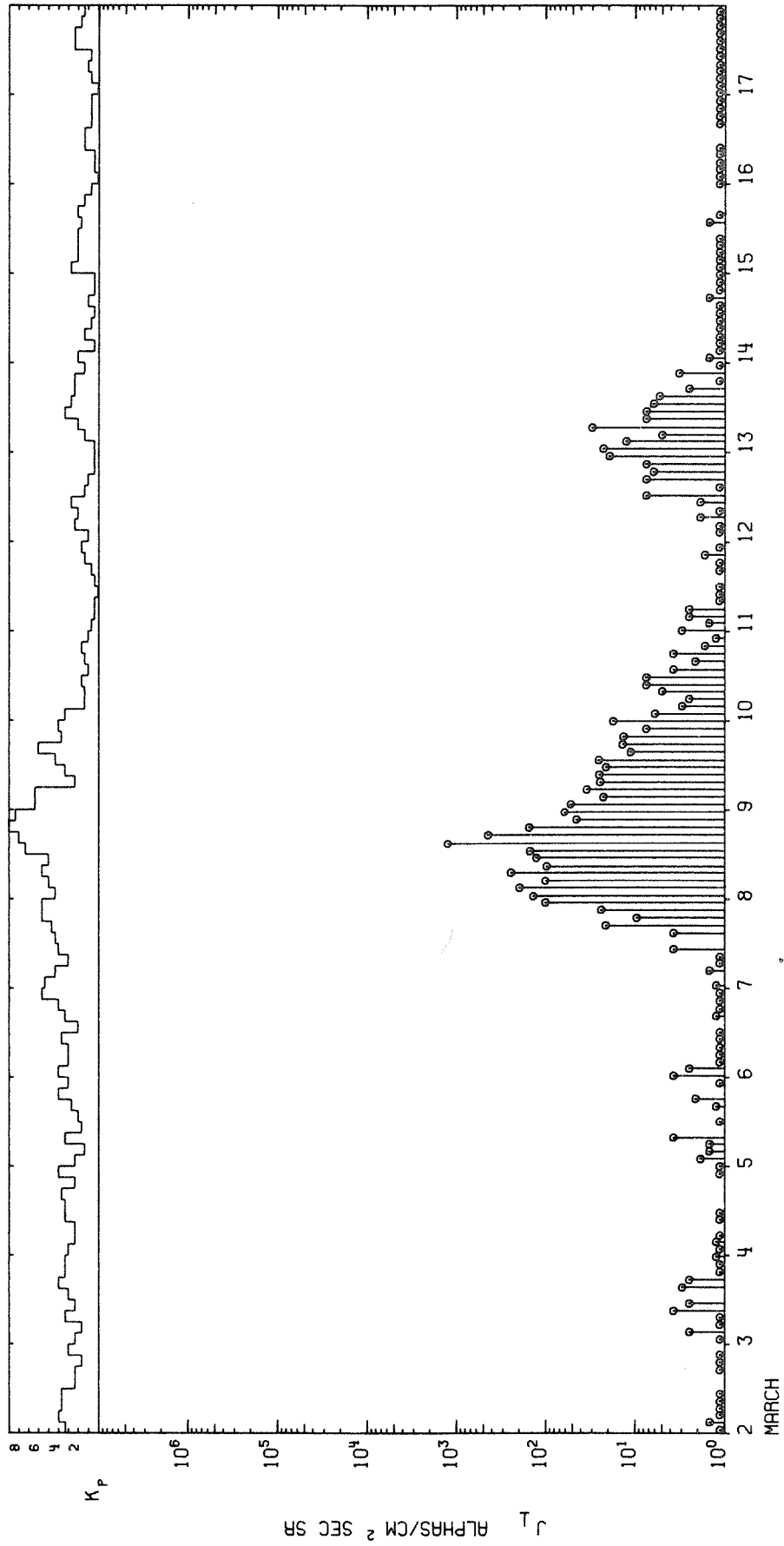
Fig. 5.

INVARIANT LATITUDE 70 (DEG), NORTH

GRS-A/AZUR

TIME DEPENDENCE OF ALPHAS

ALPHA ENERGY 2.00 - 6.40 (MEV)



YEAR 70

INVARIANT LATITUDE 70 (DEG), NORTH

Fig. 6.

"Observation of Solar Particles in March 1970 and Correlated Effects in the Outer Radiation Belt"

by

E. Achtermann, B. Häusler, D. Hovestadt and M. Scholer
Max-Planck-Institut für Physik und Astrophysik
Institut für extraterrestrische Physik
Garching

Introduction

It is the purpose of this paper to present a collection of experimental data which has been obtained during the March 1970 solar proton events. The events were associated with one of the largest geomagnetic storms which occurred to date of this solar cycle. The data we report were obtained between March 6 and March 18, 1970.

The instruments were carried by the polar orbiting satellite GRS-A/AZUR (inclination 102.94, perigee 383 km, apogee 3145 km, period = 122 min.). The satellite is magnetically stabilized. Two proton alpha-particle telescopes (88/1 and 88/2) are oriented perpendicularly (88/1) and at an angle of 45 degrees (88/2) with respect to the geomagnetic field vector. In the northern hemisphere telescope 88/2 is pointing upwards. The telescopes cover the energy range from 1.5 to 104 MeV for protons in six energy channels, and 6 to 19 MeV for alpha-particles in one energy channel. In addition, two omnidirectional proton-electron detectors are employed, which cover the energy range from 20 to 72 MeV for protons and >1.5 MeV for electrons.

Instrumentation

The telescopes 88/1 and 88/2 are particle range devices consisting of a stack of seven fully depleted silicon detectors. The energy channels are defined by the thickness of the detectors and of the absorbers placed in-between.

The stacks are surrounded by a plastic anti-coincidence scintillator and a heavy shielding (only protons with energies >75 MeV are able to penetrate).

Table 1 shows the energy ranges and the logical condition of the different channels K1 to K7.

Table 1

Channel	Logic	Particle	Energy
K1	A B \bar{C} \bar{S}	protons	1.5 - 2.7 MeV
K2	A B \bar{D} \bar{S}	alpha	6 - 19 MeV
K3	B C \bar{D} \bar{S}	protons	2.7 - 5.2 MeV
K4	C D \bar{E} \bar{S}	protons	5.2 - 10.4 MeV
K5	D E \bar{F} \bar{S}	protons	10.4 - 22 MeV
K6	E F \bar{G} \bar{S}	protons	22 - 49 MeV
K7	F G \bar{S}	protons	49 - 104 MeV

Geometrical factor: $5.80 \times 10^{-2} \text{ cm}^2 \text{ ster}$ (telescope 88/1; 90°)
 $5.95 \times 10^{-2} \text{ cm}^2 \text{ ster}$ (telescope 88/2; 45°)

Response of the telescopes 88/1 and 88/2 of the satellite AZUR.
A to G = Silicon detectors, S = Anti-coincidence scintillator.

The geometrical factor of the instruments are $5.80 \times 10^{-2} \text{ cm}^2 \text{ ster}$ for telescope 88/1 and $5.95 \times 10^{-2} \text{ cm}^2 \text{ ster}$ for telescope 88/2.

As calibration measurements show [Achtermann, *et al.*, 1970], the sensitivity of the instruments to energetic electrons is less than 10^{-6} for all coincidence channels as long as pile-up effects can be neglected. This is true for all measurements reported here.

The omnidirectional counters 93/1 and 93/2 consist of cubical lithium-drifted silicon detectors, heavily shielded on one side and covered by a hemispherical shield over a 2π solid angle on the other side. The thickness of the hemispherical shield determines the lower energy threshold for protons and electrons. The upper energy limit for protons is determined by the energy loss in the silicon cube in relation to the electronical threshold. Electrons and protons are separated by the electronical threshold (300 keV for the electron channels and 5.0 MeV for the proton channels).

Table 2 shows the relevant parameters of the devices. The geometrical factor for electrons was determined in calibration measurements. A detailed description of the experiments and an analysis of the calibration measurements are published elsewhere [Achtermann *et al.*, 1970].

Table 2

Channel	Shielding	Threshold	Particles	Energy	Geometrical Factor
K1	0.53 g/cm ² Al	0.3 MeV	e ⁻	>1.5 MeV	energy dependent
	0.53 g/cm ² Al	0.3 MeV	p	> 20 MeV	2.7 x 10 ⁻² cm ²
K2	0.53 g/cm ² Al	5.0 MeV	p	20-45 MeV	1.95 x 10 ⁻² cm ²
K3	2.34 g/cm ² Cu	0.3 MeV	e ⁻	> 4 MeV	energy dependent
	2.34 g/cm ² Cu	0.3 MeV	p	>40 MeV	4.7 x 10 ⁻² cm ²
K4	2.34 g/cm ² Cu	5.0 MeV	p	40-72 MeV	3.4 x 10 ⁻² cm ²

Response of the Omnidirectional Particle Counters of Satellite AZUR

History of the March 7 Solar Particle Event

The time history of the solar particle influx into the polar cap for different proton energy channels is given in Figure 1. The lower curves show the results of the 45° AZUR telescope (88/2) as obtained at a geomagnetic invariant latitude of $\Lambda = 70^\circ \pm 0.5$. At the time of measurement the apogee (3100 km) of the orbit was near the polar region. Therefore most of the measurements were obtained above 2900 km altitude.

A region of observation at an invariant latitude of $\Lambda = 70^\circ$ has been chosen because of an apparently easy access of solar flare particles from interplanetary space into this region [Williams and Bostrom, 1969; Evans and Stone, 1969; see also "Entry of Solar Particles into the Polar Region" of this paper].

The top curves of Figure 1 give the proton flux above 13.9 MeV [Pioneer 8 data, Solar-Geophysical Data 1970] as observed at a heliocentric longitude of about 45°E and the proton flux above 10 MeV as observed in the vicinity of the earth outside the magnetosphere [Explorer 41, Solar-Geophysical Data 1970]. In addition the time history of the proton/alpha-particle ratio:

$$\frac{\text{Protons } (5.2 < E < 22 \text{ MeV})}{\text{Alpha-particles } (6 < E < 19 \text{ MeV})} \text{ is given.}$$

In the lower part of Figure 1 we plotted the major flares, their solar longitudes [Solar-Geophysical Data 1970], and the sudden commencement which occurred in the time considered here. In Figure 2 the solar proton energy spectra are given at the times indicated in Figure 1.

Early on March 7 in nearly all energy channels there was a sudden flux increase. Since the 2B flare started at a later time, this increase may be due to the 1N flare which occurred at the western limb of the sun more than one day earlier. At the same time an enhancement in the $E > 10$ MeV proton flux at Explorer 41 can be seen. For several hours (8h) the proton flux roughly remains constant with some fluctuations. During this period the proton/alpha ratio stays also constant at a value of about 30 ± 10 .

On March 7 at about 2230 UT a second fast flux increase by about one order of magnitude occurred in all energy channels. In the following time span, until the sudden commencement on March 8, all proton channels reach their maximum flux values. During this period the proton/alpha ratio is roughly constant at a value of about 8 to 10.

Associated with the sudden commencement a sudden decrease in the counting rates occurs in all energy channels, which slowly continues for several days until nearly background level is reached. Also, the proton/alpha ratio drops to a value of about 5.

Later, on March 12, another flux increase occurs which probably is associated with a 2B flare at west 45° solar longitude, since no flux increase has been observed on Pioneer 8 at a position of 45° east solar longitude.

The second flux increase of the March 6/7 event appears about half a day earlier at Pioneer 8 than at AZUR and Explorer 41. Because of the spiral structure of the interplanetary magnetic field the lines of force at the position of Pioneer 8 are rooted about 0° east heliocentric longitude. Therefore it is very likely that this flux increase is associated with the 2B flare at 10° east solar longitude, which occurred on March 7, 0150 UT.

Entry of Solar Particles into the Polar Region

Figure 3 shows a sequence of 3 polar passes (Orbit 1415, 16, 18) at a time before, during and after a strong increase in the interplanetary proton flux (1 - 8.8 MeV) on March 7, 2228 UT [Simpson 1970]. With a delay of a few minutes the observed flux at an invariant latitude of 70° roughly represents the flux observed on IMP5 outside the magnetosphere. In the second pass (Orbit 1416) the flux of low energy protons at high latitudes $\Lambda > 75^\circ$ remains on the level of orbit 1415. Four hours later (Orbit 1418) the polar region uniformly shows the higher flux level. The short time delay at low latitudes and the longer delay at higher latitudes as well as the energy dependence suggest that for these particles diffusion across the magnetospheric tail might play an important role [Michel and Dessler, 1965; Williams and Bostrom, 1969].

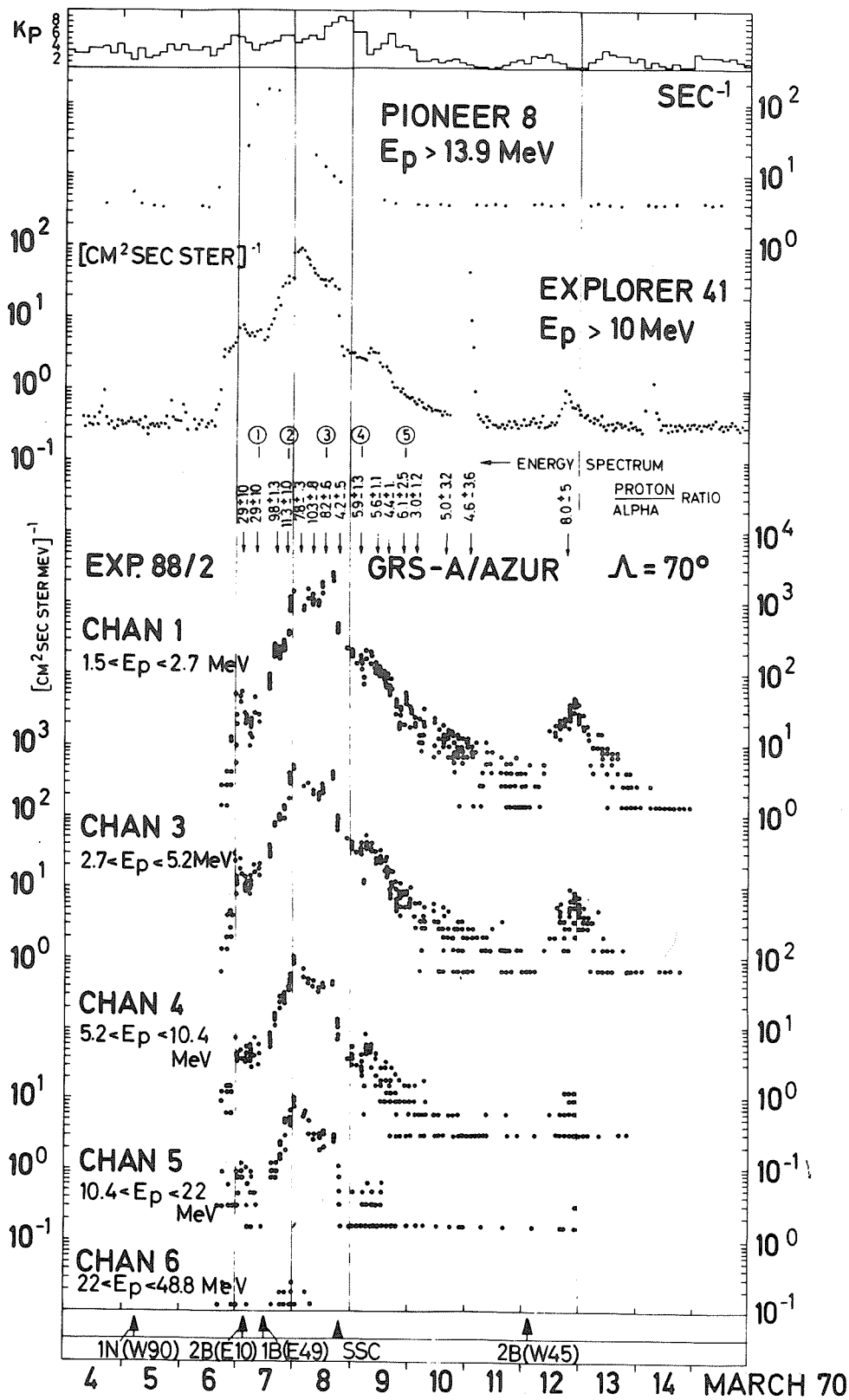


Fig. 1. Time history of the proton flux measured with telescope 88/2 at an invariant latitude of $70^\circ \pm 0.5^\circ$. The proton to alpha-particle ratio and the times, when energy spectra are obtained are indicated (see Figure 2.). In addition Pioneer 8 and Explorer 41 data on protons are included.

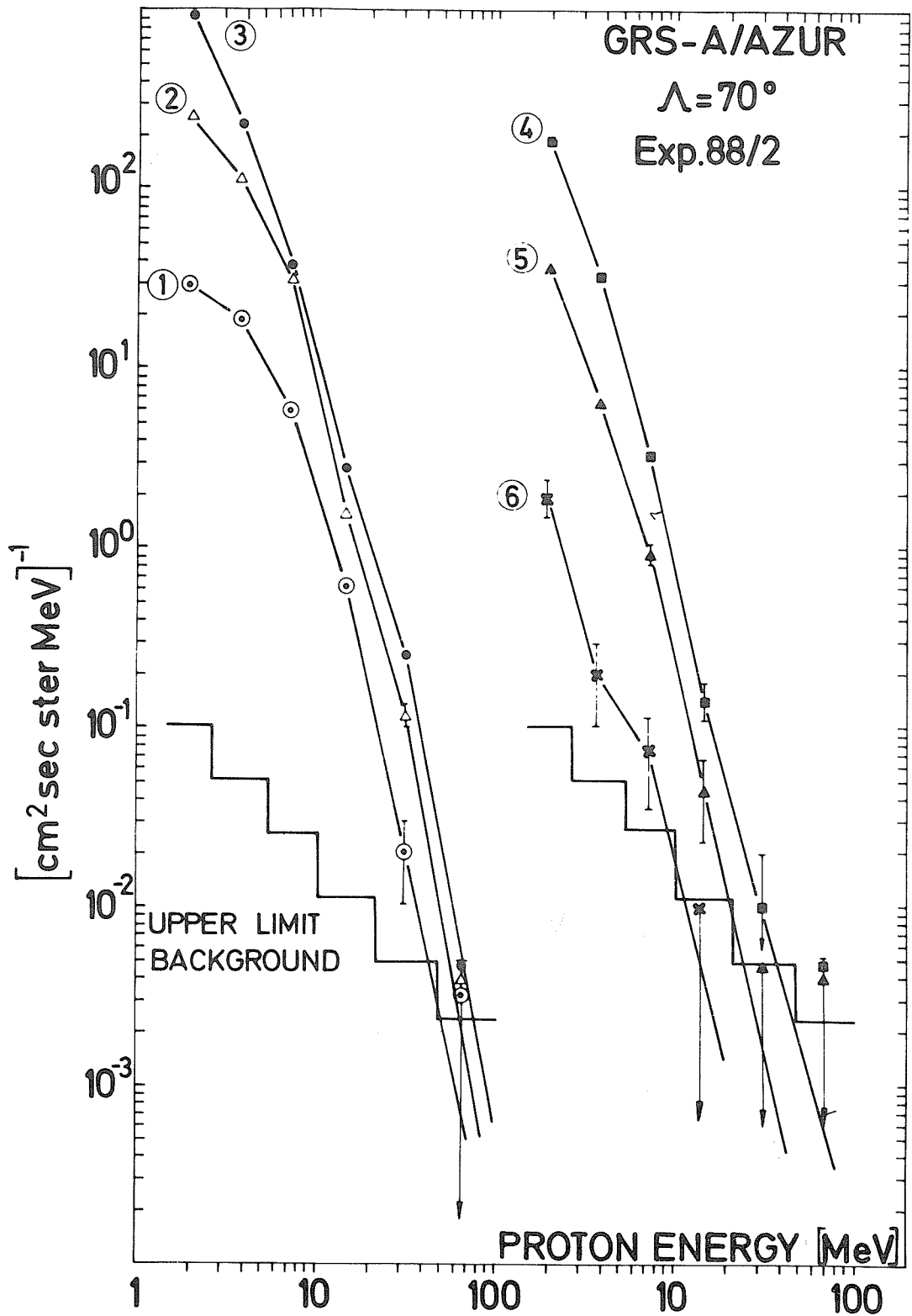


Fig. 2. Energy spectra of solar protons at the times indicated in Figure 1.

suggest that for these particles diffusion across the magnetospheric tail might play an important role [Michel and Dessler 1965, Williams and Bostrom 1969].

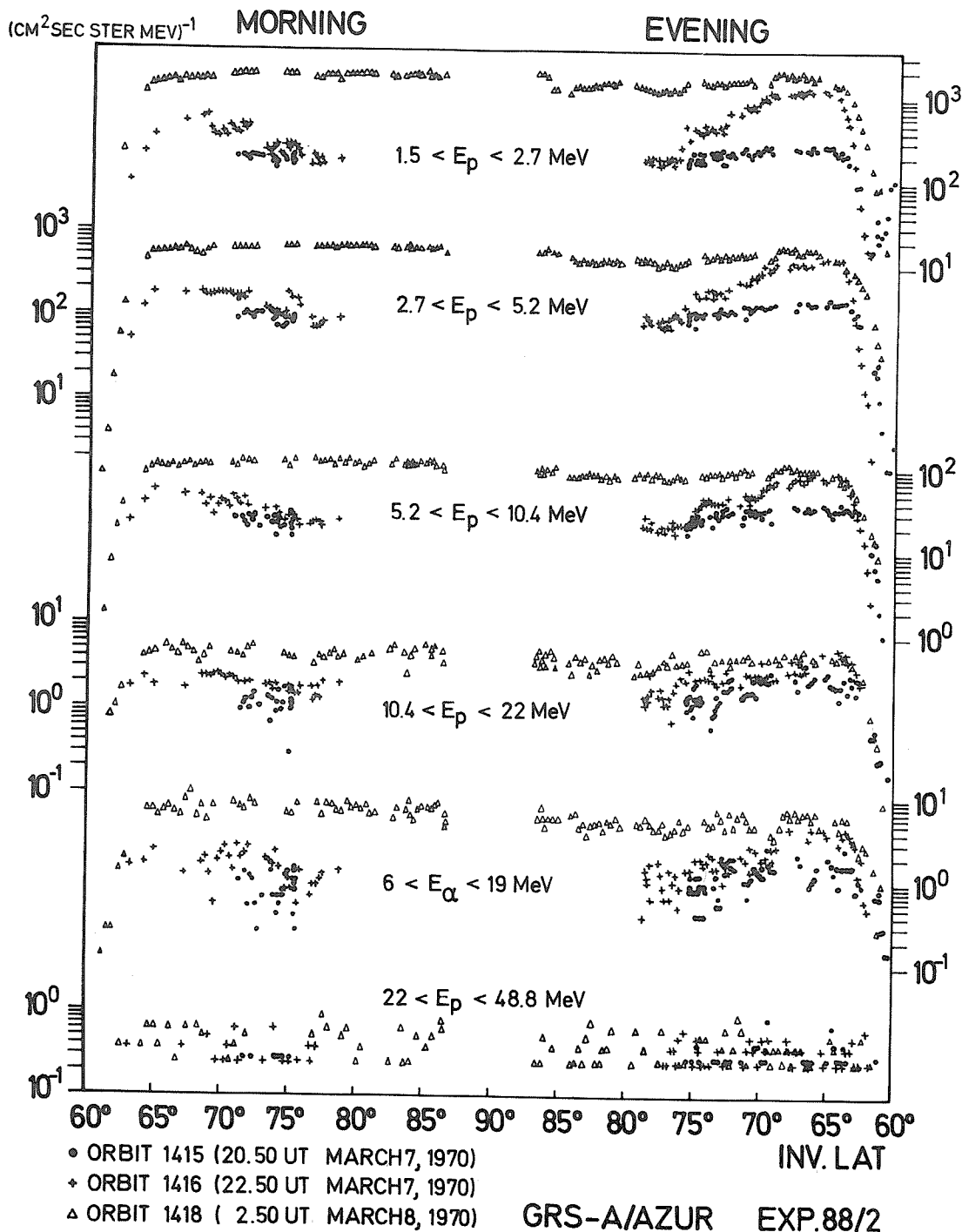


Fig. 3. Proton and alpha-particle flux as a function of the invariant latitude Λ for three polar cap passes before (Orbit 1415), during (Orbit 1416) and after (Orbit 1418) a fast flux increase in the interplanetary space.

During the period of non-uniform flux distribution over the polar cap (March 7, 2250 UT) the proton/alpha-particle ratio has been investigated. An attempt has been made to correlate the proton flux of various energy channels with the flux of alpha-particles. In Figure 4 the counting rates of the proton channels of telescope 88/2 between 1.5 MeV and 49 MeV are plotted versus the counting rate of the 6 to 19 MeV alpha-particle channel. The best correlation, a line with the slope of about 1.06 is obtained for channel 4 (5.2 - 10.4 MeV) and for the sum of channel 4 and 5 (5.2 - 22 MeV).

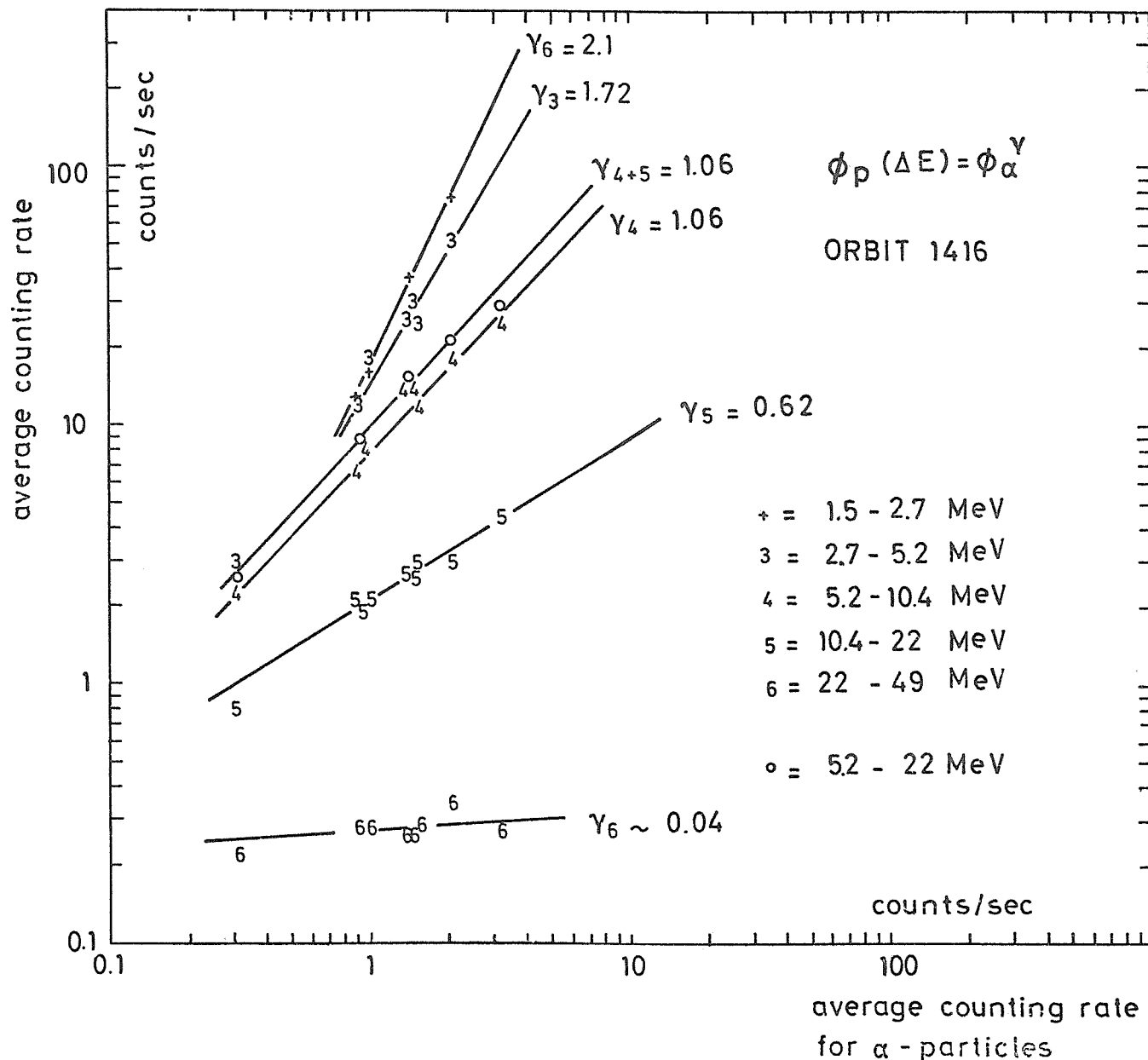


Fig. 4. Correlation of the counting rates in various proton energy channels of telescope 88/2 with the counting rate in the 6 to 19 MeV alpha-particle channel. Best correlation is given by a line with the slope equal one.

The correlation for lower and higher energy channels deviate considerably from a slope equal to one. Assuming a proton/alpha ratio outside the magnetosphere which is constant over the period of measurement we conclude that during this period the conditions for propagation into the polar cap of protons and alpha-particles of the same energy are the same. Since protons and alpha-particles of the same energy carry the same magnetic rigidity, it follows that the entry of the particles was mainly ruled by effects dependent on rigidity and not on velocity.

Variations of the Outer Zone Electron Flux

Figure 5 and Figure 6 show a sequence of polar cap passes with the time flux profiles of electrons with energies >1.5 MeV and >4 MeV as measured with the omnidirectional detectors 93/1 and 93/2. During all passes the satellite had a minimum altitude of 2900 km.

Figure 5 shows the long time behavior of the outer zone electron fluxes over a period of eight days including the time before arrival of flare particles. Figure 6 shows the short time sequence after the sudden commencement (SSC) on March 8, 1418 UT.

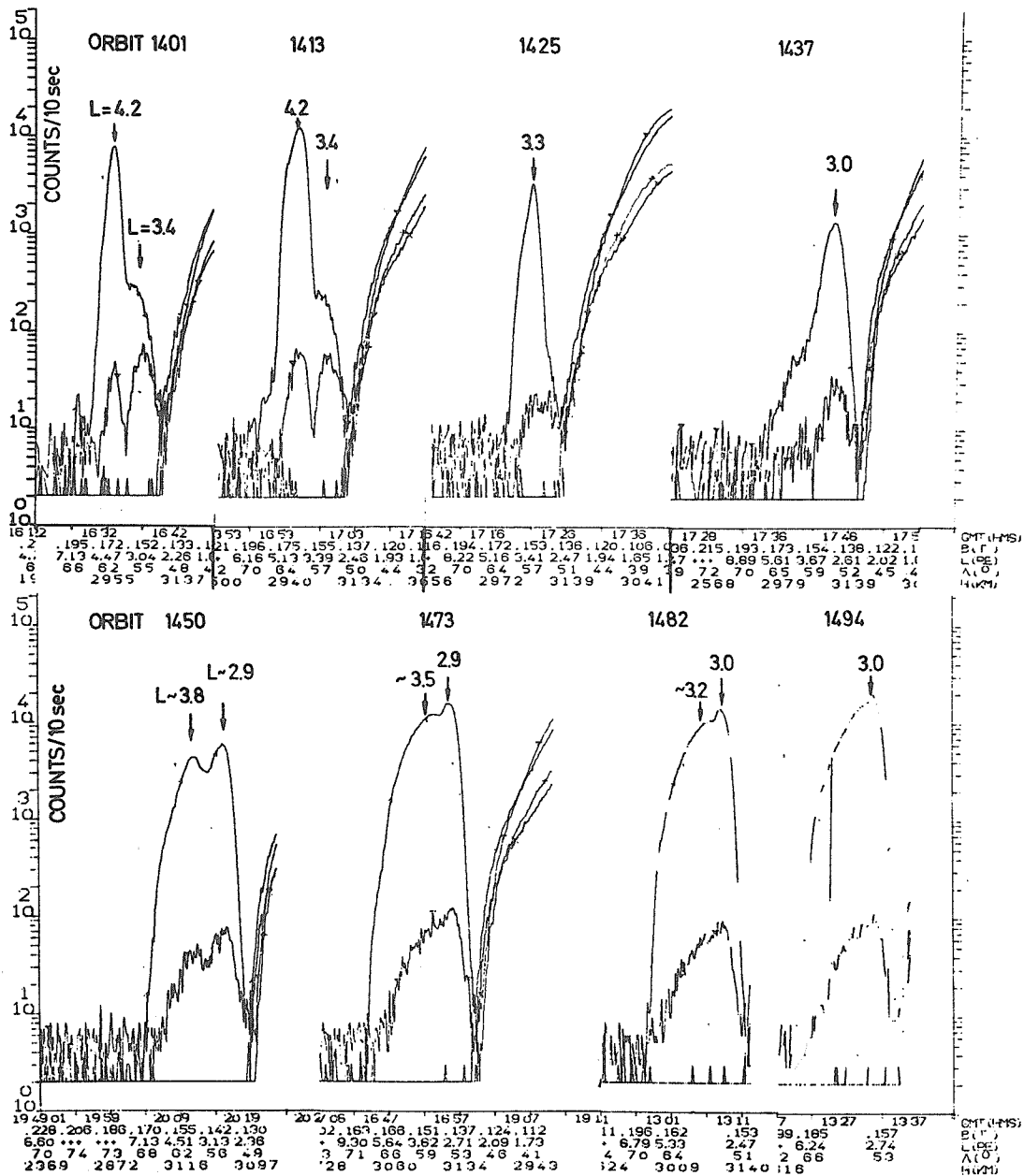


Fig. 5. Flux variations in the outer zone electron belt during the time of geomagnetic activity. Altitude 2900 to 3100 km in the region $L = 3$ to 4. The peak with the higher intensity represents electrons >1.5 MeV, the lower peaks electrons $E >4$ MeV. Orbit 1401 and 1413 were measured before the ssc.

The main features of the passes are:

- 1) Before the sudden commencement (Orbit 1401 to 1413):
 - a) A strong peak for electrons ($E >1.5$ MeV) at about $L = 4.2$ with a hump at $L \sim 3.4$.
 - b) A double peak for electrons ($E >4$ MeV) at $L \sim 4.2$ and $L \sim 3.4$ with a remarkable slot in-between at about $L = 3.8$.
- 2) In connection with the magnetic disturbances of the ssc (several hours before and after ssc):
 - a) Initially a short increase and then a fast decrease of the peak intensities for electrons ($E >1.5$ MeV).

- b) A simultaneous shift in L to lower L-values.
- c) Few (~ 4 h) hours after the ssc there remains only one electron peak at $L \sim 2.9$ for both energies. The flux peak is lowered by a factor of about 10 for $E > 1.5$ MeV and of about 10 for high energy electrons ($E > 4$ MeV).

OUTER ZONE ELECTRON FLUXES (MARCH 9 - 10, 1970) EXP.93 GRS-A/AZUR

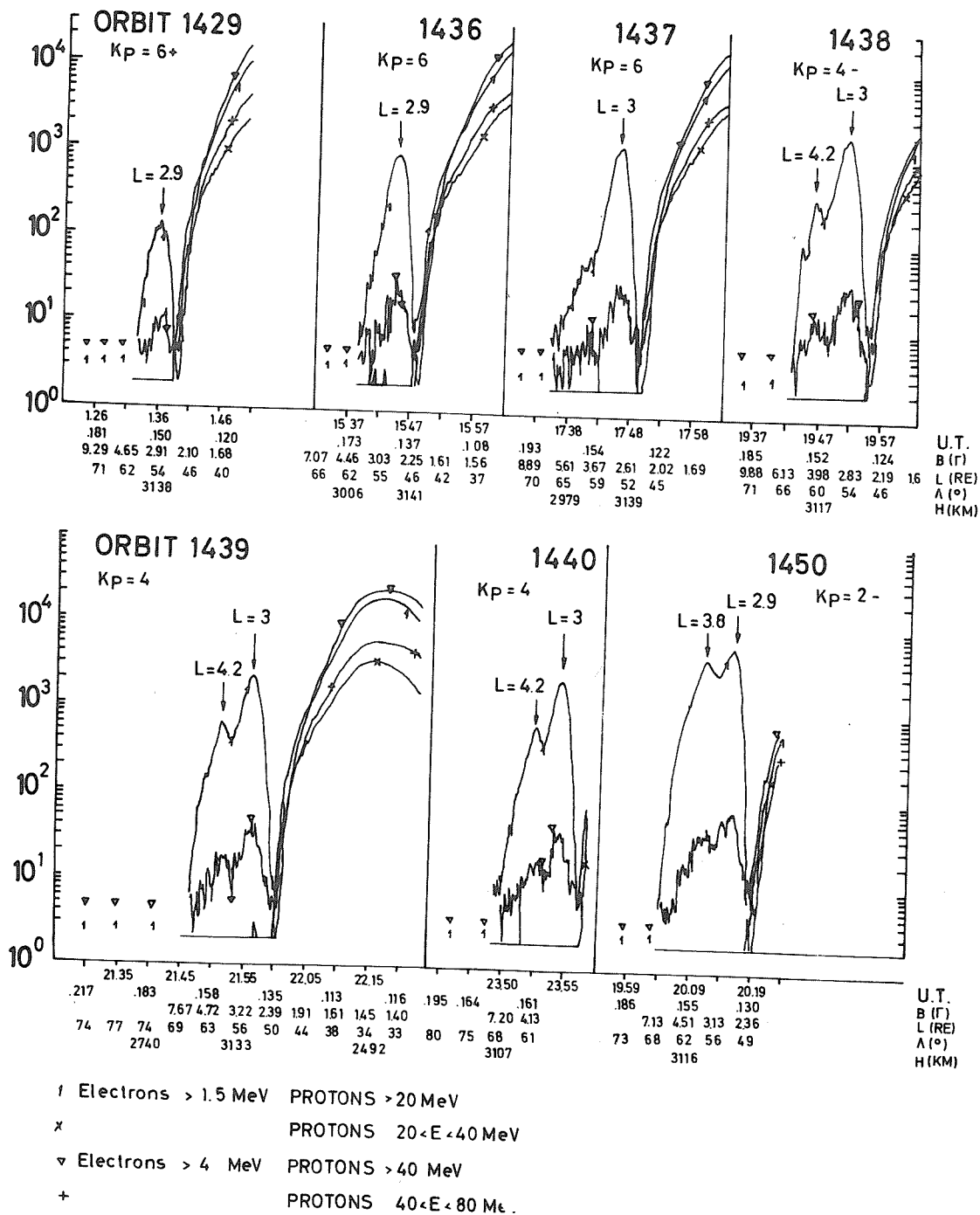


Fig. 6. Development phase of the secondary electron peak at $L = 4.2$ after the ssc.

- 3) Several hours after ssc:
 - a) Gradual recovery of low energy and high energy electron flux at $L \sim 2.9$.
 - b) Appearance of an additional peak for both electron energies at about $L \sim 4.2$ one day after ssc.
- 4) Until March 14 the second peak slowly shifts to lower L-values and finally merges with the peak at $L \sim 3.0$ to form a broad peak with a high electron flux (the peak flux is about a factor of 2 higher than before the event). This structure remains present over a long period (at least until March 18, 1970).

TIME VARIATIONS IN THE OUTER ELECTRON BELT ($E_e > 1.5$ MeV)

GRS-A/AZUR EXP 93

H ~ 3000 km

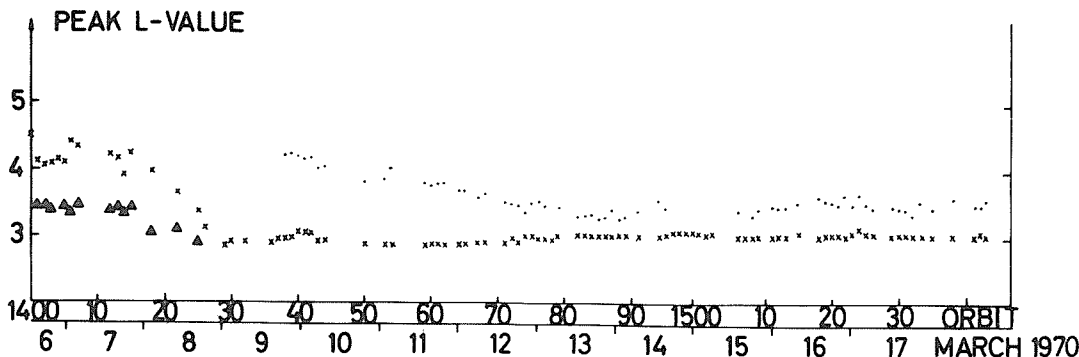
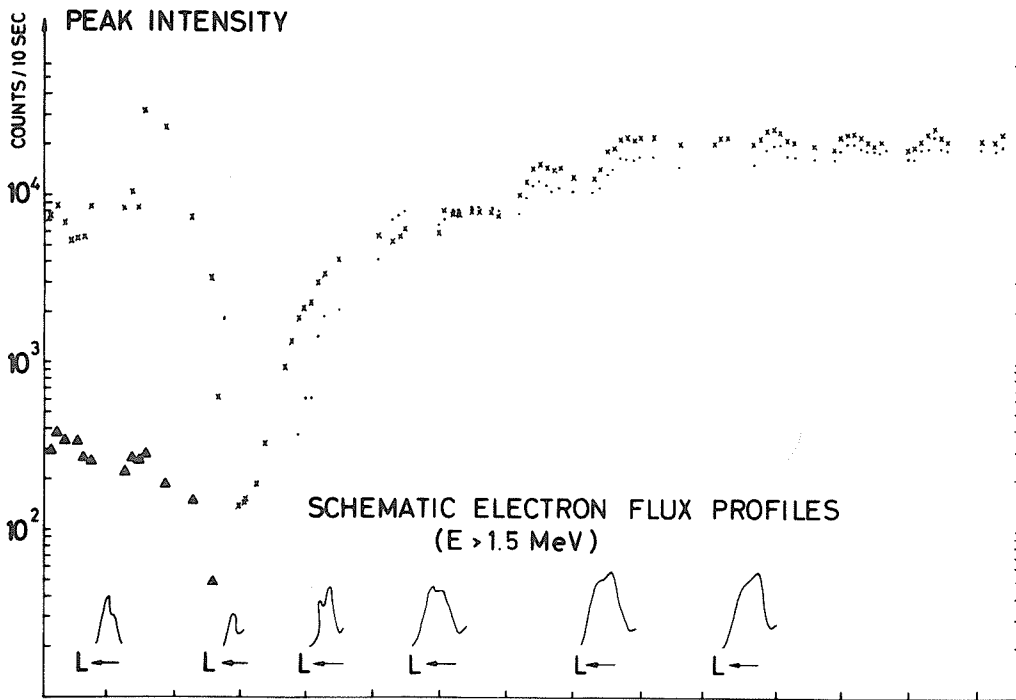
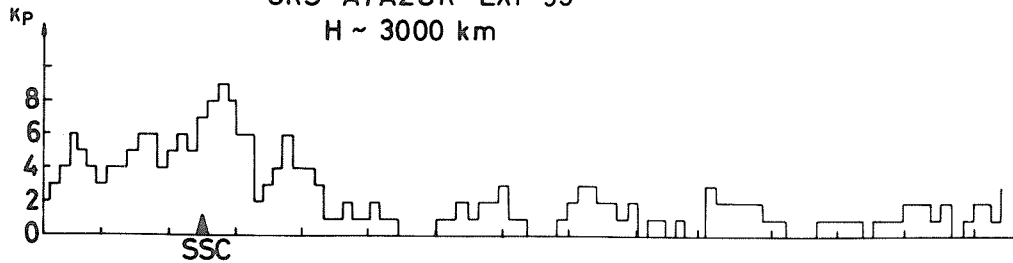


Fig. 7. Time history of the >1.5 MeV electron channel from March 6 to March 18, 1970. Lower part of the graph shows peak position in L. The middle part shows peak flux values of both $E > 1.5$ MeV peaks as a function of time.

These experimental results are summarized in Figure 7, which shows the peak intensity of the E > 1.5 MeV electron flux and the peak position in L-values as a function of time.

A comparison with the two onboard proton telescopes 88/1 and 88/2 leads to the conclusion that this time characteristic is really due to electrons. Beside this the proton channels of both omnidirectional counters do not respond at all in this region of space.

For electrons comparable with the lower energy range similar results were obtained for previous magnetic disturbances by other authors [Frank 1965; Williams 1966, 1967; Craven 1966; Williams *et al.* 1968].

An interpretation of the rather complex phenomenon is difficult and should await additional information from other experiments on electrons of lower energy. Nevertheless, the rapid shift (within ~ 1 day) of the outer electron belt from L = 4.2 to L = 2.9 during the first part of the event and the slower shift (within 4 days) of the secondary electron peak one day after the ssc from L = 4.2 to L = 3.0 probably can be attributed to radial L-shell diffusion under violation of the third adiabatic invariant.

Another question is the fact of appearance of energetic electrons well within the trapping region at L = 4.2 one day after the ssc and its slow increase in the intensity which occurs simultaneously with the inward L-diffusion. Correlated measurements at lower energies should show whether the slow flux increase for electrons E > 1.5 MeV and E > 4 MeV is due to the energizing of lower energy electrons (with a steep energy spectrum) by the inward L-shell motion.

Acknowledgements

The authors would like to thank the technical staff of the Max-Planck-Institut for the development and testing of the instrument. We acknowledge the help of the data group, especially the work of Dipl.-Math. B. Ebel.

We are grateful to Dr. G. Haerendel and Dipl.-Phys. G. Paschmann for fruitful discussions.

The work was prepared with the support of the Bundesministerium für wissenschaftliche Forschung under grant WRK 98.

REFERENCES

- ACHTERMAN, E., 1970 Die Experimente EI88 und EI93 zur Messung von energiereichen Elektronen, Protonen und Alphateilchen im Satelliten AZUR, EMBW-Bericht.
- B. HAUSLER,
D. HOVESTADT,
E. KÜNNETH,
P. LAEVERENZ and
G. PASCHMANN
- CRAVEN, J. D. 1966 Temporal variations of electron intensities at low altitudes in the outer radiation zone as observed with satellite Injun 3, J. Geophys. Res., 71, 5643.
- EVANS, L. C. and 1969 Access of solar protons into the polar cap. A persistent north-south asymmetry, J. Geophys. Res., 74, 5127.
- E. C. STONE
- FRANK, L. A. 1965 Inward diffusion of electrons of greater than 1.6 million electron volts in the outer radiation zone, J. Geophys. Res., 70, 3533.
- MICHEL, F. C. and 1965 Physical significance of inhomogeneities in polar cap absorption events, J. Geophys. Res., 70, 4305.
- A. J. DESSLER
- SIMPSON, J. 1970 Private communication.
- Solar-Geophysical Data, 309 Part I, May 1970 and 313 Part II, September 1970, U.S. Department of Commerce (Boulder, Colorado, U.S.A. 80302).
- WILLIAMS, D. J. and 1969 Proton entry into the magnetosphere on May 26, 1967, GSFC Report X-612-69-141.
- C. O. BOSTROM
- WILLIAMS, D. J., 1968 Observation of trapped electrons, J. Geophys. Res., 73, 5673.
- J. F. ARENS and
L. J. LANZEROTTI

- WILLIAMS, D. J. 1967 On the low altitude trapped electron boundary collapse during magnetic storm, J. Geophys. Res., 72, 1644.
- WILLIAMS, D. J. 1966 Outer zone electrons. In "Radiation trapped in the earth's magnetic field", Billy M. McCormac, D. Reidel Publishing Co., 263.

USCOMM-NOAA-ASHEVILLE-4-23-71--1100

Upper Atmosphere Geophysics Report UAG-1

"IQSY Night Airglow Data" by L. L. Smith, F. E. Roach and J. M. McKenna of Aeronomy Laboratory, ESSA Research Laboratories, July 1968, single copy price \$1.75. [Catalog No. C52.16/2:1]

Upper Atmosphere Geophysics Report UAG-2

"A Reevaluation of Solar Flares, 1964-1966" by Helen W. Dodson and E. Ruth Hedeman of McMath-Hulbert Observatory, The University of Michigan, August 1968, single copy price 30 cents. [Catalog No. C52.16/2:2]

Upper Atmosphere Geophysics Report UAG-3

"Observations of Jupiter's Sporadic Radio Emission in the Range 7.6-41 MHz, 6 July 1966 through 8 September 1968" by James W. Warwick and George A. Dulk, Department of Astro-Geophysics, University of Colorado, October 1968, single copy price 30 cents. [Catalog No. C52.16/2:3]

Upper Atmosphere Geophysics Report UAG-4

"Abbreviated Calendar Record 1966-1967" by J. Virginia Lincoln, Hope I. Leighton and Dorothy K. Kropp of Aeronomy and Space Data Center, Space Disturbances Laboratory, ESSA Research Laboratories, January 1969, single copy price \$1.25. [Catalog No. C52.16/2:4]

Upper Atmosphere Geophysics Report UAG-5

"Data on Solar Event of May 23, 1967 and its Geophysical Effects" compiled by J. Virginia Lincoln, World Data Center A, Upper Atmosphere Geophysics, ESSA, February 1969, single copy price 65 cents. [Catalog No. C52.16/2:5]

Upper Atmosphere Geophysics Report UAG-6

"International Geophysical Calendars 1957-1969" by A. H. Shapley and J. Virginia Lincoln, ESSA Research Laboratories, March 1969, single copy price 30 cents. [Catalog No. C52.16/2:6]

Upper Atmosphere Geophysics Report UAG-7

"Observations of the Solar Electron Corona: February 1964 - January 1968" by Richard T. Hansen, High Altitude Observatory, Boulder, Colorado and Kamuela, Hawaii, October 1969, single copy price 15 cents. [Catalog No. C52.16/2:7]

Upper Atmosphere Geophysics Report UAG-8, Parts 1 and 2

"Data on Solar-Geophysical Activity October 24 - November 6, 1968" compiled by J. Virginia Lincoln, World Data Center A, Upper Atmosphere Geophysics, ESSA, March 1970, single copy price \$1.75. Part 1 [Catalog No. C52.16/2:8/1], Part 2 [Catalog No. C52.16/2:8/2]

Upper Atmosphere Geophysics Report UAG-9

"Data on Cosmic Ray Event of November 18, 1968 and Associated Phenomena" compiled by J. Virginia Lincoln, World Data Center A, Upper Atmosphere Geophysics, ESSA, April 1970, single copy price 55 cents. [Catalog No. C52.16/2:9]

Upper Atmosphere Geophysics Report UAG-10

"Atlas of Ionograms" edited by A. H. Shapley, ESSA Research Laboratories, May 1970, single copy price \$1.50. [Catalog No. C52.16/2:10]

Upper Atmosphere Geophysics Report UAG-11

"Catalogue of Data on Solar-Terrestrial Physics", compiled by J. Virginia Lincoln and H. Patricia Smith, World Data Center A, Upper Atmosphere Geophysics, ESSA, June 1970, single copy price \$1.50. [Catalog No. C52.16/2:11]